

A thesis submitted for the Doctoral degree (Dr. rer. nat.) to the Faculty of Biology at the
Luidwig-Maximilians-University, Munich, Germany

**Addressing the Role of Mitochondrial Thioredoxin Reductase
and xCT in the Maintenance of Redox Homeostasis**

Tamara Perisic

Helmholtz Zentrum München, German Reasearch Center for Environmental Health
Institute of Clinical Molecular Biology and Tumor Genetics

Munich, October 2009

Ehrenwörtliche Versicherung

Ich versichere hiermit ehrenwörtlich, dass die Dissertation von mir selbständig, ohne unerlaubte Beihilfe angefertigt ist.

Die vorliegende Dissertation wurde weder ganz, noch teilweise bei einer anderen Prüfungskommission eingereicht.

Ich habe noch zu keinem früheren Zeitpunkt versucht eine Dissertation einzureichen oder an einer Doktorprüfung teilzunehmen.

.....

(Tamara Perisic)

Dissertation eingereicht am 8. Oktober 2009

- | | |
|----------------------|-----------------------------------|
| 1. Gutachter: | Prof. Dr. Dirk Eick |
| 2. Gutachter: | Dr. Daniel Krappmann |
| 3. Gutachter: | Prof. Dr. Hans-Ulrich Koop |
| 4. Protokoll: | Prof. Dr. Michael Boshart |

Tag der mündlichen Prüfung: 23. 03. 2010

Table of contents

LIST OF ABBREVIATIONS	I
1. INTRODUCTION	1
1.1. Biological sources of ROS and its role in diverse biological processes	1
1.2. Selenoproteins	2
1.2.1. Incorporation of selenium	3
1.2.2. Family of thioredoxin reductases	5
1.2.3 Mammalian thioredoxin system	7
1.3. Peroxiredoxins	13
1.3.1. The catalytic mechanisms of peroxiredoxins	15
1.3.2. The role of sulfiredoxin (Srx)	17
1.4. System x_c^-	19
1.5. Objectives	21
2. MATERIALS AND METHODS	23
2.1. Materials	23
RT-PCR	28
Expression and Targeting Vectors	28
2.2. Methods	31
2.2.1. Cell culture	31
2.2.2. Gene-transfer methods	34
2.2.3. Molecular biology techniques	35
2.2.4. Flow cytometry	46
2.2.5. Biochemical methods	49
2.2.6. ES cell technology	50

3. RESULTS	53
3.1. Functional analysis of mitochondrial thioredoxin reductase (Txnrd2)	53
3.1.1. Phenotype of primary MEFs lacking Txnrd2	53
3.1.3. Antioxidants rescue loss of Txnrd2	54
3.1.4. Intracellular ROS are augmented in cells lacking Txnrd2	55
3.1.5. Susceptibility of <i>Txnrd2</i> ^{-/-} cells towards pro-oxidants and genotoxic agents	56
3.1.6. Sensitivity of <i>Txnrd2</i> ^{-/-} cells towards inhibition of de novo GSH biosynthesis	59
3.1.7. Expression of mitochondrial peroxiredoxins is increased in <i>Txnrd2</i> ^{-/-} cells	61
3.1.8. Time-dependent increase of Prx III levels in response to H ₂ O ₂	62
3.1.9. Ectopic expression of Txnrd2 and Txnrd1 in <i>Txnrd2</i> ^{-/-} cells	64
3.1.10. Stable expression of Txnrd1 in <i>Txnrd2</i> knock-out cells	65
3.1.11. Add-back of mitoTxnrd2 rescues <i>Txnrd2</i> ^{-/-} cells from cell death induced by GSH depletion	67
3.1.12. The role of Txnrd2 in normal physiology and disease	69
3.2. The role of system x_C⁻ in maintenance of intracellular GSH levels and cystine/cysteine redox balance in cultured cells	75
3.2.1. The protective role of system x _C ⁻ in Burkitt lymphoma (BL) cells	75
3.2.2. The thioredoxin system as the possible driving force for the cystine/cysteine redox cycle	76
3.3. Generation of conditional xCT-knock-in mice	80
3.3.1 Gene targeting in ES cells	80
3.3.2. Analysis of the functionality of the neoR-STOP-xCT cassette	82
3.3.3. Generation of <i>R26mxCT</i> ^{flSTOP/CreERT2} mice	82
3.3.4. Breeding of xCT-transgenic mice with the Tam-inducible <i>CreERT2-Deleter</i> mouse	84
3.3.4. Phenotypic analysis of <i>R26mxCT</i> ^{flSTOP/CreERT2} mice	84
4. DISCUSSION	93
4.1. Absence of Txnrd2 causes high ROS accumulation, increased sensitivity towards pro-oxidants and impaired cell growth	93

4.2. Compensatory up-regulation of mitochondrial peroxiredoxins III and V in response to Txnrd2 disruption	98
4.3. Txnrd1 and Txnrd2 do not show functional redundancy in vivo	99
4.4. Txnrd2 is dispensable for maintaining the Cys/(Cys)₂ cycle	101
4.5. Txnrd2 protects myocardial tissue from oxidative damage and is implicated in the pathogenesis of Dilatative Cardiomyopathy	103
4.6. Inducible overexpression of xCT in mice is not protective, but causes spleen, thymus and testis atrophy and defective erythropoiesis	104
5. SUMMARY	109
6. REFERENCES	111
7. APPENDIX	129
7.1. Acknowledgements	129
7.2. Curriculum vitae	131

List of Abbreviations

2-ME	β -mercaptoethanol
Amp	Ampicillin
AmpR	Ampicillin resistance gene (β -lactamase)
AMV	Avian myeloblastosis virus
ATP	Adenosine-5'-triphosphate
BOOH	<i>t</i> -butylhydroperoxide
BSA	Bovine serum albumin
BSO	L-buthionine sulfoximine
CDK	Cycline dependent kinase
CMV	Cytomegalovirus
Cre	Cre recombinase
Cys	Cysteine
(Cys) ₂	Cystine (oxidised Cys dimer)
DAPI	4',6-diamidino-2-phenylindole, dihydrochloride
DCFH-DA	Dichlorofluorescein diacetate
DCM	Dilated cardiomyopathy
DIOs	Iodothyronine deiodinases
DMEM	Dulbecco's Modified Eagle Medium
DMSO	Dimethylsulfoxide
DNA	Deoxyribonucleic acid
dNTP	Deoxyribonucleotide
DTT	Dithiothreitol
EDTA	Ethylenediamine-N,N,N',N'-tetra-acetic acid
EFSec	Sec-specific elongation factor
EGF	Epidermal growth factor
eGFP	Enhanced green fluorescence protein
EpRE	Electrophile response element
ERK	Extracellular signal-regulated kinase
ES cells	Embryonic stem cells
FACS	Fluorescence activated cell sorting

FAD	Flavin adenine dinucleotide
FCS	Fetal calf serum
GpAATs	Glycoprotein-associated amino acid transporters
GPx	Glutathione peroxidase
GR	Glutathione reductase
GRx	Glutaredoxin
GSH	Glutathione
GSS	Glutathione synthetase
GSSG	Oxidized glutathione
GTP	Guanosine-5'-triphosphate
H ₂ O ₂	Hydrogen peroxide
HO•	Hydroxyl radical
HO ₂ •	Hydroperoxy radical
HPRT	Hypoxanthine-guanine phosphoribosyltransferase
IRES	Internal ribosomal entry site
LMP agarose	Low melting point agarose
LTR	Long terminal repeat
MAPK	mitogen activated protein kinase
MCM	MERCreMER
MEFs	Murine embryonic fibroblasts
MitoPY	Mitochondrial Peroxi-yellow
MLS	Mitochondrial leader sequence
NAC	N-Acetyl-L-cysteine
NADPH	Nicotinamide adenine dinucleotide phosphate
NeoR	Neomycin phosphotransferase
NESs	Nuclear export signals
NFκB	Nuclear factor κB
NLS	Nuclear localization signal
Nrf2	NF-E2-related factor 2
NTAPe-tag	N-terminal tandem affinity purification enhanced tag
nucmemb	Nuclear membrane anchor
O ²⁻	Superoxide anion
OVA	Ovalbumin
pA	PolyA signal

PAGE	Polyacrylamide gel electrophoresis
PBS	Phosphate buffered saline
PDGF	Platelet-derived growth factor
PEITC	Phenyl ethyl isothiocyanate
PFA	Paraformaldehyde
PI	Propidium iodide
PRE	Post regulatory element
Prx	Peroxiredoxin
PS	Phosphatidylserine
PuroR	Puromycin N-acetyltransferase gene
Py ori	Polyoma origin of replication
PYAM	Peroxi-yellow acetoxymethyl-ester
PYME	Peroxi-yellow methyl-ester
RFP	Red fluorescence protein
RNA	Ribonucleic acid
RO•	Alkoxyl radical
RO ₂ •	Peroxyl radical
ROS	Reactive oxygen species
rpL30	Ribosomal protein L30
rT3	Reverse-triiodothyronine
SA	Splice acceptor
SBP2	SECIS-binding protein 2
SDS	Sodium dodecyl sulfate
Se	Selenium
Sec	Selenocysteine
SECIS	Selenocysteine insertion sequence
Secp43	43 kDa RNA-binding protein
-SeH	Selenol group
SFFV	Spleen focus forming virus
SF-tag	Strep-FLAG-tag
SIN	Self-inactivating 3' LTR
SLA	Soluble liver antigen protein
SOD	Superoxide dismutase
Srx	Sulfiredoxin

SV40	SV-40 promoter
T3	Triiodothyronine
T4	Thyroxine
Tam	Tamoxifen
TGR	Thioredoxin-glutathione reductase (Txnrd3)
TNF	Tumour necrosis factor
TPx	Thioredoxin peroxidases
<i>Trsp</i>	Selenocysteine-specific <i>tRNA</i> gene
Trx	Thioredoxin
Txnrd	Murine thioredoxin reductase
TXNRD	Human thioredoxin reductase
UGA	“opal” stop codon
wt	Wild-type
γ -GCS	γ -glutamylcysteine synthetase

1. Introduction

1.1. Biological sources of ROS and its role in diverse biological processes

Reactive oxygen species (ROS) is a collective term and includes superoxide anion ($O_2^{\cdot-}$), hydrogen peroxide (H_2O_2), hydroxyl radical ($HO\cdot$), hydroperoxy radical ($HO_2\cdot$), peroxy radical ($RO_2\cdot$) and alkoxy radical ($RO\cdot$). Among them, hydrogen peroxide (H_2O_2) is the most extensively studied one. Most biological sources of H_2O_2 involve the spontaneous or catalytic breakdown of superoxide anion ($O_2^{\cdot-}$), generated by the partial reduction of oxygen during mitochondrial respiration (Boveris, 1984). Also, exposure of cells to a variety of physical, chemical, and biological agents causes ROS accumulation. For instance, immune cells activate the NADPH oxidase complex to generate superoxide and hydrogen peroxide as a cytotoxic agent during microbial defence. Furthermore, UV light and ionising radiation causes oxidative stress as well. There is increasing evidence that cells produce H_2O_2 transiently in response to the activation of various cell-surface receptors. Various growth factors and cytokines, including PDGF, EGF, insulin, angiotensin II, and $TNF\alpha$, generate hydrogen peroxide in target cells (D'Autreaux and Toledano, 2007; Geiszt and Leto, 2004; Park et al., 2004a). Thus, beyond its toxic effects H_2O_2 has been recognized as an important intracellular messenger that modifies protein function through the oxidation of critical cysteine residues of many proteins including protein tyrosine phosphatases (Choi et al., 2005; DeYulia et al., 2005; Finkel, 1998; Rhee, 1999; Rhee et al., 2000; Rhee et al., 2005). If the physiological threshold level of H_2O_2 is not exceeded, it will have an affirmative effect on the cell processes, such as receptor-mediated cell signalling pathways, normal cell proliferation, and transcriptional activation. On the contrary, the chronic presence of peroxides and oxygen radicals is a risk factor to cells because they may damage cellular components, which is often associated with the initiation and progression of many degenerative diseases. Therefore, it is no surprise that the generation of H_2O_2 and other reactive oxygen species (ROS) is a tightly regulated process.

In addition to non-enzymatic antioxidants, among which glutathione (GSH), cysteine, vitamin C and E are well known, cells contain a variety of antioxidant enzymes which contribute to controlling the level of cellular ROS. The major antioxidant enzymes involved in the catalytic breakdown of ROS are superoxide dismutase (SOD), catalase, thioredoxin reductase (Txnrd), peroxiredoxins (Prx) and glutathione peroxidase (GPx). Catalase is a highly efficient enzyme that utilizes a heme prosthetic group, while the catalytic reduction of hydrogen

peroxide by thioredoxin peroxidases involves the oxidation of catalytic cysteine residues. The catalytic mechanism of thioredoxin reductases and glutathione peroxidases involves the cyclic oxidation/reduction of catalytic cysteine and selenocysteine residues.

1.2. Selenoproteins

Selenium (Se) is an essential trace element whose deficiency in mammals interferes with normal embryonic development and fertility or may even favour the development of certain cancers (Beck and Levander, 1998). Evidence for a molecular link between selenium deficiency and biological disorders was provided by knock-out mouse studies. Targeted disruption of the mouse selenocysteine-specific *tRNA* gene, *Trsp*, leads to early embryonic lethality, confirming that selenoprotein synthesis is essential for mammals (Bosl et al., 1997). Further studies carried out with knock-out mice for individual selenoproteins underlined the long-discussed protective role of selenium in form of selenocysteine against free radicals and different pathologies (Bondareva et al., 2007; Brigelius-Flohe and Banning, 2006; Conrad et al., 2004; Crack et al., 2001; Hill et al., 2007; Jakupoglu et al., 2005; Rohrbach et al., 2006; Rundlof and Arner, 2004; Schneider et al., 2009; Schweizer et al., 2004; Seiler et al., 2008; Soerensen et al., 2008; Yamamoto et al., 1993; Yoshida et al., 1997). The amino acid selenocysteine (Sec) is the major biological form of selenium in bacteria and animals. It is normally found in the active site of selenoproteins and is directly involved in the catalytic reaction. In this regard, the capacity of the selenol group (-SeH) to become ionized at physiological pH is higher than that for the cysteine thiol group (-SH), which usually requires a higher pH. This fact has been considered to account for the higher rate of selenoenzyme catalysis (Stadtman, 1991). Few selenoprotein families have been characterized so far in mammals. Thioredoxin reductase and glutathione peroxidase families are crucially involved in the scavenging of ROS and maintaining the redox status of the cell. The iodothyronine deiodinases (DIOs) family consists of three Sec-containing oxidoreductases (DIO1, DIO2, DIO3) that catalyze the activation (DIO1 and DIO2) and inactivation (DIO3) of the thyroid hormones thyroxine (T4), triiodothyronine (T3) and reverse-triiodothyronine (rT3) by removing distinct iodine moieties. Mammals express various other selenoproteins whose functions are still widely unknown; likewise, knowledge on structural data is still very limited (SelH, Sell, SelO, SelT, SelV-function unknown; SelK, SelR, SelW-antioxidant enzymes; SelM, SelN, SelS-protein folding and SelP has a function of transport and storage of selenium). The reason for the lack of knowledge is either their very recent discovery or general technical difficulties in the analysis of selenoprotein function due to their relatively low abundance in cells and tissues.

1.2.1. Incorporation of selenium

Available evidence suggests that the principle of selenoprotein synthesis has been conserved during evolution (Atkins and Gesteland, 2000; Birringer et al., 2002; Driscoll and Copeland, 2003; Hirosawa-Takamori et al., 2004; Hirosawa-Takamori et al., 2000; Low and Berry, 1996). Sec is encoded by an in-frame UGA codon (opal codon), implying the existence of a machinery capable of distinguishing the UGA codon from a translational stop. Decoding UGA as Sec requires the presence of a Sec-specific tRNA, the Sec insertion sequence (SECIS) element and several protein factors acting in *trans* (Figure 1).

The Sec-specific tRNA is designated as tRNA^{[Ser]Sec}. In contrast to the other 20 amino acids, the 21st proteinogenic amino Sec is synthesised directly on the tRNA by incorporation of selenium into the amino acid serine. Seryl-tRNA synthetase attaches serine to tRNA^{[Ser]Sec} to yield seryl-tRNA^{[Ser]Sec}. The phosphoseryl-tRNA kinase phosphorylates this complex to give phosphoseryl-tRNA^{[Ser]Sec}. It is believed that the phosphate of phosphoseryl-tRNA^{[Ser]Sec} is replaced by the selenium donor selenide (H₂Se-P) which is activated by selenophosphate synthetase. The resulting selenocysteyl-tRNA^{[Ser]Sec} provides the Sec for the growing polypeptide chain (Xu et al., 2007).

One more essential factor for Sec incorporation is the SECIS element, a stem-loop-like secondary structure located in the 3'-untranslated region of selenoprotein mRNAs (Low and Berry, 1996). SECIS elements from different selenoproteins in general display low sequence similarities; however, their secondary structures are very similar and they contain consensus sequences that are necessary for Sec incorporation (Krol, 2002).

Besides these two elements, Sec-decoding requires the concerted action of several factors acting in *trans*. In mammals these are: the SECIS-binding protein 2 (SBP2) (Copeland and Driscoll, 1999; Copeland et al., 2000), the Sec-specific elongation factor (EFSec) (Fomenko and Gladyshev, 2003; Tujebajeva et al., 2000), ribosomal protein L30 (rpL30) (Chavatte et al., 2005), the 43-kDa RNA-binding protein (Secp43) and the soluble liver antigen protein (SLA) or Sec synthase (Figure 1) (Xu et al., 2005). Of these, SBP2 is the best characterised component of the UGA decoding machinery. SBP2 itself is a selenoprotein in organisms which do express selenoproteins. It is ubiquitously expressed in tissues and may be encoded by several transcripts (Copeland et al., 2000). SBP2 contains an RNA-binding domain (RBD), through which it binds to one of the consensus sequences within the SECIS elements (Fletcher et al., 2001; Walczak et al., 1998) and thereby interacts with the 28s ribosomal RNA (Copeland et al., 2001). Moreover, SBP2 contains a few other functional motifs: an

N-terminal nuclear localization signal (NLS) (Papp et al., 2006), a C-terminal NLS (de Jesus et al., 2006), two C-terminal nuclear export signals (NESs) (Papp et al., 2006), a functional domain dispensable for SECIS binding but required for Sec incorporation activity (Copeland et al., 2001), and a ribosomal interaction domain (Copeland et al., 2001; Kinzy et al., 2005). EFSec is the Sec-specific elongation factor that simultaneously interacts with Sec-tRNA^{[Ser]Sec} and SBP2 (Fagegaltier et al., 2000; Tujebajeva et al., 2000). The role of Sec-tRNA^{[Ser]Sec} has a stabilizing effect on the elongation factor in building the SBP2-EFSec complex (Zavacki et al., 2003), which might form in the nucleus as well as in the cytoplasm (Small-Howard et al., 2006).

Another trans-acting factor of the UGA translation machinery is the ribosomal protein L30. This element has an RNA-binding motif (Chen et al., 2003), which belongs to the same RBD type as the RBD of SPS2. Recent molecular and biochemical studies with rpL30 revealed that it binds specifically to the SECIS element, and thereby stimulates UGA codon read-through (Chavatte et al., 2005). It seems, however, that rpL30 and SBP2 do not bind to the SECIS element simultaneously. Rather, they mutually bind the SECIS element in a competitive manner and are able to displace each other from the SECIS element (Chavatte et al., 2005). RpL30 appears to bind preferentially to a conformationally altered SECIS element. A model has been proposed, in which rpL30-binding to the SECIS element leads to a conformational change, inducing SBP2 release and thus promoting the delivery of Sec-tRNA^{[Ser]Sec} to the ribosomal A site (Figure 1).

The roles for SECp43 and SLA in selenoprotein synthesis were recently characterized. Soluble liver antigen (SLA) was isolated by autoantibody precipitation (Gelpi et al., 1992) and the protein was found to be associated with a Sec-tRNA^{[Ser]Sec}. SECp43 was identified independently, based on its ability to specifically precipitate Sec-tRNA^{[Ser]Sec} from mammalian cell lysates. One of the identified SECp43 binding partners was a 48-kDa protein (Ding and Grabowski, 1999) now referred to as SLA (Xu et al., 2007; Xu et al., 2005). SECp43 has two ribonucleoprotein-binding domains (RNPs). Like SLA and Sec tRNA^{[Ser]Sec}, SECp43 form a complex in cell lysates, and depletion of either SECp43 or SLA decreases the binding of the remaining protein to the Sec-tRNA^{[Ser]Sec} (Xu et al., 2005). SECp43 normally resides in the nuclear compartment and is able to sequester SLA from the cytoplasm. Combined depletion of both proteins causes a global decrease in selenoprotein synthesis (Xu et al., 2005). Another study has shown that SECp43 plays an important role in the formation or stabilization of the EFSec–SBP2–Sec tRNA^{[Ser]Sec} complex (Small-Howard et al., 2006). All these studies suggest that SECp43 and SLA are involved in the mechanism of Sec biosynthesis and Sec incorporation.

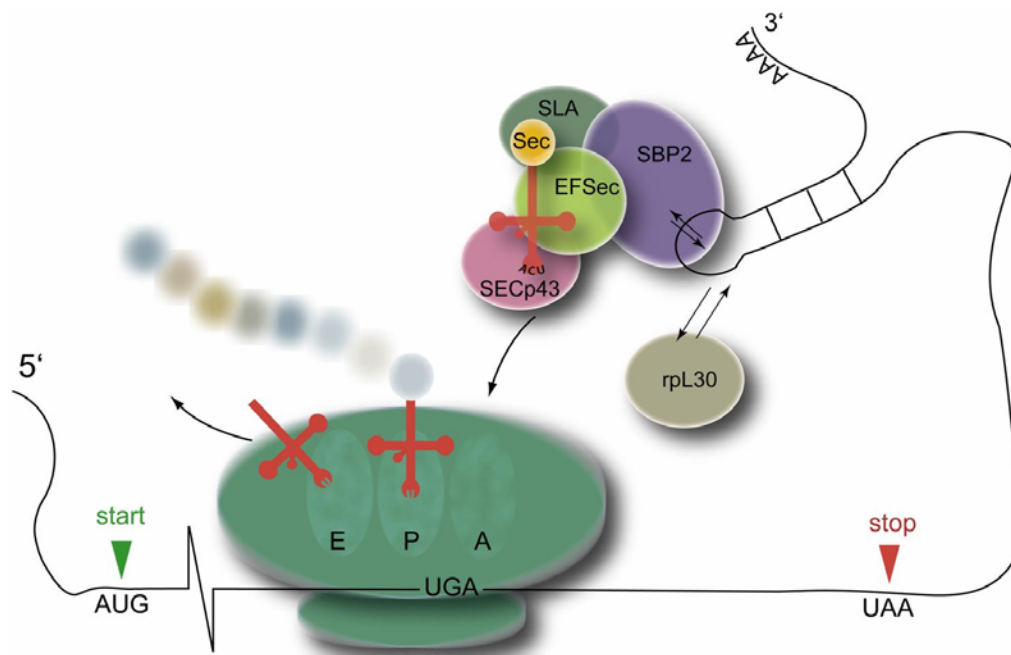


Figure 1. Mechanism of co-translational Sec incorporation. The tRNA (red), carrying Sec (yellow) is depicted in the complex required for co-translational Sec incorporation: EFsec (light green), SBP2 (blue), SLA (dark green), SECp43 (pink) and rpL30 (grey) and the SECIS element (black hairpin loop). Only when these factors are present and arranged in this manner, the opal codon (UGA) serves as a Sec codon, and Sec can be co-translationally incorporated into the nascent polypeptide chain. Translational start and stop codons of the mRNA are indicated by green and red arrows, respectively. The ribosome (large green) contains three RNA binding sites, designated as A, P, and E. The A site binds a tRNA bound to an amino acid; the P site binds a tRNA bound to the peptide being synthesized; and the E site binds a free tRNA before it exits the ribosome.

1.2.2. Family of thioredoxin reductases

The three members of the mammalian thioredoxin reductase family are homodimeric flavoproteins in which each monomer binds FAD as a prosthetic group. Each monomer has one NADPH binding site, an interface for dimerization, and two catalytic sites localised at the N- and C- termini (Holmgren, 1989).

Thioredoxin reductases differ fundamentally between lower and higher organisms. The enzyme in eukaryotic organisms is more closely related to glutathione reductase (GR) than to bacterial thioredoxin reductase, being larger, having broader substrate specificity and an additional redox-active motif, which, at least in mammals, contains Sec (Gladyshev et al., 1996; Papp et al., 2006).

The main substrates of thioredoxin reductases are oxidized thioredoxins (Trx) (Figure 2). There are two major thioredoxins in mammals, one primarily localised in the cytosol (Trx1) and one in mitochondria (Trx2). The expression of these relatively small (12 kDa), redox-active proteins is essential for embryonic development as knock-out for both Trx1 and

Trx2 is embryonic lethal at E6.5 and E10.5, respectively (Matsui et al., 1996; Nonn et al., 2003b). Thioredoxins are characterised by a conserved -Trp-Cys-Gly-Pro-Cys-Lys- catalytic site that undergoes reversible oxidation/reduction of the two Cys residues. The redox activity of this catalytic site is necessary for the biological activity of Trx (Freemerman et al., 1999; Gasdaska et al., 1994).

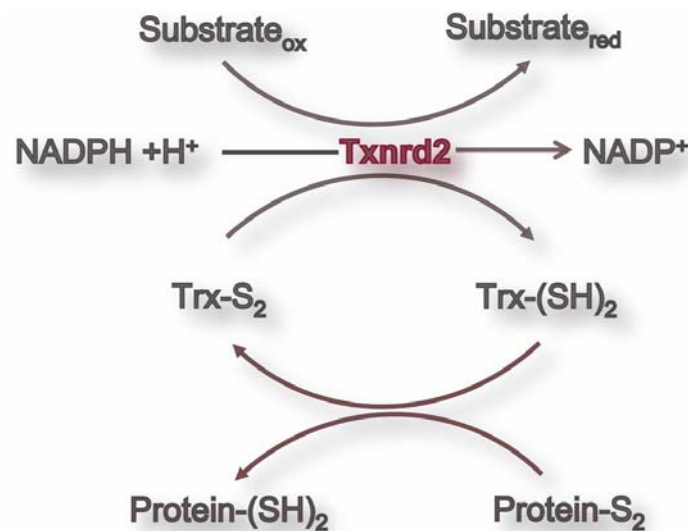


Figure 2. The thioredoxin/thioredoxin reductase system. The figure schematically depicts the reduction of the active site disulfide in oxidized thioredoxin (Trx-S₂) to a dithiol of reduced thioredoxin (Trx-(SH)₂) by mitochondrial thioredoxin reductase (Txnrd2) and NADPH. Trx-(SH)₂ reduces protein disulfides by its oxidoreductase activity, whereby it becomes oxidised (Trx-S₂). Mammalian thioredoxin reductases have various substrates other than thioredoxins (Arner and Holmgren, 2000).

The major functions of Trx are the supply of reducing equivalents to enzymes, including thioredoxin peroxidases (Chae et al., 1994; Rhee et al., 2005; Watabe et al., 1997). Moreover thioredoxin was initially described in *E.coli* as an essential co-factor for ribonucleotide reductase which converts NTPs into dNTPs (Laurent et al., 1964). Through thiol-disulphide exchange reactions, thioredoxins reduce key Cys residues in certain transcription factors, resulting in their increased binding to DNA and altered gene transcription (Nordberg and Arner, 2001). Mammalian Trxs have also been shown to function as cell growth factors and to inhibit apoptosis (Baker et al., 1997; Gasdaska et al., 1995a). Since thioredoxin reductases are the only class of enzymes known to reduce oxidized Trx, it is very likely that alterations in reductase activity may compromise Trx activities. Besides thioredoxins, a large number of small molecules have been shown to be substrates of Txnrds (Figure 2). These include lipoic acid (Arner et al., 1996), H₂O₂, lipid hydroperoxides (Bjornstedt et al., 1995), cytotoxic peptide NK-lysin (Andersson et al., 1996), vitamin K₃ (Holmgren, 1985), dehydroascorbic acid (May et al., 1998), the ascorbyl free radical (May et al., 1998) and many selenium-containing molecules, such as selenite, selenodiglutathione, methyseleninate, selenocystine, and ebselen (Bjornstedt et al., 1995; Gromer and Gross, 2002; Kumar et al., 1992; Park et al., 2004b; Persson-Moschos et al., 2000). However, the

physiological relevance in the reduction of most of these substrates by thioredoxin reductase is not known.

Three distinct mammalian thioredoxin reductases have been identified: cytosolic thioredoxin reductase (Txnrd1) (Tamura and Stadtman, 1996), mitochondrial thioredoxin reductase (Txnrd2) (Gasdaska et al., 1999b; Lee et al., 1999; Miranda-Vizuite et al., 1999; Watabe et al., 1999) and a testis-specific enzyme thioredoxin-glutathione reductase (Txnrd3/TGR) (Sun et al., 2001a; Sun et al., 1999). Mammalian thioredoxin reductases are encoded by three distinctive genes; yet, they share general domain organization (Figure 3).

Both Txnrd1 and Txnrd2 express various isoforms some of which are well characterised. An evolutionary conserved genetic mechanism contributes to the heterogeneity of Txnrds and suggests the existence of a greater variety of Txnrd species with different regulation and cellular functions (Rundlof and Arner, 2004; Rundlof et al., 2000; Rundlof et al., 2007; Su and Gladyshev, 2004; Sun et al., 2001b; Turanov et al., 2006). Both cytosolic and mitochondrial Txnrd are essential for murine embryogenesis. The genetic deletion of either gene was shown to cause embryonic lethality (Bondareva et al., 2007; Conrad et al., 2004; Jakupoglu et al., 2005).

1.2.3 Mammalian thioredoxin system

1.2.3.1. Cytosolic thioredoxin reductase (Txnrd1)

Txnrd1 is the most studied enzyme of the thioredoxin reductase family. Predominantly localised in cytosol, this enzyme has a wide range of functions in cells, including the regulation of cell proliferation and differentiation, modulation of the immune system, antioxidant defence, redox control of transcription factors, and in the development of cancer (Arner and Holmgren, 2006; Gromer et al., 2004).

Transcription of cytosolic thioredoxin reductase involves complex alternative splicing and transcription initiation leading to a large number of different isoforms that differ from each other at their N-termini (Rundlof et al., 2007; Su and Gladyshev, 2004; Sun et al., 2001b). A study by Sun QA and colleagues provided evidence for first alternative exon splicing, thus yielding various different forms of mouse and rat *Txnrd1* mRNA. Three alternative forms of *Txnrd1* mRNA were described from a single *Txnrd1* gene by transcription initiation at exons 1, 2, or 3 (Sun et al., 2001b). The next study identified six human TXNRD1 isoforms that were derived from a large number of transcripts and differed in their N-terminal sequences (Su and Gladyshev, 2004). Similarly, the study by Rundlof AK et al., provided evidence for a

core promoter region of *TXNRD1* in A549 and HeLa cells. This study identified several *TXNRD1* transcripts in the 5'-region using cDNA derived from different tissues. The results show that the core promoter governs transcription of the majority of *TXNRD1* transcripts but also shows that alternative promoters may be activated under rare conditions or in specific cell types. Furthermore, extensive alternative splicing occurred in the 5' region of *TXNRD1*. In total, 21 different transcripts were identified, potentially encoding five isoforms of *TXNRD1* carrying alternative N-terminal domains (Rundlof et al., 2007).

1.2.3.2. Txnrd3

The thioredoxin reductase isoenzyme TGR, encoded by the *Txnrd3* gene, is similar to the two other reductases, although *Txnrd3* appears to be evolutionary more distant than *Txnrd1* and *Txnrd2*. At the N-terminus it contains a monothiol Grx extension conferring both glutathione and glutaredoxin reductase activity (Sun et al., 2001a; Sun et al., 1999). The *Txnrd3* enzyme is mainly expressed in early spermatids, and is suggested to participate in redox reactions required during sperm maturation (Su et al., 2005; Sun et al., 2001a; Sun et al., 2005).

1.2.3.3. Mitochondrial thioredoxin reductase (Txnrd2)

1.2.3.3.1. The molecular structure and catalytic mechanism of Txnrd2

For the time being, four papers describing mouse, human, rat and bovine mitochondrial thioredoxin reductase, have been reported (Gasdaska et al., 1999a; Gasdaska et al., 1999b; Lee et al., 1999; Miranda-Vizueté et al., 1999; Watabe et al., 1999). When it was cloned, it was shown that *Txnrd2* has more than 50% sequence identity to both rat (Zhong et al., 1998) and human (Gasdaska et al., 1995b) *Txnrd1* (Lee et al., 1999). However, *Txnrd2* contains 36 additional amino acid residues at its N-terminus, which displays features typical of a mitochondrial leader sequences. Furthermore, rat *Txnrd2* shows 50% similarity to the human glutathione reductase (Lee et al., 1999; Watabe et al., 1999; Zhong et al., 2000)(Figure 3).

Several biochemical and computational studies have been performed to elucidate the catalytic mechanisms of *Txnrd2* and other family members. Structural analyses confirmed the “head-to-tail” arrangement with the redox-active C-terminal center of one subunit interacting with the active N-terminal site of the opposing subunit (Figure 3) (Sandalova et al., 2001; Zhong et al., 2000). More specifically, each *Txnrd2* subunit is comprised of three domains: an FAD-binding domain (residues 35–190 and 322–392), an NADPH-binding domain (residues 191–321) and an interface domain (residues 393–524) (Biterova et al., 2005; Sandalova et al., 2001).

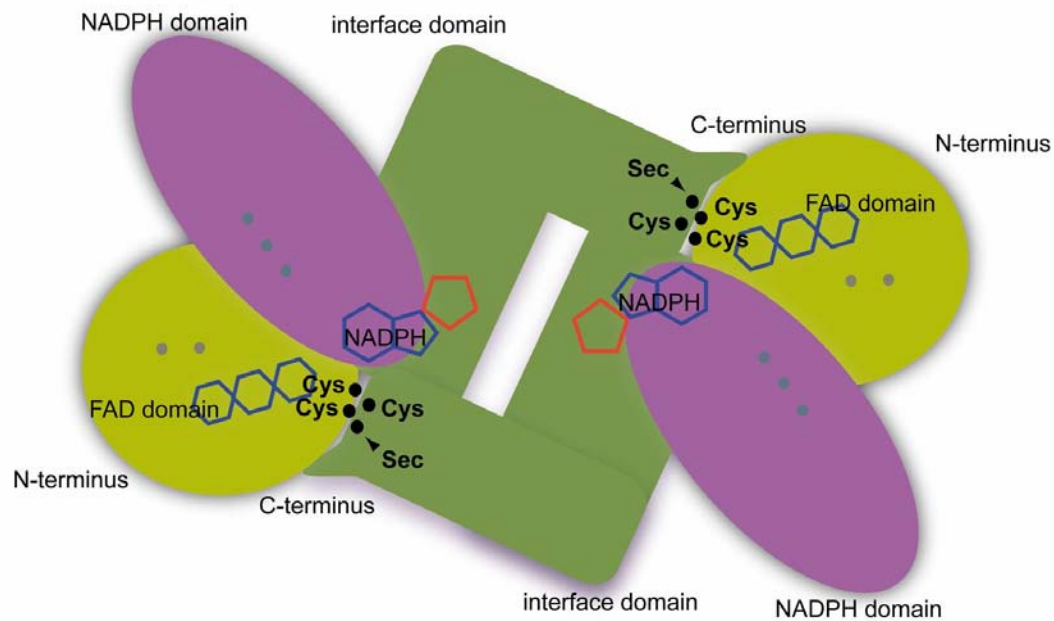


Figure 3. Model of mammalian Txnrd structure. The structure of mammalian Txnrd is based on the homology to GR. Model of Txnrd with FAD (light green), NADPH (purple) and interface domains (green) (adapted from (Zhong et al., 2000). Active-site cysteines and the Sec (filled circles) are indicated. FAD is represented only with isoalloxazine ring and NADPH with the adenosine structure.

Txnrd1 was the first thioredoxin reductase to be discovered; considering the high structural homology between Txnrds, the proposed basic mechanism by which Txnrd1 reduces its substrates is most likely the same for Txnrd2. Hence, electrons are first transferred from NADPH to FAD, which then leads to the reduction of the cysteines of the N-terminal conserved redox-active catalytic site -Cys-Val-Asn-Val-Gly-Cys- (Gasdaska et al., 1999b; Sandalova et al., 2001)(Figure 4). The electrons are further passed on to the highly flexible C-terminal catalytic site -Gly-Cys-Sec-Gly of the adjacent subunit (Gladyshev et al., 1996; Lee et al., 1999; Miranda-Vizueté et al., 1999; Sandalova et al., 2001; Tamura and Stadtman, 1996; Watabe et al., 1999; Williams et al., 2000; Zhong et al., 2000). The C-terminal catalytic site eventually reduces its substrates including oxidised thioredoxin. Once reduced, the enzyme catalyzes a selenenylsulfide exchange between the reduced C-terminus and oxidized thioredoxin (Arner and Holmgren, 2000; Bauer et al., 2003; Brandt and Wessjohann, 2005; Gilberger et al., 1997; Gromer et al., 1998; Sun et al., 2001a; Williams et al., 2000).

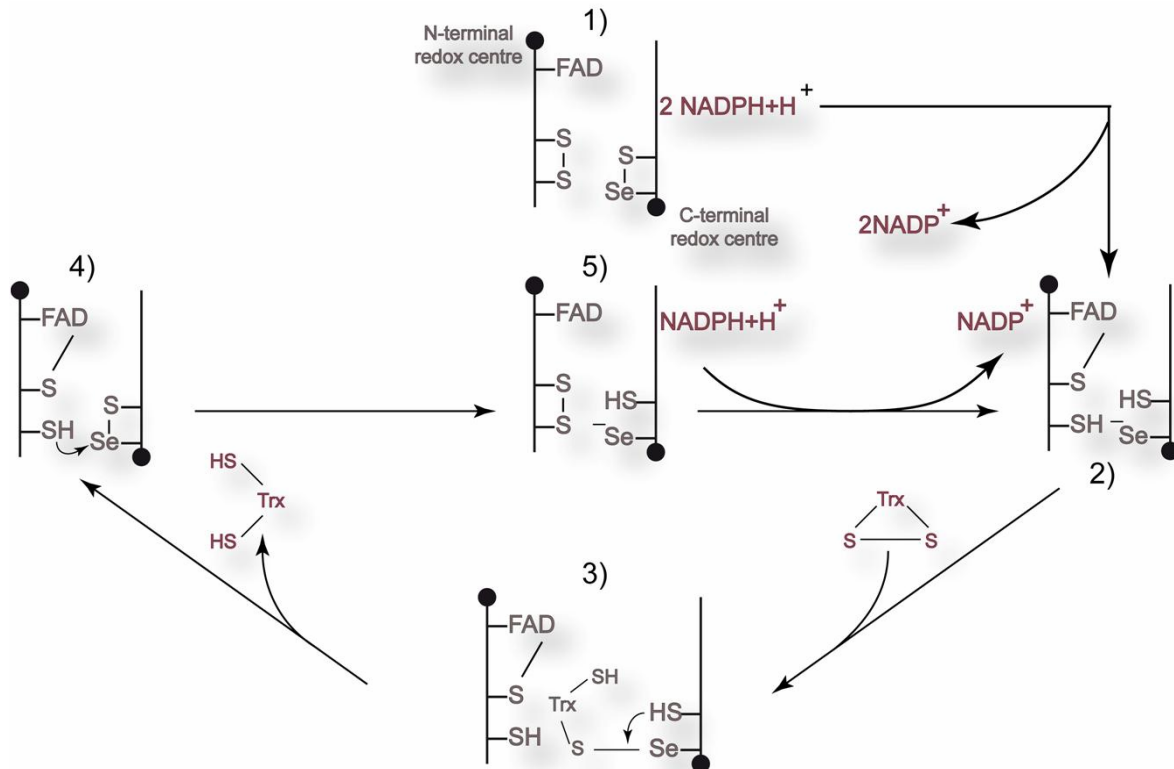


Figure 4. Postulated mechanism of Trx reduction. (1) The catalytic reaction starts by reduction of the selenenylsulfide to yield the selenolate (Se^-) anion. The selenenylsulfide receives electrons from NADPH via FAD and the N-terminal redox-active dithiol of the first subunit to generate 2) a sulfhydryl and a selenol ($-\text{SeH}$) or selenolate anion ($-\text{Se}^-$) at the C-terminus of the second subunit. The selenolate anion ($-\text{Se}^-$) performs a nucleophilic attack of the disulfide of Trx. The resulting enzyme-substrate mixed selenenylsulfide 3) is attacked by the neighbouring “releasing” Cys to release fully reduced Trx, thereby forming the selenenylsulfide. The latter 4) is then reduced by the N-terminal active-site thiolate from the other subunit. During the catalytic reaction cycle, the active-site dithiol maintains the selenol in the reduced state. The selenolate anion is both a better nucleophile and a better leaving group than the thiolate anion. Because of the low pKa of the selenol, the selenolate anion is considered to be the predominant form under physiological conditions (adopted from (Zhong et al., 2000))

The expression of multiple Txnrds isoforms was first described for Txnrd1 (Gladyshev et al., 1996; Sun et al., 2001a; Tamura and Stadtman, 1996). Later on, some splicing variants were also predicted for Txnrd2 (Lescure et al., 1999; Miranda-Vizuet and Spyrou, 2002; Sun et al., 2001a), and shortly after confirmed and further characterised (Turanov et al., 2006) (Figure 5).

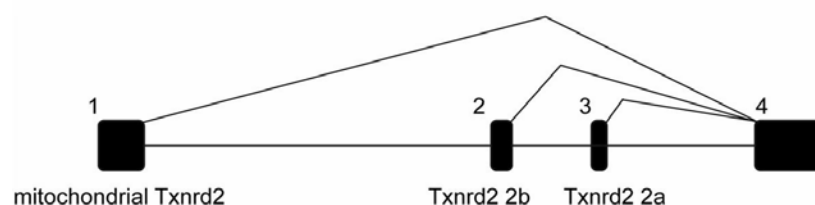


Figure 5. Structural organisation of the 5' region of the mouse, rat and human *Txnrd2* genes. Only the first four exons of a total of 18 exons are shown. Alternative transcription initiation determines which *Txnrd2* transcript is generated in cells. The three forms utilize alternative first exons 1–3, followed by the common exons 4 to 18. Exon 2a encodes only for three amino acids (in mice and rats), exon 2b encodes 12 amino acids (in mice and humans), while the classical exon 1 encodes 36 amino acids, including the mitochondrial leader sequence. (adapted from (Turanov et al., 2006)).

The three Txnrd2 isoforms are generated by alternative transcription initiation at the 5' region. Hence, the Txnrd2 variants differ in their N-termini (Turanov et al., 2006). The same genomic organisation and the same Txnrd2 variants were also detected in mouse, human and rat, suggesting a high conservation of alternative splicing among the different organisms. The predominant form of Txnrd2 contains a N-terminal signal peptide necessary for mitochondrial targeting (mitochondrial leader sequence, MLS) (Figure 5, mitochondrial Txnrd2) (Lee et al., 1999; Watabe et al., 1999; Zhong et al., 2000). The two other isoforms (Figure 5, cytoplasmatic Txnrd2 2b and 2a) have shorter N-terminal sequences and are localised in cytosol. Additionally, it was shown that the protein Txnrd2 2b resides neither in the endoplasmic reticulum nor in lysosomes (Turanov et al., 2006).

1.2.3.3.2. Cellular functions of Trx2 and Txnrd2

Eukaryotic mitochondria are equipped with a thioredoxin system, composed of mitochondrial thioredoxin (Trx2) and mitochondrial thioredoxin reductase (Txnrd2). Both enzymes are essential in mammals (Conrad et al., 2004; Nonn et al., 2003b); however the physiological functions of Trx2 and Txnrd2 are far less understood than that for the cytoplasmatic thioredoxin system, consisting of Txnrd1 and Trx1.

In fact, it has been proposed that the main function of the mitochondrial thioredoxin-dependent system is to act as the major antioxidant device, controlling the level of ROS in mitochondria. The antioxidant function of mitochondrial thioredoxin either relies on its direct scavenging properties (Tanaka et al., 2002) or by reducing the mitochondrial thioredoxin-dependent peroxidases (Araki et al., 1999; Pedrajas et al., 2000; Watabe et al., 1995; Watabe et al., 1997). Nalvarte et al. showed *ex vivo*, that cytochrome c is reduced by Txnrd2 (Nalvarte et al., 2004b). Thus it was proposed that *in vivo* Trx2 may recruit cytochrome c to keep it in closer proximity to Txnrd2, which would allow electrons to bypass complex III during cytochrome c reduction. This hypothesis might be valuable in understanding the pathophysiology of diseases induced by dysfunctional mitochondrial respiration, such as cardiomyopathies and encephalomyopathies (Keightley et al., 2000; Lerman-Sagie et al., 2001). Moreover, Txnrd2 may also be involved in the redox regulation of the mitochondrial estrogen receptor (Nalvarte et al., 2004b).

Furthermore, using a Tet-off expression system for an alternative splicing variant of TXNRD2 it was found that this form impaired Txnrd2 activity altered cellular ROS levels and increased apoptosis (Chang et al., 2005). By using a very similar system, when cells were expressing a dominant-negative form of TXNRD2 (DNTXNRD2) were stimulated with epidermal growth factor (EGF), they were found to produce more H₂O₂ than normal cells (Kim et al., 2003b).

Overexpression of dominant-negative Txnrd2 was shown to perturb proper electron flow from NADPH via Trx2 to Prx III, thus impinging on cellular redox imbalance. Stimulation of these cells with EGF then alters the cellular redox status and affects signalling pathways mediated through tyrosine phosphorylation of ERKs (extracellular signal-regulated kinases). Furthermore, another laboratory reported that overexpressing either Trx2 or Txnrd2 reduces p42/p44 MAPK signalling (Zhou et al., 2008). Collectively, these results indicate that the forced expression of Trx2 and Txnrd2 decreases intracellular ROS, leading to reduced cell growth. Contrary, the overexpression of DNTXNRD2 accelerates transition of the cells from G1 to S phase and expression of some cyclins (A, B, D₃), CDKs (2, 4), and p27 (Kim et al., 2003b).

1.2.3.3.3. Knock-out mouse model for *Txnrd2*

Mice with spatiotemporal inactivation of Txnrd2 were established in our laboratory (Conrad et al., 2004). To this end, the last four exons of *Txnrd2* gene were flanked by loxP sites. Cre-mediated deletion leads to removal of the C-terminal catalytic site including the Sec codon, which is encoded by exon 17, the SECIS element and the polyA termination signal, both encoded by the last exon (Figure 6). In the same work, it was shown that ubiquitous deletions of both Txnrd2 alleles leads to embryonic lethality around E13.5 most likely due to severe defects in foetal haematopoiesis and improper heart development. More specifically, *Txnrd2*^{-/-} embryos displayed an increased number of apoptotic cells in the foetal haematopoietic compartment and an impaired proliferative capacity of isolated haematopoietic stem cells isolated from foetal liver. Moreover, heart-specific *Txnrd2* knock-out animals died just after birth. The knock-out mice showed thinning of the ventricular walls, and a perturbation in the heart muscle architecture. On the cellular level, cardiomyocytes showed swelling of mitochondria along with a destruction of mitochondrial cristae of cardiomyocytes. All these phenotypes are hallmarks of dilated cardiomyopathy (DCM). This suggests that Txnrd2 plays a pivotal role in both foetal haematopoiesis and cardiac development and function. To bypass postnatal lethality of heart-specific *Txnrd2*^{-/-} mice, mice with Tamoxifen (Tam) inducible, cardiac tissue-restricted disruption of Txnrd2 (Figure 6) were generated (Kiermayer et al., 2007). Interestingly, inducible adult heart-specific *Txnrd2* null mice are fully viable, and cardiac tissue did not display any signs of severe histopathological abnormalities in induced knock-out mice, at least in young animals. Additionally, a conditional Txnrd2 knock-out mouse (Figure 6) lacking Txnrd2 expression in CD4⁺- and CD19-positive T- and B-lymphocytes were generated using CD4⁺- and CD19- Cre transgenic mice, respectively. However, the development and differentiation of both cell types in thymus and bone marrow was not impaired. In addition, B-cell proliferation and activation in response to CD40 and IL-4 was unaltered in *Txnrd2*-deficient B-cells

(Geisberger et al., 2007). These findings, however, do not rule out that *Txnrd2* inactivation in the myeloid compartment may provoke yet-unrecognized abnormalities in adult myelopoiesis.

In order to examine whether proliferation and/or cell death are affected in *Txnrd2*^{-/-} cells, primary mouse embryonic fibroblasts (MEFs) were established from E12.5 embryos and used as a cellular model system (Conrad et al., 2004). Although MEF cultures could be established from *Txnrd2*^{-/-} embryos, proliferation and survival of *ex vivo* cultured mouse embryonic fibroblasts (MEFs) is clearly compromised. The difference between wild-type and knock-out embryonic fibroblasts is even more pronounced when the *de-novo* synthesis of GSH is inhibited by BSO. GSH depletion rapidly induces apoptosis in *Txnrd2*^{-/-} cells, but not in wild-type cells. Treatment of cells with the antioxidant NAC rescued *Txnrd2*^{-/-} MEFs from BSO-induced cell death (Conrad et al., 2004). Taken together, these results suggest that *Txnrd2* is involved in the defence against oxidative stress *in vitro* and *in vivo*, although it remains to be formally demonstrated.

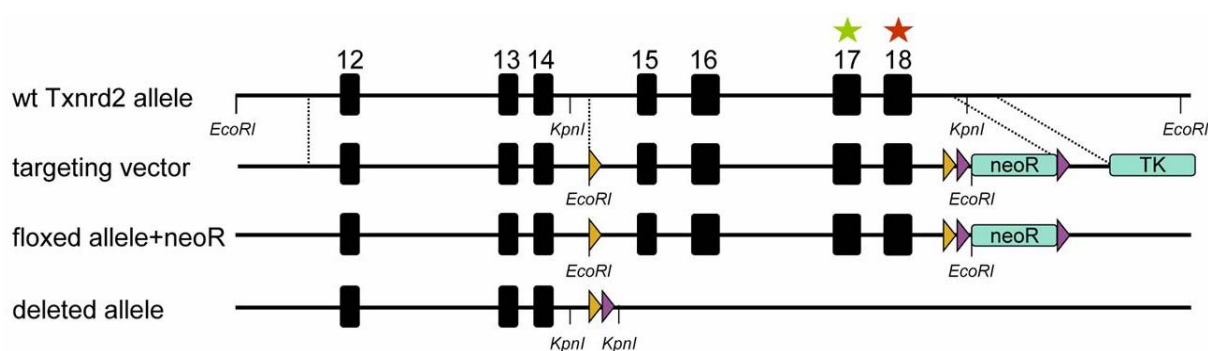


Figure 6. The conditional knock-out strategy for *Txnrd2*. The 3' region of *Txnrd2* gene is shown in the upper line. For conditional gene targeting, exons 15 to 18 were flanked by loxP sites (yellow triangles). Neomycin phosphotransferase gene (*neoR*) removal was achieved by Flp recombinase (violet triangles). Deletion of the C-terminally located redox-center is mediated by Cre. The Sec codon (red asterisk) encoded by exon 17 and the SECIS element (green asterisk) located on exon 18 are both deleted in these mice. For gene targeting the thymidine kinase gene (*TK*) was placed downstream from the 3' arm for negative selection (adopted from Conrad et al., 2004).

1.3. Peroxiredoxins

Mammals express 6 peroxiredoxins, which can be subdivided according to structural similarities or catalytic mechanism in the reduction of their substrates (Wood et al., 2003). The localisation of peroxiredoxins in different compartments, including the extracellular space (Haridas et al., 1998; Okado-Matsumoto et al., 2000), suggests that it is important that these enzymes are present at compartments where H₂O₂ is generated, as H₂O₂ is essentially involved in cell signalling and even able to cross membranes.

Previously, peroxiredoxins were named thioredoxin peroxidases (TPx), since Trx and Txnrd were initially considered to be the sole reducing systems for peroxiredoxins. But later on it was shown that mammalian cells express peroxiredoxins with only one conserved peroxidatic cysteine, capable of reducing peroxides in the presence of DTT (dithiothreitol) but not in the presence of Trx. For this reason thioredoxin peroxidases (TPx) were then redefined and named peroxiredoxins (Prx). All peroxiredoxins act as “head-to-tail” dimers, in which the larger N-terminal domain of one subunit folds over the smaller C-terminal domain of the other subunit to form an active site (Choi et al., 1998; Hirotsu et al., 1999).

Prxs I–IV belong to the category of 2-Cys Prxs and they share high sequence homology (60-80%). Prx VI is a member of the 1-Cys group. Peroxiredoxin V, for now, is the only representative of an atypical 2-Cys protein (Seo et al., 2000). Also, Prx I-IV belong to the thioredoxin peroxidase subfamily (TPx) and require thioredoxin (Trx) as an electron source, while Prx V and VI can use other cellular reducing agents, such as GSH or DTT (Fisher et al., 1999; Seo et al., 2000). Prx I, Prx II, and Prx VI are localised in the cytoplasm and in the nucleus (Kinnula et al., 2002; Mizusawa et al., 2000; Oberley et al., 2001). Other than these, Prx VI displays other cellular localisations including lysosomes and cytoplasmic vesicles. Prx IV has an N-terminal secretion signal sequence and is found in the endoplasmic reticulum as well as in the extracellular space (Okado-Matsumoto et al., 2000). Prx III and V are both expressed in the mitochondrion, although Prx V is additionally detected as a short form in peroxisomes (Seo et al., 2000) and in nuclei (Kinnula et al., 2002). Prx III and Prx V use the mitochondrial thioredoxin system (Trx2 and Txnrd2) as the main electron source for its peroxidase activity (Watabe et al., 1995; Watabe et al., 1997), but they may also use electrons from DTT *in vitro*. The specific localization of Prx III in mitochondria, along with the mitochondria-specific reducing system Trx2 and Txnrd2, suggests that these three proteins possibly together with Prx V provide a primary line of defence against H₂O₂ produced by the mitochondrial respiratory chain. The precise *in vivo* roles of Prx III and Prx V and their contribution to the maintenance of normal mitochondrial and cellular function are, however, still sparsely investigated. Specific inactivation of both Prxs has been reported to increase their sensitivity to apoptosis (Araki et al., 1999; Chang et al., 2004b; Watabe et al., 1995; Watabe et al., 1997; Zhou et al., 2000). Lowering Prx III expression increases the sensitivity of cells to TNF α - or staurosporine-induced apoptosis (Chang et al., 2004b). Studies with Prx III knock-out mice revealed that Prx III is not required for embryonic development; rather the knock-out mice were more sensitive to LPS-induced severe lung injury due to augmented levels of intracellular ROS. Thus, it has been proposed that Prx III acts as an important ROS scavenger, particularly under stress-inducing conditions (Li et al., 2007). Mice

overexpressing Prx III were shown to have decreased left ventricular remodelling and cardiac failure in response to myocardial infarction due to reduced mitochondrial oxidative stress (Matsushima et al., 2006; Tsutsui et al., 2009). Furthermore, overexpression of Prx III in thymoma cells was shown to dampen cellular H_2O_2 levels, leading to decreased growth rates and increased resistance to apoptosis induced either by high H_2O_2 , hypoxia, *t*-butylhydroperoxide and the anticancer drug imexon (Nonn et al., 2003a). Overexpression of Prx III has been reported to protect rat hippocampal neurons from excitotoxic injury (Hattori et al., 2005b). Up-regulation of Prx VI and Prx III within skeletal muscles of neuronal nitric oxide synthase (nNOS) knock-out mice functionally compensates for the absence of nNOS in superoxide scavenging (Da Silva-Azevedo et al., 2009). Increased expression of Prx V in Chinese hamster ovary cells was found to decrease mtDNA damages caused by exogenously added hydrogen peroxide (Banmeyer et al., 2005). Furthermore, Prx I and Prx II are prime candidates to regulate H_2O_2 signalling of cell-surface receptors after activation with platelet-derived growth factor (PDGF) or tumor necrosis factor (TNF) (Choi et al., 2005; Egler et al., 2005; Jin et al., 1997; Kang et al., 1998b; Kang et al., 2004; Kim et al., 2008; Kwon et al., 2004; Veal et al., 2004; Zhang et al., 1997; Zhao et al., 2009).

Furthermore, Prx expression is increased in several human cancers. Prx I levels are increased relative to normal tissue in oral cancer (Yanagawa et al., 2000), in follicular (Yanagawa et al., 2000), in breast cancer (Noh et al., 2001), and in lung cancer (Kim et al., 2003a). Noh DY et al. have shown that Prx II and III are increased in breast cancer (Noh et al., 2001), while increased expression of all peroxiredoxins has been observed in mesothelioma (Kinnula et al., 2002).

1.3.1. The catalytic mechanisms of peroxiredoxins

The catalytic mechanisms by which 2-Cys and 1-Cys Prx enzymes remove peroxides diverge (Kang et al., 1998a). In case of 2-Cys Prx (Figure 7), the N-terminal thiol group (Cys-SH) is oxidized by peroxides to sulfenic acid (Cys-SOH), which immediately reacts with the C-terminal Cys-SH of the other subunit to form an intermolecular disulfide. This disulfide is subsequently reduced by Trx and Txnrd (Seo et al., 2000). Kang et al showed that mutant 2-Cys Prx proteins that lack either the N-terminal or C-terminal Cys residues do not exhibit Trx-dependent peroxidase activity (Kang et al., 1998a).

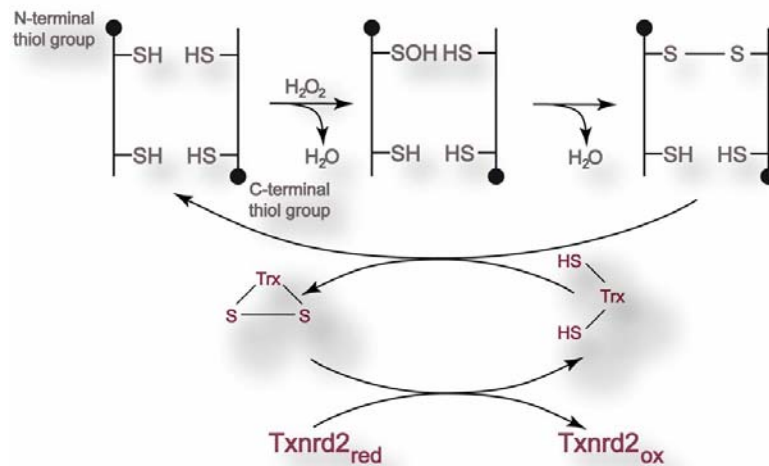


Figure 7. The catalytic mechanism by which 2-Cys peroxiredoxins reduce peroxides. In case of 2-Cys Prx, the N-terminal Cys thiol group (Cys-SH) is oxidized by peroxides to sulfenic acid (Cys-SOH), which immediately reacts with the C-terminal Cys-SH of the other subunit to form an intermolecular disulfide. This disulfide is subsequently reduced by Trx and Txnrd (adapted from (Seo et al., 2000)).

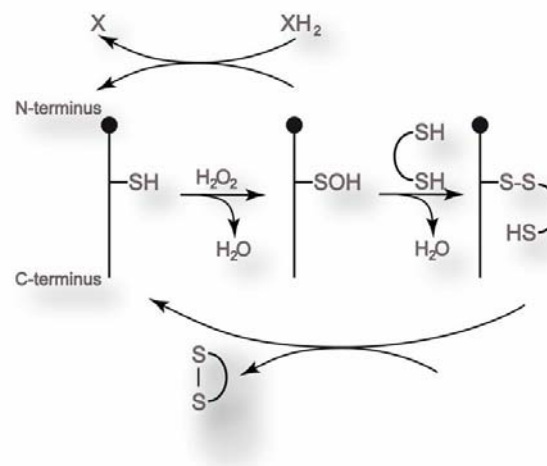


Figure 8. 1-Cys Prx catalytic mechanism. The N-terminal Cys-SH of 1-Cys Prx is oxidised by peroxides. The resulting Cys-SOH does not form a disulfide because of the unavailability of another nearby Cys-SH. The Cys-SOH of oxidized 1-Cys Prx can be reduced by non-physiological thiols such as DTT and GSH but not by Trx.

The N-terminal Cys-SH of 1-Cys Prx is also the site of oxidation by peroxides. However, the resulting Cys-SOH does not form a disulfide because of the unavailability of another nearby Cys-SH (Figure 8). The electron donor used to reduce the sulfenic acid of 1-Cys peroxiredoxins might be GSH (Fisher et al., 1999); however in *in vitro* experiments it was shown that DTT is able to effectively reduce the active site Cys (Kwon et al., 2004; Rhee et al., 2005; Rhee et al., 2001).

Prx V is an atypical 2-Cys peroxidase. Mutant analyses of human Prx V revealed that the N-terminal cysteine (Cys48) and the C-terminal cysteine (Cys152) are essential for Trx-dependent activity and that the oxidized intermediate is a monomer containing the

Cys48–Cys152 disulfide (as shown in Figure 9). The C48S mutant of Prx V is inactive, regardless of whether the reducing equivalents are provided by DTT, or by Trx, whereas the C152S mutant is active in the presence of DTT, but not in the presence of the Trx system. These results suggest that Cys48 is the catalytically active peroxidatic cysteine and that this is directly oxidized by H_2O_2 to yield H_2O and Cys48-SOH; Cys48-SOH then reacts with Cys152-SH to form an intramolecular disulfide, which is subsequently reduced by Trx. In this model, Cys48-SOH would react with one thiol of DTT to form a mixed disulfide in the absence of Cys152, whereas the second thiol of DTT would attack the disulfide to produce Cys48-SH and oxidized DTT (Figure 9) (Seo et al., 2000).

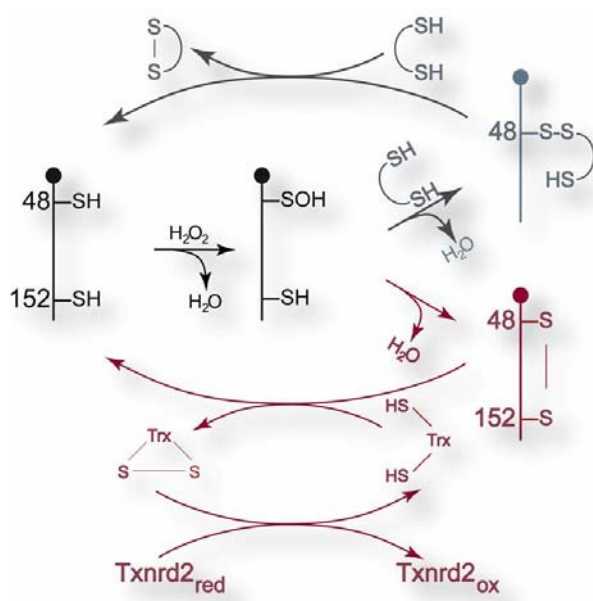
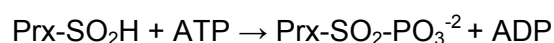


Figure 9. The catalytic mechanism of 2-Cys atypical Prx. Analysis of Prx V revealed that both Cys48 and Cys152 are essential for Trx-dependent activity. Cys48 is the site of peroxide oxidation by H_2O_2 resulting in Cys48-SOH; this reacts with Cys152-SH to form an intramolecular disulfide, which is subsequently reduced by Trx. Cys48-SOH would react with one thiol of DTT to form a mixed disulfide in the absence of Cys152, whereas the second thiol of DTT would attack the disulfide to produce Cys48-SH and oxidized DTT (adapted from(Seo et al., 2000)

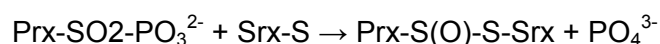
1.3.2. The role of sulfiredoxin (Srx)

The disulfide-forming cysteine residues of 2-Cys Prx enzymes are positioned far apart (Schroder et al., 2000), which significantly slows down the process of disulfide formation (Figure 7). Under strongly oxidizing conditions, the sulfenic acid intermediate (Cys-SOH) can be further oxidized to sulfinic acid (Cys-SO₂H), which cannot be directly reduced to the ground state. Neither Trx nor other cellular reductants, such as GSH, are able to reduce the sulfinic acid moiety of Prx. Therefore, the overoxidation was thought to result in permanent inactivation of Prx peroxidase activity (Chae et al., 1994; Rabilloud et al., 2002; Yang et al., 2002). Additionally, it was shown that H_2O_2 causes hyperoxidation of Prx I in different cells

which was gradually reduced to the catalytically active thiol form (Woo et al., 2003a; Woo et al., 2003b). This implied that in cells there must be a system demonstrated the ability of mammalian cells to reduce protein sulfinic acid. Subsequently, Toledano's laboratory identified sulfiredoxin (Srx) in yeast capable of reducing sulfinylated Prx and thus returning it into its fully reduced ground state (Biteau et al., 2003). Srx was initially identified as its expression is rapidly induced by high H_2O_2 concentrations. These studies further showed that Prx reduction requires a conserved cysteine residue in Srx, ATP or GTP hydrolysis, Mg^{2+} and a thiol group as an electron donor (Trx or DTT) (Biteau et al., 2003). The reductase activity of rat Srx was shown to be equally efficient with GSH or Trx as electron source (Chang et al., 2004c). Reduction of sulfinic acid by mammalian Srx is specific to 2-Cys Prx isoforms (Woo et al., 2005). Thus, the cycle of thiol to sulfinic acid might represent a redox switch by which the function of a wide variety of proteins is regulated in response to a strongly changing intracellular redox status. It was also shown that the conserved cysteine of Srx from various species is essential for enzyme activity. The catalytically active cysteine is thought to serve as the phosphate carrier in the reducing reaction (Roussel et al., 2008):



or as the removing site for phosphate in the thiol-transferase reaction:



Even when cells are exposed to high H_2O_2 concentrations Srx is not inactivated. Srx is able to keep peroxiredoxins in their reduced states, because Srx turnover by ATP is highly efficient, similar to the reduction of Trx by Txnrd2 (Chang et al., 2004c). It has been speculated that the slow rate of Prx reactivation via Srx-dependent reduction has been evolved to regulate the basal levels H_2O_2 so that it can confer its intracellular second messenger-like function (Bondareva et al., 2007; Chang et al., 2004c; Woo et al., 2003a; Woo et al., 2003b). Rapid reactivation of the inactivated Prx enzymes would reduce the time window needed for H_2O_2 accumulation and thus propagating the signal. Although sulfiredoxin is mainly localised in the cytoplasm, it was shown that *in vitro* Srx reduces not only sulfinic acids of cytosolic Prxs (I and II) but also sulfinic acid of mitochondrial Prx III (Noh et al., 2009; Woo et al., 2005). In response to oxidative stress, sulfiredoxin was shown to translocate from the cytosol to mitochondria. Moreover, overexpression of mitochondrion-targeted Srx promotes the regeneration of overoxidised Prx III and results in cellular resistance to apoptosis, accompanied by enhanced elimination of mitochondrial H_2O_2 and decreased rates of mitochondrial membrane breakdown. Therefore, Srx appear to play a

crucial role in maintaining the balance between mitochondrial H_2O_2 production and elimination (Noh et al., 2009).

1.4. System x_C^-

Cysteine is an essential amino acid and as such is indispensable for normal cell proliferation, including cultured cells. Moreover, cysteine (Cys) is unstable in the extracellular environment and becomes readily oxidised to yield cystine, $(\text{Cys})_2$ (Toohey, 1975).

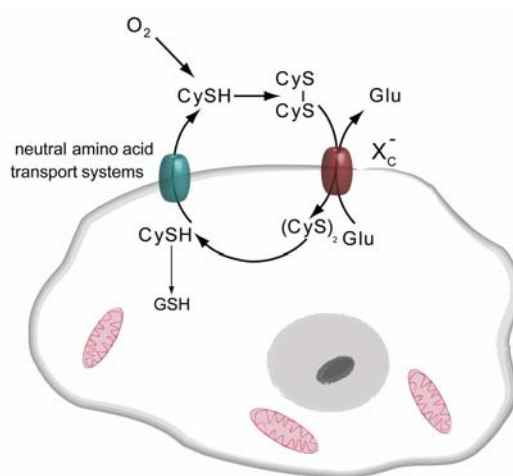


Figure 10. The Cys/ $(\text{Cys})_2$ circuit. Cysteine (CySH) is unstable in the extracellular environment and is readily oxidised to cystine $(\text{Cys})_2$. Cysteine transport is mediated by the neutral amino acid transport system ASC, while the transport of cystine is mediated by system x_C^- . System x_C^- is an antiporter for cystine and glutamate. Cystine, taken up via system x_C^- , is rapidly reduced to cysteine in the intracellular reducing environment, which is then used for protein synthesis or GSH biosynthesis. The driving force of this circuit that actually reduces cystine to cysteine is considered to be GSH, by forming mixed disulfides; yet experimental proof is still lacking.

Cysteine transport is mediated by the neutral amino acid transport system ASC, whereas the transport of cystine, the predominant form of cysteine in the extracellular space and body fluids, is accomplished by system x_C^- (Bannai and Kasuga, 1985; Sato et al., 2000). System x_C^- is a member of the glycoprotein-associated amino acid transporters (gpAATs) (Shih and Murphy, 2001). gpAAT functions as heterodimeric transmembrane proteins consisting of a highly glycosylated heavy chain (4F2hc/CD98) that is common to all gpAATs, and a light chain. The light chain component of system x_C^- is xCT which confers high substrate specificity for cystine (Bannai, 1986; Bannai and Ishii, 1982; Sato et al., 2000). System x_C^- carries one mole of cystine and at the same time releases one mole of glutamate. Upon uptake, cystine is rapidly reduced to cysteine inside cells, which is subsequently used for the synthesis of GSH or proteins (Bannai and Ishii, 1982). Since intracellular cysteine concentrations are the substrate-limiting step in GSH biosynthesis, the intracellular GSH level is considered to be coupled to systems x_C^- activity, at least in cell culture.

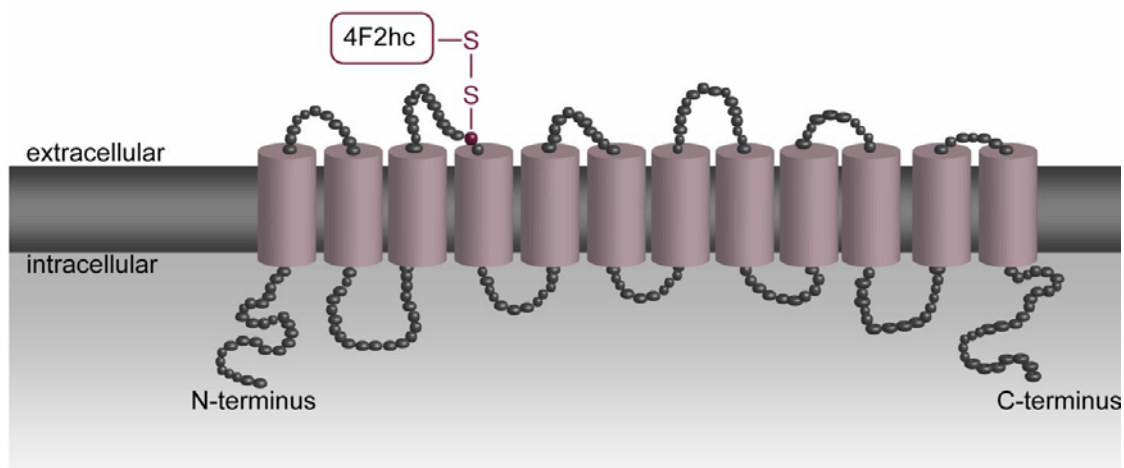


Figure 11. Schematic representation of system x_C^- . xCT light chain of system x_C^- is embedded in the plasma membrane via 12 transmembrane domains. The N- and C-termini reside in the cytosol. Cys 158 is involved in the formation of a disulfide bridge with heavy chain (4F2hc/CD98). Proper folding of xCT requires the presence of the heavy subunit (Gasol et al., 2004).

The driving force for intracellular reduction of cystine to cysteine is thought to be GSH by forming mixed disulfides, thus releasing cysteine. Since system x_C^- provides Cys for intracellular GSH levels, it is classified to the category of the stress proteins that are required for the metabolic response to oxidative stress (Sasaki et al., 2002). In fact, the activity of system x_C^- is strongly induced by electrophilic agents (Bannai, 1984; Bannai et al., 1991), LPS (Sato et al., 1991), oxygen (Sato et al., 2000) and even HIV infection (Bridges et al., 2004). Moreover, the expression of xCT is partly up-regulated by an electrophile response element (EpER), which is recognized by the oxidative stress-activated transcription factor NF-E2-related factor 2 (Nrf2). The electrophile response element (EpRE) is a gene regulatory sequence which is present in the promoter region of a variety of genes that are involved in the defence against xenobiotics (Sasaki et al., 2002). In the brain, system x_C^- is predominantly expressed in regions that are in contact with the cerebrospinal fluid, indicating that relatively high levels of ROS in these regions are counteracted by augmented cysteine supply (Burdo et al., 2006; Sato et al., 2002).

In addition, xCT has also been studied in the context of high glutamate levels in the brain (Massie et al., 2008). The latest hypothesis is that neuronal injury might be caused by high extracellular glutamate levels ultimately leading to cell damage. It has also been shown that cystine/glutamate antiporter contributes to the pathogenesis of Parkinson's disease (Massie et al., 2008). The striatal xCT protein expression level was investigated in a hemi-Parkinson rat model, using comparative western blotting. Time-dependent changes were observed after a unilateral 6-hydroxydopamine lesion of the nigrostriatal pathway with increased expression levels in the deafferented striatum. These data suggest for the first time an involvement of

the cystine/glutamate antiporter in determining the aberrant glutamate neurotransmission in the striatum of a parkinsonian brain (Massie et al., 2008).

On the other hand, high xCT expression levels have been shown to negatively correlate with the potency of the anti-tumor drug cisplatin, as shown in cisplatin-resistant human ovarian cancer cell line (Okuno et al., 2003). Accordingly, the inhibition of system x_C^- abolished the growth of primary brain tumours (Chung et al., 2005; Savaskan et al., 2008). Enforced expression of xCT protects Burkitt's lymphoma cells from cell death induced by oxidative stress and GSH depletion (Banjac et al., 2008). The studies by Banjac et al. provided strong evidence that the cystine/cysteine redox couple represents an efficient redox system, which may also act independently from intracellular GSH (Banjac et al., 2008).

It is noteworthy, that mice lacking xCT are born at the Mendelian ratio and are healthy in appearance (Sato et al., 2005). Most interestingly, xCT-deficient MEFs rapidly die in normal cell culture, if not supplemented with thiol-containing compounds, such as GSH or NAC (Qiao et al., 2008; Sato et al., 2005). This is a perfect example that one has to be extremely careful when conclusions are drawn from *in vitro* experiments, particularly when dealing with oxidative stress and redox signalling - very often *in vitro* results do not really reflect the *in vivo* situation, which calls for more specific transgenic mouse models for redox enzymes.

1.5. Objectives

The importance of the overall cellular redox balance on many cell processes has been recognized in recent years. However, the redox control of distinct cellular pathways is still poorly understood and still at its infancy. This is also supported by the fact, that interacting partners, as well as substrates of redox enzymes, are widely unknown.

To date, in *ex vivo* studies investigating the role of peroxiredoxins (Prx) in cellular redox system, the focus was placed on the biochemical characterisation of reactions which included Trx2 and Txnrd2. It was found that Trx2 is needed for maintenance of Prx in the active state. Also, from these experiments it is known that this reaction was possible only in the presence of Txnrd2. Given that a confirmation of these results *in vivo* is lacking, one of our research aims was to demonstrate that the mechanisms proposed are also operable in the cells.

Furthermore, in order to dissect the contribution of the thioredoxin 2 dependent system on the redox balance and effect on the overall physiology and pathophysiology of tissues and

organs, a mice with targeted deficiencies in mitochondrial thioredoxin reductase (Txnrd2) were created (Conrad et al., 2004). Ubiquitous inactivation of Txnrd2 revealed that mitochondrial thioredoxin reductase is essential for embryonic development, increased apoptosis of haematopoietic cells and perturbed cardiac development. Additionally, heart-specific Txnrd2 ablation shows perturbed myocyte organisation and leads to fatal cardiac insufficiency (Conrad et al., 2004). Hence, unbalanced levels of ROS due to Txnrd2 absence are probably a cause for the failing myocardium and lethality among ubiquitous and heart-specific Txnrd2 knock-out mice. The use of cells isolated from the embryos lacking Txnrd2 (MEFs and eEPCs) would therefore help us reveal the mechanisms behind cell and tissue pathological modifications caused by absence of Txnrd2. The next aim of the present study was to clone the tagged mitochondrial and cytoplasmatic isoforms of Txnrd2 and to confirm their function *in vivo*, by using the cells which lack respective enzymes. Furthermore, we have used the constructs to investigate more in detail cellular localisation of Txnrd2 isoforms, since the data on their subcellular arrangement is sparse. Moreover, it was interesting to see whether there is *in vitro* functional overlap between Txnrd1 and Txnrd2. In order to elucidate biological implications of mutation in mitochondrial Txnrd2 found in DCM patients, we have designed two different mutants and performed a functional analysis in transfected cells, as well as the repercussions of introduced changes on the protein localisation.

Over recent decades genetically manipulated mouse models have proven themselves as valuable tools to study human disease and as models to study disease mechanisms. Cystine/glutamate transporter, designated as system x_c^- , mediates cystine entry in exchange for intracellular glutamate in mammalian cells. Overexpression of xCT plays a role in maintaining the GSH intracellular levels (Bannai, 1986). As shown by Banjac et al, overexpression of xCT *in vitro* in Burkitt lymphoma cells protects them from BSO-induced cell death (Banjac et al., 2008). Moreover, it is suggested that Cys/(Cys)₂ biochemical system functions independently and could be induced by oxidative stress, mediated by electrophilic agents and by oxygen (Bannai et al., 1989; Hattori et al., 2005a) surmounting the effects of oxidative stress. In this work our aim was to extend the study of Banjac et al and to clarify the physiological roles of xCT transporter *in vivo*. Thus, we successfully generated mice overexpressing xCT. For that purpose Rosa26 locus was used. This is a mouse locus commonly used to knock-in different constructs for ubiquitous or conditional gene expression in transgenic mice. Also, since, molecular mechanisms of potential cross-talk between system x_c^- and Txnrd2 remain obscure, we sought to perform a comprehensive analysis of Txnrd-deficient cells and a putative overlap between Txnrd2 and system x_c^- seeking for the truly driving force of the Cys/(Cys)₂ circuit.

2. Materials and Methods

2.1. Materials

Chemicals	Company	Catalog-No.
4-Hydroxytamoxifen (Tam)	Sigma-Aldrich GmbH, Taufkirchen, Germany	H7904
Acrylamide	Roth Carl GmbH & Co., Karlsruhe, Germany	3426
Agarose	Invitrogen, Karlsruhe, Germany	15510-027
Agarose, low melting point	Fermentas GmbH, St. Leon-Rot, Germany	R0801
Albumin Fraction V	Roth Carl GmbH & Co., Karlsruhe, Germany	2923225
Ammonia (30%)	Merck KGaA, Darmstadt, Germany	1054231000
Ammonium persulfate	Sigma-Aldrich GmbH, Taufkirchen, Germany	A3678
Ampicillin sodium salt	Sigma-Aldrich GmbH, Taufkirchen, Germany	A9518
ANTI-FLAG M2 Affinity Gel	Sigma-Aldrich GmbH, Taufkirchen, Germany	A2220
Antimycin A	Sigma-Aldrich GmbH, Taufkirchen, Germany	A0274
Bacto yeast extracts	Difco Laboratories, Michigan, USA	
BODIPY581/591 C ₁₁	Invitrogen, Karlsruhe, Germany	D-3861
Boric acid	Merck KGaA, Darmstadt, Germany	203667
Bromophenol Blue sodium salt	Sigma-Aldrich GmbH, Taufkirchen, Germany	B8026
L-Buthionine Sulfoximine (BSO)	Sigma-Aldrich GmbH, Taufkirchen, Germany	B2640
Calcium chloride	Sigma-Aldrich GmbH, Taufkirchen, Germany	C7902
Chloroquine diphosphate salt	Sigma-Aldrich GmbH, Taufkirchen, Germany	C6628
cis-Platinum(II) dichloride	Sigma-Aldrich GmbH, Taufkirchen, Germany	P4394
Citric acid	Sigma-Aldrich GmbH, Taufkirchen, Germany	C4540
DAPI	Invitrogen, Karlsruhe, Germany	D1306
DCF, DCFDA	Invitrogen, Karlsruhe, Germany	C-13293
Dimethyl sulfoxide (DMSO)	Sigma-Aldrich GmbH, Taufkirchen, Germany	D2650
Disodium hydrogen orthophosphat	Merck KGaA, Darmstadt, Germany	1065855000
Dithiothreitol (DTT)	Sigma-Aldrich GmbH, Taufkirchen, Germany	D8161
dNTP/dUTP Mix	Fermentas GmbH, St. Leon-Rot, Germany	R0241
Doxorubicin hydrochloride	Sigma-Aldrich GmbH, Taufkirchen, Germany	D1515
ECL	GE Healthcare, Freiburg, Germany	RPN2106
Ethanol p.a	Merck KGaA, Darmstadt, Germany	1.00983.2500
Ethidium bromide	Merck KGaA, Darmstadt, Germany	70257083
EDTA	Sigma-Aldrich GmbH, Taufkirchen, Germany	E9884
Foetal Bovine Serum (FCS)	PAA, Pasching, Austria	A15-043
Formaldehyde (38%)	Sigma-Aldrich GmbH, Taufkirchen, Germany	F8775
Formamide	Merck KGaA, Darmstadt, Germany	344205
Gelatine from porcine skin	Sigma-Aldrich GmbH, Taufkirchen, Germany	G2500
Glacial acetic acid	Merck KGaA, Darmstadt, Germany	8187552500
Glutaraldehyd (25%)	Merck KGaA, Darmstadt, Germany	354400
Glutathione (GSH)	Sigma-Aldrich GmbH, Taufkirchen, Germany	G6013

Chemicals	Company	Catalog-No.
Glycerol	Sigma-Aldrich GmbH, Taufkirchen, Germany	G8773
Glycine	Merck KGaA, Darmstadt, Germany	2002722
HEPES	Invitrogen, Karlsruhe, Germany	15630-080
Hydroperoxide	Sigma-Aldrich GmbH, Taufkirchen, Germany	H1009
Iodoacetamide	Sigma-Aldrich GmbH, Taufkirchen, Germany	I6125
Isopropanol p.a.	Merck KGaA, Darmstadt, Germany	1.09634.2511
LIF (ESGRO)	Millipore, Billerica, MA, USA	ESG1107
Luria Broth Base	Invitrogen, Karlsruhe, Germany	12795-019
Magnesium sulfate	Merck KGaA, Darmstadt, Germany	105886
Mounting medium	Dako Cytomation, Hamburg, Germany	S3023
N-Acetyl-L-cysteine (NAC)	Sigma-Aldrich GmbH, Taufkirchen, Germany	A9165
Oligonucleotides	Metabion international AD, Martinsried, Germany	
Paraformaldehyde (PFA)	Roth Carl GmbH & Co., Karlsruhe, Germany	0335.3
Penicillin-Streptomycin solution	Invitrogen, Karlsruhe, Germany	15140-122
Perchloric acid (70%)	Merck KGaA, Darmstadt, Germany	1005191001
Phenethyl isothiocyanate (PEITC)	Fluka Chemie GmbH, Buchs, Switzerland	77972
Phenol/Chloroform/Isoamyl alcohol	Roth Carl GmbH & Co., Karlsruhe, Germany	A156
Ponceau S	Sigma-Aldrich GmbH, Taufkirchen, Germany	P3504
Potassium acetate	Merck KGaA, Darmstadt, Germany	1048201000
Potassium dihydrogen phosphate	Merck KGaA, Darmstadt, Germany	104873
Propidium iodide (PI)	Sigma-Aldrich GmbH, Taufkirchen, Germany	P4170
Puromycin dihydrochloride	Sigma-Aldrich GmbH, Taufkirchen, Germany	P7255
RPMI 1640 medium	Invitrogen, Karlsruhe, Germany	31870025
Rubidium chloride	Sigma-Aldrich GmbH, Taufkirchen, Germany	215260
Silver nitrate	Sigma-Aldrich GmbH, Taufkirchen, Germany	S8157
Skim Milk Powder	Fluka Chemie GmbH, Buchs, Switzerland	70166
Sodium acetate	Sigma-Aldrich GmbH, Taufkirchen, Germany	S8750
Sodium chloride	MP Biomedicals, Eschwege, Germany	194848
Sodium deoxycholate	Sigma-Aldrich GmbH, Taufkirchen, Germany	D6750
Sodium dodecyl sulfate (SDS)	Fluka Chemie GmbH, Buchs, Switzerland	71729
Sodium hydroxide	Roth Carl GmbH & Co., Karlsruhe, Germany	2151855
Sodium phosphate	Merck KGaA, Darmstadt, Germany	567550
Sodium pyrophosphate tetrabasic	Sigma-Aldrich GmbH, Taufkirchen, Germany	S6422
Sodium selenite	Sigma-Aldrich GmbH, Taufkirchen, Germany	S5261
Tetramethylethylenediamine (TEMED)	Fluka Chemie GmbH, Buchs, Switzerland	87689
Trichloroacetic acid	Sigma-Aldrich GmbH, Taufkirchen, Germany	T8657
Tris(hydroxymethyl)aminomethane	Merck KGaA, Darmstadt, Germany	108382
Tris-sodium citrate	Merck KGaA, Darmstadt, Germany	1110371000
Triton X-100	GE Healthcare, Freiburg, Germany	17-1315-01
Trypan Blue (0.4%)	Sigma-Aldrich GmbH, Taufkirchen, Germany	T8154
Trypsin-EDTA	Invitrogen, Karlsruhe, Germany	25300
Tryptone	Difco Laboratories, Michigan, USA	
Tween 20	Sigma-Aldrich GmbH, Taufkirchen, Germany	P5927
β -Mercaptoethanol (2-ME)	Invitrogen, Karlsruhe, Germany	31350-010
α -Tocopherol (Toc)	Sigma-Aldrich GmbH, Taufkirchen, Germany	T3251

<u>Radioactive Isotopes</u>	<u>Company</u>	<u>Catalog-No.</u>
[gamma- ³² P]-dCTP	GE Healthcare, Freiburg, Germany	PT10165
L-[¹⁴ C (U)] Cystine	Perkin Elmer Life Sciences Inc., Boston, USA	NEC465050UC

<u>Bacteria</u>	<u>Company</u>
TOP 10 <i>E.coli</i> cells	Invitrogen, Karlsruhe, Germany

<u>Enzymes</u>	<u>Company</u>	<u>Catalog-No.</u>
DNA Polymerase I (Klenow)	New England Biolabs GmbH, Frankfurt, Germany	M0210S
Pfx DNA Polymerase	Invitrogen, Karlsruhe, Germany	11708-013
Phosphatase, alkaline	Roche Diagnostics, Mannheim, Germany	713 023
Protease Inhibitor Cocktail Tablets	Roche Diagnostics, Mannheim, Germany	1 697 498
Proteinase K	Roth Carl GmbH & Co., Karlsruhe, Germany	7528.1
Restriction Endonucleases	MBI Fermentas GmbH, St. Leon-Rot, Germany	
Restriction Endonucleases	New England Biolabs GmbH, Frankfurt, Germany	
RNAse A	QIAGEN GmbH, Hilden, Germany	19101
T4 DNA Ligase	Promega GmbH, Mannheim, Germany	M180A
Taq DNA Polymerase	Invitrogen, Karlsruhe, Germany	18038-026

<u>Antibodies</u>	<u>Company</u>	<u>Catalog-No.</u>
anti-actin	Santa Cruz Biotechnology, Heidelberg, Germany	sc-58679
anti-FLAG	Sigma-Aldrich GmbH, Taufkirchen, Germany	F2555
anti-mouse-HRP conjugate	Santa Cruz Biotechnology, Heidelberg, Germany	sc-2354
anti-mouse-Alexa Fluor 488	Invitrogen, Karlsruhe, Germany	A-11001
anti-peroxiredoxin-III	LabFrontier, Seoul Korea	LP-PA0030
anti-peroxiredoxin-SO ₃	LabFrontier, Seoul Korea	LF-PA0004
anti-rabbit-HRP conjugate	Santa Cruz Biotechnology, Heidelberg, Germany	sc-2768
anti-rat-HRP conjugat	Santa Cruz Biotechnology, Heidelberg, Germany	sc-2006
anti-Txnrd1 polyclonal antisera	Dr. Vladim Gladyshev, University of Nebraska, Lincoln, USA	
anti-Txnrd2 monoclonal antisera	Dr. Elisabeth Kremmer, Helmholtz Zentrum München, Germany	
anti-Txnrd2 polyclonal antisera	Dr. Vladim Gladyshev, University of Nebraska, Lincoln, USA	
anti-xCT monoclonal antisera	Dr. Elisabeth Kremmer, Helmholtz Zentrum München, Germany	
anti-α-tubulin	Sigma-Aldrich GmbH, Taufkirchen, Germany	T6199

<u>Disposables and Kits</u>	<u>Company</u>	<u>Catalog-No.</u>
CEA RP NEW	CEA AB, Martinsried, Germany	C011824
DC Protein Assay	Bio-Rad, Munich, Germany	500-0112
DMEM lacking L-cystine	Invitrogen, Karlsruhe, Germany	21013
DMEM	Invitrogen, Karlsruhe, Germany	41966
Gel Extraction Kit	QIAGEN GmbH, Hilden, Germany	28704
Hybond-C super membrane	GE Healthcare, Freiburg, Germany	RPN203G
Illustra MicroSpin™ Columnx	GE Healthcare, Freiburg, Germany	27-3565-01
Immobilon-Ny+	Millipore, Schwalbach, Germany	HAHY13750
JETstar Plasmid purification system	Genomed GmbH, Loehne, Germany	220020
LightCycler Capillaries	Roche Diagnostics, Mannheim, Germany	11 909339 001

<u>Disposables and Kits</u>	<u>Company</u>	<u>Catalog-No.</u>
LightCycler FastStart DNA Master ^{PLUS}	Roche Diagnostics, Mannheim, Germany	03515869001
LS 5000 TA Scintillation Counter	Beckman Coulter GmbH, Krefeld, Germany	
Parafilm M®	Pechiney Plastic Packaging Company	
PCR Cloning Kit	QIAGEN GmbH, Hilden, Germany	231122
Plasmid Maxi Kit	QIAGEN GmbH, Hilden, Germany	12163
Random Prime DNA Labeling Kit	Roche Diagnostics, Mannheim, Germany	11 004 760 001
Reverse Transcription System	Promega GmbH, Mannheim, Germany	A3500
RNase-Free DNase Set	QIAGEN GmbH, Hilden, Germany	79254
RNeasy Mini Kit	QIAGEN GmbH, Hilden, Germany	74104

<u>Equipment</u>	<u>Company</u>	<u>Catalog-No.</u>
250/SE 260 Mini-Vertical Gel Unit	GE Healthcare Europe GmbH, Freiburg, Germany	
Axiovert 200M	Carl Zeiss, Jena GmbH, Germany	
Bench-top radioisotope counter	Bioscan, Washington D.C., USA	
Eurostar RW16, IKA-Labortechnik	IKA Werke GmbH, Staufen, Germany	2572100
FACS Calibur	BD GmbH, Heidelberg, Germany	
GenAmp PCR system 2700	Applied Biosystems, Darmstadt, Germany	
Gene Pulser II System	Bio-Rad, Munich, Germany	
GenPulser Cuvettes, 0.4 cm gap	Bio-Rad, Munich, Germany	
Heraeus Incubator, Modell B 5060	Heraeus Holding GmbH, Hanau, Germany	
Leica DM IRBE confocal microscope	Leica Microsystems GmbH, Wetzlar, Germany	
Leica TCS SP2 scanner	Leica Microsystems GmbH, Wetzlar, Germany	
Light-Cycler 1.5	Roche Diagnostics, Mannheim, Germany	
Microscope Axiovert 135	Carl Zeiss Jena GmbH, Germany	
Mini-PROTEAN 3 Electrophoresis Cell	Bio-Rad, Munich, Germany	
Mini-Sub Cell GT Electrophoresis Cell	Bio-Rad, Munich, Germany	
OTD Combi Ultracentrifuge	Sorvall, Langenselbold, Germany	
Overhead stirrer	Eurostar RW, IKA-Labortechnik, Staufen, Germany	2572100
Photometer Bio	Eppendorf, Hamburg, Germany	
PowerPac 200 Power Supply	Bio-Rad, Munich, Germany	
RF-10A XL Spectrophotometer	Shimadzu, Duisburg, Germany	
Sephadex G-50 columns	GE Healthcare, Freiburg, Germany	27-5330-01
Spectrophotometer DU-64	Beckman Coulter GmbH, Krefeld, Germany	
Stereomicroscope	Nikon, Tokyo, Japan	
Supelclean LC-18 columns	Sigma-Aldrich, Stockholm, Sweden	57012
Trans-Blot Semi-Dry	Bio-Rad, Munich, Germany	
UZ-PA-38,5-1 Ultracentrifuge Tubes	Kisker GbR, Steinfurt, Germany	
X-ray film	GE Healthcare, Freiburg, Germany	RPN16778K

<u>Oligonucleotides</u>	<u>Sequence</u>
<u>Genotyping</u>	
Cre D	5'-CACGACCAAGTGACAGCAATGCTG-3'
Cre E	5'-CAGGTAGTTATTCGGATCATCAGC-3'
TR2_Del_for	5'-TGCTTCCAGGCCCACTGCTCTGACTGG-3'

Oligonucleotides	Sequence
Genotyping	
TR2_Del_rev	5'-CAGGCTCCTGTAGGCCCATTAAGGTGC-3'
TR2_flox_for	5'-CAGGTCACTAGGCTGTAGAGTTTGC-3'
TR2_flox_rev	5'-ATGTCCCAGTGTACTTATGATGAATC-3'
TrxR2E15	5'-TTCACGGTGGCGGATAGGGATGC-3'
TrxR2E18	5'-TGCCCAGGCCATCATCATCTGACG-3'
xCT for	5'-CCTGAAACATAGAATGAATGCA-3'
xCT for1	5'-GGCACCGTCATCGGATCAGGCATC-3'
xCT KO for I	5'-TCACGACCGAACAGTGATCAGTC-3'
xCT KO rev I	5'-ATCCGATGACGGTGCCGATGATG-3'
xCT KO rev II	5'-GCTCATATTGCCCTGCAGGTAAC-3'
xCT rev	5'-CCTTTGGAGATGGTGGCCA-3'
xCT rev1	5'-CACGAGCTTGATTGCAAGTTCAGG-3'
Cloning	
Olig_SECI_BglII_for	5'-TCTCAGAGATCTGAGAAGATGTGGATGGAAC-3'
Oligo TR2 A59T for	5'-AGCGGGAATCGATTATAAAGAT-3'
Oligo TR2 A59T rev	5'-GCCAGAAGCTTTCTTGCCTTGATAGC-3'
Oligo TR2 G375R for	5'-GCTATCAAGGCAAGAAAGCTTCTGGC-3'
Oligo TR2 G375R rev	5'-GCCAGAAGCTTTCTTGCCTTGATAGC-3'
Oligo_ClaI_for	5'-TCGCCGCCACCATCGATTATAAAGATGA-3'
Oligo_ClaI_rev	5'-TCATCTTTATAATCGATGGTGGCGGCGA-3'
Oligo_KpnI_for	5'-CAGCCAGAAGATGTCGTCACCTTGAT-3'
Oligo_mTxnrd2_Cla I	5'-ATTGAATTCCATGGCGGCGATGGTGGCGGCGA-3'
Oligo_SECIS_rev	5'-GTTTGAACCCCTGGCATTCTAGAGCACT-3'
Oligo_TR2_NheI_&_SacI_rev	5'-ATGAGCTCGCTAGCAGATCAAAGCTCTGCTGCCC-3'
Oligo_Txnrd2_ATG_MLS_EcoRI	5'-ATTGAATTCCATGGCGGCGATGGTGGCGGCGA-3'
RT-PCR	
18s RNA for	5'-GGACAGGATTGACAGATTGATAG-3'
18s RNA rev	5'-CTCGTTCGTTATCGGAATTAAC-3'
Prx I for	5'-GGGAATTGAACCTGGGTCTT-3'
Prx I rev	5'-CGAAAAACAAAAGGCCAACT-3'
Prx II for	5'-TTGACTGTGATCTGGCGAAGG-3'
Prx II rev	5'-CTCTTGCTCACGCAGTCATGG-3'
Prx III for	5'-GTCTGCCTCTGCCCAAGGAAA-3'
Prx III rev	5'-CTTGGTGTGTTGATCCAGGCA-3'
Prx IV for	5'-CACAAAGGTCAAATCCAGTGGG-3'
Prx IV rev	5'-TTAGCTGGCTGCCTGGCGGAGG-3'
Prx V for	5'-AATCTCATCAAAGTTCCTGCCC-3'
Prx V rev	5'-ACCACAGAACTTGGCAGAGCTGC-3'
Prx VI for	5'-CCGATCAAGGTGGGAGATGCC-3'
Prx VI rev	5'-TCTGGCTCCACGTTCAGTGCC-3'
TrxR2E15	5'-TTCACGGTGGCGGATAGGGATGC-3'

Oligonucleotides	Sequence
RT-PCR	
TrxR2E18	5'-TGCCCAGGCCATCATCATCTGACG-3'
xCT for1	5'-GGCACCGTCATCGGATCAGGCATC-3'
xCT rev1	5'-CACGAGCTTGATTGCAAGTTCAGG-3'
Srx fov	5'-AGACACGGGGTTTTTCTGTG-3'
Srx rev	5'-ACGAACTGACCAACGGAAAC-3'
Sequencing	
Cter	5'-TCTGAGAGGCAGCAAGGCCTTC-3'
IRES rev1	5'-CTTCGGCCAGTAACGTTAGG-3'
LTR 3'-for1	5'-GCTCACAACCCCTCACTC-3'
ROSA26 flox for	5'-CCCAAGTGGTTCAGACGATTA-3'
ROSA26 flox rev	5'-GGTGGCCACAACCTGGCTT-3'
Sp6 promoter	5'-ATTTAGGTGACACTATAGAA-3'
T7 promoter	5'-TAATACGACTCACTATAGGG-3'
TR2 mid	5'-GTCATCTTTGGTCACAGAG-3'

All DNA-oligonucleotides were obtained from Metabion GmbH, Martinsried, Germany.

Expression and Targeting Vectors

Depicted are the expression vectors pCAG-3SIP (Figure 12), the lentiviral vector p442 (Figure 13), and the targeting vectors pTVRosa26-mxCT (Figure 14) and pMB-mxCT (Figure 15).

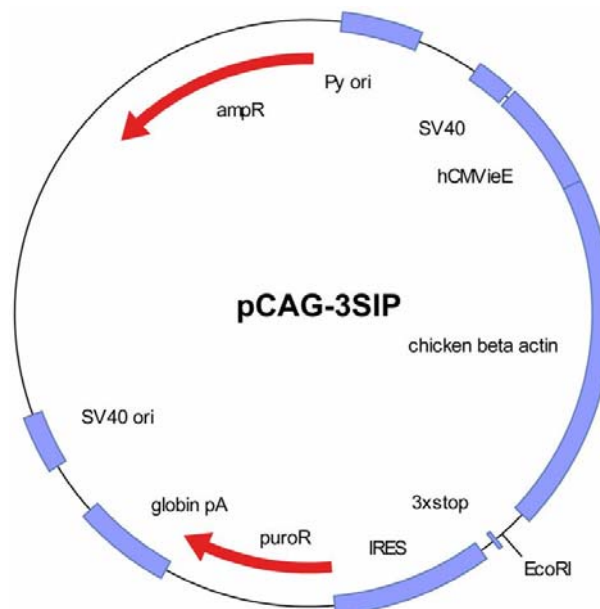


Figure 12. Map of the expression vector pCAG-3SIP. Abbreviations: SV40 (early SV-40 promoter), hCMVieE (human cytomegalovirus immediate early-enhancer modified chicken β -actin promoter), *EcoRI* (unique restriction site used for cloning), 3 x stop (three stop codons in all three open reading frames), IRES (internal ribosomal entry site), PuroR (*puromycin N-acetyltransferase* gene), globin pA (globin poly A signal), SV40 ori (simian virus 40 origin of replication), ampR (β -lactamase: ampicillin resistance gene), Py ori (Polyoma origin of replication).

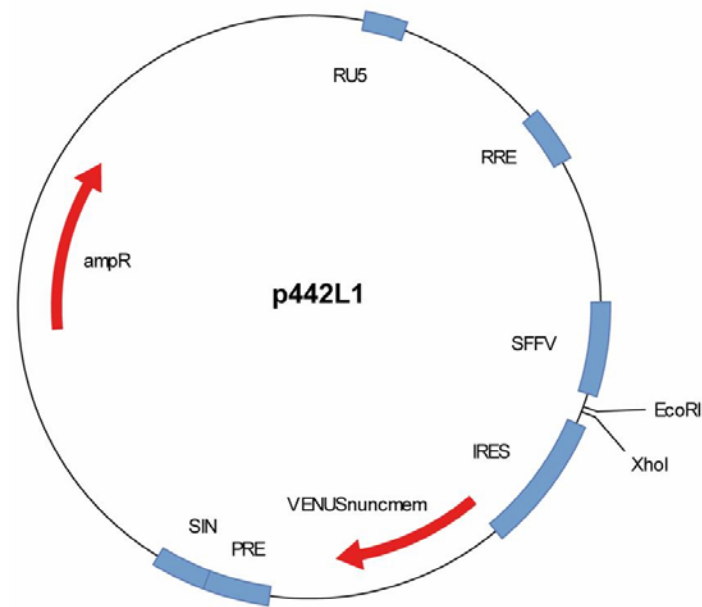


Figure13. Map of the lentiviral vector p442L1. Abbreviations: ampR (β -lactamase), RU5 (HIV 5' LTR splice donor site, necessary for the integration of gene in to host genome), RRE (Rev responsive element, splice acceptor site), SFFVp (spleen focus forming virus promoter), *EcoRI/XhoI* (restriction sites used for cloning), IRES (internal ribosome entry site), VENUSnucmem (fluorescent protein with nuclear membrane anchor), PRE (post regulatory element), SIN (self-inactivating 3' LTR).

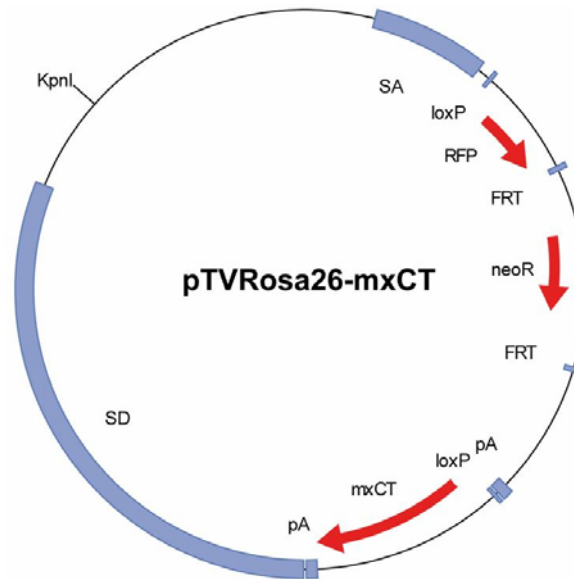


Figure 14. Map of the targeting vector pTVRosa26-mxCT. Abbreviations: SA (splice acceptor), RFP (*red fluorescence protein*), neoR (*neomycin phosphotransferase*), FRT (34 bp palindromic sequence, which allows Fip-mediated removal of *neoR*), pA (bidirectional polyA signal), loxP (34 bp palindromic sequence, which is the target for Cre recombinase), mxCT (murine *xCT* cDNA), pA (polyA signal), SD (splice donor), *KpnI* restriction unique site used for linearization of the plasmid.

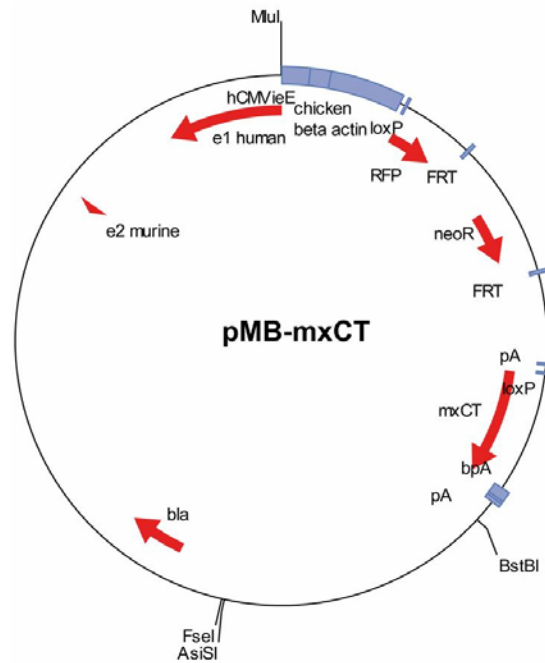


Figure 15. Map of the HPRT targeting vector. hCMVieE (human CMV early immediate enhancer/CAG chicken β -actin promoter), *loxP* (34 bp palindromic sequence, which is the target for Cre recombinase), RFP (*red fluorescence protein*), FRT sequence (34 bp palindromic sequence, which allows Flp-mediated removal of neoR), pA (three polyA signals), mxCT (murine *xCT* cDNA), *FseI*/*AsiSI* (restriction sites used for linearization of the plasmid), *bla* (ampicillin resistance gene).

Cell lines

Primary mouse embryonic fibroblasts (MEFs) were isolated from E12.5 mouse embryos arising from breeding pairs that were heterozygous for *Txnrd2* (wt/ko). Isolated MEFs were stably transfected with the pCAG-3SIP-mxCT and pCAG-3SIP-EGFP expressing vectors yielding the respective cell lines.

Murine E14tg2a embryonic stem (ES) cells were a kind gift from Dr. W. Wurst's laboratory (Helmholtz Zentrum München). E14tg2a 129/Ola-derived HPRT-negative ES cells were used for the generation of the transgenic mouse line *R26mxCT^{fSTOP}*.

HH514 is a human, EBV-positive Burkitt's lymphoma cell line (Y163H + frame shift: E287stop). This cell line was already stably transfected with the expression constructs pCAG-3SIP-mxCT and pCAG-3SIP by Ana Banjac (Banjac, 2005).

HEK293 T cells were used for the production of lentiviral particles, based on the third generation lentiviral vector p442L1 (kind gift from Dr. T. Schroeder, Helmholtz Zentrum München).

Probes for Southern Blot analysis

The **Rosa26-Probe** was a kind gift from Dr. Cornelia Hoemig (Hömig, 2005). A 550 bp long fragment encompassing the first intron of the Rosa26 locus was cloned via *EcoR* und *PacI* sites into the plasmid pBSIIKS.

The **Neo-Probe** was a kind gift from Dr. Cornelia Hoemig (Hömig, 2005). The probe (466 bp) was isolated with *RsrII* and *PstI* from the pBSIIKS-Neo plasmid.

Probes for Northern Blot analysis

The **mxCT-Probe** was amplified by PCR using the pCAG-mxCT plasmid as template and xCT for1/xCT rev1 as primer pair.

2.2. Methods

2.2.1. Cell culture

Bacterial cells

The bacterial strain TOP10 was cultured either on LB agar plates or in LB liquid medium, in an incubator at 37°C over night. Selection of transformed bacteria on agar plates or in liquid medium was achieved by use of the corresponding antibiotics.

LB medium: 20 mM MgSO₄, 10 mM KCl, 1% (w/v) Tryptone, 0.5% (w/v) Bacto yeast extracts, 0.5% (w/v) NaCl

LB agar: 20 mM MgSO₄, 10 mM KCl, 1% (w/v) Tryptone, 0.5% (w/v) Bacto yeast extracts, 0.5% (w/v) NaCl, 1.2% (w/v) Bacto-agar

Murine embryonic fibroblasts (MEFs)

Hemizygous *Txnrd2* knock-out mice were mated and females were checked daily for vaginal mucous plugs. A vaginal mucous plug was considered as embryonic day 0.5 (E0.5). Pregnant mice were sacrificed at E12.5 by cervical dislocation. Uterine horns were dissected under sterile conditions and placed into a Petri dish containing PBS. Each embryo was separated from its placenta and surrounding membranes. The body trunk was dissected from the organs and washed with fresh PBS to remove blood and other tissue debris. Embryo tails were used for determination of the genotype by using TR2_Del_for/TR2_Del_rev and

TR2_flox_for/TR2_flox_rev primer pairs. Only when the floxed allele is deleted by Cre recombinase, the distance between TR2_Del_for/TR2_Del_rev primer binding sites is small enough to be amplified by standard PCR. The second primer pair, TR2_flox_for/TR2_flox_rev, was used to detect the wt allele, and thus to determine genotype (either *Txnrd2*^{-/-} or *Txnrd2*^{+/-}) of the cells. By using two forceps embryo trunks were minced, suspended in trypsin-EDTA and incubated at 37°C for 15 min. The suspension was homogenized by vigorous pipetting, the cells were collected by centrifugation (1,200 rpm/5 min) and washed in Standard DMEM to remove trypsin. After washing, the cells were plated in 6 cm diameter cell culture dishes (referred to as passage No. 0). Cells were cultured at 37°C in a 5% O₂, 5% CO₂ water-saturated atmosphere. After the cell lines reached confluency, they were split at a ratio of 1:3 on to a larger cell culture dishes. Cells from early passage numbers were harvested by trypsinization and aliquots were stored by cryo-conservation in liquid nitrogen. Primary cells cultured in Standard DMEM were routinely split by trypsinization at a ratio of 1:3 every 4th to 5th day.

PBS: 80.0 g NaCl, 2.0 g KCL, 14.4 g Na₂HPO₄, 2.4 g KH₂PO₄ in 1 l H₂O, pH 7.4

Standard DMEM: DMEM, 10% FCS, 1% glutamine, 50 U/ml penicillin G, 50 µg/ml streptomycin

HH514 Burkitt's lymphoma cell line

The Burkitt's lymphoma cell line HH514 was cultured at 37°C and 6% CO₂ under water-saturated atmosphere. Cells were grown in Standard RPMI medium and routinely split at a ratio of 1:3 every 3rd day.

Standard RPMI: RPMI 1640-medium, 10% FCS, 1% glutamine, 50 U/ml penicillin G, 50 µg/ml streptomycin

HEK293 T cells

Cells were cultured at 37°C in a 5% O₂, 5% CO₂ water-saturated atmosphere in Standard DMEM. HEK293 T cells were routinely split by trypsinization at a ratio of 1:5 every 2nd or 3rd day.

Determination of cell number

Cells were detached from cell culture dishes by trypsinization and suspended by adding 2.5 volumes of Standard DMEM. Thereafter, 30 µl of the cell suspension was mixed with an equal volume of 0.4% trypan blue solution, and cells were counted using the

Fuchs-Rosenthal haemocytometer. Trypan blue is excluded from viable cells, whereas dead cells stain blue due to plasma membrane disruption.

Cryo-conservation and thawing of cells

Cells were grown in 10 cm diameter culture dishes until they reached approximately 80% confluency, trypsinized, and collected by centrifugation. The cell pellets were resuspended in FCS containing 10% DMSO, transferred to cryo-vials in 1 ml aliquots and frozen in propanol containers at -80°C over night. On the following day, vials were transferred to a liquid nitrogen tank. Stocks of all cell lines were stored in liquid nitrogen.

When needed, frozen cells were defrosted in a water bath at 37°C , immediately transferred to 5 ml Standard DMEM and collected by centrifugation. Cell pellets were resuspended in 10 ml Standard DMEM and plated in 10 cm diameter cell culture dish.

Cell fractionation by digitonin method

For the purpose of cell fractioning, cells were collected from 15 cm cell culture dishes. The medium was aspirated and cells were washed two times with ice cold PBS. Cells were scraped off with a cell scraper and were resuspended in Digi-buffer. For plasma membrane rupture digitonin was added in Digi-buffer in the final concentration of 0,007%. Cells were incubated on ice for 15-30 min. Plasma membrane rupture was followed by staining cells with Trypan Blue. When the majority of cells ($> 95\%$) were Trypan Blue-positive, they were centrifuged for 15 min/ 4°C /15,000 rpm. The supernatant (cytoplasmic fraction) was stored at -20°C until needed. The cell pellet containing plasma membranes and organelles was washed in $\sim 200\ \mu\text{l}$ of Digi-buffer and centrifuged once more at 4°C /15,000 rpm. The resulting supernatant was discarded, and the cell pellet was lysed in 50-100 μl of LCW and stored at -20°C until further needed.

Digi-buffer: 100 mM HEPES (pH 7.4), 250 mM Saccarose, protease inhibitor

100X digitonin: 0.7% in DMSO (freshly prepared)

LCW: 0.5% TritonX-100, 0.5% Sodium Deoxycholate Salt, 150 mM NaCl, 20 mM Tris, 10 mM EDTA, 30 mM Na-Pyrophosphate, pH 7.5

2.2.2. Gene-transfer methods

Electroporation of MEFs

Cells were grown on 15 cm cell culture dishes to ~80% confluency, harvested by trypsinization, washed in PBS and resuspended in 800 µl DMEM. Primary MEFs were electroporated with a Gene Pulser II (Bio Rad, Munich, Germany) at 240 V, 1,000 µF in cuvettes with 0.4 cm gap width. For each transfection, ~20 µg plasmid DNA was used. Immediately after the pulse, FCS (500 µl) was applied to the cells. The cell suspension was plated in a 10 cm diameter cell culture dish in Standard DMEM. Selection for antibiotic resistance was initiated 24 h after electroporation with 0.5 µg/ml puromycin, gradually increasing to 2 µg/ml over a period of one to three weeks.

Lentiviral infection

Lentiviruses are retroviruses capable of integrating DNA into the target cells. Lentiviruses enter the nucleus of dividing and resting cells and are therefore one of the most efficient methods for gene delivery into cells. Lentiviral particles were produced in HEK293 T cells using a third generation lentiviral packaging system, which provides maximal biosafety. For lentivirus production, four different plasmids were co-transfected into the producer cell line (HEK293 T). Three plasmids encode all necessary and structural proteins for lentivirus production: (i) pEcoEnv-IRES-puro expresses the structural gene *env*, which encodes the surface and transmembrane glycoprotein; (ii) plasmid pMDLg_pRRE expresses the structural gene *gag* that encodes for capsid and matrix proteins and also the enzyme cluster *Pol* which encodes for provirus-integrase, reverse transcriptase, as well as the protease indispensable for post-translational modification of the fusion proteins; and (iii) pRSV_Rev plasmid which expresses *rev* (regulator of virion), which promotes the cytoplasmic accumulation of unspliced and single spliced viral transcripts. Third generation packaging systems are Tat-independent, as the transfer vector pRRL.PPT.SF.IRES-VENUSnucmem (p442L1) contains an additional SFFV promoter.

For the generation of lentiviruses, 5×10^6 human embryonic kidney cells (HEK293 T) were plated in Standard DMEM in 10 cm diameter cell culture dishes and incubated for 24 h. Plasmids (2 µg pEcoEnv-IRES-puro, 5 µg pMDLg_pRRE, 10 µg pRSV_Rev, 5 µg p442-based vector) were diluted in 450 µl 12.5 mM CaCl₂ and mixed with 500 µl HBS by air-bubbling. Cell culture medium was replaced with TF medium, in which chloroquine was added to a final concentration of 25 µM. For calcium phosphate transfection, the plasmid mix

was vortexed, incubated for 20 min at room temperature and applied drop wise onto the HEK293 T cells. Cells were incubated for another 8-12 h. The transfection medium was replaced with fresh TF medium, and the transfected packaging cells were incubated for further 36 h. Virus-enriched TF medium was recovered from the cell culture dish, filtrated through a 0.22 µm sterile filter and ultracentrifuged in a swing rotor for at least 16 h at 10,000 x g. The virus-containing pellet was resuspended in 200 µl Standard DMEM and stored at -80°C until used.

1 x 10⁵ MEFs were transduced in a 3.5 cm diameter cell culture dish by adding 30 µl of the virus concentrate, followed by another incubation period for 48 h. Infection efficiency was monitored by flow cytometry (BD FACSCalibur), with excitation wavelength at 488 nm and analysed using CellQuest™ software (Becton Dickinson). In experiments where the p442L1-based vectors, which contain an IRES-*puromycin N-acetyl-transferase* cassette, were used, infected cells were selected with 0.5 µg/ml puromycin 24 h after infection, gradually increasing from 0.5 µg/ml puromycin to 1 µg/ml over a period of one to two weeks.

1000X chloroquine : 25 mM chloroquine in PBS

2X HBS: 50 mM HEPES, 280 mM NaCl, 1.5 mM Na₂HPO₄, pH 7.05 adjusted with NaOH

TF medium: Standard DMEM, 20 mM HEPES

2.2.3. Molecular biology techniques

Cloning

Preparation of competent bacterial cells

The *E.coli* TOP10 bacterial strain (Invitrogen) was grown on LB plates at 37°C overnight. A single colony from the plate was used to inoculate 2.5 ml medium in a loose-capped vessel with constant shaking. An overnight culture was diluted 1:100 (250 ml) in LB medium containing 100 mM KCl and 200 mM MgCl₂. Bacterial cells were grown in 1 l flasks until A₆₀₀ reached 0.4-0.6. Bacteria were harvested by centrifugation (4,000 rpm/10 min/4°C). The pellet was resuspended in ~40% of the original volume of ice cold TFB1. For the remaining steps the cells were kept on ice. Finally, bacterial cells were concentrated in 0.04 original volume of ice-cold TFB2. Aliquots of 100 µl of the bacterial suspension were snap-frozen in liquid nitrogen and stored at -80°C until further use.

TFB1: 15% (w/v) glycerol, 100 mM RbCl, 10 mM CaCl₂, 50 mM MgCl₂, 30 mM KAc. Adjust pH to 5.8 with acetic acid. Filter-sterilize (0.45 µm) and store at room temperature.

TFB2: 10 mM MOPS or PIPES (pH 6.5), 75 mM CaCl₂, 10 mM RbCl, 15% glycerol. Adjust pH to 6.5 with 1 M KOH. Filter-sterilize (0.45 µm) and store at room temperature.

Transformation of bacteria by heat shock

Aliquots of frozen competent cells were removed from –80°C and thawed on ice. The cells were gently mixed by flicking the tube. For transformation, 100 µl of competent cells were transferred to pre-chilled sterile polypropylene tubes and either 10 µl of the ligation mixture (see below) or 1-10 pg purified plasmid DNA was added to the cell suspension. After incubation on ice for 15-20 min, cells were heated to 42°C for 1-2 min and placed on ice for 10 min. 1 ml of LB medium was added to the cell suspension and incubated with shaking (~750 rpm) for 45 min at 37°C. Cells were harvested by centrifugation (4,500 rpm for 5 min), and LB excess was discarded. The transformation mixture was resuspended in 200 µl of LB and plated on an LB plate containing 50 µg/ml ampicillin (all plasmids used in this study expressed β-lactamase for selection). Plates were incubated for 12-16 h at 37°C until single cell colonies became visible.

Preparation of plasmids by the alkaline lysis method

After transformation, single colonies were inoculated in 2.5 ml LB medium, containing 100 µg/ml ampicillin. The inoculum was incubated with vigorous shaking (~200 rpm) at 37°C for 5-7 h or overnight. The volume of 2 ml of the bacterial suspension was centrifuged at 4,500 rpm for 5 min. The remaining cell suspension (~500 µl) was stored at 4°C until needed. The cell pellet was resuspended in 200 µl E1 resuspension buffer by vortexing. E2 lysis buffer (200 µl) was added to the cell suspension, mixed by inverting the tubes and incubated no longer than 5 min at room temperature. 200 µl of neutralisation buffer E3 was added, mixed by inverting the tubes and centrifuged for 8 min at 15,000 rpm. For DNA precipitation 0.7 volumes of isopropanol was added to the supernatant, and the plasmid DNA was recovered by centrifugation (15,000 rpm) for 15 min at 4°C. The DNA pellet was washed with 70% ethanol, air-dried at room temperature and resuspended in 30 µl TE.

The isolated plasmids were subjected to analytic restriction digestions to identify the correct construct and orientation of the insert. After identification of positive clones, the amount of plasmid DNA was augmented using the *Qiagen Plasmid Maxi Kit*. Plasmid concentrations were quantified by measuring the absorbance at 260 nm in a spectrophotometer (Spectrophotometer DU-64, Beckman Coulter GmbH, Krefeld, Germany).

E1 (resuspension buffer): 50 mM Tris, 10 mM EDTA, pH 8.0

E2 (lysis buffer): 200 mM NaOH, 10% w/v SDS, RNaseA 7,000 U/ml

E3 (neutralisation buffer): 3.1 M potassium acetate, adjust to pH 5.5 with acetic acid

TE: 10 mM Tris pH 7.5; 1 mM EDTA

Restriction digestion

DNA restriction digestion was performed with respective endonucleases according to manufacturer's instructions (New England Biolabs GmbH or MBI Fermentas GmbH).

For cloning, DNA fragments were separated and visualised by electrophoresis in a 0.8% low melting point (LMP) agarose gel, stained with ethidium bromide, at 50 V in 1X TAE buffer. The desired fragment was isolated from the gel with a scalpel and processed with a *Qiagen Gel Extraction Kit*, according to the manufacturers' instructions. For analytical purposes, digested DNA was separated and visualised by electrophoresis in a 1-2% agarose gel at 80 V in 1X TAE buffer.

50X TAE: 2 M Tris-acetate (2 M Tris and 5.71% v/v acetic acid); 50 mM EDTA/NaOH pH 8.0

Phenol/chloroform extraction and precipitation of DNA

DNA fragments, obtained from enzyme digestions or other modifications, such as dephosphorylation reactions or fill-in reactions by Klenow DNA polymerase, were purified by phenol/chloroform/isoamylalcohol treatment and ethanol precipitation. An equal volume of phenol/chloroform/isoamyl alcohol (ratio of 25:24:1) was added to the digestion reaction, briefly vortexed and centrifuged for 8 min at 15,000 rpm. The upper aqueous phase was recovered and the DNA was precipitated by adding 2 volumes of absolute ethanol and 0.1 volume of 3 M sodium acetate (pH 5.5; adjusted with potassium acetate), followed by centrifugation at 4°C, 15,000 rpm for 15 min. The DNA precipitate was washed with 70% ethanol, centrifuged as above for 10 min and air-dried at room temperature. The DNA was dissolved in 30 µl TE, incubated at 65°C for 10 min in order to fully dissolve the DNA and stored at -20°C.

DNA ligation

Ligation reactions were prepared with T4 DNA ligase (New England Biolabs GmbH) according to standard procedures as described in the manufacturers' instructions. Depending on the size of the fragments to be ligated, the protocol was adjusted to optimize the insert:vector ratio for ligation. The ligation mix was incubated at 16°C for 12-24 h. To quantify

the specificity of the ligation reaction, respective backbone and insert DNA were subjected to separate control ligations. The ligation reactions were used in subsequent heat shock transformation of competent bacteria and further analysed.

Klenow fragment fill-in reaction

For blunt-end cloning DNA fragments were treated with DNA Polymerase I (Klenow fragment) according to the manufacturers' instructions (New England Biolabs GmbH). The Klenow fragment retains polymerization fidelity and 3'-5' exonuclease activity, but is devoid of 5'-3' exonuclease activity. Hence, the Klenow fragment forms blunt ends by either filling-in 5'-overhangs or by removing 3'-overhangs. Linearised DNA was subjected to fill-in reaction by Klenow DNA polymerase for 30 min at room temperature.

Dephosphorylation of linearized plasmid DNA

Dephosphorylation of backbone DNA favours the integration of DNA inserts with phosphorylated 5' ends, since re-ligation of the backbone is prevented. Vector DNA was dephosphorylated with CIP (calf alkaline phosphatase) (Roche Diagnostics). Pico-mol of 3' or 5' ends were calculated according to the average molecular weight of a nucleotide pair (660 Da), concentration ($\mu\text{g}/\mu\text{l}$) of DNA to be used and the size of the fragment (bp) to be used. One unit of CIP per 1 pmol 3' or 5' terminal phosphorylated DNA fragments was used, and the reaction was incubated for 1 h at 37°C. After dephosphorylation of DNA fragments, phenol/chloroform/isoamyl alcohol extraction was performed to remove CIP.

Polymerase chain reaction (PCR)

The standard polymerase reaction (PCR) was performed according to manufacturer's instructions (Invitrogen). The individual PCR steps were optimized for each template and primer pair combination. For standard (analytical) amplifications, Taq polymerase (Invitrogen) was used, whereas the high fidelity polymerase, Platinum Taq DNA Polymerase (Invitrogen) was used for cloning purposes according to the manufacturers' instructions. The DNA to be amplified (1-20 ng) was mixed with 1-2.5 units DNA polymerase, 0.5 μM oligonucleotide primers (Metabion International AG), 0.2 mM each dNTP (Fermentas GmbH), 1X PCR buffer (Invitrogen) and 1.5 mM MgCl_2 (Invitrogen). After PCR amplification, the product was analyzed for size, quantity, and/or sequence and used in further experimental procedures.

Site-directed Txnrd2 mutagenesis

Exchange of single amino acids within Txnrd2 was performed by site-directed PCR mutagenesis in a final volume of 50 µl. Primers of 21 nucleotides were designed such that the primer sequence contains a mutated codon approximately in the centre of the primer. Codons were chosen according to the highest murine codon usage of the respective amino acid. Prior to transformation of competent bacteria, PCR products were digested with *DpnI*. *DpnI* cleaves only methylated DNA, and is thus suitable to remove template DNA prior to transformation of the PCR products in bacteria. Mutations were verified by sequencing.

cDNA preparation

Isolated RNA was first reverse-transcribed to cDNA to provide the necessary DNA template for Taq polymerase. Single-stranded cDNA was synthesized from 1 µg of isolated mRNA by Reverse Transcription System (Promega) according to manufacturers' instructions (0.5 U/µl Avian myeloblastosis virus (AMV) reverse transcriptases, 1 U/µl RNasin® broad-spectrum RNase inhibitor, 50 ng random primer, 0.25 mM each dNTP, 1X reaction buffer and 5 mM MgCl₂). The incubation time was extended to 60 min to obtain more abundant transcripts. The cDNA amplification was performed with random primers at 42°C. After elongation the samples were denatured at 95°C for 5 min and then placed on ice for 5 min. The 20 µl first-strand cDNA synthesis reaction mix was finally diluted to 100 µl with nuclease-free water and subjected to semi-quantitative and quantitative PCR.

Real-time PCR

For expression analysis the LightCycler FastStart DNA MasterPLUS SYBR Green I Kit in combination with LightCycler 1.5 System (Roche) was used. Each RT-PCR reaction mix contained the respective primer pair, cDNA and the LightCycler Master Mixes (Taq DNA polymerase and SYBR Green I dye for detection) according to manufacturers' instructions (Roche). During each PCR cycle, SYBR Green I intercalates specifically into the double strand of the amplified PCR products; ongoing amplification is monitored by measuring the increase in fluorescence after each cycle. RT-PCR primers were designed with software Primer3 (Rozen and Skaletsky, 2000), standardizing optimal T_M of approximately 58°C and a product size of 200-300 bp. If possible, primer pairs hybridizing on different exons were used to minimize unspecific amplification of possible genomic DNA contaminations. Expression levels of the target gene were normalized on *18s* or *aldolase* expression levels. To control the specificity of the RT-PCR reaction, the synthesized PCR product was correlated to a

specific melting point, which was assessed by running a melting curve program after the final cycle.

primer mix: oligonucleotide primer stock solution 5 μ M for each primer

Cloning of expression and targeting vectors

pCAG-3SIP-based vectors (xCT, EGFP, MCM)

pCAG-3SIP-based vectors contain a strong hybrid promoter, consisting of the chicken β -actin promoter and the CMV enhancer, which is highly active in many cell types and organisms (Sawicki et al., 1998).

The pCAG-3SIP-based vectors, expressing EGFP or xCT, were a kind gift from Dr. Ana Banjac (pCAG-3SIP-EGFP and pCAG-3SIP-mxCT (Banjac, 2005) and Dr. Alexander Seiler (pCAG-3SIP-MCM) (Seiler, 2008) (Figure 12). The vector pCAG-3SIP-mxCT contained the coding region of murine xCT-light chain, pCAG-3SIP-EGFP contained the red-shifted variant of wild-type *GFP* and pCAG-3SIP-MCM is a vector expressing the Cre recombinase with murine estrogen receptor binding domains (Mer) fused at both the N- and C-terminus of Cre. This MerCreMer recombinase does not bind to estrogen but retains binding activity to tamoxifen (Tam, selective estrogen receptor modulator). In the absence of Tam the MerCreMer fusion protein is bound to the hsp90 complex, and thus retained in the cytoplasm. Upon Tam administration the hsp90-MerCreMer complex dissociates and the Cre translocates from the cytoplasm to the nucleus, where Cre-mediated removal of the loxP-flanked cassette occurs.

p442L1-based Txnrd2 expression vectors

The vector pGEM-Teasy-mTxnrd2 was a kind gift from Dr. Antonio Miranda-Vizuet (Centro Andaluz de Biología del Desarrollo, Espania). The vector contained the partial 5' sequence of murine *Txnrd2*. 3'-UTR region containing the SECIS element was missing. The remaining part was amplified from murine liver cDNA with the primes "Olig_SECI_BglII_for" and "Olig_SECIS_rev". The resulting 160 bp PCR product including the entire SECIS element was purified, cloned into pDrive (Qiagen, Hilden, Germany) to give SECIS-pDrive and sequenced. The SECIS element coding sequence was isolated from the SECIS-pDrive with *PaeI* and *BglII* and inserted into the same restriction enzyme sites of pGEM-T-Easy-Txnrd2 (4702 bp), yielding pGEM-T-Easy-Txnrd2-SECIS.

To generate a cytoplasmic version of Txnrd2 (cyto-Txnrd2) (see also Turanov et al 2005), a second PCR was performed with primers “Oligo_TR2_NheI_&_SacI_rev” and “Oligo_KpnI_for”. This amplified the 5’ region of Txnrd2 (551 bp), which, however, lacks the coding sequence for the MLS. The PCR was designed as such that a *SacI* site and *NheI* site were generated (*NheI* was needed for cloning into the NTAPe vector). The purified PCR product was digested with *SacI* and *KpnI* and ligated into the same sites of pGEM-T-Easy-Txnrd2-SECIS, yielding pGEM-T-Easy-cyto-Txnrd2.

For purification of protein complexes, Txnrd2 was additionally tagged with a Tandem Affinity Purification enhanced (TAPe) tag, which was a kind gift from Dr. Marius Ueffing and Dr. Johannes Gloeckner (Helmholtz Zentrum München). pcDNA3-NTAPe and pGEM-T-Easy-cyto-Txnrd2 were digested with *NheI* and *XhoI*. The resulting backbone of pcDNA3-NTAPe and the corresponding fragment of pGEM-T-Easy-cyto-Txnrd2 (cyto-Txnrd2) were ligated to obtain pcDNA-NTAPe-cyto-Txnrd2.

To create the TAPe-tagged mitochondrial version of Txnrd2, the start codon of the NTAP had to be removed prior to fusing the MLS of Txnrd2 to the 5’ end of the TAPe. At first, the MLS was amplified by PCR with pGEM-TEasy-mTxnrd2 as template and the primer pair: “Oligo_Txnrd2_ATG_MLS_EcoRI” / “Oligo_mTxnrd2_ClaI”. Since a *ClaI* site was included in the resulting 136 bp fragment, encoding the MLS, the product was cut with *EcoRI* and *ClaI*. In parallel, the start codon of the NTAPe in pcDNA-NTAPe was removed by means of site-directed mutagenesis (primer pair “Oligo_ClaI_for” / “Oligo_ClaI_rev”), yielding the vector pcDNA3-NoMetNTAPe. Subsequently, pcDNA3-NoMetNTAPe was digested with *EcoRI* and *ClaI* and ligated with MLS to generate pcDNA3-MLS-NoMetNTAPe. pcDNA3-MLS-NoMetNTAPe and pcDNA-NTAPe-cyto-Txnrd2 were then digested with *EcoRI* and *NheI*, and the 7156 bp backbone of the pcDNA-NTAPe-cyto-Txnrd2 vector and the 249 bp fragment of pcDNA3-MLS-NoMetNTAPe were ligated to obtain pcDNA3-NTAPe-mito-Txnrd2.

The expression vector p442L1 (kind gift from Dr. Tim Schroeder, Helmholtz Zentrum München) was used for efficient gene transfer and protein expression in MEFs by viral transduction.

Two fragments carrying mitochondrial (1992 bp) or cytosolic (1887 bp) NTAP-tagged versions of *Txnrd2* were cloned via *EcoRI* and *XhoI* into the backbone of p442L1 (7870 bp) to generate p442L1-NTAPe-cyto-Txnrd2 and p442L1-NTAPe-mito-Txnrd2. In any of these vectors the VENUS nuclear membrane anchor protein (VENUSnucmem) was replaced by the puromycin resistance cassette. This cassette was isolated from the plasmid

p442L1-NTAPe-Txnrd1 (kind gift from Pankaj Kumar Mandal, PhD thesis, 2009) using the restriction enzymes *BsrGI* and *SnaBI*. This fragment replaced VENUSnucmem in the p442L1-NTAPe-cyto-Txnrd2 and p442L1-NTAPe-mito-Txnrd2 plasmids to gain the p442L1-NTAPe-cyto-Txnrd2-puro and p442L1-NTAPe-mito-Txnrd2-puro vectors.

Generation of the xCT knock-in targeting vector (Rosa26 locus)

Murine *xCT* cDNA was isolated from the pCAG-3SIP-xCT. To this end, the vector was first linearised with *EcoRI*, blunt-ended by Klenow fill-in reaction, and the resulting vector was digested with *NheI* to obtain a 1653 bp long xCT-containing fragment. This fragment was ligated into the dephosphorylated backbone of the pBSIIKS-LMP1 (3133 bp) generated with *PmeI* and *XbaI*. pBSIIKS-mxCT was digested with *AscI* and the resulting 1913 bp fragment was then ligated into the *AscI*-digested and dephosphorylated pTVRosa26-EBNA1 (Hömig, 2005). The pTVRosa26-mxCT vector was then used for gene targeting in ES cells.

Generation of the xCT knock-in targeting vector (HPRT locus)

A 1913 bp long fragment containing the murine *xCT* cDNA was isolated from pBSIIKS-mxCT using *AscI*. The fragment was then ligated into the *AscI*-digested and dephosphorylated backbone pCAG-3SIP-STOP-EBNA1. The resulting vector pCAG-3SIP-STOP-mxCT was finally digested with *MluI* and *BstBI* to obtain the hCMVieE/chicken β -actin promoter, *mxCT* cDNA, *neoR* cassette that was then cloned into the backbone of pMB digested with *MluI* and *BstBI*. The vector pMB-mxCT was used for gene targeting.

Analysis of genomic DNA, RNA and proteins

Isolation of genomic DNA

Tissues and cultured cells were lysed in buffer containing 50 μ g/ml proteinase K. After lysis at 55°C overnight, DNA was subjected to phenol/chloroform/isoamyl alcohol extraction.

Lysis buffer: 10 mM Tris pH 7.6; 10 mM EDTA; 0.5% SDS; 10 mM NaCl

Proteinase K buffer: 50 mM Tris-HCl, pH 7.6, 5 mM EDTA pH 8

RNA isolation

For Northern blot analysis and RT-PCR total RNA from cultured cells (up to 1×10^6) or tissues (approx. 30 mg) was isolated with RNeasy Mini Kit (Qiagen) according to

manufacturers' instructions. In brief, the samples were lysed and homogenized in the appropriate amount of the denaturing guanidine-thiocyanate containing buffer, which immediately inactivates RNases to ensure purification of intact RNA. Ethanol was added to provide the proper binding conditions. The sample was then applied onto RNeasy Mini spin column, where the total RNA binds to the column and contaminants can be efficiently removed. To avoid DNA contaminations, on-column DNase digestion with the RNase-Free DNase Set (Qiagen) was performed. Total RNA was then eluted in 30–100 µl RNase-free water. RNA is generally stable at –80°C for up to one year without degradation. Final RNA concentrations were determined by measuring the absorbance at 260 nm in a spectrophotometer in triplicate (Spectrophotometer DU-64, Beckman Coulter GmbH, Krefeld, Germany).

Radioactive labelling of DNA fragment

Radioactively labelled DNA probes were used for Southern and Northern blots. The DNA fragments were labelled using Random Primed DNA Labeling Kit (Roche Diagnostics) and 50 µCi [gamma-³²P]-dCTP (3,000 Ci/mmol, 10 mCi/ml, GE Healthcare) according to manufacturers' instructions. The method of "random primed" DNA labelling (Feinberg et al 1983) is based on the hybridization of a mixture of all possible hexanucleotides to the DNA to be labelled. In brief, ~25 ng of linearised DNA template, dATP, dGTP, dTTP (25 µM each), hexanucleotide primer mixture, 1X reaction buffer, 50 µCi [gamma-³²P]-dCTP and 2 U Klenow enzyme were mixed in this order with denatured probe and incubated for 1 h at 37°C. Non-incorporated nucleotides were separated from the labelled probe by using Sephadex G-50 columns (GE Healthcare). Labelling efficiency was detected by using a bench-top radioisotope counter (Bioscan, Washington D.C., USA). Immediately before hybridisation, the probe was heat-denatured at 95°C for 5 min and placed on ice to prevent re-annealing of the labelled fragments.

Northern blot

Total RNA was isolated with RNeasy Mini Kit (Qiagen) according to manufacturers' instructions. Briefly, 10 µg of total RNA was dissolved in 1X volume of RNA loading buffer and incubated at 65°C for 5 min to minimize RNA secondary structures. RNA was separated on a 1% denaturing agarose gel, containing 2.2 M formaldehyde. Gels were run in 20 mM MOPS overnight in 1X MOPS buffer at 20 V. Upon separation equal loading of RNA samples was assessed by visualisation of the gel using UV (254 nm) trans-illuminator. Afterwards, RNA was transferred to an Immobilon-Ny+ membrane by capillary forces using 10X SSC

solution. The gel was placed up-side down on a glass plate and Whatman filter papers (dipped in reservoirs with 10X SSC solution). On top of the gel, the Immobilon-Ny+ membrane (humidified in deionised water), two Whatman filter papers and several layers of paper towel were placed. Finally, a glass plate and a weight were put on top of the staple. On the next day the RNA was cross-linked to the membrane by UV light (1,200 J/cm²), and thereafter pre-hybridised in Church buffer at 62°C for at least 1 h. Hybridisation was performed at 62°C overnight in 15-20 ml of fresh Church buffer, containing radioactively labelled probe. The membrane was washed twice with 2X SSC, 1% SDS for 15 min at 62°C and then twice with 0.1X SSC, 0.5% SDS for 10 min at 62°C. Subsequently, the membrane was exposed to an X-ray film (Amersham HyperfilmTMMP) overnight at -80°C.

Formaldehyde agarose gel: 2.2 M formaldehyde, 20 mM MOPS, 1% (w/v) agarose

MOPS buffer: 0.4 M MOPS (free acid), 100 mM Na-acetate, 10 mM EDTA/NaOH pH 8.0, pH 7.0 adjusted with 10 N NaOH

RNA loading buffer: 50% (v/v) formamide, 2.2 M formaldehyde, 1X MOPS buffer, 50 µg/ml ethidium bromide, 0.2% (w/v)

20X SSC: 3 M NaCl, 300 mM Tris-sodium citrate/NaOH pH 7.0

Immunoblotting

For Western blotting, tissue and cell lysates were prepared in LCW lysis buffer containing Protease Inhibitor Cocktail (Roche Diagnostics), sonicated (50% duty cycle and 5 ms of pulse width) and incubated for 15 min on ice. Prior to sonication tissue was additionally minced by using an overhead stirrer (Eurostar RW16, IKA-Labortechnik). Cell debris was removed by centrifugation at 15,000 rpm/4°C for 20 min. The protein concentration was determined by the DC Protein Assay (Bio-Rad) according to manufacturers' instructions. Equal amounts of protein lysates were mixed with sample loading buffer and heated for 5 min at 95°C prior to gel electrophoresis. The proteins were separated by 12% SDS-PAGE at constant 100 V in a 250/SE 260 Mini-Vertical Gel electrophoresis unit (Bio-Rad). After electrophoresis the proteins were transferred to a Hybond-C super nitrocellulose membrane (GE Healthcare) in blotting buffer with a Trans-Blot Semi-Dry Blotter (Bio-Rad) at ~800 µA constant current per 1 cm² of membrane for 1 h. The efficiency of protein transfer from the gel to the membrane was confirmed by staining the membrane with Ponceau S. The blots were blocked with 5% skim milk in TBST for 60 min and hybridized with a primary antibody in 5% BSA 1X TBS-T at 4°C overnight. On the next day, the blots were incubated with a HRP-conjugated secondary antibody for 60 min at room temperature. Afterwards, they were washed three times in 1X TBS-T for 15 min and visualized by ECL detection on Hyperfilm. Stripping of Hybond-C super membranes was performed with 0.2 M NaOH for 15 min at

room temperature. Prior to second hybridisation, the blots were blocked with 5% skim milk in 1X TBS-T for 60 min. All following steps were performed as described above.

6X sample loading buffer: 375 mM Tris pH 6.8, 9% (w/v) SDS, 9% (v/v) β -mercaptoethanol, 50% (v/v) Glycerol, 0.03% (w/v) Bromophenol Blue

10X running buffer: 250 mM Tris, 1% SDS, 2.5 M Glycine

Blotting buffer: 1X Running Buffer (10X), 20% Methanol

Ponceau S: 2% (w/v) Ponceau S in 30% TCA

TBS-T: 25 mM Tris, 125 mM NaCl, 0.1% Tween-20, pH 8.0

The production of antibodies against xCT and murine Txnrd2

The generation of antibodies, specific for human xCT, murine xCT and murine Txnrd2, was performed in collaboration with Dr. Elisabeth Kremmer (Helmholtz Zentrum München). Antibodies were raised against the different peptide sequences in rats. The peptides HHHHGRLPSLGNKEPPGQEKVGLKC and HHHHDKKPRWFRIMSEKITRC (both human xCT) and the peptides HHHHGRLPSMGDQEPGQEKVVLKC and HHHHDKKPKWFRRLSDRITRC (both murine xCT) were used to immunize rats. One peptide sequence was used to raise monoclonal antibodies for Txnrd2: VKLHISKRSGLIPTVTG. The peptides were obtained from Peptide Specialty Laboratories, Heidelberg, Germany and were coupled to ovalbumin (OVA) or bovine serum albumin (BSA) at the C-terminus (peptide-OVA/KLH). Monoclonal antibodies were produced by hybridoma fusion technology. Two hybridoma clones that produced antibodies specific for human xCT and six for Txnrd2 were identified among numerous supernatants that were tested by immunoblotting.

Immunocytochemistry and confocal microscopy

MEFs were plated on cover slips in 6-well cell culture dishes at ~75,000 cells per well and cultured in standard DMEM. For fixation, the medium was aspirated from the cell culture dish, and the cover slips were rinsed with PBS. The cells were fixed for 15 min in a 2% PFA solution. The cover slips were washed with PBS, and the cells were permeabilized three times for 5 min with 0.15% Triton X-100 in PBS. Subsequently, unspecific binding was blocked by using PBS⁺ three times for 10 min. The cover slips were incubated overnight with the primary antibody at 4°C in a humidified chamber. Thereafter, cover slips were washed for 5 min with PBS and subsequently with PBS/Triton (0.15%) for 10 min twice and finally for 10 min in PBS⁺. Cells were then incubated with a fluorophore-labelled secondary antibody in the dark for 45 min. Cover slips were washed twice for 5 min in PBS/Triton (0.15%) and twice for 7 min in PBS. Finally, DAPI-solution was added for 90 s, and the cells were subjected to

two final washing steps with PBS for 2 min. The glasses were mounted onto microscope slides, using mounting medium (Dako, Cytomation). The slides were dried overnight at 4°C, protected from light and sealed with nail polish. The pictures were taken by confocal microscopy with Leica DM IRBE microscope, Leica TCS SP2 scanner by using Leica Confocal software.

2% PFA: 2% (w/v) PFA in PBS

PBS⁺: 1% (w/v) BSA, 0.15% (w/v) Glycin in PBS

DAPI-solution: 1:10,000 in PBS

2.2.4. Flow cytometry

Detection of intracellular ROS

Dichlorofluorescein diacetate (DCFH-DA, Invitrogen) was used as an indicator for monitoring intracellular ROS. DCFH-DA is cell permeable and diffuses across cell membranes, whereupon it is hydrolysed by intracellular esterases to yield dichlorofluorescein (DCFH), a nonfluorescent compound. DCFH can be oxidized by various types of ROS to the fluorescent compound DCF. In order to monitor cellular ROS, cells ($\sim 5,5 \times 10^4$) were plated and incubated with 2 μ M dichlorofluorescein diacetate (DCFH-DA) in DMEM for 1 h at 37°C, 5% CO₂ in a water-saturated atmosphere in the dark. After incubation cells were harvested, transferred into the round bottom polypropylene tubes, washed in PBS and resuspended in ~ 200 μ l PBS. Cellular fluorescence intensity was measured in a flow cytometer (BD FACSCalibur) using an excitation wavelength of 448 nm and measured at 530 nm emission (FL-1). The recorded results were analysed using CellQuest™ software (Becton Dickinson). As a cut-off value for obtaining significant values the number of at least 8,000 cells was used.

DCFH-DA solution: 2 mM DCFH-DA in ethanol

Detection of lipid peroxidation

BODIPY581/591 C₁₁ is a lipophilic fluorescent compound that readily intercalates into membranes and upon oxidation shifts its fluorescence from red to green. Thus, it can be used to efficiently monitor lipid peroxidation. For this purpose, $\sim 5,5 \times 10^4$ cells were plated and incubated with 2 μ M BODIPY in DMEM for 1 h at 37°C in a 5% CO₂ water-saturated atmosphere in the dark. After incubation, the cells were harvested and treated as described above (2.5.1). Cellular fluorescence intensity was measured in a flow cytometer (BD

FACSCalibur) in the FL-1 (green) and FL-3 (red) channels. Cell populations of interest were gated and analysed using CellQuest™ software (Becton Dickinson). As a cut-off value for obtaining significant values the number of at least 8,000 cells was used.

BODIPY581/591 C₁₁ solution: 2 mM BODIPY581/591 C₁₁ in DMSO

Specific detection of hydrogen peroxide in living cells

New boronate-based compounds (kind gift of Dr. Christopher J. Chang, University of California, Berkeley, California (Chang et al., 2004a; Dickinson and Chang, 2008; Miller et al., 2005) allow the specific detection of H₂O₂ within the cell, which is produced due to environmental stress and/or accumulate due to genetic manipulation of antioxidant enzymes. These new fluorophores allow to measure H₂O₂ levels also in different subcellular compartments including mitochondria (mitochondria peroxy yellow 1). For H₂O₂ determination by flow cytometry, ~5,5 x 10⁴ cells were plated one day prior to analysis. After overnight cultivation, the standard medium was exchanged with DMEM. The cells were incubated with 2.5 µM of Peroxi-yellow acetoxy methyl-ester (PYAM), Peroxi-yellow methyl-ester (PYME) and mitochondrial Peroxi-yellow (mitoPY) for 1 h at 37°C in a 5% CO₂ water-saturated atmosphere protected from the light. After incubation, cells were treated as described under 2.5.3. Cellular fluorescence intensity was measured with a flow cytometer (BD FACSCalibur) in FL-1 (green) channel with an excitation wavelength of 450 nm. Cells were gated and analysed using CellQuest™ software (Becton Dickinson). As a cut-off value for obtaining significant values the number of at least 8,000 cells was used.

Boronate-based compounds: 2 mM in DMSO

Determination of cell viability by flow cytometry

Assessment of cellular DNA content

To measure genomic DNA fragmentation and nuclear DNA content, propidium iodide (PI) staining of DNA was used. The cells were harvested by trypsinisation, washed with PBS and fixed in 2% of formaldehyde for 30 min on ice. After fixation, cells were permeabilised with ice cold 100% ethanol for 15 min, pelleted and resuspended in PBS containing RNAase A (40 µg/ml). After 30 min incubation at 37°C, cells were harvested and diluted in ~200 µl of PBS. The cells prepared in this way are stable for 1 month at 4°C. The fluorogenic dye PI intercalates into double-stranded DNA. Cell suspensions were excited with 488 nm and PI emission was recorded on channel FL3 at 661 nm.

2% formaldehyde: 2% v/w formaldehyde in PBS

PI solution: 1 mg/ml PI in PBS

Staining of apoptotic cells by Annexin V-FITC/PI

One hallmark of apoptotic cells is the translocation of the membrane glycerophospholipid, phosphatidylserine (PS), from the inner to the outer leaflet of the plasma membrane. Annexin V is a 35-36 kDa Ca^{2+} -dependent phospholipid-binding protein that has high affinity for PS. Annexin V is very sensitive and detects PS exposure occurring early in the onset of apoptotic cells. Annexin V-FITC is typically used in conjunction with a dye that stains for dead cells, such as propidium iodide (PI), to distinguish early apoptotic cells (Annexin V-FITC-positive, PI-negative) from late cell death (Annexin V-FITC-positive, PI-positive). During the various steps of classical apoptosis, cells are first Annexin V-FITC-positive/PI-negative and then during late phases Annexin V-FITC-/PI-double positive. In non-classical forms of apoptotic cell death, it has been described that Annexin V-FITC-positive/PI-negative can never be detected and only Annexin V-FITC-/PI-double positive cells are evident. To detect apoptotic cells, approximately 1×10^5 cells were harvested and washed with PBS. Collected cells were resuspended in ~150 μl binding buffer containing Annexin V-FITC at a concentration of 1 mg/ml and incubated in the dark at room temperature. After 30 min of incubation, 50 $\mu\text{g}/\text{ml}$ propidium iodide (PI) in PBS was added and cells were subjected to flow cytometry (BD FACSCalibur) with FL-1 (green) and FL-3 (red) channels with an excitation wavelength of 488 nm. Cell populations of interest were analysed using CellQuestTM software (Becton Dickinson). Data were collected from at least 8,000 cells.

10X Annexin V binding buffer: 0.1 M Hepes/NaOH (pH 7.4), 1.4 M NaCl, 25 mM CaCl; Store at 4 °C.

Microscopy pictures

Pictures of cells were taken with Axiovert Microscopes (Carl Zeiss, Jena GmbH, Germany) and processed using Improvision Openlab 3.0.8 software.

2.2.5. Biochemical methods

Determination of cellular cystine uptake activity

Cystine uptake activity was determined by measuring the time-dependent increase of radioactively labelled L-[^{14}C (U)] cystine inside cells as described (Bannai and Kasuga, 1985). Approximately 1×10^6 cells were plated per 6 cm cell culture dish in DMEM, and incubated for 24 h. Cells were washed with pre-warmed PBS(+), followed by the addition of 500 μl uptake solution and further incubation at 37°C for 90 s. To control for the specific uptake activity of system x_c^- , 2.5 mM glutamate was added to the uptake solution. The uptake solution was aspirated, cells were quickly washed with ice-cold PBS and lysed in 500 μl 0.5 M NaOH overnight. The protein concentration of the samples was determined by the DC Protein Assay (Bio Rad). Then, 200 μl cell lysate, 3 ml scintillation cocktail and 100 μl 0.2 M Tris-HCl were mixed in a scintillation tube. The amount of L-[^{14}C (U)] cystine was determined by a LS 500 TA Scintillation Counter. To correlate cystine concentration and radioactivity, 5 μl Uptake Solution (50 μM cystine) was mixed with 500 μl 0.5 M NaOH and the “specific activity” of L-[^{14}C (U)] cystine was measured. The cellular cystine uptake activity is expressed as nmol cystine $\text{min}^{-1} \text{mg}^{-1}$.

Uptake solution: 50 μM cystine, 0.2 $\mu\text{Ci/ml}$ [^{14}C (U)] cystine, 10% glucose, 1% CaCl_2 , 1% MgCl_2 in PBS. 5 mM cystine stock solution was dissolved in 0.05 M HCL with stirring for several hours at room temperature.

PBS(+): PBS, 10% glucose, 1% CaCl_2 , 1% MgCl_2

GSH determination by HPLC

Estimation of glutathione was done by method described for estimation of homocysteine with slight modification (Feussner et al., 1997). The HPLC system consisted of a System Gold 126 pump, connected to a System Gold 508 autosampler (both Beckman Coulther GmbH, Krefeld, Germany) and a RF-10A XL fluorescence spectrophotometer (Shimadzu, Duisburg, Germany). The mobile phase consisted of 95% of 30 mM ammonium-formiate, 40 mM ammonium-nitrate buffer (adjusted to pH 3.65 with formic acid) and 5% of acetonitrile. The column effluent was monitored by fluorescence detection with an excitation wavelength of 385 nm and an emission of wavelength of 515 nm.

Intracellular GSH levels were measured in *Txnrd2* knock-out cells. Cells were plated 24 h prior to GSH measurements in 10 cm diameter dishes. Cells were harvested from cell culture dishes with the cell scraper, washed in PBS, resuspended in 500 μl Borate Buffer 1 and

homogenized by sonication (50% duty cycle, 5 ms of pulse width). For GSH determinations, samples (200 µl) were treated on ice with 20 µl 100 µl/l tri-*n*-butylphosphine in dimethylformamide for 30 min in order to reduce thiols and liberate them from proteins. 200 µl perchloric acid was added to the samples, mixed and incubated for 10 min on ice. Proteins were removed by centrifugation at 10,000 x g for 10 min at 0°C. 100 µl of the supernatant, 250 µl Borate Buffer 2 and 100 µl (SBDF) were mixed and incubated at 60°C for 60 min. To terminate the SBDF derivatization step, the solutions were snap-cooled on ice and transferred to a pre-cooled autosampler vial. Aliquots of 50 µl were injected into the column. Standard samples of GSH (1 to 25 µM) were prepared by serial dilution in Borate Buffer 1.

Borate buffer 1: 0.2 M boric acid, containing 2 mM Na₂EDTA, pH 9.5

Borate buffer 2: 0.2 M boric acid, containing 5 mM Na₂EDTA, pH 10.5

Perchloric acid: 0.5 M perchloric acid, containing 1 mM Na₂EDTA

SBDF: 1.0 g/l 7-fluoro- benzo-2-oxa-1.3-diazole-4- sulphonate in 0.1 M Borate Buffer 1

2.2.6. ES cell technology

E14tg2a ES cell line

The maintenance of ES cell cultures is far more elaborate than that of many other cell lines. The major reason for this is to maintain the pluripotent state of ES cells. The E14tg2a ES cell line had been previously adapted for the growth on 0.1% gelatine-coated cell culture dishes. ES cells were cultured at 37°C in a 5% CO₂ water-saturated atmosphere in E14 media containing LIF (leukaemia inhibitory factor) to prevent differentiation of ES cells. To minimize the risk of differentiation, ES cells were plated as a single cell suspension of approximately 1.5×10^5 - 4×10^5 cells per cm². The medium was replaced every day and the cells were generally split every other day at ~80% confluency at ratios between 1:4 and 1:10.

ES cell medium: Stempan medium (PAN-Biotech GmbH, Stempan GMEM prepared mix: L-Glutamine, 3.7 g/l NaHCO₃), ESGRO (LIF) 500 U/ml

Gene targeting in E14tg2a ES cells

ES cells were grown to ~80% confluency and harvested by trypsinization. A small aliquot was taken to determine the cell number. The rest of the cells were collected by centrifugation, resuspended in PBS to a density of 7×10^6 and washed two times in PBS and kept on ice. Twenty µg of linearised targeting vector was used for each transfection using an electric pulse of 240 V and a capacitance of 500 µF in electroporation cuvettes with 0.4 cm

gap width (Bio-Rad). After transfection, cells were allowed to recover at room temperature for 10 min. The cell suspension was transferred into E14 medium and plated in 10 cm diameter cell culture dishes coated with 0.1% gelatine. Selection for antibiotic resistance was initiated 36 h after electroporation with 200 µg/ml G418-Sulfate. As a control, one plate of non-transfected ES cells was plated and treated as transfected cells. Cells were kept under selection pressure for the next 9-10 days. Neomycin-resistant single cell colonies appeared and were visible by eye. Approximately 10 days after electroporation, individual ES cell clones were picked with a pipette and transferred to a gelatine-coated 96-well containing ES cell medium. The clones were left over night to attach to the dish, and on the next day they were washed in PBS and trypsinized to obtain single cells. These were re-plated in a fresh 96-well plate and allowed to grow until ~80% confluency was reached. Afterwards, cells were split 1:3. Two replica plates were frozen after they reached ~80% confluency for expansion of positive clones. One replica plate was further expanded (1:3) for Southern blot analysis in order to identify the clones with homologous recombination.

E14 medium: Stempan medium (PAN-Biotech GmbH; Stempan GMEM already prepared mix: L-Glutamine, 3.7 g/l NaHCO₃), ESGRO (LIF) 100 U/ml)

Freezing of ES cells in 96 well plates

ES cells that were used for further electroporation or used in blastocyst injection were frozen in E14 medium containing 10% DMSO. ES cell clones that were picked after electroporation with the targeting construct and selection were frozen in E14 medium containing 10% DMSO directly in the 96 plates. After reaching proper confluency cells were washed with PBS, trypsinized in 25 µl trypsin and resuspended. 200 µl of 10% DMSO E14 medium was used to inactivate the trypsin and as a freezing medium. The 96-well dishes were wrapped with Laboratory Parafilm M (Pechiney Plastic Packaging Company) and paper towels and stored at -80°C not longer than 6 weeks.

Isolation of genomic DNA

To screen for homologous recombination of the targeting construct by Southern blot, genomic DNA was isolated directly from 96 wells. The amount of DNA obtained with this method is sufficient for Southern blot analysis in a 96 well format. After cell lysis overnight, DNA was precipitated in 2X volumes of 100% ethanol/150 mM NaCl at constant shaking for 15 min at room temperature. DNA was collected by centrifugation of the 96 well plates at 1,000 rpm for 5 min at 4°C. Afterwards, the DNA was washed three times with 70% ethanol.

After air-drying, DNA samples were dissolved in 50 µl 1X TE and stored at -20°C until further analysis.

Southern blot

Approximately 10 µg of DNA was digested with the corresponding endonuclease at 37°C overnight. Since DNA isolated in described way (as described in subsection 2.2.3.) was not very pure, spermidine (4 mM final concentration) was added to allow more efficient DNA digestion. The next day DNA fragments were separated on a 1% 1X TAE ethidium bromide-stained agarose gel in 1X TAE. Before blotting the DNA on the Immobilon-Ny+ membrane (Millipore), the gel was incubated in 0.25 N HCl with gentle shaking for 15 min and for DNA denaturation for 1 h in denaturation buffer. DNA was transferred to the Immobilon-Ny+ membrane by capillary forces overnight. After blotting, the membrane was shortly washed in 2X SSC and pre-hybridised for at least 1 h at 62°C in Church buffer (hybridisation buffer). Finally radioactively labelled probe was added to the hybridisation buffer and hybridised overnight at 62°C in hybridisation buffer. The next day the membrane was washed three times for 10 min in washing buffer at 62°C and exposed to an X-ray film (Amersham HyperfilmTMMP) overnight at -80°C.

Denaturation buffer: 1.5 M NaCl, 0.5 N NaOH

20X SSC: 3 M NaCl, 300 mM Trisodiumcitrat, NaOH pH 7.0-optional

Church buffer (hybridisation buffer): 200 mM NaH₂PO₄, 400 mM Na₂HPO₄, 7% (w/v) SDS, 1 mM EDTA, pH 7.1-7.2

Washing buffer: 0.5% SDS, 0.2X SSC

Blastocyst injection of ES cells

Clones with successful homologous recombination were identified by Southern blot (as described in section 2.2.3). Positive clones were thawed and individually expanded for blastocyst injection. The clone was split 1:2 24 h before blastocyst injection. On the day of blastocyst injection the cells were harvested in the usual way, washed in PBS and injected into C57BL/6 blastocysts at the Institute of Experimental Genetics (IEG), Helmholtz Zentrum München. Embryonic Stem cells reintroduced into host blastocysts can contribute to all adult tissues, including germ cells, if the cells used for blastocyst injection were still pluripotent. After injection, 15-20 manipulated blastocysts were re-implanted in pseudo-pregnant foster mice. Chimeric mice were born and subsequently bred with C57BL/6 for germ line transmission.

3. Results

3.1. Functional analysis of mitochondrial thioredoxin reductase (Txnrd2)

3.1.1. Phenotype of primary MEFs lacking Txnrd2

To explore the functions of thioredoxin reductase 2 (Txnrd2) in physiology and disease development, *Txnrd2* knock-out mice have been previously created in our laboratory (Conrad et al., 2006) (Figure 6). To establish *Txnrd2*^{-/-} and *Txnrd2*^{+/-} cell lines, mice heterozygous for *Txnrd2* allele were mated and inspected daily for vaginal mucous plug. Since *Txnrd2* knock-out mice die between E13.5 and E15.5, primary MEFs were isolated from E13.5 embryos. To verify the knock-out, semi-quantitative RT-PCR with mRNA isolated from the cells was performed (Figure 16 A). A primer pair covering the deleted region (Txnrd2E15-18) of the *Txnrd2* gene was used. *18s rRNA* transcripts served as a control. The absence of Txnrd2 protein in the MEFs was further confirmed by immunoblotting using an anti-Txnrd2 antibody (Figure 16 B). As illustrated in Figure 16, full-length *Txnrd2* mRNA and Txnrd2 protein levels were absent in knock-out cells, but clearly detectable in the control cell lines.

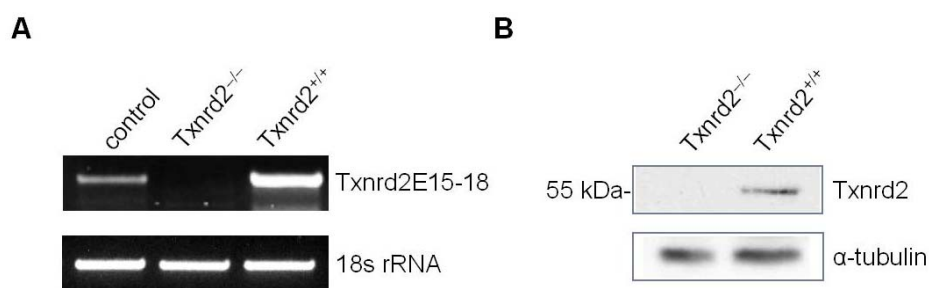


Figure 16. Analysis of Txnrd2 expression in isolated primary MEFs. (A) Semi-quantitative RT-PCR analyses of mRNA isolated from primary MEFs was conducted using a primer pair spanning the coding region of exon 15 to exon 18 (for further details see figure 6). (B) Lack of Txnrd2 expression was also confirmed by Western blotting. The 55 kDa band corresponds to the expected molecular weight of Txnrd2 that was detectable in *Txnrd2*^{+/-} cells, but not in *Txnrd2*^{-/-} cells.

As previously shown (Conrad et al., 2004), cell proliferation rates of primary *Txnrd2*^{-/-} MEFs were significantly lower than that of wild-type counterparts, although the underlying reasons remained widely elusive. To recapitulate the previously observed proliferation defects, equal cell numbers were plated and cell proliferation was monitored over a period of six days. As shown in Figure 17 A, cell proliferation of knock-out cells was markedly decreased compared to wild-type cells.

To compare the cell cycle profiles of primary *Txnrd2*^{-/-} and *Txnrd2*^{+/+} fibroblasts, total DNA was stained with PI. Flow cytometry analysis revealed no alterations in cell cycle distribution between wild-type and knock-out cells (Figure 17 B). Likewise, the size (FSC) and granularity (SSC) of the cells was not changed in *Txnrd2*^{-/-} cells (Figure 17 C and D).

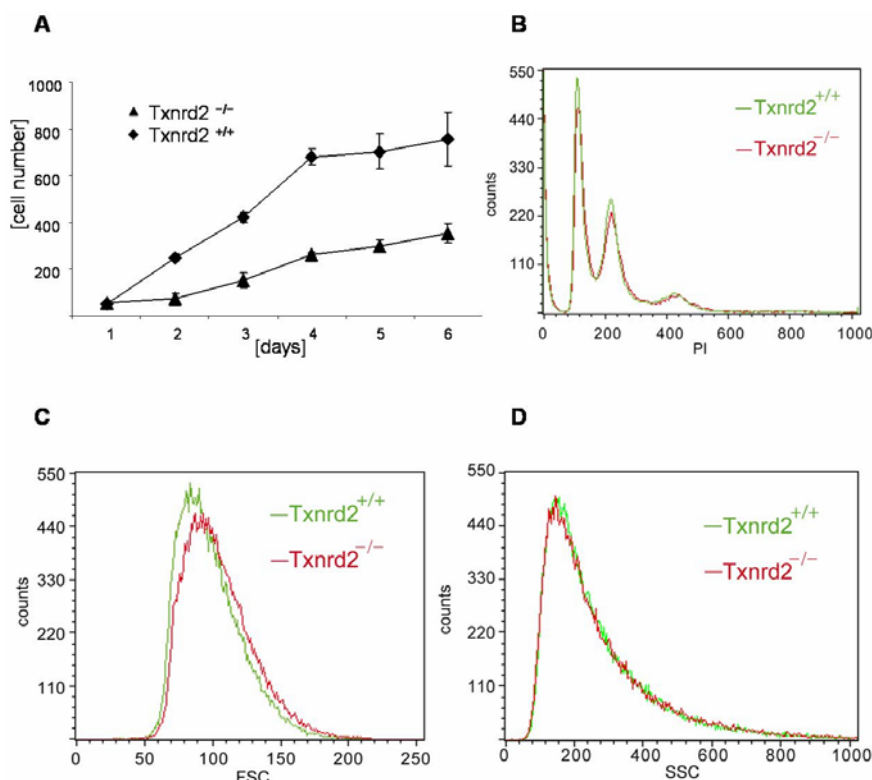


Figure 17. Determination of cell proliferation, cell cycle distribution, cell size and cell granularity of *Txnrd2*^{+/+} versus *Txnrd2*^{-/-} primary MEFs. (A) Primary *Txnrd2*^{-/-} fibroblasts showed a strongly decreased proliferation rate compared to *Txnrd2*^{+/+} cells, confirming previous findings. (B) Cell cycle analysis by measuring total DNA content by PI did not reveal any differences in the cell cycle distribution of KO and WT cells. (C, D) The intensity of the forward and side scatter did not show any alterations in cell size nor in the granularity between wild-type and knock-out cells.

3.1.3. Antioxidants rescue loss of *Txnrd2*

In order to investigate whether the impairment of cell growth of the knock-out cells is due to high levels of intracellular ROS, various antioxidants were included in the proliferation experiments. N-acetylcysteine (NAC), α -Tocopherol (α -Toc), glutathione (GSH) and sodium-selenite (NaSe) were used to test this hypothesis. Increasing concentrations of water-soluble (NAC, GSH and NaSe) and lipophilic (α -Toc) antioxidants were added to the cell culture medium at the same time when the cells were plated. The number of viable cells was determined 72 h later by trypan blue exclusion. The growth of *Txnrd2*^{-/-} cells was clearly augmented with increasing concentrations of GSH compared to untreated *Txnrd2*^{-/-} cells.

When compared to *Txnrd2*^{+/+} cells, *Txnrd2*^{-/-} cells showed an equal proliferation rate at 2 mM GSH (Figure 18 A). Addition of 500 nM α-Toc (Figure 18B) and 1mM NAC (Figure 18 B) increased the proliferation rate of *Txnrd2*^{-/-} cells so that knock-out cells proliferated similarly to wild-type cells (Figure 18 C). 100 nM NaSe fully restored proliferation of *Txnrd2*^{-/-} as compared to *Txnrd2*^{+/+} cells, while higher concentrations of NaSe slowed down rather than accelerated the proliferation of knock-out cells (Figure 18 D).

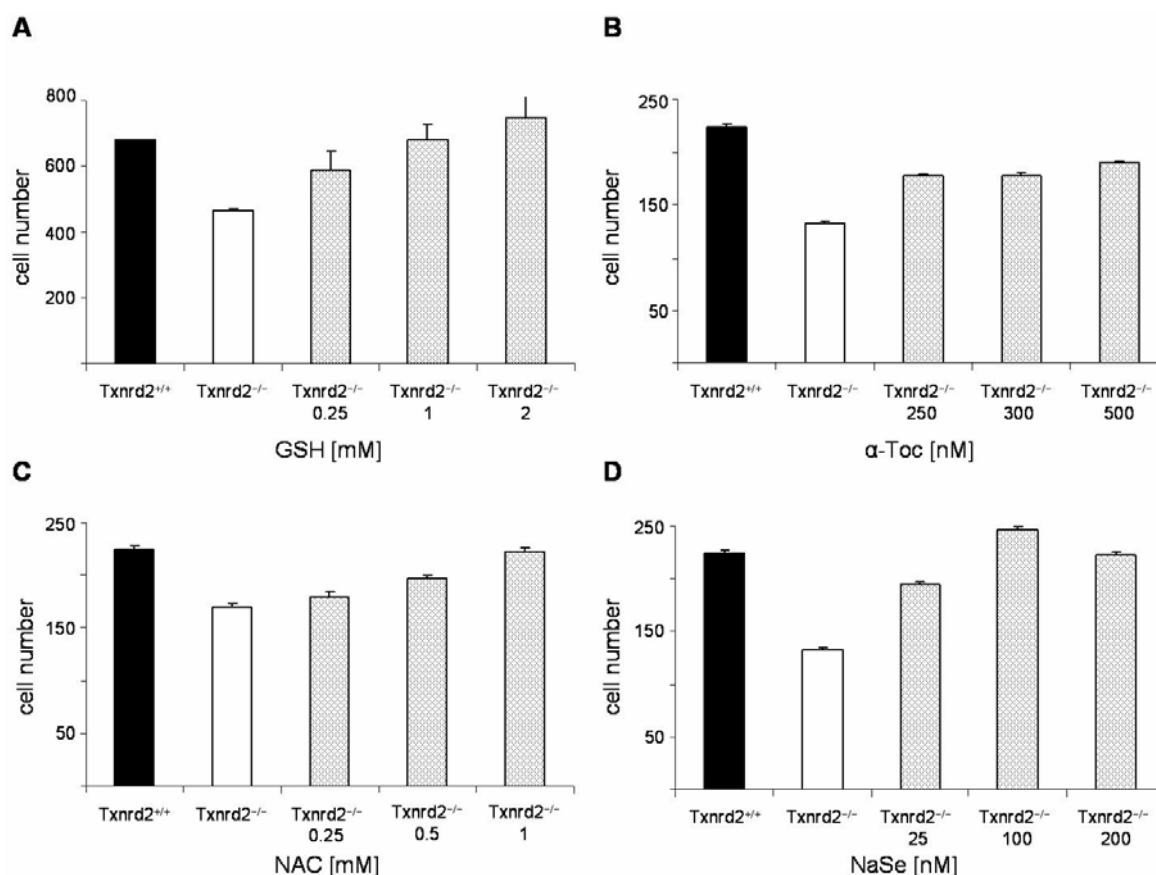


Figure 18. Antioxidant supplementation restored the proliferation defects of *Txnrd2*^{-/-} cells. (A, B, C) At any concentration used, addition of GSH, α-Toc and NAC improved growth of *Txnrd2*^{-/-} cells. (D) At lower concentrations, NaSe supplementation was beneficial, whereas at higher concentrations became toxic.

3.1.4. Intracellular ROS are augmented in cells lacking *Txnrd2*

Since the thioredoxin 2/thioredoxin reductase 2/peroxiredoxin 3 system has been considered to play a major role in controlling mitochondrial ROS levels, it was hypothesised that the impairment of this system may lead to increases in cellular ROS concentrations. To address this question, MEFs were seeded in the presence or absence of different antioxidants and stained 24 h later with different fluorescent dyes to monitor for intracellular ROS accumulation. Compared to control cells, *Txnrd2*^{-/-} cells exhibited a significant increase (one order of magnitude) in basal ROS content, as quantified by flow cytometry using DCFH-DA

as a non-specific ROS sensor (Figure 19 A). The ROS accumulation in *Txnrd2*^{-/-} cells could be strongly decreased by antioxidant supplements, such as NAC or α -Toc, compared to untreated cells, however not to wild-type levels (Figure 19 B).

Since DCFH-DA does not allow discriminating between soluble ROS, such as H₂O₂, O₂⁻ and lipid peroxides (Bilski et al., 2002; Ohashi et al., 2002), BODIPY 581/591 C₁₁ was utilized to assess the amount of lipid peroxidation (Drummen et al., 2002; Itoh et al., 2007). BODIPY 581/591 C₁₁ intercalates into lipid bilayers and shifts its fluorescence from red to green upon oxidation. As shown in Figure 19 C (left), *Txnrd2* knock-out cells showed clearly increased lipid peroxidation when compared with wild-type cells. Culturing *Txnrd2*^{-/-} cells in the presence of NAC for 24 h did not decrease the amount of lipid peroxides in knock-out cells (Figure 19 C middle), whereas treatment of *Txnrd2*^{-/-} cells with α -Toc reduced the amount of lipid peroxides almost to wild-type background levels (Figure 19 C, right).

For specific H₂O₂ measurements, we obtained boronate-based fluorophores, such as peroxi-yellow acetoxymethyl-ester (PYAM), peroxi-yellow methyl-ester (PYME) and mitochondrial peroxi-yellow (mitoPY) from Dr. Christopher Chang (University of California, Berkeley, California, USA) (Chang et al., 2004a; Dickinson and Chang, 2008; Miller et al., 2005). These reagents are passively loaded into living cells and detection of H₂O₂ is based on the hydrolytic deprotection of the boronates with H₂O₂ which produce fluorescent product. When PYAM was used as an H₂O₂ indicator, *Txnrd2* knock-out cells displayed significantly higher fluorescence compared to wild-type cells (Figure 19 D left). Also, when PYME and mitoPY were used, knock-out cells exhibited a higher shift in green fluorescence (Figure 19 D middle and right), indicating an increase of basal H₂O₂ in the cytosol and mitochondria.

3.1.5. Susceptibility of *Txnrd2*^{-/-} cells towards pro-oxidants and genotoxic agents

As *Txnrd2*^{-/-} cells showed higher levels of ROS, it was hypothesized that *Txnrd2*^{-/-} cells are more susceptible towards genotoxic agents and agents which induce additional oxidative stress. Therefore, knock-out and wild-type cells were treated with pro-oxidants and genotoxic agents over a wide range of different concentrations, and the cell viability was analysed by trypan blue exclusion 72 h after the onset of treatment.

As illustrated in Figure 20, *Txnrd2* knock-out cells were only marginally more sensitive to the two anticancer drugs doxorubicine and cisplatin (Figures 20 A and B), whereas H₂O₂ and

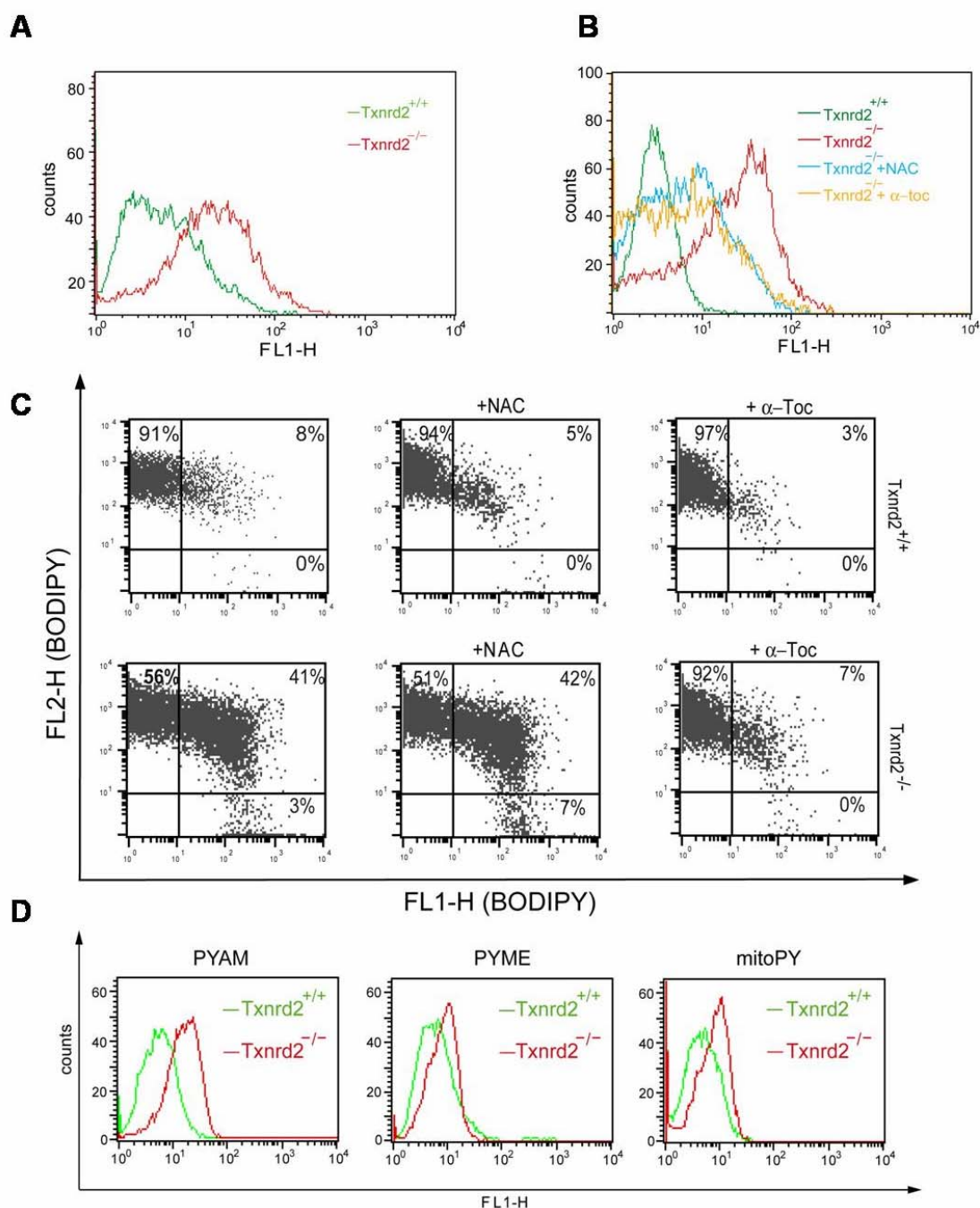


Figure 19. Txnrd2 ablation *in vitro* caused high intracellular ROS levels. (A) High levels of ROS were detected by flow cytometry in *Txnrd2* knock-out MEFs using the non-selective ROS sensor DCFH-DA. Cells were analysed 24 hours after seeding. (B) The strong increase of intracellular ROS in knock-out cells could be dampened by the antioxidants NAC (500 μ M) and α -Toc (500 nM) to some extent, but not to background levels. (C) BODIPY 581/591 C₁₁ staining revealed substantial lipid peroxidation in knock-out cells which was insensitive to NAC, but which could be prevented by the lipophilic antioxidant α -Toc. Antioxidants were added to the cells at the time of plating. (D) Monitoring cellular ROS with the H₂O₂-specific boronate-based fluorophores PYAM, PYME and mitoPY revealed markedly increased H₂O₂ concentrations in the cytosol (PYAM, PYME) and mitochondria (mitoPY).

t-butylhydroperoxide (BOOH) readily induced cell death in *Txnrd2* null cells even at very low concentrations compared to wild-type cells (Figures 20 C and D). β -phenylethyl isothiocyanate (PEITC), which is present in consumable cruciferous vegetables (Yu et al., 1998), was also used in these experiments, because recent studies suggested that this

compound increases ROS and induces apoptosis in cancer cell lines (Trachootham et al., 2006; Wu et al., 2005; Yu et al., 1998; Zhang et al., 2003). In addition, it was shown that PEITC causes rapid oxidation of mitochondrial Prx III (Brown et al., 2008). Similarly to H_2O_2 and *t*-butylhydroperoxide, *Txnrd2*^{-/-} cells were clearly more vulnerable to increasing PEITC concentrations than wild-type cells (Figure 20 E).

The antibiotic antimycin A interrupts the electron flow from semiquinone to ubiquinone in the Q-cycle of complex III of the respiratory chain. Antimycin A is thus regarded to trigger the formation of large quantities of superoxide anion. When *Txnrd2*^{-/-} cells were treated with antimycin A, they died already at very low concentrations, while wild-type cells were clearly more resistant to antimycin A (Figure 20 F).

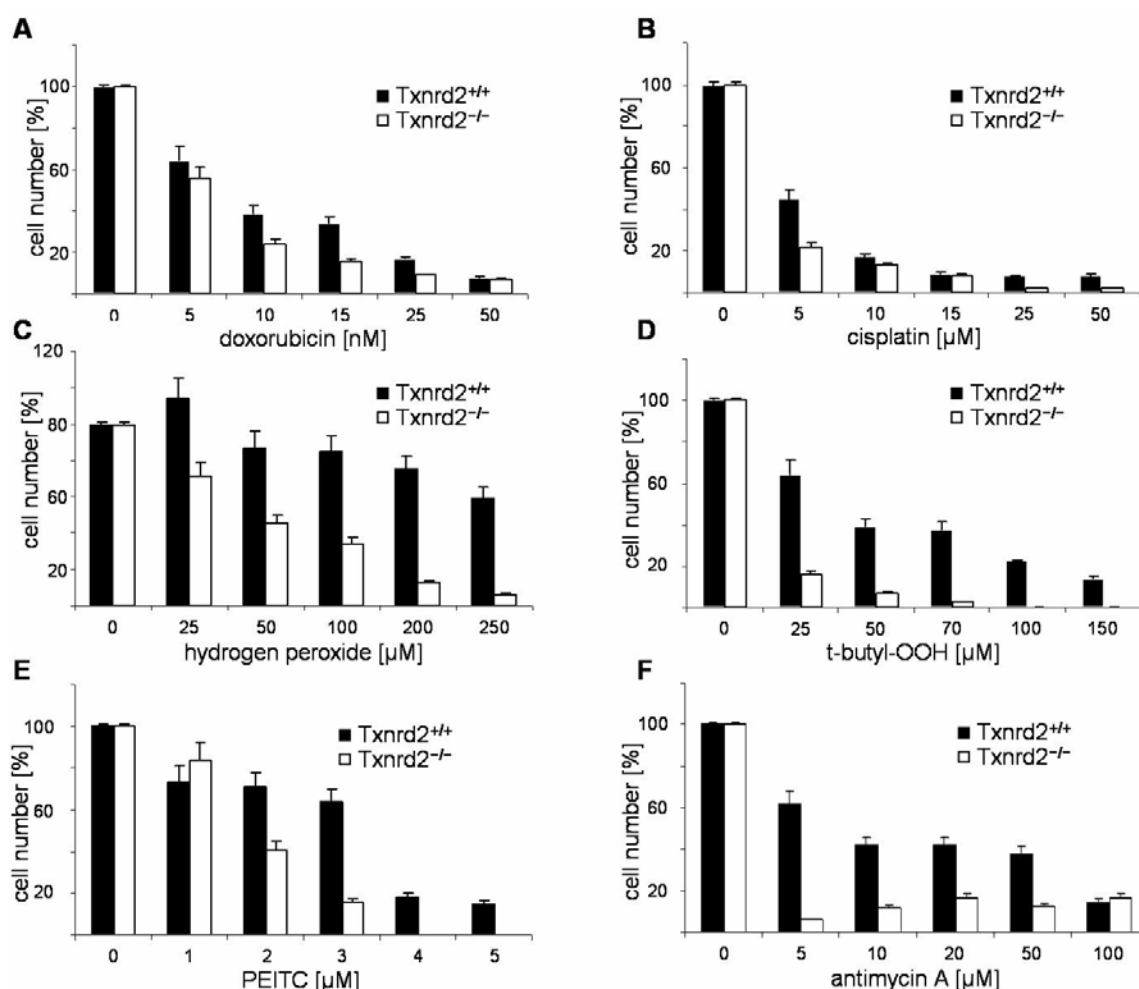


Figure 20. *Txnrd2*^{-/-} cells are highly sensitive to pro-oxidants, but almost equally resistant to genotoxic agents. The same number of the knock-out and wild-type cells was seeded in the presence of different pro-oxidants and genotoxic agents, and cell viability was determined 72 h later by trypan blue exclusion. (A, B) *Txnrd2*^{-/-} and *Txnrd2*^{+/+} control cells were almost equally resistant to the anticancer drugs doxorubicin and cisplatin. (C, D) *Txnrd2*^{-/-} MEFs rapidly died in response to increasing concentrations of H_2O_2 and *t*-butylhydroperoxide and to a lesser extent when PEITC was used (E). (F) Antimycin A triggered rapid cell death in *Txnrd2*^{-/-} cells already at very low concentrations. Each value represents the mean \pm S.D from triplicate assays.

From these findings one can conclude that *Txnrd2*^{-/-} cells show high levels of overall cellular ROS, which can be partially blunted by antioxidants, and that *Txnrd2*^{-/-} cells are highly susceptible to pro-oxidants but not to genotoxic agents.

3.1.6. Sensitivity of *Txnrd2*^{-/-} cells towards inhibition of de novo GSH biosynthesis

Reportedly, *Txnrd2* knock-out cells are highly susceptible to GSH depletion induced by L-buthionine sulfoximine (BSO), a highly specific and irreversible inhibitor of γ -glutamyl-cysteinyl-synthetase (γ -GCS) (Conrad et al., 2004). γ -GCS catalyses the first and rate-limiting step of GSH synthesis. To test whether *Txnrd2*^{-/-} cells may show differences in basal intracellular GSH concentrations, total (GSH) and oxidised (GSSG) GSH levels were determined by HPLC analysis. Interestingly, *Txnrd2*^{+/+} cells showed considerably higher level of GSH than knock-out cells, while GSSG levels were comparable in both cell types (Figure 21 A). As the ratio between the level of glutathion (GSH) and oxidised glutathione (GSSG) determines the capability of the cells to buffer an increase in ROS, this finding explains the highly increased sensitivity of *Txnrd2*^{-/-} cells to additional exogenous oxidative stress.

Next, the effects of experimental GSH depletion on cell survival and cell death was investigated more thoroughly. Preferential killing of the *Txnrd2*^{-/-} cells was further demonstrated by treatment of the cells with increasing BSO concentrations. As illustrated in Figure 21 B, *Txnrd2*^{-/-} cells rapidly died already at very low BSO concentrations. 72 h after treatment, 5 μ M BSO caused cell death in 59% of the knock-out cells and only in 16% of *Txnrd2*^{+/+} cells. Overall, *Txnrd2*^{+/+} cells were much more resistant to BSO: about 50% of *Txnrd2*^{+/+} cells were still viable at 20 μ M BSO, whereas *Txnrd2*^{-/-} cells had invariably been killed by this BSO concentration (Figure 21 B).

Next, total ROS levels were measured in wild-type and knock-out cells by DCFH-DA in response to BSO-induced GSH depletion. Treatment of *Txnrd2*^{-/-} cells with increasing concentrations of BSO caused a strong increase of ROS in these cells (almost 2 orders of magnitude) compared to untreated knock-out and wild-type as well as BSO-treated wild-type cells (Figure 22 A). Interestingly, ROS levels in *Txnrd2*^{+/+} cells treated with 15 μ M BSO were comparable to that of untreated *Txnrd2*^{-/-} cells (Figure 22 B).

In order to address whether *Txnrd2* knock-out cells die in an apoptotic manner in response to BSO-mediated GSH depletion, cells were stained with AnnexinV-FITC/PI and analysed by

flow cytometry. During “classical” apoptosis, phosphatidylserine (PS), which normally resides at the inner side of the plasma membrane, is externalised, and thus can be used to detect

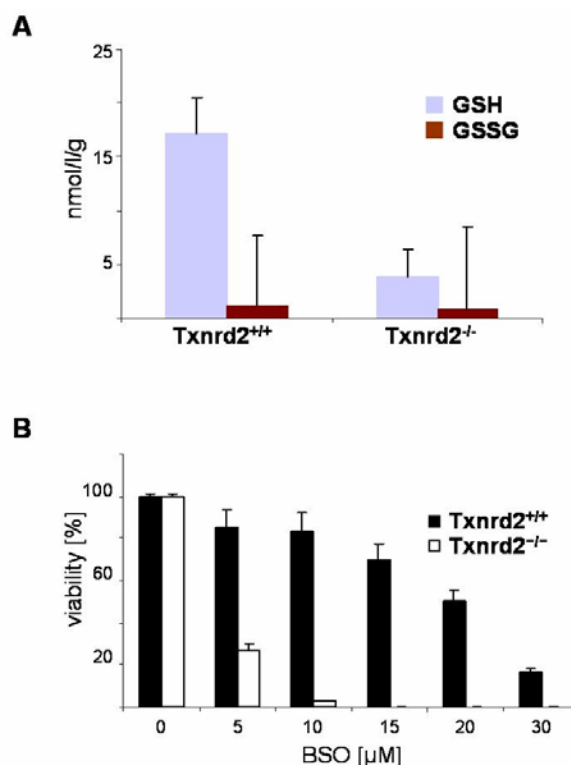


Figure 21. *Txnrd2*^{-/-} cells have strongly diminished levels of reduced glutathione. (A) HPLC analysis of glutathione (GSH) and oxidised glutathione (GSSG) in *Txnrd2*^{-/-} and *Txnrd2*^{+/+} cells revealed that knock-out cells had strongly decreased levels of reduced GSH (3.8±2.5 nmol/l/g) compared to wild-type cells (17.1±3.4 nmol/l/g). (B) Accordingly, *Txnrd2*^{-/-} cells were highly sensitive to increasing BSO concentrations compared to *Txnrd2*^{+/+} cells. Cell numbers were evaluated by trypan blue exclusion 72 h after BSO treatment.

early apoptotic cells by Annexin-V, a specific PS-binding protein. Annexin-V in combination with propidium iodide (PI) can be used to monitor for early and late apoptotic cells and/or necrotic cells. Early apoptotic cells are positive for Annexin-V, but negative for PI. Late apoptotic cells and necrotic cells are double positive for Annexin V and PI. Figure 22 C shows that when *Txnrd2*^{-/-} cells were treated with 5 μM BSO for 72 h, they had an increased number of Annexin-V-positive cells, reaching almost one third of the complete cell population (R1=30%), in comparison to *Txnrd2*^{+/+} cells in which 12% of the cells were Annexin-V positive (R1=12%). There was also a considerable increase in Annexin-V/PI-double positive cells among BSO-treated *Txnrd2*^{-/-} cells, which was about one third of the whole cell population (R2=29%) as compared to BSO-treated *Txnrd2*^{+/+} cells (R2=4%). Accordingly, 84% of the *Txnrd2*^{+/+} cells and only 41% of the *Txnrd2*^{-/-} cells were viable at 72 h post-treatment.

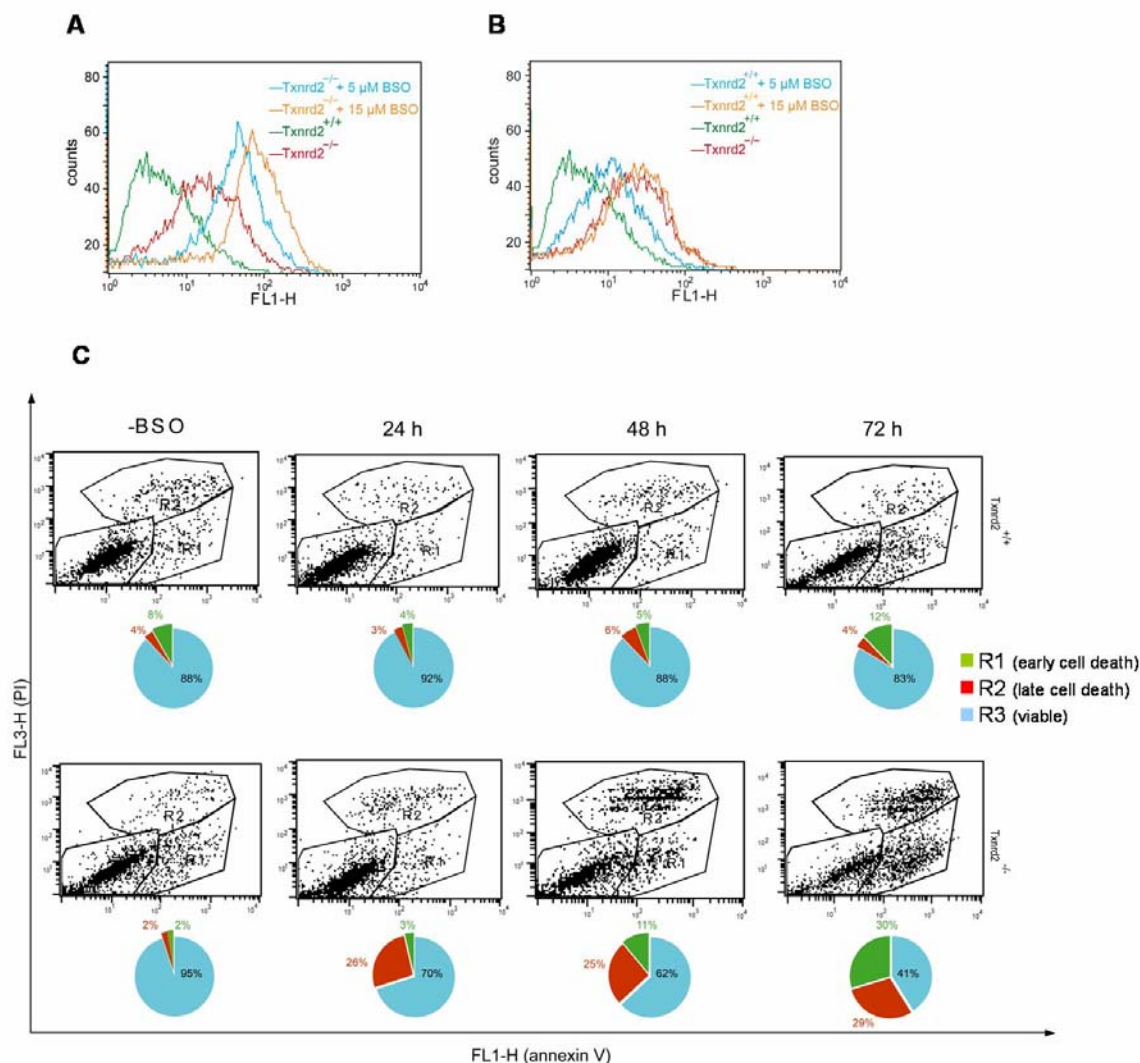


Figure 22. BSO-treatment exacerbates ROS production and cell death in *Txnrd2* knock-out cells. (A, B) ROS formation was strongly induced by BSO in *Txnrd2*^{-/-} cells (A) and to a lesser extent in wild-type cells (B). (C) Cell death was measured by Annexin-V/PI staining. *Txnrd2*^{-/-} and *Txnrd2*^{+/+} cells were cultured in the presence of 5 μ M BSO for 72 hours. Annexin V and PI staining revealed an increasing number of Annexin V-positive and PI-positive *Txnrd2*^{-/-} compared to control cells.

3.1.7. Expression of mitochondrial peroxiredoxins is increased in *Txnrd2*^{-/-} cells

The mitochondrial thioredoxin system has been postulated to be the major system to provide reducing equivalents to mitochondrial peroxiredoxins (Prx III and V), which are critically involved in the detoxification of H₂O₂ and other peroxides generated as a side product of mitochondrial respiration.

Since *Txnrd2* knock-out cells were shown to have strongly elevated ROS levels (see section 3.1.4.), it was interesting to see whether *Txnrd2*-deficiency may impinge on the expression and regulation (oxidation) of the different peroxiredoxins.

First, mRNA levels of the different peroxiredoxins (*Prx I-VI*) were analysed by semi-quantitative RT-PCR analysis in *Txnrd2^{+/+}* and *Txnrd2^{-/-}* cells either treated with BSO or left untreated. Semi-quantitative RT-PCR showed that the basal transcript levels of *Prx III* and *Prx V* were strongly increased in *Txnrd2^{-/-}* cells as compared to *Txnrd2^{+/+}* cells, whereas *Prx I*, *Prx II*, *Prx IV* and *Prx VI* mRNA levels did not differ between wild-type and knock-out cells (Figure 23 A). Only when the cells were treated with 15 μ M BSO for 12 h, *Prx III* and *Prx V* expression could be induced in *Txnrd2^{+/+}* cells to levels comparable to that in untreated *Txnrd2^{-/-}* cells. Exposure of *Txnrd2^{-/-}* cells to 15 μ M BSO for 12 h did not further enhance *Prx III* and *Prx V* expression. Next, the protein levels of *PrxIII* were examined in cells treated with increasing H_2O_2 concentrations. *Prx III* was strongly up-regulated in knock-out cells by treatment with 10 μ M H_2O_2 for 15 min, while a concentration of 750 μ M H_2O_2 was required to achieve the same response in wild-type cells (Figure 23 B).

Next, the cells were exposed to t-butyl-hydroperoxide (BOOH) for different time periods to explore whether loss of *Txnrd2* causes increased oxidation of peroxiredoxins in the cells after exogenous oxidative stress. To this end, an antibody was used which recognizes the sulfinic (Cys-SO₂H) and sulfonic (Cys-SO₃H) forms of the active site cysteines of peroxiredoxins. Without BOOH treatment, overoxidation of the different peroxiredoxins was neither detectable in *Txnrd2^{+/+}* nor in *Txnrd2^{-/-}* cells. However, when cells were treated with BOOH, *Prx I/Prx II* and *Prx III* appeared to be oxidised to a larger extent in knock-out as compared to wild-type cells (Figure 23 C). Due to the same molecular size of *Prx I* and *Prx II*, one cannot discriminate both peroxiredoxins by one dimensional SDS-PAGE and immunoblotting (Figure 23 C).

3.1.8. Time-dependent increase of *Prx III* levels in response to H_2O_2

To further explore the kinetics of *Prx III* up-regulation at the transcription and protein level in more detail, *Txnrd2^{+/+}* and *Txnrd2^{-/-}* cells were treated with a given concentration of H_2O_2 (250 μ M) over a time period of 120 min and the expression analysed by semiquantitative RT-PCR and Western blotting. *Prx III* transcript levels were induced in *Txnrd2^{+/+}* cells 5 min after H_2O_2 treatment and remained almost constant up to 60 min after which the transcript levels decreased. In *Txnrd2^{-/-}* cells, due to the higher basal *PrxIII* expression in untreated cells (see Fig. 23 A), *Prx III* mRNA levels increased only slightly, after 5 min of treatment and remained constant during the remaining time period (Figure 24 A). *Prx III* protein levels were high and stayed almost constant in *Txnrd2^{+/+}* cells, regardless of H_2O_2 treatment, whereas *Prx III* protein levels were clearly induced in knock-out cells 5 min after H_2O_2 exposure (Figure 24 B). While in control cells the level of *Prx III* mRNA and *Prx III* protein appeared to

decrease 60 min after treatment, in knock-out cells both mRNA and protein levels were increased irrespective of H₂O₂ treatment (see Figure 23 A and 24 B).

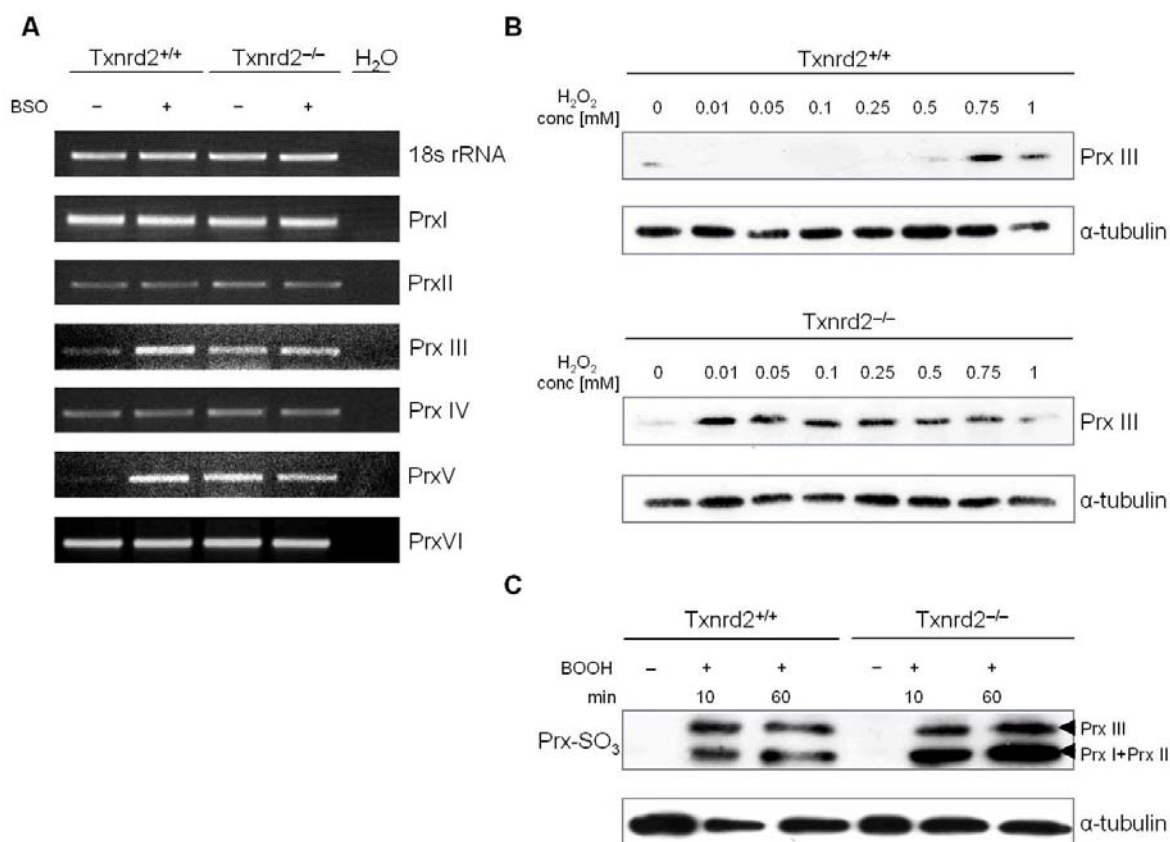


Figure 23. Mitochondrial Prx III and Prx V are strongly up-regulated in *Txnrd2* knock-out cells. (A) Semi-quantitative RT-PCR analysis showed that *Prx III* and *Prx V* are strongly up-regulated in *Txnrd2*^{-/-} cells in a manner similar to wild-type cells treated with 15 μM BSO for 12 hours. Treatment of *Txnrd2*^{-/-} cells with BSO did not further induce *Prx III* and *Prx V* expression. 18s rRNA served as control. (B) Treatment of *Txnrd2*^{+/+} and *Txnrd2*^{-/-} fibroblasts with increasing H₂O₂ concentrations (0.01, 0.05, 0.1, 0.25, 0.5, 0.75 and 1 mM) for 15 min strongly induced Prx III protein levels in *Txnrd2*^{-/-} fibroblasts at very low concentrations. (C) *Txnrd2*^{+/+} and *Txnrd2*^{-/-} cells were treated with 500 μM t-butyl-hydroperoxide for 10 and 60 min. Immunoblot analysis with a sulfinylation/sulfonylation-specific antibody (Prx-SO₃) revealed overoxidation of Prx I/Prx II and Prx III, which appeared to be stronger in *Txnrd2*^{-/-} than in *Txnrd2*^{+/+} wild-type cells.

Reduction of the sulfinic acid in the active site cysteine of peroxiredoxins, formed under prolonged exposure to oxidants, was shown to require sulfiredoxin (Srx) (Biteau et al., 2003; Bondareva et al., 2007; Jeong et al., 2006; Jonsson et al., 2008; Lim et al., 2008; Rhee et al., 2007; Roussel et al., 2008). It was thus hypothesised that the level of Srx might be elevated in the knock-out cells at high H₂O₂ concentration. Indeed, when the cells were treated for different time intervals with H₂O₂, *Srx* transcript levels were higher in *Txnrd2*^{-/-} than in control cells, while the *Srx* mRNA levels in the *Txnrd2*^{+/+} control cells were not affected (Figure 24 A).

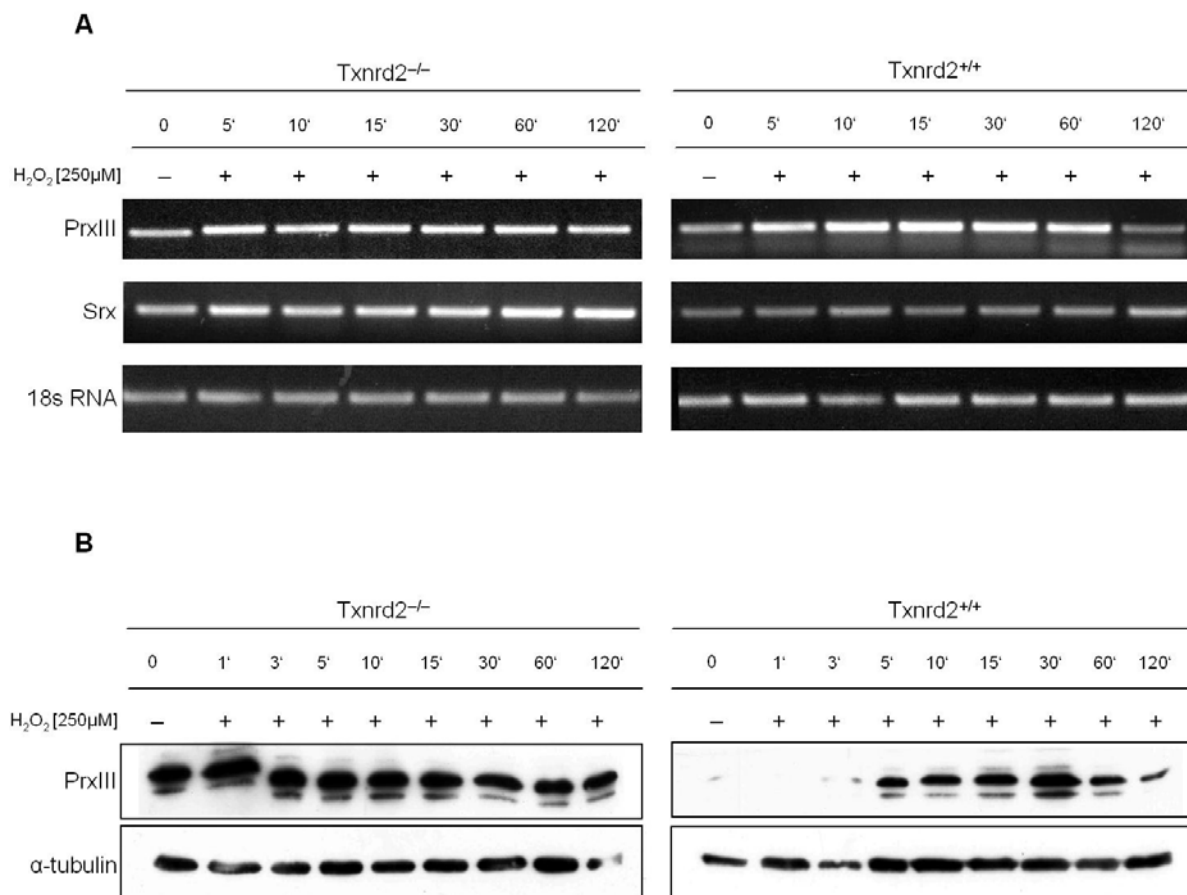


Figure 24. Different kinetics in the regulation of Prx III in *Txnrd2* wild-type and knock-out cells in response to H₂O₂. (A) *Txnrd2^{-/-}* and *Txnrd2^{+/+}* fibroblasts were treated with 250 μM H₂O₂ for the indicated time intervals. Semi-quantitative RT-PCR showed that the *Prx III* mRNA levels were only slightly induced in *Txnrd2^{-/-}* cells 5 min after treatment and remained constant throughout the 120 min of treatment, presumably due to the higher basal expression of *PrxIII* in these cells. In contrast, *Prx III* mRNA expression was clearly induced in *Txnrd2^{+/+}* cells after 5 min and down-regulated at 120 min. The level of the *Srx* mRNA was elevated at any tested time point in *Txnrd2^{-/-}* cells but not in *Txnrd2^{+/+}* cells. *18s rRNA* served as control. (B) Coinciding with the increased Prx III transcript levels, there was also an increase in the Prx III protein levels 5 min after H₂O₂ treatment, which reached a maximum at 30 min. In knock-out cells Prx III expression was high and remained constant.

3.1.9. Ectopic expression of Txnrd2 and Txnrd1 in *Txnrd2^{-/-}* cells

At least three N-terminal splicing variants with different subcellular localisation of Txnrd2 have been described (Turanov et al., 2006) (Figure 25 A). To answer the question whether the phenotype of *Txnrd2* knock-out cells is due to specific inactivation of Txnrd2 and not due to possible secondary side-effects, Txnrd2 expression was reconstituted in *Txnrd2^{-/-}* cells. As a control *Txnrd2* wild-type cells were included. Two of the three reported isoforms were generated: one is the predominant mitochondrial version of Txnrd2 with the N-terminal mitochondrial leader sequence (MLS) (Figure 25 A), the second variant lacks the MLS and accordingly has been reported to reside in the cytoplasm (Figure 25 A; Txnrd2a). The cytoplasmatic Txnrd2b form, which has an N-terminal extension of 12 amino acids in mice and humans was not included in this study (Turanov et al., 2006). To reconstitute Txnrd2

expression of both forms, a lentivirus-based system was used (Figure 13). Lentiviral transduction is highly efficient in primary cells and expression of the gene of interest is very stable. The vectors used for transduction of the cells express the *puromycin N-acetyltransferase* gene for stable selection of transduced cells with puromycin. Of note, exogenous Txnrd2 expression was much more pronounced than expression of endogenous Txnrd2 in wild-type MEFs (Figures 25 B and C). To assure that Sec is incorporated at the UGA codon, cells were supplemented with 25 nM NaSe (Nalvarte et al., 2004a). When the lysates of cells overexpressing mitoTxnrd2 were probed with an anti-Txnrd2 antibody, two bands appeared (Figure 25 B, second panel), whereas overexpression of Txnrd2a (referred to as cytoTxnrd2 in the following) revealed only one band. When the lysates were probed with the FLAG antibody only one band was obtained for both mitoTxnrd2 and cytoTxnrd2. The origin of the second band has remained elusive.

The subcellular localization of the two isoforms was additionally studied by immunocytochemistry using a FLAG-specific antibody and confocal microscopy. As predicted, mitoTxnrd2 was clearly detected in mitochondria (Figure 25 D), whereas cytoTxnrd2 was found in the cytoplasm (Figure 25 E), thus confirming the previous reports by Turanov et al. (Turanov et al., 2006). This indicates that the presence of the N-terminal tag had no effect on the subcellular localisation of Txnrd2. Next, the proliferation rates of *Txnrd2* knock-out and wild-type cells expressing either empty-virus (mock), or mitoTxnrd2 and cytoTxnrd2 were compared. Compared to mock-transduced *Txnrd2*^{-/-} cells, knock-out cells expressing either mitoTxnrd2 or cytoTxnrd2 had a higher proliferation rate than mock-transduced cells (Figure 25 F). Intriguingly, wild-type cells transfected with either Txnrd2 variant decreased the growth rate to some minor extent (Figure 25 G).

3.1.10. Stable expression of Txnrd1 in *Txnrd2* knock-out cells

Since it was shown previously that Txnrd2 reduces thioredoxin 1 and 2 (Trx1 and Trx2) equally well and that there is some kind of *in vitro* redundancy between Txnrd1 and Txnrd2 (Conrad et al., 2006; Turanov et al., 2006), it was intriguing to see whether overexpression of *Txnrd1* had any effect on the formation of ROS and proliferation of *Txnrd2*^{-/-} cells. To express *Txnrd1* in the *Txnrd2* knock-out cells, the lentiviral expression vector p442L1 was used (a kind gift from Pankaj Kumar Mandal) (Figure 26 A). Figure 26 A shows that that NTAPe- (N-terminal Tandem Affinity Purification enhanced, TAPe)-tagged Txnrd1 is highly expressed in *Txnrd2* knock-out cells (for details regarding the TAPe tag see 3.1.12.). Confocal microscopy after staining with a FLAG-specific antibody confirmed that NTAPe-tagged Txnrd1 is expressed in the cytoplasm (Figure 26 C).

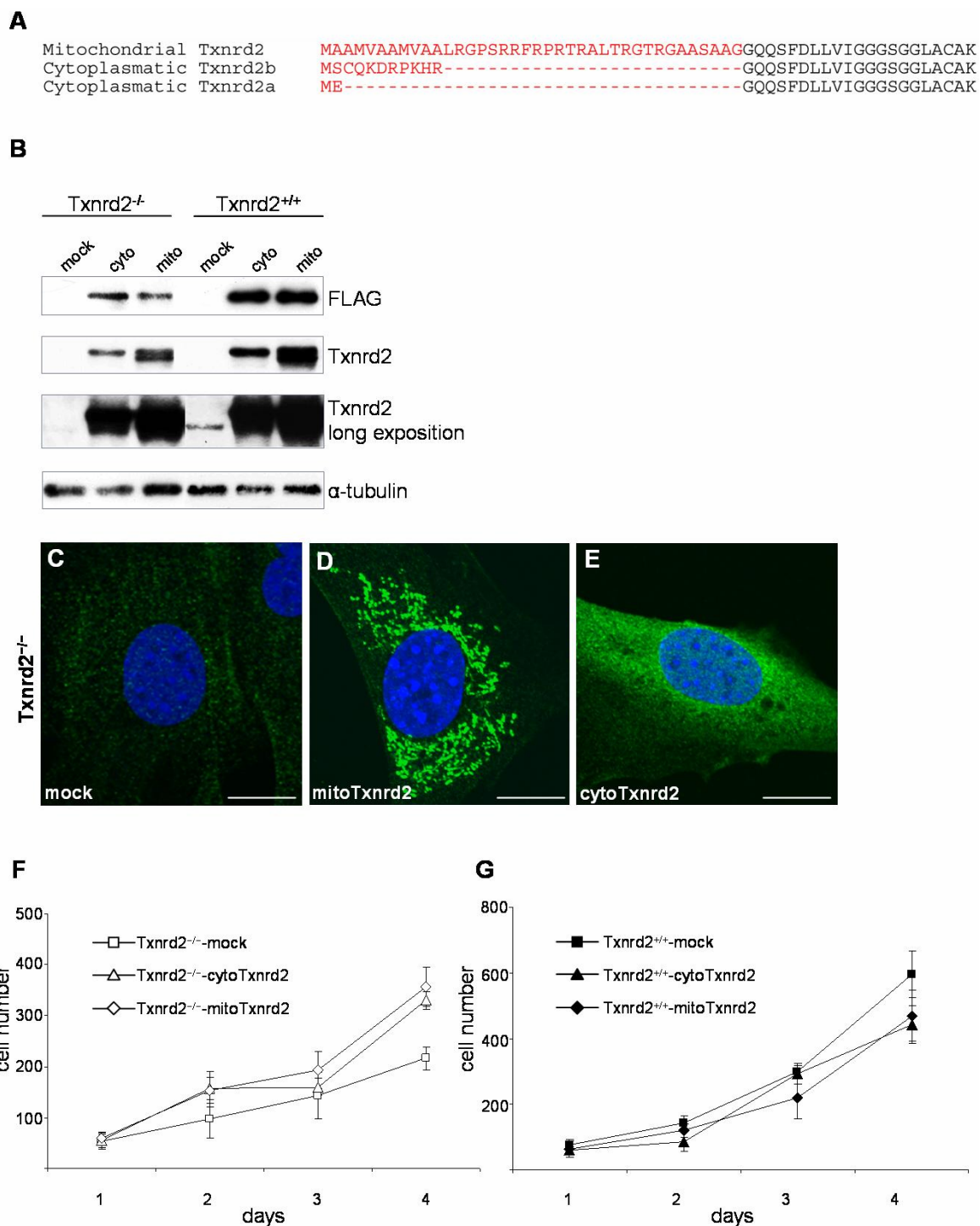


Figure 25. Stable expression of mitochondrial Txnrd2 and cytoplasmatic Txnrd2 in *Txnrd2*^{-/-} and *Txnrd2*^{+/+} cells. (A) Depicted are the three alternative N-terminal variants of Txnrd2 (Turanov et al., 2006). (B) Immunoblotting performed with an anti-FLAG or an anti-Txnrd2 antibody revealed high expression of mitoTxnrd2 and cytoTxnrd2 in *Txnrd2*^{-/-} and *Txnrd2*^{+/+} cells. Endogenous Txnrd2 is detectable after longer exposure in wild-type but not in knock-out cells. (C-E) The subcellular localization of mitoTxnrd2 and cytoTxnrd2 was further analysed by immunocytochemistry and confocal microscopy using an anti-FLAG antibody. Scale bars 10 μm. (F, G) Add-back of both mitoTxnrd2 and cytoTxnrd2 into *Txnrd2*^{-/-} cells restored proliferation of *Txnrd2*^{-/-} cells, and slowed down the proliferation of wild-type cells to a minor extent.

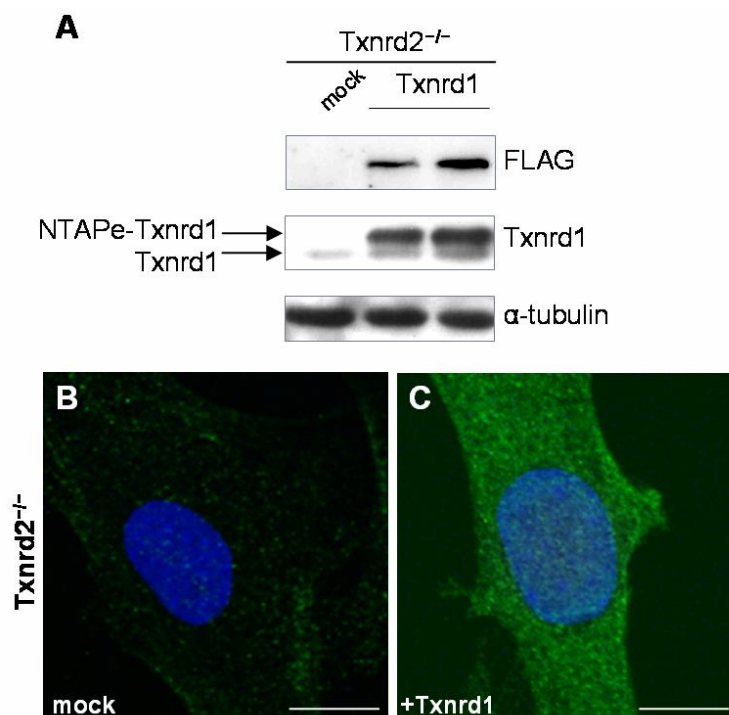


Figure 26. Stable expression of Txnrd1 in *Txnrd2*^{-/-} cells. (A) Western blot analysis of two independent *Txnrd2*^{-/-} cell clones stably expressing TAPe-tagged Txnrd1. While the FLAG antibody only detects the tagged protein, the Txnrd1-specific antibody also reveals endogenous Txnrd1 levels. (B) The subcellular localization of Txnrd1 in *Txnrd2*^{-/-} MEFs was demonstrated by immunocytochemistry using the FLAG antibody and confocal microscopy. Scale bars 10 μM.

3.1.11. Add-back of mitoTxnrd2 rescues *Txnrd2*^{-/-} cells from cell death induced by GSH depletion

To investigate whether the add-back of the different Txnrd2 variants has any impact on intracellular ROS levels, *Txnrd2*^{-/-} cells expressing mitoTxnrd2, cytoTxnrd2 or Txnrd1 were stained with DCFH-DA and analysed by flow cytometry. Figure 27 shows that intracellular ROS accumulation was effectively dampened in *Txnrd2*^{-/-} cells expressing mitoTxnrd2, cytoTxnrd2 or Txnrd1 as compared to mock-transfected *Txnrd2*^{-/-} cells. This finding was surprising because it had been anticipated that ROS generated by mitochondria would be effectively cleared only by the mitochondrial thioredoxin system, but apparently cytoTxnrd2 and Txnrd1 were also functional.

To investigate whether the different enzyme forms are able to protect *Txnrd2*^{-/-} cells from BSO-induced cell death, *Txnrd2*^{-/-} cells were treated with different BSO concentrations and cell viability was determined 48 h after treatment. As shown in Figure 28, knock-out cells stably expressing mitoTxnrd2 were highly resistant to BSO-mediated GSH depletion and these cells were even slightly more resistant than mock-transfected *Txnrd2*^{+/+} cells.

Overexpression of cytoTxnrd2 in *Txnrd2*^{-/-} cells provided partial rescue of cell viability after BSO treatment compared to mock-transduced and Txnrd1-transduced *Txnrd2*^{-/-} cells.

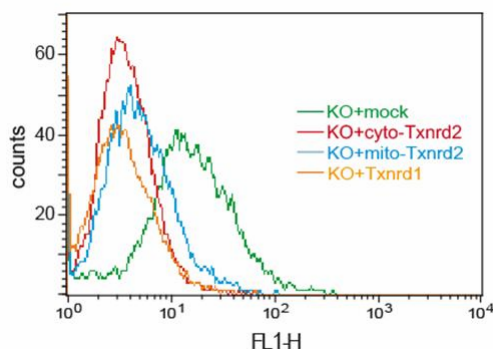


Figure 27. Overexpression of Txnrd2 and Txnrd1 reduced ROS levels in *Txnrd2*^{-/-} cells. *Txnrd2*^{-/-} cells overexpressing the different forms of Txnrd2 and Txnrd1 were plated and stained for ROS with DCFH-DA 24 h after BSO treatment.

From this experiment one may conclude that efficient dampening the intracellular ROS levels by overexpression of the Txnrd1 and mitochondrial and cytoplasmic Txnrd2 is not necessarily coupled to rescue from GSH-depletion-induced cell death.

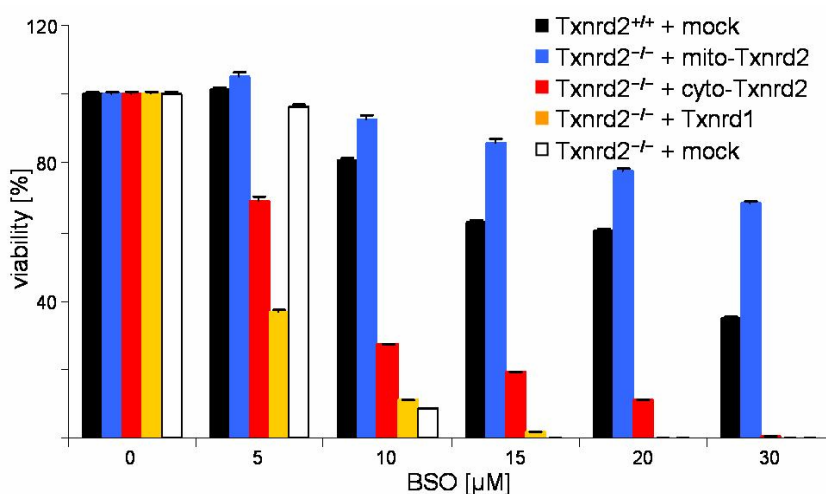


Figure 28. Re-expression of mitoTxnrd2 rescues *Txnrd2*^{-/-} MEFs from BSO-induced cell death. Reconstitution of mitochondrial Txnrd2 rescued the cells from BSO-induced cell death, whereas cytoplasmic Txnrd2 could only partially rescue viability and Txnrd1 was ineffective. Cell viability was determined by trypan blue exclusion 48 h after BSO treatment.

3.1.12. The role of *Txnrd2* in normal physiology and disease

3.1.12.1. Identification and functional characterisation of two novel *Txnrd2* mutations in patients suffering from dilated cardiomyopathy (DCM)

It had been shown previously in our laboratory that mice lacking *Txnrd2* die during embryonic development due to impaired foetal haematopoiesis and perturbed cardiac development (Conrad et al., 2004). In the same study it was also demonstrated that heart-specific inactivation of *Txnrd2* resulted in a cardiac phenotype reminiscent of human dilated cardiomyopathy (DCM) with biventricular dilatation of heart chambers and thinning of ventricular walls. Transmission electron microscopy (TEM) analysis of cardiac tissue of heart-specific *Txnrd2* knock-out mice showed swelling of mitochondria and partial destruction of mitochondrial cristae (Conrad et al., 2004).

The phenotype of mice with heart-specific deletion of *Txnrd2* suggested that *Txnrd2* might be involved in the pathogenesis of DCM. To address the question whether this is indeed the case, a collaborative study was initiated in collaboration with Dr. N. v. Beckerath and Dr. D. Sibbling, Klinikum rechts der Isar and Deutsches Herzzentrum, Technische Universität München) and Dr. Arne Pfeufer (Institute of Human Genetics, Helmholtz Zentrum München) searching for mutations in the *Txnrd2* gene of DCM patients. In the course of this study the genomic structure of the *Txnrd2* gene has been analysed in 227 DCM patients by cycle sequencing including the respective forward and reverse primers and BigDye-Terminator 3.1 (Qiagen, Hilden, Germany) sequencing technology. Two mutations have been identified in three patients suffering from DCM.

In this study the Ala codon (GCC) at position 59 was found to be changed to Thr (ACC) and the Gly codon (GGG) at position 375 was exchanged to Arg (AGG) (Figure 30). Both mutations were not observed in healthy subjects. The presence of these mutations was further verified with a additional matrix-assisted laser ionization (MALDI), a technique allowing the analysis of proteins by ionization. The ionization is triggered by a laser beam and matrix is used to protect the biomolecule from being destroyed by direct laser beam and to facilitate vaporization and ionization. The first mutation (Ala59Thr) was found in two out of 227 DCM patients ($2/227=0.88\%$). The second mutation (Gly375Arg) was found in one out of the 227 DCM patients ($1/227=0.44\%$). As identification of amino acid changes in a given gene does not imply that the protein is functionally impaired and the molecular aetiology of congestive heart failure due to dilated cardiomyopathy (DCM) remains poorly understood, it was mandatory to demonstrate that the mutations found in DCM patients impact on the

function of Txnrd2. To this end, we used Txnrd2^{+/-}- and Txnrd2^{-/-}-MEFs as a cellular model system. As shown in Figure 29, the amino acid sequence of Txnrd2 among mammals is highly conserved. Moreover, the positions of the altered amino acid residues are located in highly conserved regions of Txnrd2; yet, it was not clear whether the two amino acid exchanges may have any impact on Txnrd2 function. To test the functional activity of the mutated Txnrd2 forms in cells, the corresponding mutants were generated in the murine mitochondrial form of Txnrd2 by site-directed PCR mutagenesis, designated as mitoA59T and mitoG375R.

The mitochondrial Txnrd2 variant (mitoTxnrd2) was chosen for mutagenesis because this form is the predominant form in cardiac tissue and probably also in most other tissues (Kiermayer et al., 2007). Moreover, mitochondrial Txnrd2 was shown to rescue Txnrd2^{-/-} cells from BSO-induced cell death (see also Figure 28). Both mutant forms, mitoA59T and mitoG375R, were cloned into the lentiviral vector p442L1 and stably expressed in Txnrd2^{-/-} and Txnrd2^{+/+} control cells. The expression levels of mitoTxnrd2 and both mutant forms, mitoA59T and mitoG375R, were determined by immunoblotting using an anti-Txnrd2 and a FLAG-specific antibody (Figures 30 A and B). While the expression level of mitoA59T was similar to the expression level of mitoTxnrd2 (Figure 30 A) in both knock-out and control cells, the expression of mitoG375R was strongly reduced in both cell lines (Figure 30 B). The expression of mitoG375R in Txnrd2^{+/+} cells was very low and could not be detected by anti-FLAG antibody either by Western blotting (not shown) or by immunocytochemistry (Figure 30 H). To determine the subcellular localisation of mitoTxnrd2 and both mutant forms, immunocytochemical staining using an anti-FLAG antibody and confocal microscopy were carried out. Unmutated mitoTxnrd2 was localised to mitochondria in wild-type and knock-out cells (Figures 30 C and F). Intriguingly, the number of mitochondria appeared to be reduced in Txnrd2^{-/-} as compared to Txnrd2^{+/+} wt cells. Expression of the mutants revealed that mitoA59T was localised in the cytosol and in particulate structures, which might represent structurally abnormal mitochondria in Txnrd2 knock-out cells (Figure 30 D). In Txnrd2^{+/+} control cells, mitoA59T showed a predominant mitochondrial localisation pattern (Figure 30 G). Confocal microscopy of the Txnrd2^{-/-} cells transfected with mitoG375R revealed that the protein was expressed close to the nucleus, within structures similar to aggregated mitochondria (Figure 30 E). Besides the aberrant localisation of both mutant forms, the proliferation rates of Txnrd2^{+/+} cells expressing either of the two mutant forms were markedly reduced (Figure 31 A). In Txnrd2^{-/-} cells, expression of both mutant forms did neither rescue nor further impair proliferation of Txnrd2 knock-out cells (Fig. 31 B), whereas expression of mitoTxnrd2 completely rescued the proliferation defect (as had been also previously shown in Fig. 25 F).

Canis familiaris	MSSCGIRAP-ALTWP---FLSPLS-----AA-----GQQNYDLLVIGGGSGGLACAKEAAQLGKKVAVV
Pan troglodytes	MAAMAV----ALRGLGGRFRWRQTQAVAGGVRGAARGAA---GQRDYDLLVVGSGSGGLACAKEAAQLGRKVAVV
Bos taurus	MA-----ALRGAAARFRGRAP---GGARGAA-----GRQCYDLLVIGGGSGGLACAKEAAQLGKKVAVL
Rattus norvegicus	MAAIVA----ALRGSSGRFRPQTRVLTRGTRGAA-GAASAAGGQNFDDLVIIGGGSGGLACAKEAAQLGRKVAVA
Mus musculus	MAAMVAAMVAALRGPSRRFRPRTRALTRGTRGAA----SAAGGQSFDDLVIIGGGSGGLACAKEAAQLGKKVAVA
Homo sapiens	MAAMAV----ALRGLGGRFRWRQTQAVAGGVRGAARGAAA---GQRDYDLLVVGSGSGGLACAKEAAQLGRKVAVV
Canis familiaris	DYVEPSPRGTKWGLGGTCVNVGCIIPKKLMHQAALLGSMIRDAPHYGWDVAQPVLDHWRMTMAEAVQNHVKSLNWGH
Pan troglodytes	DYVEPSPOGTRWGLGGTCVNVGCIIPKKLMHQAALLGGLIQDAPNYGWEVAQPVPHDWRKMAEAVQNHVKSLNWGH
Bos taurus	DYVEPSPOGTRWGLGGTCVNVGCIIPKKLMHQAALLGGMIRDAPHYGGWGAQA-PHSWATLADAVQNHVKSLNWGH
Rattus norvegicus	DYVEPSPRGTKWGLGGTCVNVGCIIPKKLMHQAALLGGMIRDAQHYGWEVAQPVQHNWKMAEAVQNHVKSLNWGH
Mus musculus	DYVEPSPRGTKWGLGGTCVNVGCIIPKKLMHQAALLGGMIRDAHHYGWEVAQPVQHNWKMAEAVQNHVKSLNWGH
Homo sapiens	DYVEPSPOGTRWGLGGTCVNVGCIIPKKLMHQAALLGGLIQDAPNYGWEVAQPVPHDWRKMAEAVQNHVKSLNWGH
Canis familiaris	RVQLQDRKVYFNKASVFNEHTVCGVAKGKETLLSAEHIVATGGRPRYPHTHIEGALEYGITSDDIFWLKESP
Pan troglodytes	RVQLQDRKVYFNKASVFDEHTVCGVAKGKEIILSADHIIATGGRPRYPHTHIEGALEYGITSDDIFWLKESP
Bos taurus	RIQLQDRKVYFNKASFVDTHTVCGVSKGEETLLSAEHIVATGGRPRYPHTHIEGALEYGITSDDLFWLKESP
Rattus norvegicus	RVQLQDRKVYFNKASVFNEHTVHGVKAGKVTQLSAKHIVATGGRPKYPTQVKGALHEGITSDDIFWLKESP
Mus musculus	RVQLQDRKVYFNKASVFDEHTVVRGVDKGGKATLLSAEHIVATGGRPRYPHTQVKGALHEGITSDDIFWLKESP
Homo sapiens	RVQLQDRKVYFNKASVFDEHTVCGVAKGKEIILSADHIIATGGRPRYPHTHIEGALEYGITSDDIFWLKESP
Canis familiaris	GKTLVVGASYVALECAAGFLTGLGLDITIMIRSIPLRGFDQMQSSLVTEYMASQGRFLRGCTPSRVRRLLPDGQLQ
Pan troglodytes	GKTLVVGASYVALECAAGFLTGLGLDITIMIRSIPLRGFDQMQSSMVEHMHASHGTRFLRGCAPSRVRRLLPDGQLQ
Bos taurus	GKTLVVGASYVALECAAGLLTGGLDITVMIRSVPLRAFDQMQASLVTEHMHASHGTRILRGCAPEKVEKLPGQQLR
Rattus norvegicus	GKTLVVGASYVALECAAGFLTGLGLDITVMIRSVPLRGFDQMQASLVTEHMHASHGTRFLRGCAVPSLIRKLPTNQLQ
Mus musculus	GKTLVVGASYVALECAAGFLTGLGLDITVMIRSVPLRGFDQMQSSLVTEHMHASHGTRFLRGCAVPSLIRKLPTNQLQ
Homo sapiens	GKTLVVGASYVALECAAGFLTGLGLDITIMIRSIPLRGFDQMQSSMVEHMHASHGTRFLRGCAPSRVRRLLPDGQLQ
Canis familiaris	VTWENLTSGKEDVGTFTDVLWAIGRVPETKSLNLEKAGVNTNPNKQKILVNAQEATSIPHIYAIGDVAEGRPELTP
Pan troglodytes	VTWEDCTTGKEDTGTFTDVLWAIGRVPDTRSLNLEKAGVDTSPDTQKILVDSREATSVPHIYAVGDVVEGRPELTP
Bos taurus	VTWVDLTSDRKDACTFTDVLWAIGRVPETASLNLEKAGVHTNPVTGKILVDAQETTSVPHIYAIGDVAEGRPELTP
Rattus norvegicus	VTWEDLASGKEDVGTFTDVLWAIGRVPETRLNLEKAGVNTNPNKQKIIVDAQEATSVPHIYAIGDVAEGRPELTP
Mus musculus	VTWEDHASGKEDTGTFTDVLWAIGRVPETRLNLEKAGISTNPNKQKIIVDAQEATSVPHIYAIGDVAEGRPELTP
Homo sapiens	VTWEDSTTGKEDTGTFTDVLWAIGRVPDTRSLNLEKAGVDTSPDTQKILVDSREATSVPHIYAIGDVVEGRPELTP
Canis familiaris	TAIMAGRLLAQRLCGQASDVMDYDNVPTTVFTPLEYGCVGLSEEEAVTRHGEHVEVYHAYYKPLEFTVAERDASQ
Pan troglodytes	TAIMAGRLLVQRLFGGSSDLMDYDNVPTTVFTPLEYGCVGLSEEEAVAHHGQEHVEVYHAYYKPLEFTVAGRNASQ
Bos taurus	TAIMAGRLLAQRLSGRTSDLMYSSVPPTTVFTPLEYGCVGLSEEEAVARHGEHVEVYHAFYKPLEFTVTPQRNASQ
Rattus norvegicus	TAIKAGKLLAQRLFGKSSSTLMYSNVPTTVFTPLEYGCVGLSEEEAVALHGQEHVEVYHAYYKPLEFTVADRNASQ
Mus musculus	TAIKAGKLLAQRLFGKSSSTLMYSNVPTTVFTPLEYGCVGLSEEEAVALHGQEHVEVYHAYYKPLEFTVADRNASQ
Homo sapiens	IAIMAGRLLVQRLFGGSSDLMDYDNVPTTVFTPLEYGCVGLSEEEAVARHGEHVEVYHAYYKPLEFTVAGRNASQ
Canis familiaris	CYVKMVCRLRPPQLVLGLHFLGPNAGEVTQGFALGKCGASYAQVMRTVGIHPTCAEEVAKLRITKRSGLDPTVTGCG
Pan troglodytes	CYVKMVCRLRPPQLVLGLHFLGPNAGEVTQGFALGK
Bos taurus	CYIKMVCRLRPPQLVLGLHFLGPNAGEVTQGFALGKCGASYQQLMRTVGIHPTCAEEVAKLRISKRSGLDPTVTGCGUG
Rattus norvegicus	CYIKMVCMLRPPQLVLGLHFLGPNAGEVTQGFALGKCGASYAQVMQTVGIHPTCSEEVVKLHISKRSGLDPTVTGCGUG
Mus musculus	CYIKMVCMLRPPQLVLGLHFLGPNAGEVTQGFALGKCGASYAQVMQTVGIHPTCSEEVVKLHISKRSGLDPTVTGCGUG
Homo sapiens	CYVKMVCRLRPPQLVLGLHFLGPNAGEVTQGFALGKCGASYAQVMRTVGIHPTCSEEVVKLRISKRSGLDPTVTGCGUG

Figure 29. Amino acid sequence alignment of mammalian Txnrd2s. Identical amino acids shared between Txnrd2 of the different organisms are shaded in grey. The N-terminal catalytically active site (CVNVGC) and the Sec-containing C-terminal active site (GCUG) involved in electron transport are indicated in blue. Sequences that constitute the FAD-binding domains are marked as red boxes and sequences that constitute the NADPH-binding domain as a green box. The positions of the conserved amino acids, that were found to be mutated in the DCM patients (A59T and G375R) are indicated by red letters. NCBI accession numbers: Canis Familiaris (XM_845088.1), Pan Triglodytes (XM_001166615.1), Bos Taurus (NM_174626.2), Rattus Norvegicus (NM_022584.1), Mus Musculus (NM_013711.2) and Homo Sapiens (NM_006440.3).

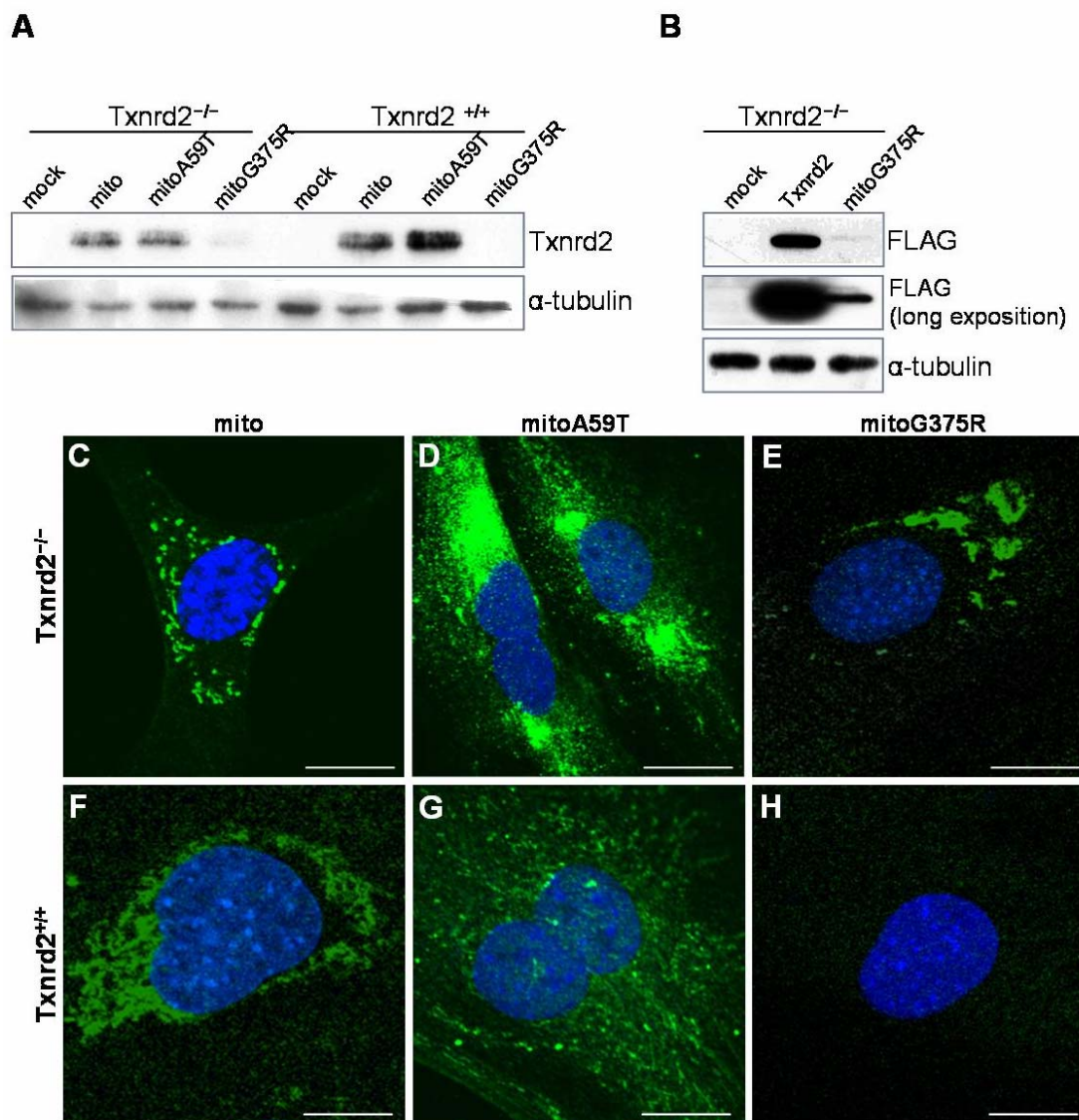


Figure 30. Stable expression of the Txnrd2 mutants, Ala59Thr and Gly375Arg, in *Txnrd2*^{-/-} and *Txnrd2*^{+/+} cells. (A-B) Expression of both mutant forms of Txnrd2 (mitoAla59Thr and mitoGly375Arg) in wild-type and knock-out cells was monitored by Western blot analysis using an anti-Txnrd2 and anti-FLAG antibody. The expression level of mitoA59T was similar to the expression level of mitoTxnrd2, the predominant form of Txnrd2 in the cells. Expression of the mutant mitoG375R was strongly reduced in Txnrd2 knock-out cells and even more reduced in Txnrd2^{+/+} wt cells when compared with the level of expression of the mitoAla59Thr mutant. (C-H) Immunocytochemistry with an anti-FLAG antibody showing an aberrant localisation of the Txnrd2 mutant forms (mitoA59T and mitoG375R) expressed either in *Txnrd2*^{-/-} or *Txnrd2*^{+/+} MEFs. Scale bars 10 μ m.

Next, it was asked whether the expression of the mutated forms of Txnrd2 is able to rescue cells from cell death induced by GSH depletion. In *Txnrd2*^{-/-} cells transduced with the mutant and wt form of mitoTxnrd2, the number of viable cells was determined by trypan blue exclusion 48 h after the addition of increasing BSO concentrations. As shown in Figure 33, the add-back of mitoTxnrd2 prevented cell death of knock-out cells induced by increasing concentrations of BSO (Figure 32 A). By stark contrast, *Txnrd2*^{-/-} cells expressing either of the two mutant forms died very rapidly already at very low BSO concentrations (Figure 32 A). Remarkably, these cells died even significantly more rapidly than mock-infected *Txnrd2*^{-/-}

cells. In *Txnrd2*^{+/+} MEFs, survival was also substantially impaired when the mitoA59T- and mitoG375R-forms were expressed in wild-type cells, (Figure 32 B), indicating that both mutant forms act in a dominant-negative fashion.

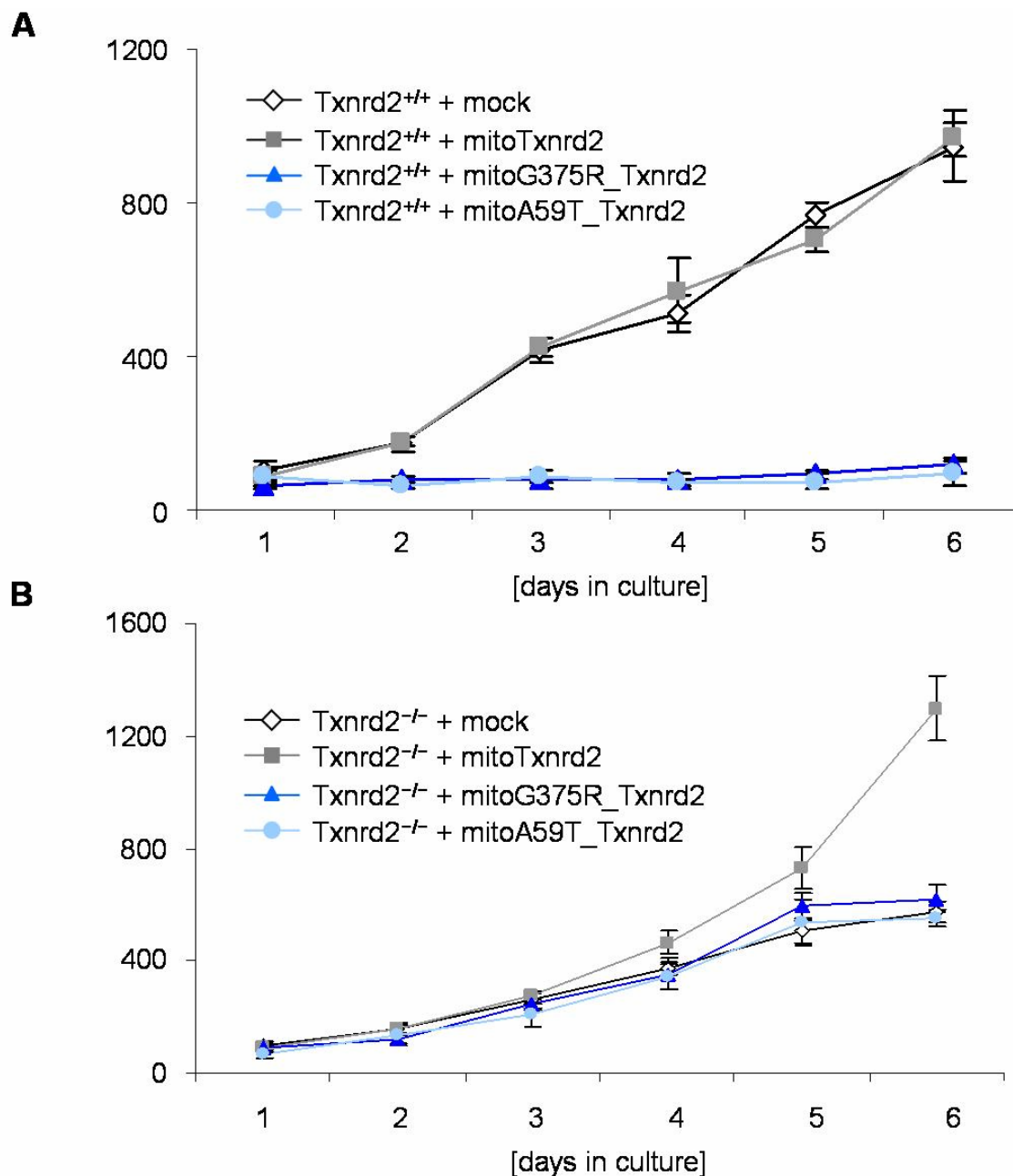


Figure 31. Growth properties of *Txnrd2*^{-/-} and *Txnrd2*^{+/+} cells expressing either mitoAla59Thr or the mitoGly375Arg mutant forms of Txnrd2. (A) Proliferation was strongly impaired when the two mutant forms of Txnrd2 were stably expressed in *Txnrd2*^{+/+} cells. (B) The slow proliferation rate of *Txnrd2*^{-/-} cells was not substantially affected by expression of the same mutant forms, whereas expression of the unmutated mitoTxnrd2 form completely rescued the proliferation defect of Txnrd2 knock-out cells (see also Fig. 25 F).

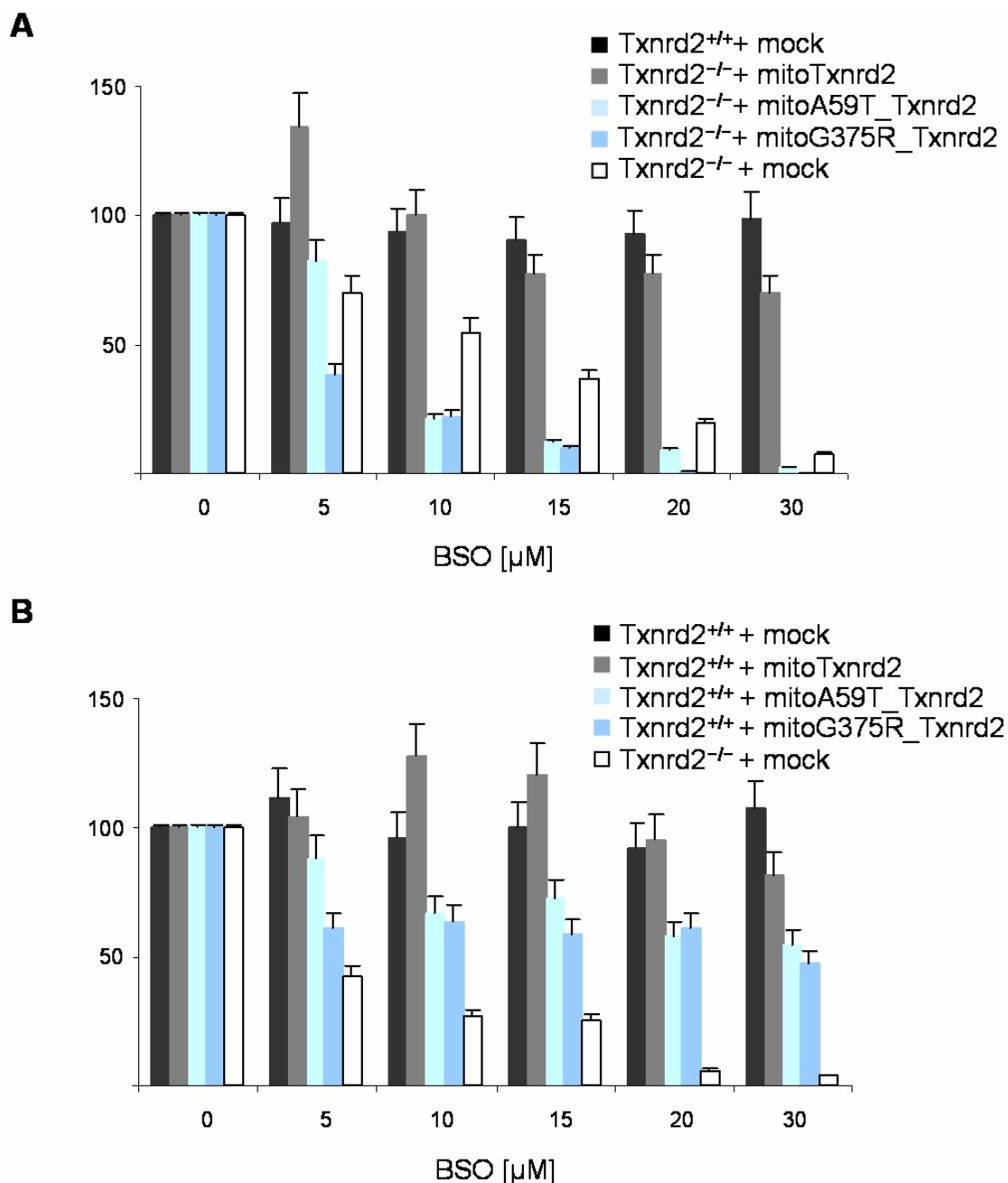


Figure 32. MitoA59T and mitoG375R do not rescue BSO-mediated cell death of *Txnrd2*^{-/-} cells. Cells were treated for 48 h with the indicated BSO concentrations and cell survival was monitored by trypan blue exclusion. (A) Stable expression of Ala59Thr and Gly375Arg mutants in *Txnrd2*^{-/-} cells did not rescue GSH depletion-induced cell death. In contrast, cells overexpressing the mutant forms died even more rapidly than mock-transduced *Txnrd2*^{-/-} cells. (B) Cell survival of *Txnrd2*^{+/+} cells transduced with either mitoA59T or mitoG375R was impaired in response to increasing BSO concentrations, indicating that both mutant forms act in a dominant-negative fashion.

3.2. The role of system x_c^- in maintenance of intracellular GSH levels and cystine/cysteine redox balance in cultured cells

3.2.1. The protective role of system x_c^- in Burkitt lymphoma (BL) cells

To address the role of system x_c^- in cell proliferation and cell death, xCT light chain was stably expressed in the Burkitt's lymphoma (BL) cell line HH514 (Banjac, 2005; Banjac et al., 2008).

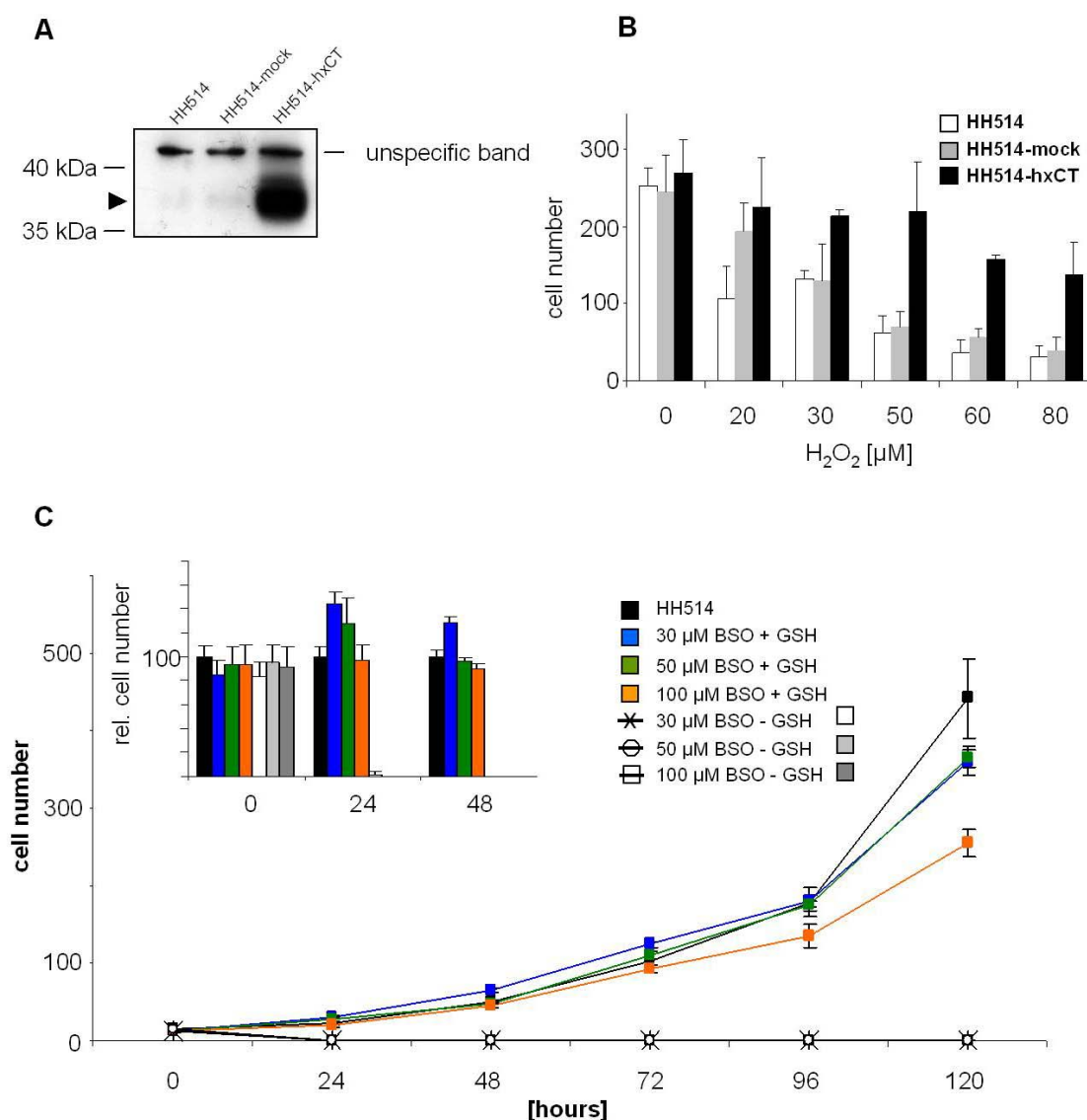


Figure 33. Stable expression of xCT in the Burkitt's Lymphoma cell line HH514. (A) Stable expression of xCT in the BL cell line HH514 was analysed by immunoblotting using a monoclonal antibody (clone 1B1) specific for human xCT. The parental cell line and mock-transfected HH514 cell line served as negative control. The arrow points to the xCT protein of approx. 37 kDa. The unspecific band of approx. 40 kDa served as loading control. (B) Cells were incubated with increasing concentrations of H_2O_2 and the number of viable cells was determined 48 h after treatment by trypan blue exclusion. (C) Glutathione (2.5mM) supplementation efficiently rescued cell death induced by BSO treatment.

It was shown that xCT-overexpressing cells were highly resistant to oxidative stress imposed by seeding the cells at low cell density or by GSH depletion induced by BSO. In the same study, initial evidence was provided that the cystine/cysteine redox cycle may act independently of intracellular GSH (Banjac et al., 2008). In the following, antibodies against human xCT were generated. This was performed in close collaboration with Dr. Elisabeth Kremmer (Helmholtz Zentrum München). Two peptide sequences complementary to the N-terminal cytoplasmic domain of human xCT were used to raise hybridoma clones that generated antibodies specific for human xCT. Out of 34 supernatants, two antibodies that recognise human xCT were identified (3A12 and 1B1) (Figure 33 A). The xCT-overexpressing HH514 cells were used to screen the supernatants for the specific antibodies.

Using the same cell lines, it was shown that xCT-overexpressing HH514 cells became highly resistant to increasing concentrations of H_2O_2 as illustrated in Figure 33 B (Banjac et al., 2008). Addition of 2.5 mM GSH to the cell culture medium rescued the BSO-mediated detrimental effects on the proliferation and survival of HH514 cells, ruling out any toxic side effects of BSO (coloured boxes in Figure 33 C).

To address whether GSH-depleted cells die in an apoptotic manner, cells were stained with Annexin V and propidium iodide (PI) at various time periods after the addition of 30 μM BSO. Apoptotic cells, defined by Annexin V-positive, PI-negative staining, could not be detected at any time point after BSO treatment, indicating that BSO-treated cells do not undergo a classical form of cell death (Figure 34) (Banjac et al., 2008).

3.2.2. The thioredoxin system as the possible driving force for the cystine/cysteine redox cycle

GSH is believed to mediate efficient reduction of cystine $(\text{Cys})_2$, that is taken up by system xc⁻ into the cells, by forming a mixed disulfide (GS-Cys). A second molecule of GSH is then releasing cysteine from the mixed disulfide resulting in the formation of oxidised glutathione (GSSG). Oxidised GSH (GSSG) is then recycled by glutathione reductase and NADPH/ H^+ . As overexpression of xCT rescues BL cells from cell death also in the presence of the GSH synthesis inhibitor BSO (see Fig. 34 C), it is an intriguing question which other redox system may compensate for the lack of GSH, i.e. which cellular system besides GSH is capable of reducing oxidised cysteine. The need for a second redox system capable of reducing cystine was additionally reinforced by the finding that xCT overexpression renders $\gamma\text{-GCS}^{-/-}$ cells,

which lack endogenous GSH biosynthesis, independent of exogenous GSH or NAC in the medium (Seiler, 2008).

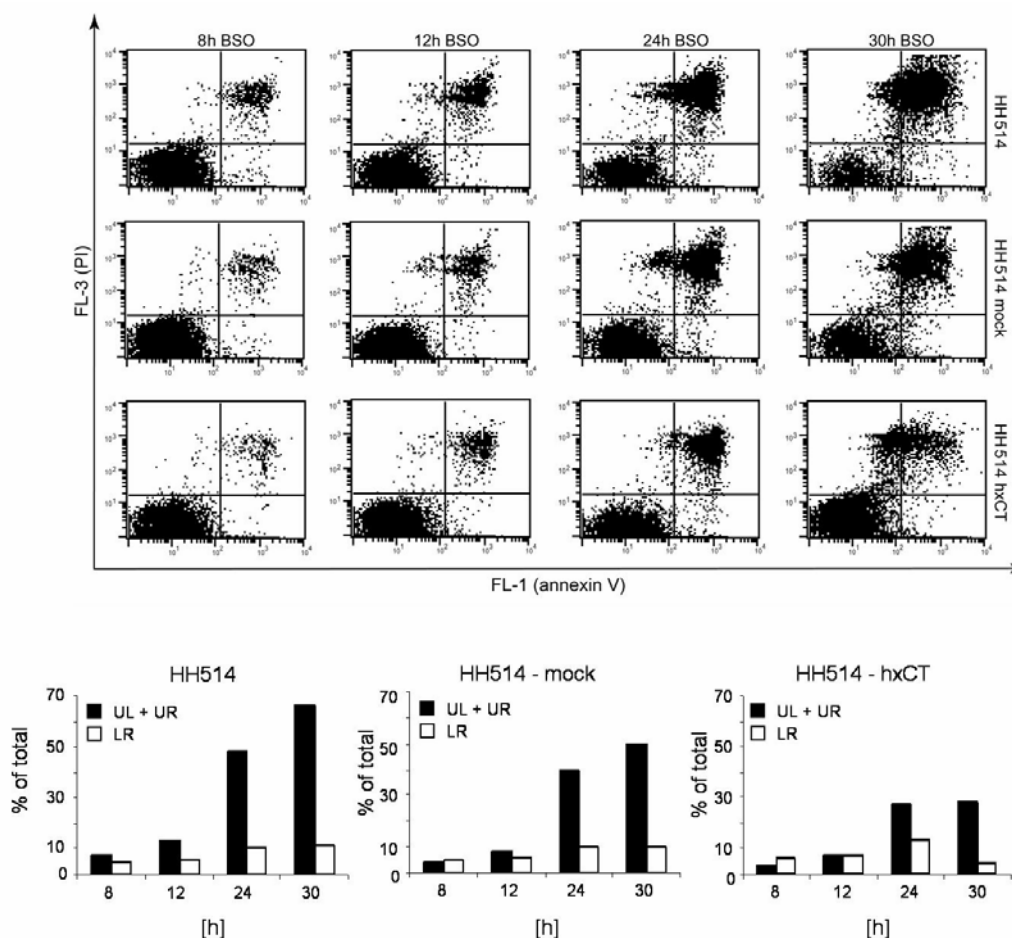


Figure 34. HH514 cells do not die in an apoptotic manner in response to GSH depletion. HH514, HH514-mock and HH514-hxCT cell lines were treated with 30 μ M BSO and stained with Annexin V/PI for the indicated time points (8 h, 12 h, 24 h, 30 h). While no Annexin V-positive/PI-negative cell population could be detected at any time point, Annexin V-positive/PI-positive cells were detectable in all cell lines to varying degree in response to BSO treatment. This indicates that these cells did not undergo a classical form of apoptosis.

To address the question whether the thioredoxin dependent system is able to reduce cystine in the absence of GSH, *Txnrd2*-deficient cells were stably transfected with the pCAG-3SIP-based vectors (Figure 35) pCAG-3SIP-EGFP and pCAG-3SIP-mxCT (mxCT = mouse xCT). The absence of *Txnrd2* in EGFP- or mxCT-transfected *Txnrd2*^{-/-} cells was confirmed by Western blotting (Fig. 35 A). As monitored by fluorescence microscopy and by flow cytometry for EGFP, stable selection of pCAG-3SIP-EGFP-transfected cells with puromycin was highly efficient (Figure 35 B). To assess xCT expression in these cells, Northern blot analysis, qRT-PCR, immunoblotting and cystine uptake measurements were performed (Figure 50 C-F). Northern blot analysis revealed strong hybridisation signals for *mxCT* in xCT-transfected *Txnrd2*^{+/+} and *Txnrd2*^{-/-} cells (Figure 35 C), but not in EGFP-transfected cells. The hybridisation signal obtained by Northern blot corresponds to the bicistronic xCT-

IRES-puromycin mRNA sequence of 2.7 kb. The Northern blot results were confirmed by quantitative Real Time-PCR in *Txnrd2*^{-/-} cells, which showed approximately 10-fold higher expression levels of xCT in xCT-transfected as compared to EGFP-transfected cells (Figure 35 D). By using an xCT-specific antibody (kind gift of Dr. Ann Massie, Brussels, Belgium), high expression of murine xCT could be detected (Figure 35 E). Finally, system x_C⁻ activity was determined in xCT-overexpressing and EGFP-transfected *Txnrd2*^{-/-} cells by measuring the (Cys)₂ uptake capacity using radioactively labelled L-[¹⁴C(U)] (Cys)₂. xCT overexpressing cells displayed an about threefold higher cystine uptake capacity than EGFP-transfected cells (Figure 35 F).

Next, intracellular GSH levels were measured by HPLC in EGFP- and xCT-transfected *Txnrd2*^{-/-} cells (Figures 36 A and B). xCT-overexpressing cells appeared to have a higher intracellular content of glutathione (Figure 36 A), but the levels of GSH were not significantly different between xCT overexpressing and EGFP expressing control cells, although a tendency to higher intracellular GSH levels was detectable (Figure 36 A). Then, it was asked whether the enforced expression of xCT in *Txnrd2*^{-/-} cells provides a growth advantage to EGFP expressing control cells, particularly when cells were depleted from intracellular GSH by BSO. As illustrated in figure 36 B, xCT-expressing *Txnrd2*^{-/-} cells became highly resistant to BSO-mediated GSH depletion, whereas EGFP-expressing *Txnrd2*^{-/-} control cells rapidly died. This finding perfectly fits with the previous finding, where xCT overexpressing HH514 cells were shown to be highly resistant to various triggers of oxidative stress including GSH depletion (Banjac et al., 2008). In the same study it was also shown that xCT expressing HH514 cells secrete vast amounts of reduced cysteine into the medium. Therefore, it was investigated whether xCT expressing *Txnrd2*^{-/-} cells can rescue EGFP expressing *Txnrd2*^{-/-} cells from cell death induced by BSO. In fact, co-culture experiments revealed that EGFP-transfected cells survived and proliferated at the same rate as xCT-transfected cells in the presence of BSO (Figure 36 C). This strongly favors the idea that xCT-expressing cells protect EGFP-transfected cells from BSO-induced cell death by secretion of reduced cysteine, which is then readily taken up by EGFP-transfected cells, thus bypassing the requirement for intracellular GSH for EGFP-transfected cells. On the other hand, these findings also imply that *Txnrd2* is not responsible for (Cys)₂ reduction in the cells. In a parallel study by Pankaj Kumar Mandal in our laboratory (PhD thesis submitted to LMU, Munich, July 2009), evidence has been provided that cytosolic thioredoxin reductase (*Txnrd1*) is the driving force for (Cys)₂ reduction in xCT overexpressing cells when GSH is depleted by BSO treatment.

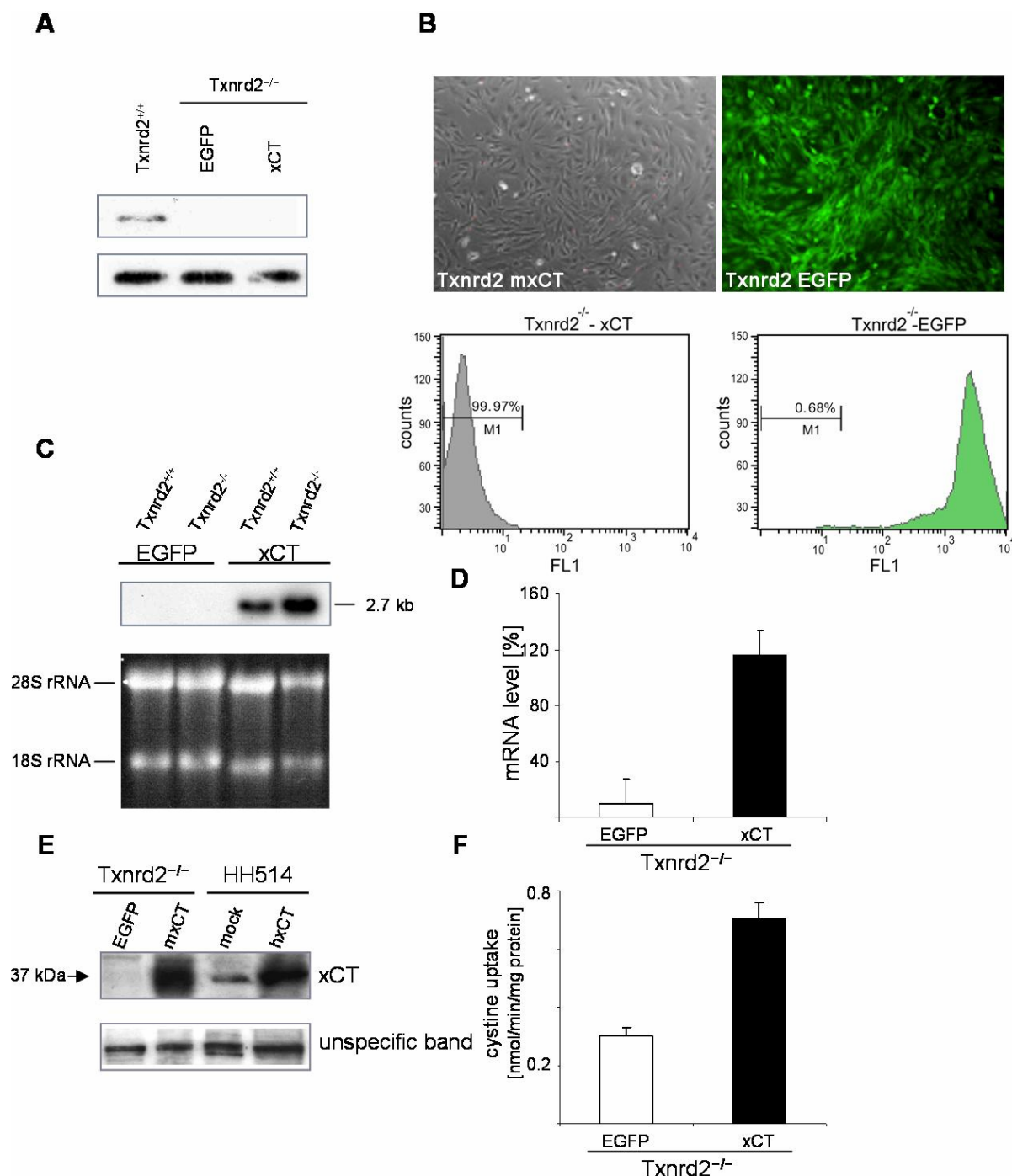


Figure 35. Stable expression of xCT in *Txnrd2*-deficient MEFs. (A) Loss of Txnrd2 in *Txnrd2*^{-/-} cells stably expressing murine xCT or EGFP was confirmed by Western blotting. (B) Stable transfection of *Txnrd2*^{-/-} cells with an EGFP expressing plasmid was monitored by fluorescence microscopy and quantified by flow cytometry one week after selection with 2 µg/ml puromycin. (C) Northern blot analysis of xCT expression in *Txnrd2*^{+/+} and *Txnrd2*^{-/-} cells stably transfected with EGFP or xCT. Equal loading of samples was assessed by visualizing 28S and 18S rRNA bands of the corresponding agarose gel. (D) xCT expression in *Txnrd2*^{-/-} cells was confirmed by qRT-PCR. (E) xCT expression was analysed by immunoblotting of cells expressing mouse xCT in *Txnrd2*^{-/-} MEFs. HH514 cells overexpressing human xCT served as positive control. Note, murine and human xCT (37 kDa) migrate faster than predicted (55 kDa) in SDS-PAGE, which is line with previous reports. An unspecific band was used as loading control. (F) Cystine uptake measurements showed a 3-fold increased cystine uptake activity of xCT-overexpressing cells as compared to EGFP-transfected cells.

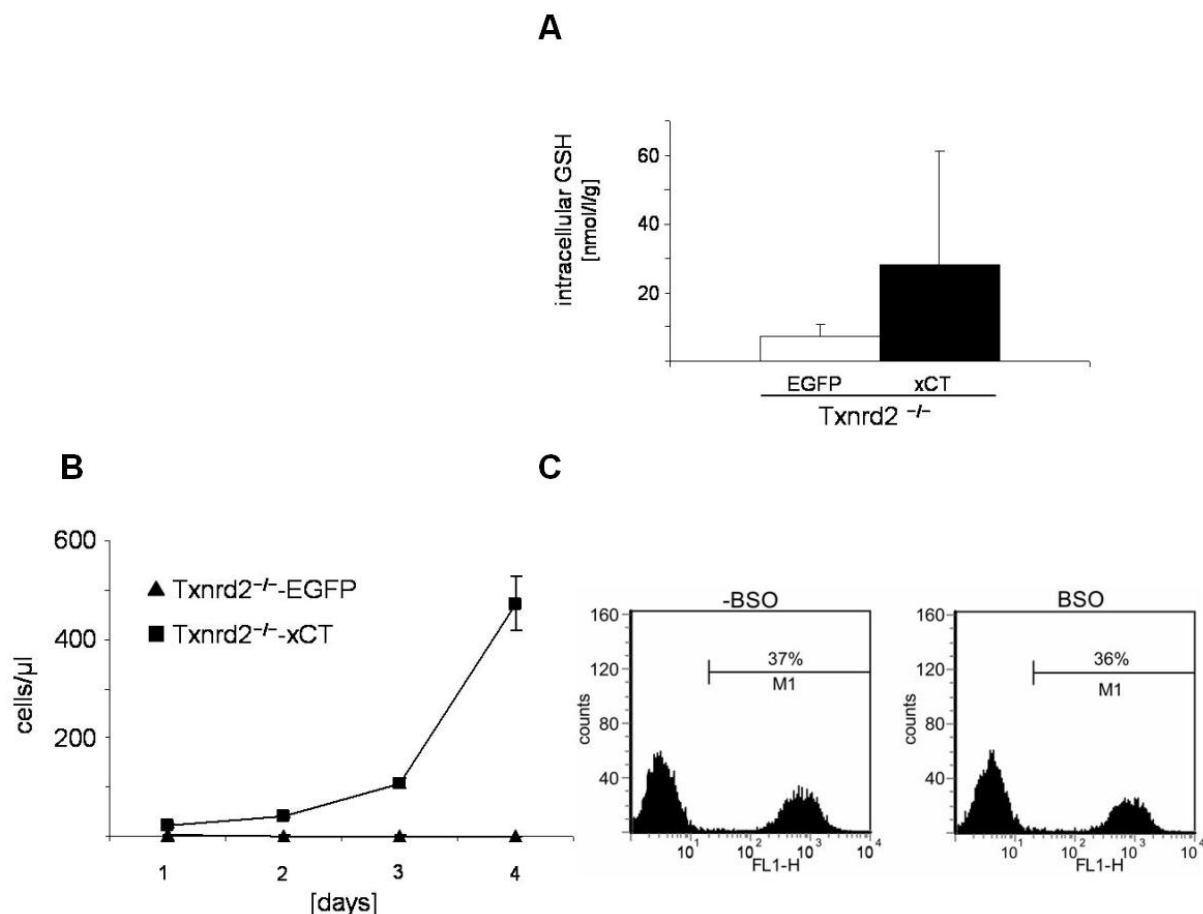


Figure 36. xCT overexpression in *Txnrd2*^{-/-} cells increases the levels of intracellular GSH and rescues *Txnrd2*^{-/-} cells from cell death induced by GSH depletion. (A) Intracellular glutathione levels were measured by HPLC, revealing an approx. 3-fold increase in glutathione level in xCT-expressing cells. (B) Overexpression of xCT in *Txnrd2*^{-/-} MEFs protected cells from cell death induced by GSH depletion (10 μ M BSO). (C) Co-culture experiments were conducted to address whether xCT expressing *Txnrd2*^{-/-} cells may protect EGFP-transfected *Txnrd2*^{-/-} cells from cell death induced by GSH depletion. Both cell lines were plated at the same cell number in the presence of 10 μ M BSO, and the number of EGFP-positive cells was evaluated 48 h after plating by flow cytometry. xCT overexpressing cells protected EGFP-transfected cells from BSO-induced cell death. xCT overexpressing cells reduce cystine and secrete the surplus of reduced cysteine. xCT overexpressing cells thus act as feeder cells by providing cysteine and thus rescue EGFP-expressing cells from cell death.

3.3. Generation of conditional xCT-knock-in mice

3.3.1 Gene targeting in ES cells

To study the contribution of system x_c⁻ to cellular redox balance, its role in antioxidant defense, and its function in the immune system and brain development, transgenic knock-in mice (designated as R26mxCT^{flSTOP}) that allow spatio-temporal expression of xCT light chain were generated. To this end, the *Rosa26* locus was chosen for two reasons: (i) the *Rosa26* promoter is ubiquitously active, and (ii) the *Rosa26* locus had been frequently and successfully used to express numerous genes in mice in a conditional fashion (Farley et al.,

2000; Hameyer et al., 2007; Homig-Holzel et al., 2008; Ivanova et al., 2005; Jager et al., 2004; Soriano, 1999; Srinivas et al., 2001). To be able to target the xCT expression cassette into the *Rosa26* locus of the E14tgTG2 ES cell line (Figure 37 A), a targeting vector for homologous recombination in ES cells was generated. Namely, the murine xCT cDNA was inserted behind a loxP-flanked cassette consisting of the FRT-flanked *neomycin phosphotransferase* gene followed by a transcriptional STOP (Figure 37 A). The entire cassette was additionally flanked by two arms for homologous recombination in ES cells. After successful recombination of this cassette into the *Rosa26* locus and Cre-mediated removal of the *neomycin phosphotransferase*-STOP element, xCT expression is driven by the endogenous *Rosa26* promoter.

After electroporation of E14tgTG2a ES cells with the targeting construct *Rosa26-neoR-STOP-xCT*, approximately 300 G418-resistant clones were picked and individually expanded. Genomic DNA was isolated and digested with *EcoRI*. ES cell clones carrying the targeted *Rosa26-neoR-STOP-xCT* allele were identified by Southern blotting (Figure 37 B).

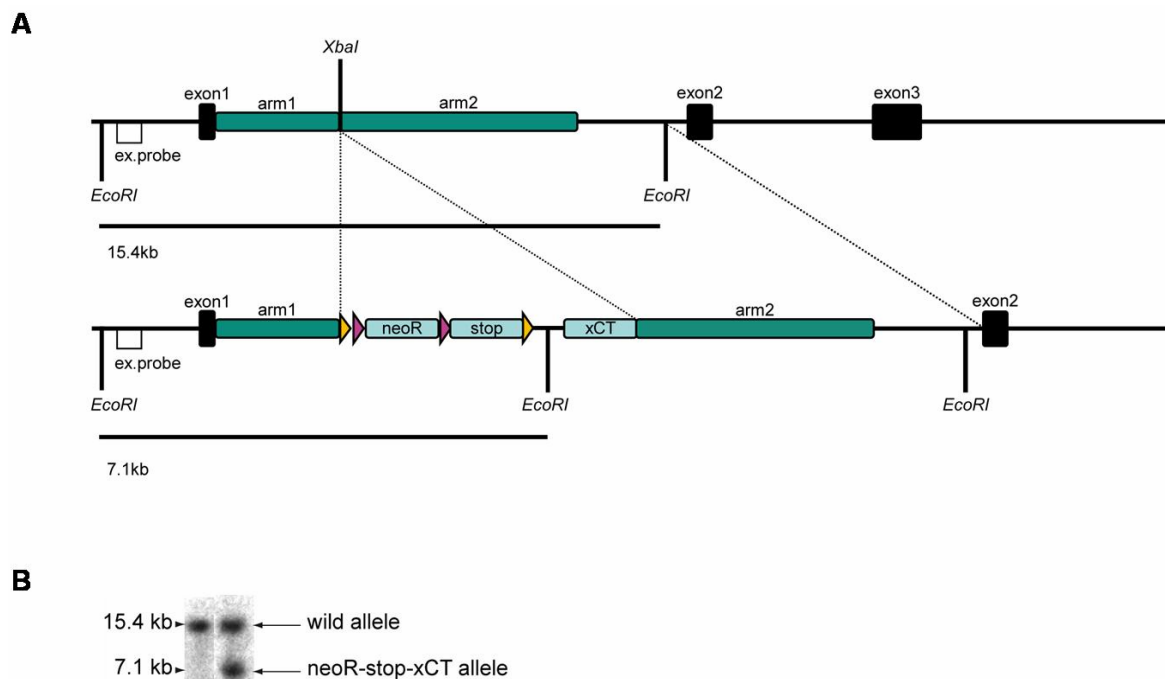


Figure 37. xCT knock-in strategy into the *Rosa26* locus of murine ES cells. (A) In the upper line, the wild-type *Rosa26* gene locus is shown. Below, the strategy for the xCT knock-in into the *Rosa26* locus is depicted. Cre-mediated removal of the *neo* (*neomycin phosphotransferase*)-STOP cassette induces gene expression of the xCT transgene. Depending on the promoter used for Cre expression, expression of xCT is achieved in a tissue-specific manner (loxP sites are depicted by yellow triangles and FRT sites by violet triangles). (B) Homologous recombination in ES cell clones was confirmed by Southern blotting. The cassette inserted into the unique *XbaI* site in *Rosa26* locus introduced an additional *EcoRI* site. *EcoRI*-digested ES cell DNA was separated by gel electrophoresis, the fragments transferred onto a nitrocellulose filter and visualized by hybridization with an external probe (Ex.probe), depicted in (A).

Eleven clones out of 300 were obtained which successfully harboured the *Rosa26-neoR-STOP-xCT* allele. Thus, homologous recombination occurred at approximately 3% frequency. Two of these cell lines (E14tg2a-tvRosa26-xCT2 and E14tg2a-tvRosa26-xCT4) were then used for blastocyst injection (see subsection 2.2.6).

3.3.2. Analysis of the functionality of the neoR-STOP-xCT cassette

To test for the functionality of xCT expression, ES cell clones with successful homologous recombination of the *neoR-STOP-xCT* allele were stably transfected with the pCAG-3SIP-based plasmids MerCreMer-IRES-Puro and EGFP-IRES-Puro as control, allowing stable selection of transfected clones with puromycin. The presence of Cre in MerCreMer-IRES-Puro-transfected cells was confirmed by PCR of genomic ES cell DNA (Figure 38 A).

Expression of EGFP in control-transfected cells was determined by flow cytometry (Figure 38 B). MerCreMer-IRES-Puro-transfected ES cells were treated with 4-OH-tamoxifen (Tam) for 48 h and cystine uptake was measured using ^{14}C -labelled cystine. Cells, in which the floxed *neo-STOP* cassette had been removed by Cre, displayed an approximately 3-fold increase in cystine uptake activity compared to non-treated or EGFP-transfected cell lines. Although expression of xCT appears to be rather low, this finding is in line with previous studies, which showed that the *Rosa26* promoter is a rather weak to moderately active promoter.

3.3.3. Generation of *R26mxCT^{flSTOP/CreERT2}* mice

Seven chimeric mice were obtained from the E14tg2a-tvRosa26-xCT4 cell line and three additional chimeric mice from the E14tg2a-tvRosa26-xCT2 cell line (Table 1) (Figure 39 A).

Table 1. Percentage of black and chinchilla coat colour of chimeras obtained by injecting two independent E14tg2a cell clones into C57BL/6 blastocysts.

E14tg2a-TVROSA26-xCT-4	black [%]	chinchilla [%]
1	10	90
2	0	100
3	40	60
4	5	95
5	10	90
6	5	85
7	0	100
E14tg2a-TVROSA26-xCT-2	black [%]	chinchilla [%]
1	0	100
2	0	100
3	80	20

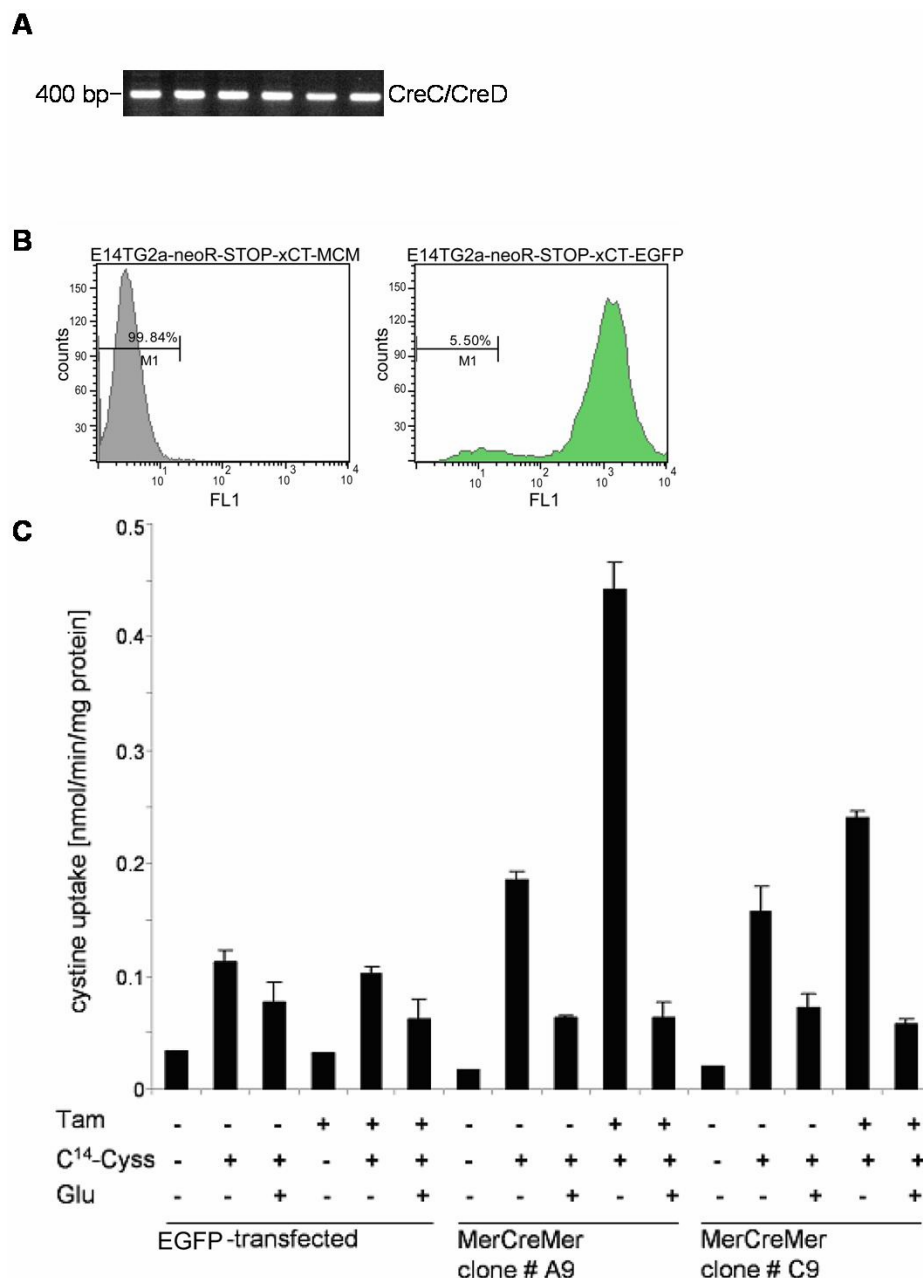


Figure 38. Cystine uptake is significantly increased in xCT-expressing ES cells. (A) Transfection of the ES cell clones with MerCreMer (MCM)-IRES-Puro vector was confirmed by PCR. The primer pair CreE/CreD specifically detects the *Cre-recombinase* gene (400 bp). (B) Flow cytometry analysis of ES cells after stable transfection and 5 days of puromycin selection with the MerCreMer-pCAG and EGFP-pCAG expression vectors. (C) L-[¹⁴C(U)]cystine uptake was measured in xCT knock-in ES cell lines, transfected with either EGFP (mock) or with the Tam-inducible MerCreMer (two independent clones A9 and C9). 2.5 mM glutamate (Glu) was used to specifically inhibit system x_c⁻ activity.

All chimeras were backcrossed to C57BL/6 mice for germline transmission. Finally all mice with agouti coat colour transmitted the targeted *neoR-STOP-xCT* allele to progeny mice (*R26mxCT^{flSTOP}*) at a frequency of 24% (Figures 39 B and C).

3.3.4. Breeding of xCT-transgenic mice with the Tam-inducible *CreERT2-Deleter* mouse

To activate the xCT transgene in every tissue, the *R26mxCT^{flSTOP}* mice were crossed to Cre-transgenic mice expressing CreERT2 (Hameyer et al., 2007). These mice express the Cre-estrogen receptor fusion protein (CreERT2) under the control of the Rosa26 promoter in all tissues except brain (Hameyer et al., 2007).

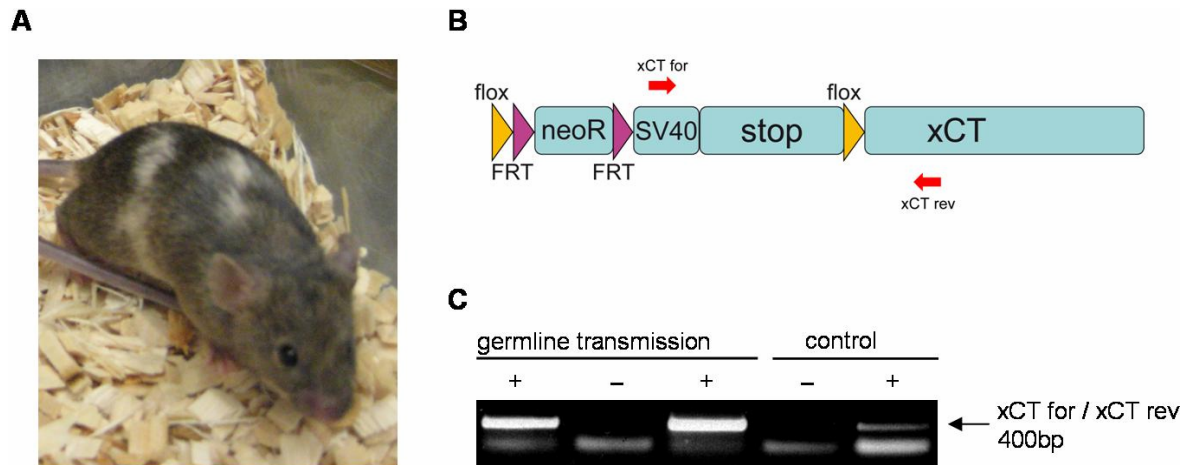


Figure 39. Germline transmission of the targeted xCT knock-in allele. (A) Ten chimeras were generated by injecting two different 129/Ola-derived E14tg2a-tvRosa26-xCT cell lines into C57BL/6 blastocysts (see also Table 1). (B) The position of the primer pair used for the identification of targeted *Rosa26* allele is depicted. (C) Confirmation of germline transmission of the targeted *Rosa26* allele was performed by PCR of tail biopsies using the primer pair that gives a 400 bp fragment, which is specific for the knock-in allele. The targeting vector tvRosa26-mxCT was used as a positive control.

This fusion protein is retained in the cytoplasm by binding to the heat shock protein 90 via the estrogen receptor. Only upon Tam administration, CreERT2 is liberated from this complex and translocates to the nucleus, where Cre-mediated deletion of the loxP-flanked *STOP* cassette occurs. *R26mxCT^{flSTOP/CreERT2}* mice were obtained at the Mendelian ratio from breeding of *Rosa26-CreERT2 deleter*-mice with *R26mxCT^{flSTOP}* mice. *R26mxCT^{flSTOP/CreERT2}* mice were fully viable, grossly normal and fertile.

3.3.4. Phenotypic analysis of *R26mxCT^{flSTOP/CreERT2}* mice

3.3.4.1. Analysis of adult haematopoiesis of *R26mxCT^{flSTOP/CreERT2}* mice

To activate xCT expression, *R26mxCT^{flSTOP/CreERT2}* mice were fed a Tam-containing diet as described previously (Kiermayer et al., 2007). Tam administration induced xCT expression, as shown for brain, spleen and kidney (Figure 40 A). Thus, apparently there is some

contradiction with regard to expression of Cre in brain tissue (see (Hameyer et al., 2007)). Already three to four weeks after Tam feeding, *R26mxCT^{flSTOP/CreERT2}* transgenic mice started to loose weight (Figures 40 B and C) and were suffering as judged by their bristle coat and by an abnormal posture. Five to six weeks after Tam administration the xCT transgenic mice had to be euthanatized (Figure 40 C).

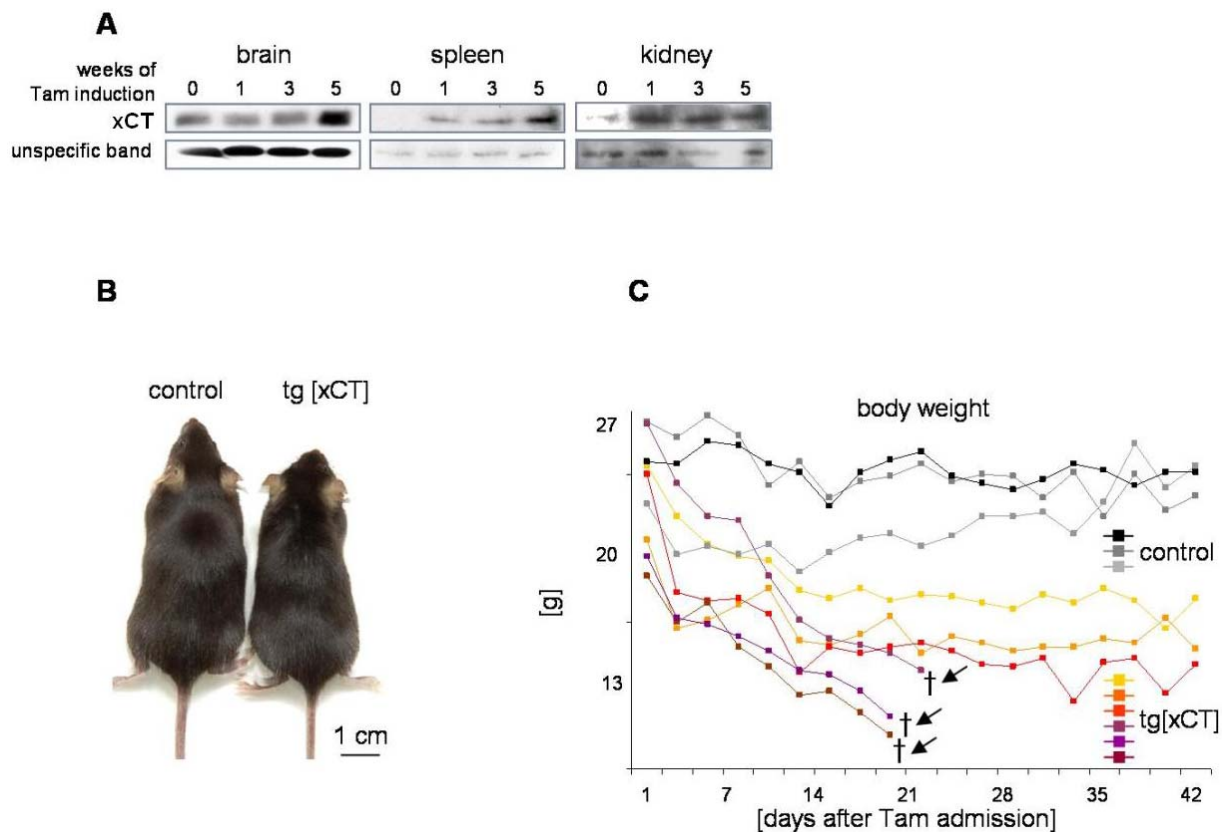


Figure 40. Inducible xCT expression appears to be toxic to mice. (A) Protein lysates were prepared from snap-frozen tissues from the xCT/CreERT2 double transgenic (tg[xCT]) mice at different time periods after Tam induction (0, 1, 3 and 5 weeks), the proteins separated by PAGE, blotted onto nitrocellulose and xCT visualized with a xCT-specific antibody (B and C) Double transgenic mice lost body weight two to three weeks after Tam feeding. Three to four weeks after Tam feeding, three of six tg[xCT] mice had to be euthanatized. Single transgenic mice (control) survived Tam treatment. Body weights were measured from a cohort of 9 mice ($n=3$ control animals and $n=6$ transgenic animals).

Hemogram analysis revealed that the transgenic animals suffered from severe anaemia. This was evidenced by a decrease in the number of red blood cells (RBC), lowered haemoglobin and a decline in hematocrit value (Figures 41 A-C). The mean cell volume (MCV) was decreased, indicating the appearance of microcytic RBCs in the circulation and iron deficiency (Figure 41 C).

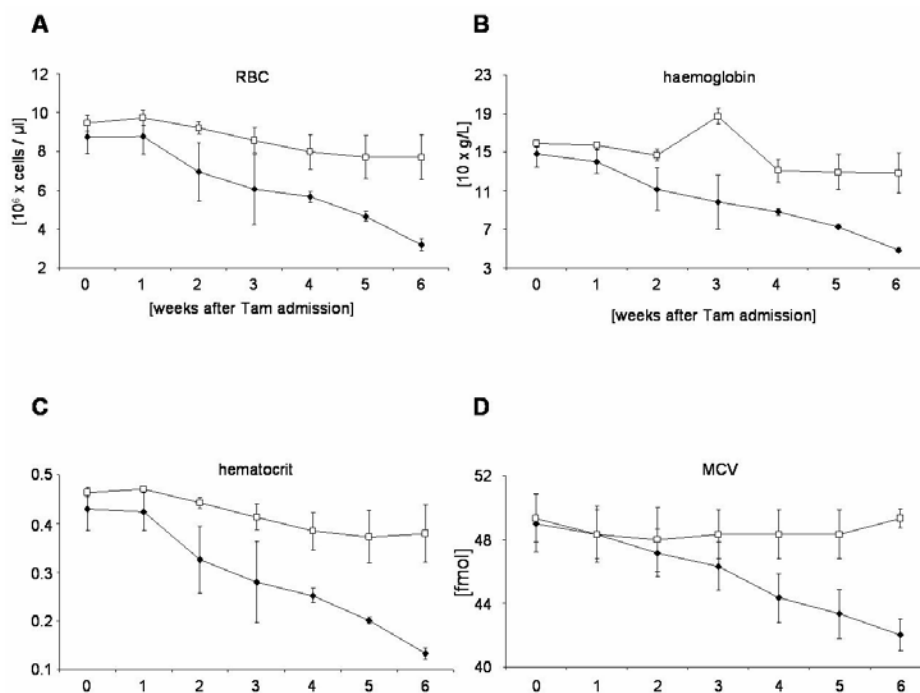


Figure 41. xCT expressing mice suffer from severe anemia as judged by hemogram analysis. (A) Shown are the average number of red blood cells (RBC), (B) the average level of haemoglobin, (C) hematocrit, and (D) mean cell volume (MCV). In each graph, the mean values are depicted \pm SD calculated from $n = 6$ double transgenic animals (filled boxes) and $n = 3$ for control animals (empty boxes).

In contrast to the severe anaemic phenotype of xCT transgenic mice, the platelet counts in transgenic animals were slightly higher than in control animals (Figure 42 A). There were no apparent differences in white blood cell (WBC) counts (Figure 42 B) and differential leukocyte counts (lymphocytes, monocytes, granulocytes and eosinophiles) when transgenic and control animals were compared (Figures 42 C-F). The anaemic phenotype of transgenic animals prompted us to investigate the development of haematopoietic cells in the bone marrow of transgenic animals in more detail.

3.3.4.2. xCT transgenic mice have a higher percentage of haematopoietic stem cells and uncommitted progenitor cells

Haematopoietic stem cells (HSCs) in the adult bone marrow are characterized by a unique combination of surface markers. The most primitive HSCs population is characterized by high levels of c-kit (c-kit⁺) and Sca-1 (Sca-1⁺) and the absence or very low expression of lineage markers (CD3, CD19, Gr-1, B220, Mac-1, Ter119, and CD41) (Lin⁻) (Osawa et al., 1996). This c-kit⁺, Sca-1⁺, Lin⁻ cell population is termed KSL cells representing multipotent progenitor cells.

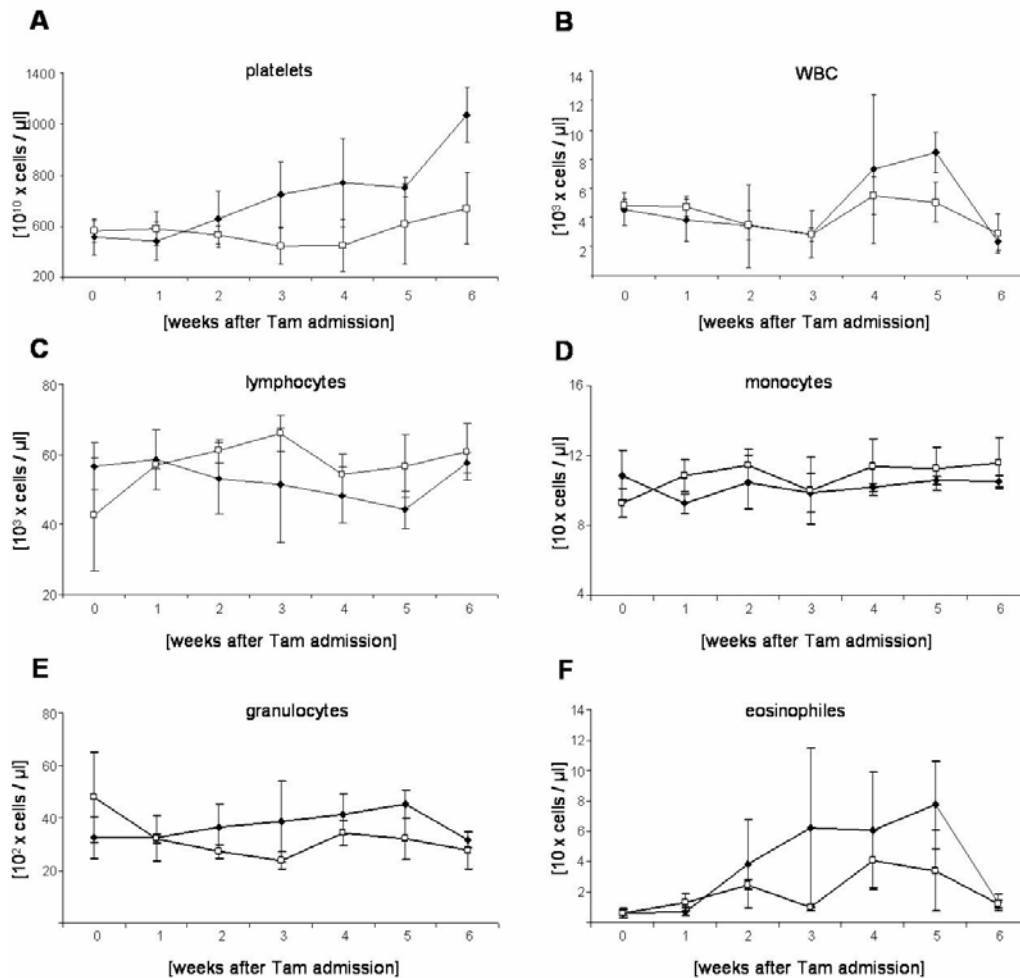


Figure 42. The number of platelets and white blood cells (WBC) was not grossly changed in xCT transgenic mice. (A) The average number of platelets appeared to be slightly higher for double transgenic animals, while the overall number of WBC (B) and differential leukocyte counts (lymphocytes, monocytes, granulocytes and eosinophiles) remained unchanged (C-F). Mean values \pm SD are shown that were calculated from $n = 6$ double transgenic animals (filled boxes) and $n = 3$ for control animals (empty boxes).

Low levels of ROS and a hypoxic microenvironment has been implicated in self-renewal of HSCs and cancer stem cells and the maintenance of stemness (Diehn et al., 2009b; Ito et al., 2004; Ito et al., 2006). Since redox regulation is emerging as a regulator of stem cell differentiation (Ogasawara and Zhang, 2008), the effect of xCT overexpression on the pool of HSCs was investigated by analyzing the KSL population by flow cytometry.

The Lin⁻ cells and c-kit⁺, Sca-1⁺ positive cells were first gated (Figure 43 A). They represented 0.06% of the initial population in *R26mxCT^{CreERT2}* mice in the absence of Tamoxifen, whereas for xCT expressing, Tamoxifen-treated mice the values reached 0.34% of the starting population. In terms of the KSL population this is a considerable difference. Hence, the transgenic mice have more cells in the KSL compartment, which indicated that there is a preferential accumulation of undifferentiated non-committed progenitor cells in the bone marrow of transgenic mice as compared to control mice.

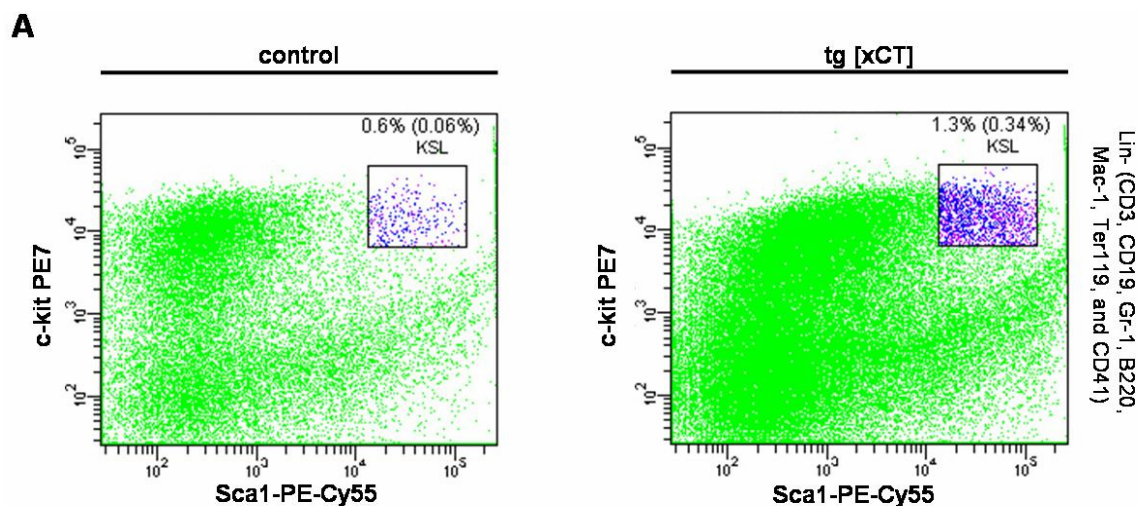


Figure 43. Analysis of the KSL population in the bone marrow of xCT transgenic and control mice. (A) Bone marrow cells were isolated from 20 weeks old mice maintained for four weeks on a Tam-containing diet. Bone marrow cells were stained with c-kit and Sca-1 antibodies to identify haematopoietic progenitor cells. The KSL cell population is characterised by undetectable levels of the lineage markers (Lin⁻), expressed on mature haematopoietic cells, and by high levels of c-kit (c-kit⁺) and Sca-1 (Sca-1⁺). All progenitors were quantified and the numbers presented as percentage of total bone marrow cells. The xCT-expressing mice were found to have more cells in the KSL compartment, i.e. they have a higher percentage of non-committed progenitors.

3.3.4.4. xCT expression leads to defective erythropoiesis

Since constitutive xCT expression was associated with a severe anemia in xCT transgenic mice, we were interested in a development of erythroid lineages of this mice. A scheme of erythroid differentiating progenitors is provided in figure 44 A, which are identified on the basis of the expression of the cell surface markers CD71 (CD71⁺, transferring receptor) and Ter119 (Ter119⁺ glycoprotein A-associated protein). A slightly higher percentage of Lin⁻ (CD3, CD19, Gr-1, B220 and Mac-1), CD71-negative and Ter119-negative cells representing CMPs was found in xCT expressing mice (Figure 44 B). All erythroid precursors like pro-, basophilic-, polychromatic- and orthochromatic-erythroblasts were considerably decreased in the bone marrow of *R26mxCT^{fSTOP/CreERT2}* mice. This clearly indicates that the anaemia observed in xCT expressing mice is caused by impaired development of erythrocytes. Since the bone marrow analysis of adult *R26mxCT^{CreERT2}* mice after four weeks of Tam feeding did not show dysplastic changes, it would be interesting to examine the cell cycle profile of the bone marrow cells in transgenic mice by flow cytometry. So far, flow cytometry analyses provided initial evidence that xCT expression affects bone marrow cell differentiation and impairs erythropoiesis.

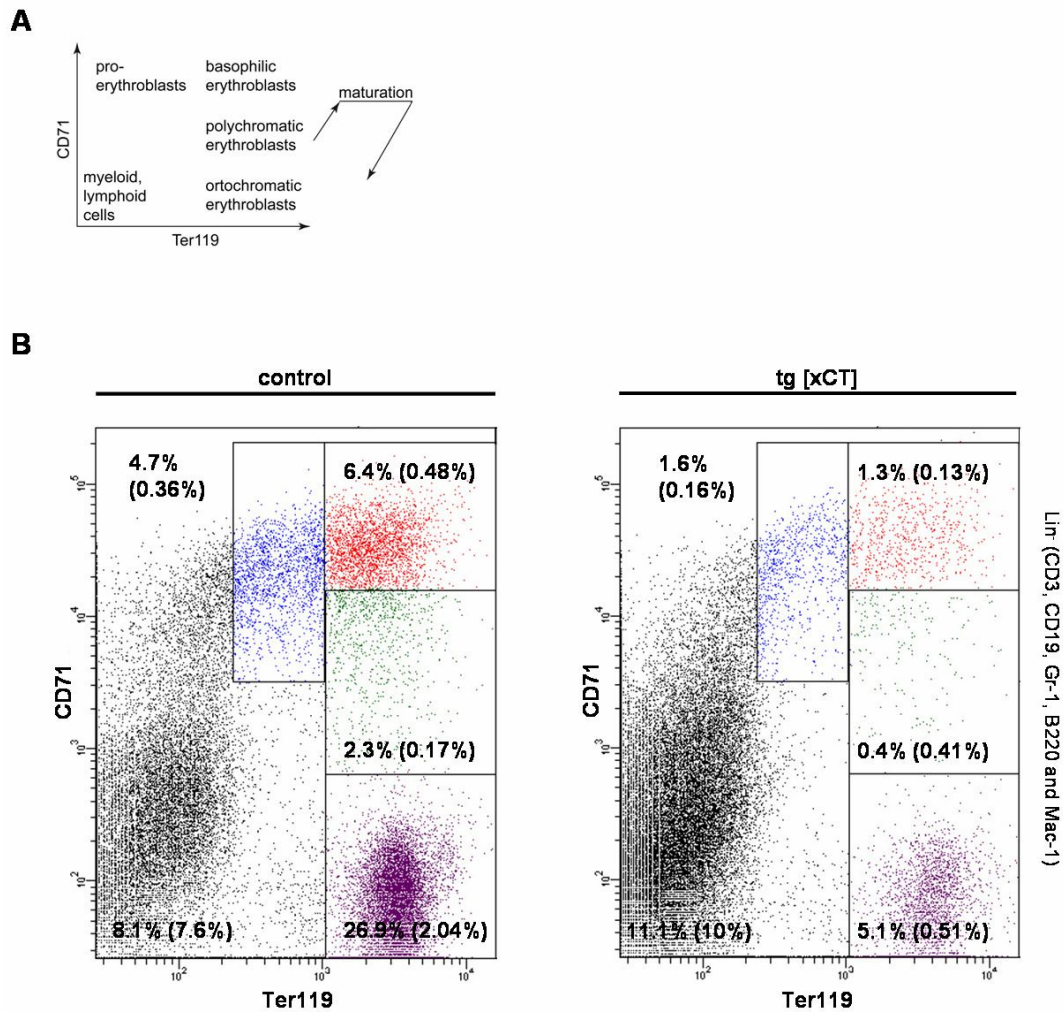


Figure 44. Analysis of the erythroid progenitors in the bone marrow of xCT expressing and control mice. (A) A scheme of erythroid progenitor cells, identified on the basis of the expression of CD71 and Ter119 cell surface markers. (B) Bone marrow cells were isolated from 20 weeks old mice maintained for four weeks on a Tam-containing diet. Bone marrow cells were stained with anti-CD71 (transferrin receptor) and anti-Ter119 (glycophorin A-associated protein) to identify erythroid progenitor cells. Erythroid maturation was determined in control and transgenic bone marrow. All progenitors were quantified and are expressed as percentage of total bone marrow cells. The CD71 and Ter119 profiles of bone marrow cells showed abnormal erythroid maturation in xCT expressing mice.

3.3.4.5. Constitutive expression of xCT leads to atrophy of spleen and testes and thymic aplasia

Already during autopsy of xCT expressing mice it was apparent that the size of some organs of the transgenic mice was strongly diminished and that some organs of these mice were paler compared to control littermates. As illustrated in Figure 41, the spleen and testis of transgenic mice were markedly reduced in size and the weight was reduced by approximately 3-fold compared to control mice (Figures 45 A and B). The relative size of the other organs like liver, heart and kidney did not show major size differences (Figures 45 C-E). Furthermore, the thymus was completely absent from xCT transgenic mice.

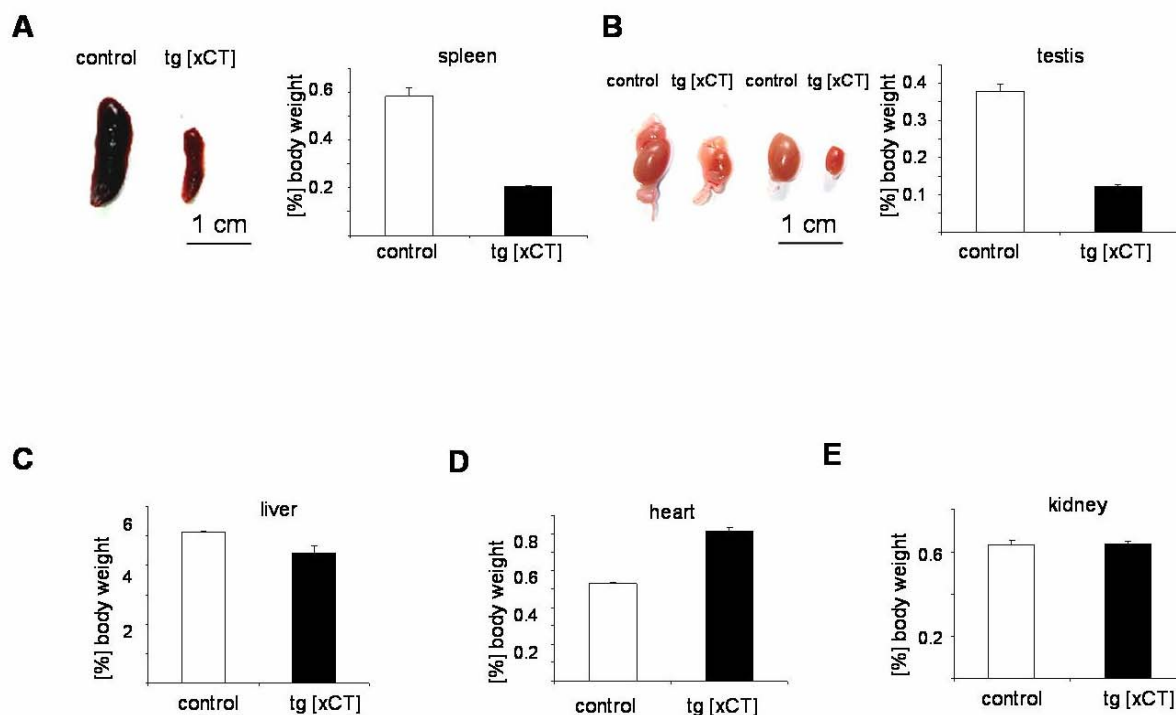


Figure 45. Spleen and testis of xCT expressing mice are strongly reduced in size. (A-E) Age-matched animals of the indicated genotypes (tg[xCT]-*transgen/cre*; control-*transgen/wt*) were sacrificed between 20 and 30 weeks of age after feeding with Tam. (A-B) The size of spleen (A) and testis (B) was strongly diminished, whereas liver, heart and kidney did not show major differences (C-E). The mean organ weight is presented as percentage of the body weight ($n=3$ transgenic and $n=3$ control animals).

Examination of histological sections of the testis stained with H&E disclosed the complete absence of spermatozooids (Figure 46 B, black arrowheads). In contrast, control mice had fully mature and healthy spermatozooids (Figure 46 A, violet arrowheads). Micrographs exhibited degenerative structures (Figure 46 A). TUNEL staining in histological sections revealed an increase in the number of apoptotic cells in the testis of transgenic animals (Figure 46 C and D).

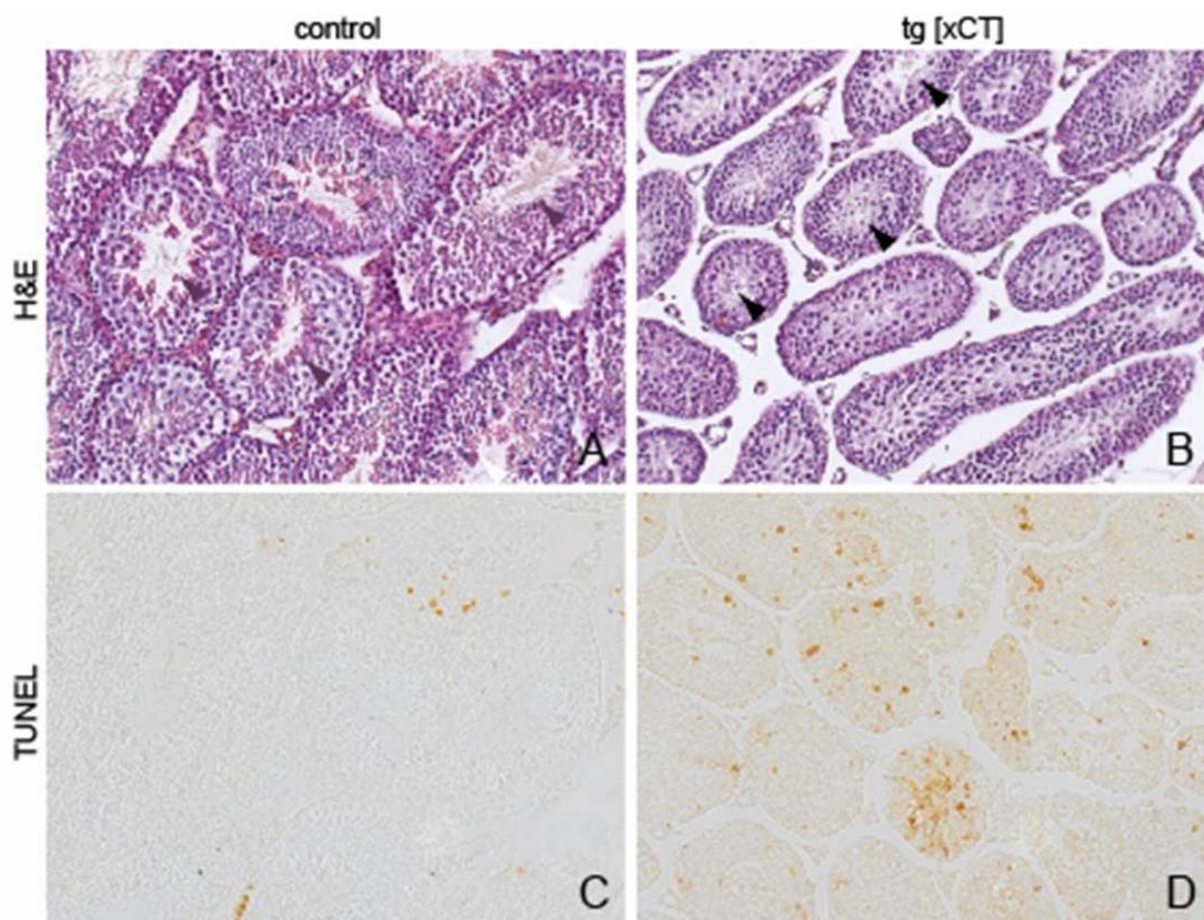


Figure 46. Increased apoptosis in testis of transgenic animal. Staining of formalin-fixed, paraffin-embedded (FFPE) cross sections of testis from control (*transgen/wt*); and transgenic mice (*tg[xCT]-transgen/cre*) are shown. Displayed are 10X H&E (haematoxylin and eosin) and TUNEL micrographs. (A-B) H&E micrographs show overall testis structure that depict degeneration of testis of xCT transgenic animal. Violet arrowheads are showing mature sperm and black arrowheads are indicating absence of the sperm in the testis of the transgenic animals. TUNEL staining of the testis cross sections revealed increased number of the apoptotic cells.

Furthermore, histopathological examinations of hematoxylin and eosin (H&E) stained sections of the spleen revealed that the spleen of xCT-expressing mice had prominent white pulp (Figure 47 B, black arrowheads). Spleen of the *tg[xCT]* mice also contained increased numbers of apoptotic cells in the red pulp, as judged by TUNEL staining (Figures 47 C-F). This result suggest that perturbed cystine/cysteine imbalance and/or altered GSH metabolism triggers apoptosis in this tissue. Observed decrement of the spleen (Figure 45 A) could result from an increased rate red pulp apoptosis (Figures 47 C-F). A destruction of red blood cells, being a normal spleen function, could be in transgenic animals changed due to a lack of red blood cells in the circulation, as already shown in this study.

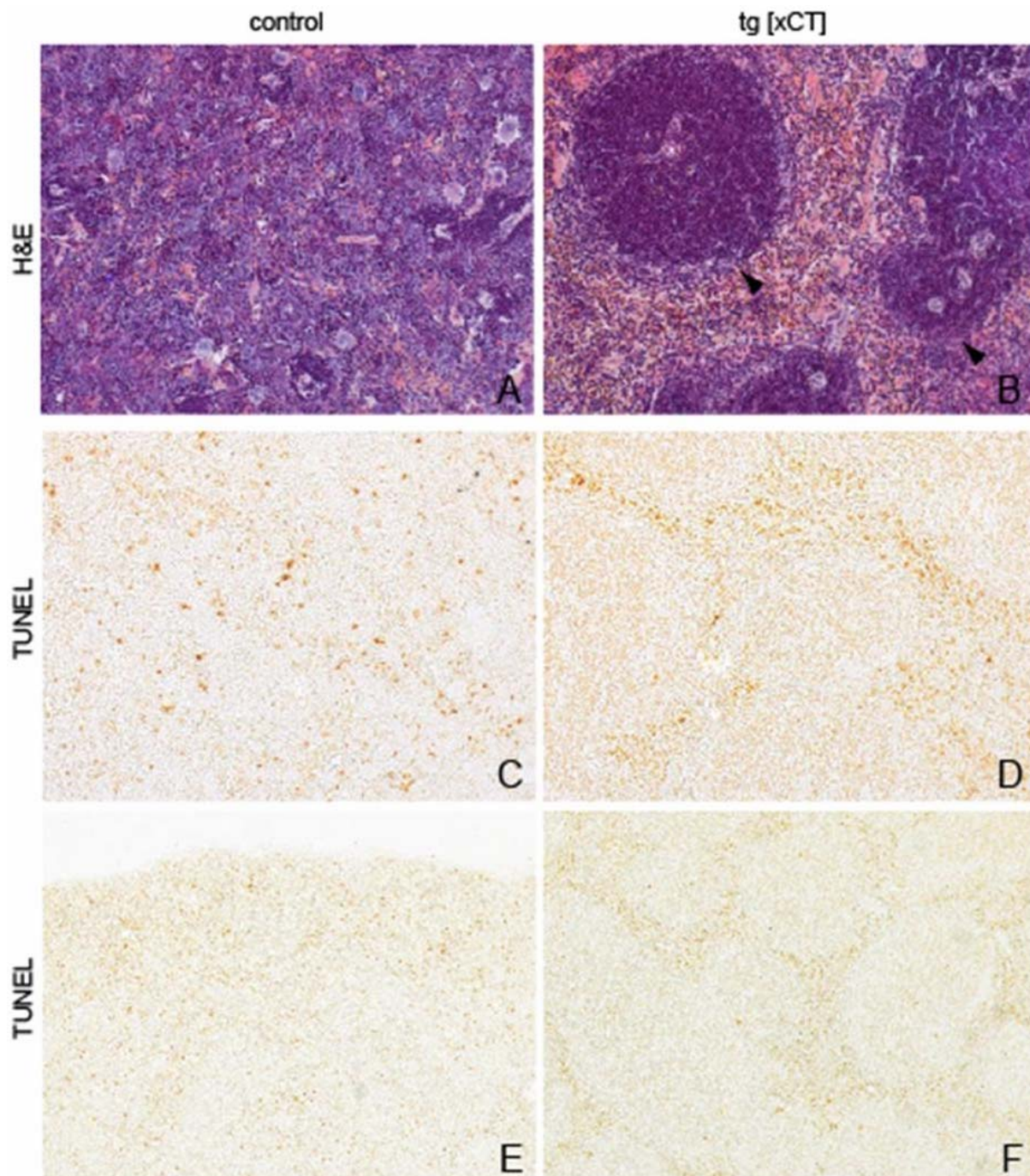


Figure 47. Increased apoptosis in spleen of transgenic animal. Staining of formalin-fixed, paraffin-embedded (FFPE) cross sections of spleen from control (*transgen/wt*); and transgenic mice (*tg[xCT]-transgen/cre*) are shown. Displayed are 10X H&E (haematoxylin and eosin) and TUNEL micrographs. (A-B) H&E micrographs show overall splenic architecture. Black arrowheads are indicating white pulp. (C-D) TUNEL micrographs of the spleen of transgenic animal revealed increased apoptosis in the red pulp (E-D) which is more prominent on the micrographs with 5X magnification.

4. Discussion

4.1. Absence of Txnrd2 causes high ROS accumulation, increased sensitivity towards pro-oxidants and impaired cell growth

Impairment or ablation of enzymes, which are critically involved in the control of cellular ROS concentrations, might cause or aggravate the development of diseases, such as myocardial infarction, stroke, neurodegeneration and tumor development (Anversa et al., 1998; Crack et al., 2001; Diehn et al., 2009b; Francis, 2001; Griendling and FitzGerald, 2003a; Griendling and FitzGerald, 2003b; Ide et al., 2000; Laurent et al., 2005; Lebovitz et al., 1996; Maulik et al., 1998; Nguyen et al., 2006; Pennington et al., 2007; Seiler et al., 2008; Selenius et al., 2008; Talbot et al., 2008; Yang et al., 1996; Yoo et al., 2007). While some recent biochemical and computational studies have revealed the mechanism of Txnrd2 catalysis, understanding the physiological role of Txnrd2 in cells and tissues is still at its infancy. Txnrd2 is predominantly localised in mitochondria, which are the cells' major site of energy production, but which are also involved in the regulation of key cellular processes, such as cell growth, and cell death (Cregan et al., 2004; Gustafsson and Gottlieb, 2008; Karunagaran et al., 2007; Mazumder et al., 2007; Saelens et al., 2004). Although we have provided initial evidence that Txnrd2 is important for the maintenance of mitochondrial function, presumably due to scavenging of mitochondrial ROS (Conrad et al., 2004), the underlying cellular and biochemical mechanisms have only been partially addressed.

Our cellular system with targeted disruption for *Txnrd2* is thus a highly suitable tool for the thorough investigation of Txnrd2-dependent cellular processes. To specifically interfere with Txnrd2 function, Kim and colleagues established on the other hand a cellular system in which a dominant-negative form of Txnrd2 (TXNR2DN) is overexpressed in a tetracycline-regulatable manner (Tet-off-system) (Kim et al., 2003b). The construct was designed such that it lacks the SECIS element. Thereby the UGA codon is read as a translational stop codon and thus yields a truncated mutant lacking the two C-terminal residues Sec and Gly. The dominant negative effect of this mutant was confirmed by measuring decreased Txnrd activity. Moreover, cells expressing TXNR2DN were shown to produce more hydrogen peroxide than non-induced cells when stimulated with EGF (Kim et al., 2003b). In a follow-up study, Chang et al., 2005 overexpressed an alternative splicing variant of TXNRD2 under Tet-off control, which had 3 independent point deletions in the coding region and an insertion of 1228 bp in the 3'-UTR, between the stop codon and the SECIS element (Chang et al.,

2005). Again, TXNRD activity in whole cell lysates was decreased which resulted in alterations of cellular ROS levels and increased apoptosis.

A genetic model is certainly preferable to ablate Txnrd2 function because overexpression of dominant negative mutants of Txnrd2 may cause side effects as artificial gain of function. For instance, it has been shown that a C-terminally truncated form of Txnrd1 acquires NADPH oxidase activity as gain-of function and causes increased oxidative stress and apoptosis (Anestal et al., 2008). Moreover, it was also shown recently that the N-terminal catalytic site alone may harbour specific functions independently of the C-terminal catalytic site (Lothrop et al., 2009). Pharmacological studies that would specifically target Txnrd2 might be interesting, but certainly hardly feasible, since Txnrd1 and Txnrd2 are highly homologous and the basic catalytic mechanisms are virtually identical. In general, inhibiting either Txnrd1 or Txnrd2 specifically will be a major challenge, but certainly worthwhile as Txnrd1 and Txnrd2 are involved in different cellular functions. For instance, overexpression of Txnrd1 (and Txn1) has been frequently linked to tumor growth, and thus targeting Txnrd1 alone might be an interesting strategy for cancer treatment (Brigelius-Flohe, 2008; Nguyen et al., 2006; Pennington et al., 2007; Selenius et al., 2008; Talbot et al., 2008; Yoo et al., 2007).

As described earlier (Conrad et al., 2004), primary *Txnrd2*^{-/-} MEFs showed reduced proliferation and/or increased apoptosis compared to wild-type counterparts. Since Txnrd2 has been implicated in the protection of cells from toxic amounts of mitochondrial ROS, *Txnrd2*^{-/-} cells were treated with different antioxidants, such as NAC, GSH and α -Toc, to substantiate this notion: NAC, a frequently used antioxidant providing cells with cysteine for GSH biosynthesis, is reported to protect cells against various triggers of oxidative stress (van Zandwijk, 1995); GSH is a cofactor of GSH-dependent enzymes, including GSH peroxidases; α -Toc disrupts the lipid peroxidation chain by one electron reduction of alkyl radicals or peroxy radicals (Ikeda et al., 2003; Seiler et al., 2008; Tagami et al., 1998). By using these different antioxidants it was possible to complement the lack of Txnrd2: knock-out cells were thus able to proliferate in a manner similar to Txnrd2 wild-type cells.

Damdimopoulos and colleagues have previously shown that overexpression of human mitochondrial Trx (Trx2) in HEK-293 cells confers resistance towards etoposide and increases the mitochondrial membrane potential (Damdimopoulos et al., 2004). Furthermore, mice specifically lacking Trx2 die during midgestation due to massive apoptosis (Nonn et al., 2003b). Since under physiological conditions Txnrd2 is the main enzyme for maintaining Trx2 in its reduced state, it was hypothesized that loss of Txnrd2 causes an increase in intracellular (mitochondrial) ROS. The flow cytometry analyses of *Txnrd2*^{-/-} MEFs, stained

with redox-sensitive dyes CM-H2DCF-DA, BODIPY 581/591 C₁₁ and boronate- based fluorophores (PYAM, PYME and mitoPY) revealed strongly elevated ROS levels, such as lipid peroxides and H₂O₂, in mitochondria and in the cytosol of knock-out cells. This rise in ROS could be even exacerbated when GSH was depleted from the cells. On the contrary, the amount of total ROS, as monitored by the non-specific ROS sensor CM-H2DCF-DA, could be dampened by using the antioxidants NAC and α -Toc. Lipid peroxidation, as determined by BODIPY 581/591 C₁₁, could also be detected in the knock-out cells, which was insensitive to NAC but sensitive to α -Toc. These results confirmed that NAC has no scavenging activity towards lipid peroxides, while α -Toc efficiently scavenges lipid peroxides which might be the initial source of ROS. More specifically boronate-based fluorophores which are highly specific for H₂O₂, unmasked higher amounts of H₂O₂ in the cytoplasm as well as in mitochondria of *Txnrd2*^{-/-} cells when compared to wild-type cells. Of course, more studies are required to answer whether lipid peroxidation is the cause or secondary to the generation of other oxygen radical species. Nonetheless, the use of the redox-sensitive dyes corroborates the generation of significant amounts of ROS in cells lacking *Txnrd2* which supports the hypothesis that an increase in ROS is the primary culprit in the impairment of cellular growth. Since the *Txnrd2* knock-out was designed as such that all *Txnrd2* isoforms are simultaneously inactivated, it was an obvious question whether the increase in cellular ROS can be blunted by overexpression of either mitochondrial or cytoplasmic variants of *Txnrd2*. The complex mammalian selenoprotein translational machinery has previously been considered to be the main hurdle when overexpressing selenoproteins in mammalian cells. Yet, in this study it was possible to stably express two wild-type and the two mutant forms of *Txnrd2* in *Txnrd2* knock-out (and wild-type) cells. To achieve this, a lentiviral system was used for expression of TAPE-tagged *Txnrd2* in MEFs. For the mitochondrial and cytoplasmic isoforms, the TAPE-tags were placed after the N-terminal mitochondrial leader sequence (MLS) or directly at the N-terminus, respectively. Since the C-terminus harbouring the catalytic site -Gly-Cys-Sec-Gly- is highly flexible and important for thioredoxin reductase function (Gasdaska et al., 1999b; Gladyshev et al., 1996; Lee et al., 1999; Miranda-Vizuete et al., 1999; Sandalova et al., 2001; Tamura and Stadtman, 1996; Watabe et al., 1999; Zhong and Holmgren, 2000), the N-terminus was used for fusion with TAPE-tag. When the cell lysates of mito*Txnrd2* overexpressing cells were immunoblotted with an anti-*Txnrd2* antibody, two bands appeared. This was not the case when the lysates were blotted against anti-FLAG, suggesting that upon transport into mitochondria the MLS of mito*Txnrd2* was processed as such that either the MLS alone or the MLS along with the TAPE-tag were removed (Chang et al., 2005); apparently, both forms were produced at an equal ratio. On the other hand, for the cytoplasmic form there was only one single band detectable with both antibodies, which was equal in size with the larger mitochondrial form due to the tag. To

further confirm their subcellular localisation, immunocytochemical staining with the anti-FLAG antibody and confocal microscopy were performed. The mitochondrial form of Txnrd2 was in fact localised in mitochondria and the cytoplasmatic form was evenly distributed throughout the cytosol.

It is highly likely that the mitochondrial isoform plays an important role in the scavenging of mitochondrial ROS generated as a side product of oxidative phosphorylation. On the other hand, the role of cytoplasmatic form, e.g. in ROS removal, is not known. The add-back of the cytoplasmatic variant of Txnrd2 was also shown to decrease the level of ROS in Txnrd2 knock-out cells, which was unexpected. However, as the uncharged H₂O₂ can freely diffuse across membranes it may be concluded that the major form of ROS released by mitochondria might be H₂O₂. Needless to say, many questions regarding the nature and the spatiotemporal generation of ROS remain to be addressed in the future. Recently, a novel method was developed that allows to monitor the dynamic changes of redox-based processes in living cells by using appropriate redox biosensors (Gutscher et al., 2008). This biosensor is a fusion protein between human glutaredoxin-1 (Grx1) and the sensor protein roGFP2. Stable expression of the Grx1-roGFP2 fusion protein allows dynamic live imaging of the cellular redox potential, which is mainly based on the pool of intracellular reduced glutathione (glutathione is present up to 10 mM in cells). Since the biosensor can be targeted to different subcellular compartments one may also study the redox potential in the different compartments. It thus facilitates the real-time determination of redox changes in response to growth factor stimulation, cell density, mitochondrial depolarization, respiratory burst activity and immune receptor stimulation. Hence, this technique offers new opportunities to analyze in more detail the intracellular generation and distribution of ROS in *Txnrd2* knock-out cells.

Reportedly, MEFs overexpressing Txnrd were shown to have slightly retarded growth (Patenaude et al., 2004; Powis et al., 1997a; Powis et al., 1997b; Spyrou et al., 1997). The overexpression of Trx2 and Txnrd2 efficiently lowered the level of ROS and consequently reduced p42/p44 MAPK phosphorylation, which was proposed to be the mechanism that slows down cell proliferation (Zhou et al., 2008). It thus appears that the redox status in cells controlled by the thioredoxin/thioredoxin reductase system affects growth and differentiation and is involved in fine tuning of molecular signalling pathways.

To address whether *Txnrd2*^{-/-} MEFs are also more sensitive to exogenous stress, cells were treated with compounds, such as doxorubicin, cisplatin, peroxides, antimycin A and PEITC, all known to induce the generation of free radicals. It is well established that doxorubicin

intercalates into DNA, but also induces ROS (Bachur et al., 1977; Gutierrez et al., 1983) by using electrons from mitochondrial complex I (Davies et al., 1983). Cisplatin, another anticancer drug, was included in these studies. cis-Diammineplatinum(II) dichloride causes the formation of cisplatin-platinum complexes in cells, which bind and lead to cross-linking of DNA, ultimately triggering cell death and the generation of ROS (Martins et al., 2008). *Txnrd2* knock-out cells were only moderately more sensitive to the treatment of the anticancer drugs in terms of cell death; however in the presence of peroxides, antimycin A and PEITC treated *Txnrd2* knock-out cells readily died. Thus, the higher ROS content of *Txnrd2* null cells was apparently exacerbated by these compounds, eventually triggering the rapid onset of cell death due to the severe impairment of *Txnrd2* null cells to cope with the additional ROS.

The initial observation that *Txnrd2*^{-/-} cells are highly sensitive to GSH depletion induced by BSO (Conrad et al., 2004), prompted us to study the GSH levels in *Txnrd2* knock-out cells. The determination of GSH levels in the knock-out and control cells showed that wild-type cells had three times higher GSH levels than *Txnrd2*^{-/-}. This confirmed that *Txnrd2* knock-out cells apparently compensate for the lack of *Txnrd2* by consuming higher levels of GSH thus leaving the cells highly sensitive towards the GSH-depleting compound BSO. These results demonstrated that cells lacking only one of the key enzymes of the thioredoxin system, when devoid of glutathione, the second important intracellular antioxidant system, undergo cell death due to the additive adverse effects. Thus, the two pathways act in a collaborative manner to protect cells against oxidative stress. Recently, Lu and colleagues showed that inhibition of thioredoxin reductase by arsenic trioxide (ATO) in human breast MCF-7 cancer cells sensitizes them to apoptosis, particularly when used in combination with agents that reduce the intracellular GSH concentrations, such as BSO (Lu et al., 2007). The authors discussed several mechanisms, which may lead to this phenotype. The combination of ATO and BSO may result in the disruption of the electron supply for DNA synthesis and simultaneously induce augmented oxidative stress which cooperates in the induction of cell death. These effects are considered to be the reason for H₂O₂ accumulation in cells upon ATO treatment (Jing et al., 1999). Trx provide electrons to peroxiredoxins for scavenging H₂O₂ and alkyl peroxides (Kang et al., 2004). GSH also participates in removing hydroperoxides by acting as a cofactor for glutathione peroxidases (Conrad, 2009). Both thioredoxins and glutaredoxins/GSH provide electrons to ribonucleotide reductase (RNR), which is essential for DNA synthesis (Holmgren, 1985; Holmgren, 1989; Lammers and Follmann, 1984; Reichard, 1988; Thelander and Reichard, 1979). Moreover, DNA repair activity through Ref1, p53, and RNR is also controlled by Trx, and inactivation of the Trx system presumably impedes DNA repair process (Seemann and Hainaut, 2005; Tanaka et al., 2000). Trx is also cofactor of methionine sulfoxide reductases, and thus is involved in the

repair of oxidised proteins (Hoshi and Heinemann, 2001). Yet, the use of ATO does not discriminate between the two thioredoxin reductases and thus does not allow to specifically target either mitochondrial or cytoplasmatic thioredoxin reductase. Also bearing in mind the *in vitro* observation of Turanov and colleagues (Turanov et al., 2006) that Trx1 can be equally well reduced by Txnrd2 as Trx2, the role of Txnrd2 on some of the processes that take place in cytoplasm should not be underestimated, particularly considering the presence of two Txnrd2 isoforms localised in cytoplasm.

4.2. Compensatory up-regulation of mitochondrial peroxiredoxins III and V in response to Txnrd2 disruption

Mammalian cells express two peroxiredoxins that are mainly localised in mitochondria: Prx III and Prx V. Prx III is exclusively expressed in mitochondria, Prx V is also localised to peroxisomes (Seo et al., 2000) and the nucleus (Kinnula et al., 2002). The mitochondrial thioredoxin system was already shown to provide electrons for peroxiredoxin III in *ex vivo* studies. It was shown that SP-22 (= Prx III) along with Trx2, partially purified mitochondrial thioredoxin reductase from bovine adrenocortical mitochondria, and NADPH had the ability to protect oxyhemoglobin against ascorbate-induced damage (Watabe et al., 1995; Watabe et al., 1997; Zhang et al., 2007). Furthermore, NADPH was consumed in equimolar amounts by Txnrd2, Trx2, and Prx III to reduce hydrogen peroxide and *t*-butylhydroperoxide (Watabe et al., 1997). Only the combination of all these factors conferred the hemoglobin-protecting and peroxide reducing activities. Evidence for these *in vitro* findings at the cellular level could be provided by this work. Here, it could be shown that basal Prx III and Prx V protein levels were increased in *Txnrd2*^{-/-} cells and that the expression of Prx III and Prx V could be further stimulated by various triggers of oxidative stress. The analysis of the oxidation state of the catalytically active site cysteines with an antibody specifically detecting the sulfenic and sulfinic forms of Prx I and Prx II (Woo et al., 2003a; Woo et al., 2003b) provided initial insights that the overoxidised forms of Prx I and PrxII/PrxIII were present at higher levels in knock-out than in wild-type cells in response to increasing H₂O₂ concentrations. However, it still remains to be clarified whether this is in fact due to overoxidation or due to augmented transcription and/or translation of the respective genes and proteins. The rapid H₂O₂-induced up-regulation, in particular of Prx III and Prx V, suggests that this is regulated at the translational and posttranslational rather than at the transcriptional level. It is tempting to speculate that there are systems in cells which sense and swiftly respond to increasing concentrations of ROS by enhancing the translation efficiency of antioxidant enzymes through binding to yet-unrecognized regulatory elements on their mRNAs.

The fact that the mRNA and protein levels of other Prxs were not changed suggests that the impairment of Txnrd2 function mainly affects mitochondrial peroxiredoxins. This implies that Txnrd2, Trx2 and Prx III and Prx V are indeed functionally connected *in vivo*. Similarly, in yeast the lack of the Trx enzyme induced increased expression of thioredoxin-dependent peroxidases, encoded by TSA1 (thiol-specific antioxidant protein encoding the major cytosolic form 2-Cys Prx), AHP1, YDR453C, YBL064C and YIL010W (Carmel-Harel et al., 2001). Hence, it seems that the role of the thioredoxin dependent system is phylogenetically conserved: its proper function is vital for protection from oxidative stress, and also for ensuring tightly controlled levels of ROS so that H₂O₂ can be used as signalling molecules (Veal et al., 2007).

It has been postulated that peroxiredoxins evolved in eukaryotes to remove even low levels of H₂O₂ as they have the potential to modulate cell signalling pathways. When H₂O₂ levels exceed a certain threshold, peroxiredoxins are oxidized and inactivated (Woo et al., 2003a). Previously, it was believed that the sulfinic forms of the active site cysteines of peroxiredoxins are irreversibly oxidised. Toledano's laboratory then identified a yeast enzyme, sulfiredoxin (Srx), which in the presence of ATP or GTP is capable of reducing the sulfinic form of peroxiredoxins thus preventing them from further and irreversible oxidation to sulfonic acid (Biteau et al., 2003). Srx was considered to be solely localised in the cytoplasm, however, recent data revealed that under stress conditions Srx translocates from the cytosol into mitochondria and regenerates hyperoxidized Prx III (Noh et al., 2009). Here it could be shown that disruption of Txnrd2 increased Srx transcript levels in *Txnrd2*^{-/-} cells, most likely to prevent Prx III and Prx V from overoxidation and inactivation. This cellular knock-out model could be further used to shed more light on the role of mitochondrial ROS on the regulation of sulfiredoxin at the transcriptional and translational level as well as of its subcellular trafficking (Figure 50).

4.3. Txnrd1 and Txnrd2 do not show functional redundancy *in vivo*

Gene targeting of Txnrd1 and Txnrd2 in mice showed that both enzymes play distinct and essential roles in embryonic development and organ functions and that they can not substitute each other (Conrad et al., 2004; Jakupoglu et al., 2005). Txnrd1 knock-out mice die during early development and knock-out embryos display severe overall developmental and growth retardation - only the embryonic heart was spared from the Txnrd1 knock-out and developed normally. The dispensable role for Txnrd1 in cardiac tissue was underlined by heart-specific disruption of Txnrd1, which did not affect viability of mice or caused any

apparent phenotype (Jakupoglu et al., 2005). Numerous studies showed that Txnrd1 is involved in cell growth and differentiation and both, protein level and thioredoxin reductase activity have been shown to be elevated in several tumors and tumor cell lines (Arner and Holmgren, 2006; Biaglow and Miller, 2005; Fujino et al., 2006; Moos et al., 2003; Pennington et al., 2007; Rundlof and Arner, 2004; Yoo et al., 2007).

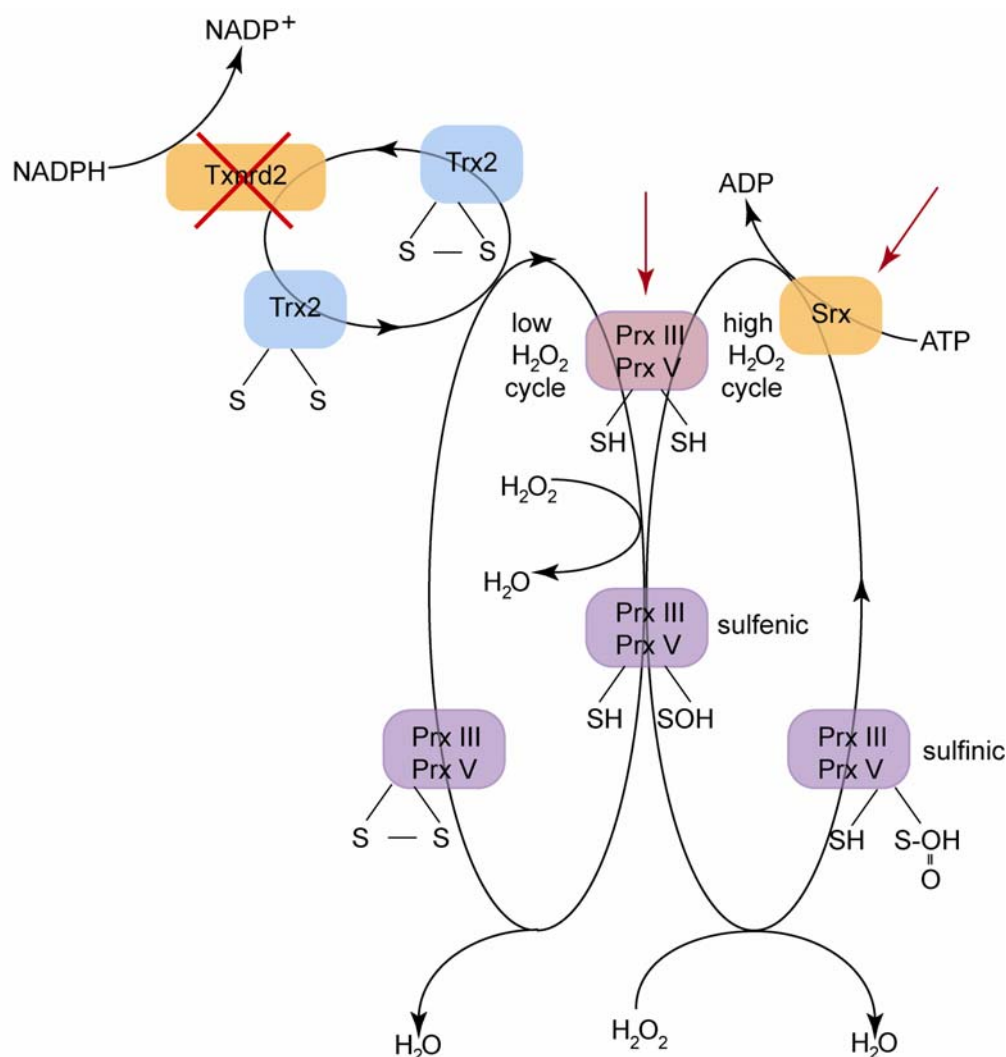


Figure 48. Model for the intertwined thioredoxin-dependent ROS-regulating system in mitochondria. The presumed Prx catalytic cycles in mitochondria and inferred compensation for Txnrd2 disruption (adopted and modified from (Bondareva et al., 2007)). Characteristic for eukaryotic 2-Cys Prxs is the slow formation of an intermolecular disulfide bridge. Even at moderate H_2O_2 concentrations, the sulfenic acid intermediate can react with a second H_2O_2 molecule to form a sulfinic acid before it reacts with the resolving cysteine to form a disulfide. Sulfinic acid cannot be reduced by Trx. The left cycle is Txnrd2 dependent and functions to reduce H_2O_2 at low concentrations. The right cycle is Txnrd2-independent and mainly active at high H_2O_2 concentrations. Disruption of Txnrd2 is expected to ablate the cycle responsible for removal of low H_2O_2 concentrations. In $\text{Txnrd2}^{-/-}$ cells mitochondrial peroxiredoxins (Prx III and Prx V) are strongly upregulated especially when the cells are exposed to additional oxidative stress. To compensate for the lack of Txnrd2, cells induce the expression of Prx III, Prx V and Srx which allows them to control increased ROS to some extent.

On the contrary, *Txnrd2* knock-out mouse die at the foetal stage between E13.5 and E15.5 due to improper heart development and perturbed haematopoiesis (Conrad et al., 2004). In a

study by Turanov and colleagues (Turanov et al., 2006) a certain overlap between Trx1 and Trx2 was postulated. By a proteomic approach it was found that Trx1 is the major target of Txnrd2 in the cytosolic fraction of rat and mouse hepatocytes. Given that Txnrd2 may also play an important role in the cytoplasm, it was important to study whether Txnrd1 or Txnrd2 specifically targeted to the cytoplasm, is capable to rescue loss of Txnrd2. To this end, Txnrd1 (a kind gift from, Mandal Kumar Pankaj, PhD thesis 2009) and Txnrd2 lacking a mitochondrial leader sequence (MLS) were stably expressed in Txnrd2 knock-out cells. These experiments showed that Txnrd1 overexpression could only partially prevent cell death of *Txnrd2*^{-/-} cells treated with increasing BSO concentrations. Partial protection of *Txnrd2*^{-/-} cells by Txnrd1 overexpression appeared to be comparable to the effect of overexpression of cytosolic Txnrd2: only re-expression of Txnrd2 harbouring a MLS fully rescued the Txnrd2 knock-out cells confirming that the observed phenotypes were solely caused by Txnrd2 inactivation and were not due to other side effects. This also implies that subcellular localisation of Txnrd2 is of major importance for proper cell function. To address the question whether both enzymes harbour distinct and non-redundant functions apart from the different tissue-specific expression patterns, one should insert mitochondria-targeted Txnrd1 into the *Txnrd2* locus and cytoplasmic Txnrd2 into the *Txnrd1* locus in mice and ask whether the mice are viable and develop normally. The present findings obtained by tissue-specific disruption of either gene indicated that both enzymes exert non-redundant functions. Yet, it cannot be excluded that the differences observed are due to the different tissue- and time-specific expression pattern of Txnrd1 and Txnrd2 (Conrad et al., 2004; Jakupoglu et al., 2005; Soerensen et al., 2008).

4.4. Txnrd2 is dispensable for maintaining the Cys/(Cys)₂ cycle

In normal cell culture conditions, the major part of intracellular Cys derives from the (Cys)₂, the oxidized and predominant form of Cys in the extracellular space. (Cys)₂ is transported into the cells via the cystine/glutamate amino acid antiporter, system x_C⁻, and then reduced to Cys. Cysteine is used for protein and GSH synthesis, however quite a substantial fraction may be released back into the medium via neutral amino acid transport systems. Thus, system x_C⁻ is regarded to be the central constituent of the Cys/(Cys)₂ cycle, which is essential for the maintenance of cellular GSH levels (Bannai, 1986) and the sustaining of the Cys/(Cys)₂ redox balance (Bannai et al., 1989). In our laboratory it was shown recently that enforced expression of xCT, the substrate-specific subunit of system x_C⁻, in Burkitt's lymphoma cell drives the Cys/(Cys)₂ cycle, characterized by uptake of (Cys)₂, intracellular reduction to Cys, secretion of Cys and re-oxidation to (Cys)₂ (Banjac et al., 2008), and

renders the cells resistant to inhibition of GSH synthesis by BSO. In a subsequent study it was also shown by our laboratory that genetic GSH-deficiency could be bypassed by stable expression of xCT in γ -GCS knock-out cells, further corroborating the Cys/(Cys)₂ cycle as an independent redox circuit (Mandal et al., submitted). Anderson et al. showed that HT-29 cells have the capacity to regulate the extracellular Cys/(Cys)₂ redox state by mechanisms that are independent of cellular GSH (Anderson et al., 2007). Earlier Jones et al. showed that the steady-state redox potential of the cysteine/cystine couple provides a redox node that is independent and distinct of the two redox couples, reduced and oxidized thioredoxin at one hand and reduced and oxidized glutathione at the other hand (Jones et al., 2004).

Therefore, the question arose what is the intracellular driving force behind the Cys/(Cys)₂ redox cycle. Under normal conditions, it is conceivable that GSH is the prime candidate. By forming mixed disulfides with (Cys)₂ it first yields Cys and GS-S-Cys, the latter releases Cys with a second molecule GSH to form GSSG. At the expense of NADPH, GSSG is then recycled by glutathione reductase to yield 2 molecules of GSH. But what occurs in cells which lack endogenous GSH biosynthesis like in γ -GCS null cells or cells depleted of GSH by BSO? In fact, initial *in vitro* observations by Holmgren implicated bovine thioredoxin reductase in (Cys)₂ reduction in a manner independent of thioredoxin (Holmgren, 1977). Therefore, xCT was stably expressed in *Txnrd2*^{-/-} cells. xCT overexpressing cells were challenged with BSO to address the role of thioredoxin reductases in intracellular (Cys)₂ reduction. As shown previously, *Txnrd2*^{-/-} cells rapidly died in response to GSH depletion, which could be prevented by NAC (Conrad et al., 2004). Overexpression of xCT in *Txnrd2*^{-/-} cells efficiently rescued the cells from BSO-mediated cell death and even prevented cell death of eGFP-expressing *Txnrd2*^{-/-} control cells when these were co-cultured with xCT-overexpressing *Txnrd2*^{-/-} cells. This finding fits very well with our previous observations that enforced expression of xCT rescues BL cells from cell death induced by BSO-mediated GSH depletion (Banjac et al., 2008). The results obtained with *Txnrd2*^{-/-} and γ -GCS^{-/-} cells (Pankaj Kumar Mandal, PhD thesis submitted) provided conclusive evidence that the (Cys)₂/Cys redox cycle is functional and intact even in the absence of GSH and/or *Txnrd2*. In a parallel study by Pankaj Kumar Mandal strong evidence could be provided that it is *Txnrd1* which is the driving force behind the Cys/(Cys)₂ redox cycle: xCT-transfected *Txnrd1*^{-/-} cells were unable to exploit the beneficial and protective effects of this cycle, but they rapidly died in response to BSO-mediated GSH depletion (Pankaj Kumar Mandal, PhD thesis submitted). Thus, by using three genetically defined cellular systems, we could show that *Txnrd1* is essential for the utilization and recycling of small thiol-containing compounds and is the main driving force for the (Cys)₂/Cys redox cycle (Pankaj Kumar Mandal, PhD thesis submitted).

4.5. Txnrd2 protects myocardial tissue from oxidative damage and is implicated in the pathogenesis of Dilatative Cardiomyopathy

Cardiac tissue has a particularly high demand for energy in form of ATP, which is mainly produced by oxidative phosphorylation. Hence, cardiomyocytes are packed with mitochondria, and up to 40% of the cellular mass is made up of mitochondria. Reduction of O_2 to H_2O is a highly dangerous process as it requires the transfer of four electrons and the intermediates of the electron transfer reaction are not stable. Single electron reduction of O_2 leads to the generation of substantial amounts (up to 4% of total oxygen) of superoxide anion ($O_2^{\cdot -}$) as a toxic by-product (Forman et al., 1982; Shigenaga et al., 1994). Oxidative stress has been associated with many cardiovascular diseases, including infarction (ischemia/reperfusion injury) and heart failure (Francis, 2001; Griendling and FitzGerald, 2003a; Ide et al., 2000). Ischemia causes alterations in cellular defense mechanisms against oxygen free radicals, mainly a reduction in the activity of SOD and GSH, yielding oxidized glutathione (GSSG) (Ferrari et al., 2004). Then, the condition is exacerbated following reperfusion due to increased ROS production, although the molecular mechanisms are still widely unclear. Myocardial infarction after ischemia/reperfusion is a consequence of profound cell death (either necrosis or apoptosis), and excessive ROS production has been considered to be the major trigger of cell death (Anversa et al., 1998; Maulik et al., 1998). Hence, cardiac tissue needs effective antioxidant and antiapoptotic systems like the thioredoxin (Trx) and the glutaredoxin (Grx) systems to maintain cellular redox balance. The mitochondrial thioredoxin system has been shown to be crucial for cardiac tissue (Bodenstein et al., 1993; Conrad et al., 2004), and in general, its expression pattern and distribution correlates well with the metabolic activity of the tissue (Spyrou et al., 1997). As mentioned earlier, mice that ubiquitously lack Txnrd2 die at E13.5, and perturbed heart development was identified as one of the underlying reasons for embryonic death. This was further corroborated by heart-specific disruption Txnrd2, which causes post-natal death due to biventricular dilatation of the heart and mitochondrial aberrations of cardiomyocytes (Conrad et al., 2004).

Additional suggestive evidence for a possible involvement of Txnrd2 in the pathogenesis of cardiac disease stems from patients who suffered from Keshan disease, an endemic cardiomyopathy resulting from severe nutritional deficiency of the trace element selenium (Xu et al., 1997) in combination with a coxsackie B virus infection (Beck et al., 2003a; Beck et al., 2003b). In a collaborative study with Dr. N. von Beckerath (Deutsches Herzzentrum München) and Dr. A. Pfeufer (Institute of Human Genetics, Helmholtz Zentrum München) sequencing of all TXNRD2 exons of DNA samples from Dilatative Cardiomyopathy (DCM)

patients ($n = 227$) along with controls ($n = 683$) identified two novel mutations in three heterozygous carriers of 227 patients ($3/227=1.3\%$). Both 175G>A (Ala59Thr) and 1124G>A (Gly375Arg) were not observed in the general population (Sibbing D, Perisic T 2009, in preparation). The recently published crystal structure of Txnrd2 (Biterova et al., 2005) allowed to precisely locate the two identified mutations of Txnrd2, which are positioned in highly conserved regions within the FAD binding domain of Txnrd2. It is noteworthy, that both mutations that had been engineered into the murine Txnrd2 protein, failed to rescue *Txnrd2*^{-/-} cells from BSO-mediated cell death when stably expressed in *Txnrd2*^{-/-} cells. When expressed in wild-type cells, cell death of these cells was accelerated compared to mock-transfected cells. Moreover, *Txnrd2*^{+/+} cells expressing the mutated forms proliferated very slowly, unlike *Txnrd2*^{-/-} fibroblasts transfected with these mutants. In conclusion, these data strongly suggest that both mutants behave like dominant-negative forms. In this context, it should be stressed that the patients carrying these mutations were heterozygous. Hence, *Txnrd2*^{+/+} or *Txnrd2*^{-/-} cells expressing mutated Txnrd2 represent an appropriate model to describe the *in vivo* condition found in the DCM patients with mutated Txnrd2. From these investigations one may conclude that a small percentage of DCM cases might be caused by these novel Txnrd2 mutations. After the identification of four mutations in the SelN gene that cause muscle disorders in humans (*SEPN1*-related myopathy) (Allamand et al., 2006; Maiti et al., 2009; Moghadaszadeh et al., 2001; Tajsharghi et al., 2005), Txnrd2 is the second selenoenzyme in which mutations were found that predispose to a distinct human disease.

4.6. Inducible overexpression of xCT in mice is not protective, but causes spleen, thymus and testis atrophy and defective erythropoiesis

A large part of this thesis has been devoted to better understand possible redundancies between different redox systems, i.e. of the thioredoxin and the glutathione system. It was shown above that cells deficient for Txnrd2 are more sensitive to agents causing oxidative stress than wildtype cells and that Txnrd2 knock-out cells are particularly susceptible to depletion of glutathione by BSO. As uptake of cystine is the limiting step for glutathione synthesis in many cellular systems, the cystine/glutamate exchange transporter xC⁻, had initially been regarded as an important part of the glutathione system. Yet, overexpression studies of xCT in wildtype cells (Banjac et al., 2008), in γ -GCS^{-/-} cells (Mandal et al., submitted) and *Txnrd2*^{-/-} cells (this thesis) performed in our laboratory had revealed that the cystine/cysteine cycle driven by system xC⁻, represents a redox system that can operate also independently of glutathione *in vitro*. Hence, system xC⁻, plays a dual role: it may increase

the level of glutathione in cells in which GSH synthesis is intact and cystine uptake is limiting, and alternatively, it may sustain the redox balance on its own when glutathione is depleted and/or glutathione synthesis is inhibited.

So far, little is known about the biological role of system x_C^- , *in vivo*. Previously, Sato and colleagues showed that loss of function of xCT by targeted disruption of the gene in mice did not cause any overt phenotype in terms of viability, fertility and gross morphological changes (Sato et al., 2005). xCT knock-out mice only showed an imbalance in plasma Cys levels. Oppositely, it was our aim to generate a gain of function system for xCT. Since xCT has been mainly associated with the protection of cells and tissues from oxidative stress, it was hypothesized that gain of function of xCT would render transgenic mice more resistant to oxidative damage. If ageing is indeed associated with increased oxidative stress and tissue damage, overexpression of xCT might even prolong the life of transgenic mice. This assumption had been corroborated by the finding of showed that xCT is central for glutathione metabolism in rat brain and its overexpression is neuroprotective by enhancing glutathione export from non-neuronal cells (Shih and Murphy, 2001). But also adverse effects of ectopic xCT expression might have to be envisioned: Massie et al. reported the involvement of the xCT in aberrant glutamate neurotransmission in the striatum of a rat Parkinsonian brain (Massie et al., 2008), and Savaskan et al. found that pharmacological inhibition of xCT or silencing by small interfering RNAs in human malignant brain tumours inhibited neurodegeneration and alleviated brain edema most likely by decreasing glutamate-induced excitotoxicity (Savaskan et al., 2008). A transgenic mouse with inducible xCT expression was thus regarded as a valuable tool to investigate the role of xCT in various models of neurodegeneration including stroke and Parkinson's disease.

Beside this, we sought to study the role of ROS, of an hypoxic microenvironment and of the intracellular redox balance for stem cell maintenance and differentiation (Diehn et al., 2009a; Diehn et al., 2009b; Ito et al., 2006). Evidence has been accumulated over the last years showing that stem cell maintenance requires an hypoxic, ROS-free environment, i.e. the osteoblastic niche, whereas hematopoietic differentiation is associated with leaving the niche, a normoxic environment and increased ROS levels (Diehn et al., 2009a; Diehn et al., 2009b; Ito et al., 2006). Moreover, since system x_C^- , is the major amino acid transporter induced in response to LPS and cytokine treatment in macrophages (Sato et al., 1991; Sato et al., 1987; Watanabe and Bannai, 1987), it was hypothesized that xCT transgenic mice might be more resistant towards bacterial infection and LPS-mediated toxicity, and hence could serve as a valuable mouse model to study the involvement of ROS in inflammation.

To express xCT in a spatio-temporal manner, the *Rosa26* locus was chosen, as the *Rosa26* promoter is ubiquitously active and this locus has been frequently used for ectopic gene expression in mice (Farley et al., 2000; Hameyer et al., 2007; Homig-Holzel et al., 2008; Ivanova et al., 2005; Jager et al., 2004; Soriano, 1999; Srinivas et al., 2001). After successful generation of conditional xCT knock-in mice, these mice were crossed to tamoxifen-inducible CreERT2-deleter mice. To our surprise, induction of xCT expression upon tamoxifen feeding resulted in severe symptoms like gradual weight loss, abnormal posture, and suffering of the mice so that the tamoxifen-fed transgenic mice eventually had to be euthanized after 5 weeks. Careful examination of these mice revealed that many organs were pale suggestive of anemia. Moreover, there was an atrophy of spleen and testes and the thymus was completely lacking. Histological analysis of the spleen revealed a clear reduction in the red pulp. The decrease in splenic size probably resulted from the increase in the number of apoptotic cells, the reasons for which are not understood yet. According to the hemogram analysis xCT transgenic mice were severely anaemic. This phenotype prompted us to further investigate the haematopoietic system in more detail. Analysis of bone marrow cells by flow cytometry revealed that transgenic mice expressing xCT had a 6-fold increase in undifferentiated non-committed progenitor cells (KSL population) in the bone marrow as identified on the basis of the high expression of c-kit and Sca-1 and the absence of lineage markers on the cell surface (Lin⁻). Unfortunately, the available data did not allow to draw the conclusion whether there is an absolute increase in the number of KSL cells or a relative increase that might be caused merely by the decrease of differentiated cells. Further investigation of erythrocyte differentiation showed that all committed erythrocytic precursors like pro-erythroblasts, as well as basophilic-, polychromatic- and orthochromatic-erythroblasts were decreased in transgenic mice, whereas the percentage of megakaryocytic and erythroblastic precursor cells was relatively increased. The impaired differentiation of cells of the erythrocytic lineage may explain the anaemic phenotype of the xCT transgenic animals. Our preliminary investigation thus showed that transgenic animals have dysfunctional erythropoiesis that possibly resembles a refractory anemia/myelodysplastic syndrome. Whether increased destruction of mature RBCs in the spleen may also contribute to the anaemic phenotype, remains open at present. This will be answered by kinetic studies determining the half life of mature erythrocytes *in vivo*. But it is noteworthy that the phenotype is clearly different from a haemolytic anemia that is characterized by increased spleen weight due to increased degradation of erythrocytes and compensatory overproduction of red blood cell precursors.

The phenotype described here is compatible with published reports that a low level of ROS and hypoxic microenvironment promotes self-renewal of HSCs (Diehn et al., 2009a; Diehn et

al., 2009b; Ito et al., 2004; Osawa et al., 1996). Thus, by promoting the cystine uptake and boosting the intracellular cysteine level, xCT overexpression may reduce the overall ROS burden to a minimal level. By generating a highly reducing intracellular environment xCT overexpression may shift the balance between self renewal and differentiation towards self renewal and may thus inhibit differentiation of uncommitted progenitors into mature red blood cells. This may be corroborated experimentally by showing that not only the relative number but also the absolute number of KSL cells (harbouring the stem cells) has increased in xCT transgenic mice. To address the question whether the phenotype observed is due to a cell-autonomous effect of xCT overexpression in hematopoietic cells or due to a cell non-autonomous action of xCT in stroma cells supporting hematopoiesis, bone marrow cells of xCT-transgenic mice have to be transplanted into wildtype mice and vice versa, wildtype bone marrow cells into xCT transgenic mice.

Although the phenotype observed in hematopoietic cells is exciting and promising, a note of caution is also required regarding the interpretation of data obtained from xCT transgenic mice. *In vivo*, xCT overexpression may not only lead to an increase in the intracellular supply of cysteine (and thus in an increase in reduced intracellular glutathione), it may also lead – due to the export of glutamate coupled to the import of cystine – to a decrease in the intracellular glutamate and an increase in the extracellular glutamate concentration both of which might be harmful to the cell. Thus, intracellular depletion of glutamate may impact on the physiology of hematopoietic cells or alternatively, xCT overexpression may cause glutamate-mediated toxicity in a manner similar to that in neurons. Recent studies have shown that glutamate not only acts as a neurotransmitter, it also has been reported to have immunomodulatory function. This is supported by the finding that glutamate receptors are expressed on T-cells and glutamate transporters in antigen presenting cells like dendritic cells and macrophages (Pacheco et al., 2007). A final caveat is necessary also regarding the intracellular supply of NADPH. The continuous import of oxidized cystine and export of reduced cysteine represents a steadily ongoing loss of reducing equivalents. Regardless whether glutathione or thioredoxin reductase 1 are used for reduction of cystine, the reducing equivalents finally stem from the degradation of glucose in the pentose phosphate cycle and glucose-6-phosphate dehydrogenase (G6PDH) that is generating NADPH as the universal supplier of electrons for various biosynthetic pathways. Regarding the phenotype of xCT overexpression *in vivo*, it may be necessary to show that the supply of NADPH is ensured also *in vivo* and that the cells are not exhausted due to the continuous loss of reducing equivalents. Yet, even though the *in vivo* phenotype of xCT overexpression is difficult to interpret for the reasons mentioned above, the importance of xCT expression for culturing cells *in vitro* is well established: *in vitro*, the supply of glutamate is guaranteed by the uptake

of glutamine from the medium and the intracellular deamination of glutamine to glutamate. Likewise, the generation of reducing equivalents through glucose and G6PDH is not limiting in culture conditions *in vitro*. We are thus left with the curious situation that the relevance of the phenotype observed by xCT overexpression *in vivo* has to be verified *in vitro* culture systems, in which all confounding parameters may be controlled and the impact of xCT overexpression on metabolic parameters can be dissected experimentally. It will be particularly important to study differentiation of hemaptoietic cells in colony assays in methylcellulose *in vitro* to which tamoxifen can be added at different time points, by following the fate of single cells (Eilken et al., 2009; Rieger et al., 2009).

Besides the role of xCT overexpression for renewal and differentiation of hematopoietic cells, it will be particularly interesting to study the impact of xCT overexpression in the brain. It is impossible to predict which of two opposing phenotypes may prevail: protection of neuronal cells from oxidative stress by increasing the intracellular glutathione concentration, or increased neurotoxicity due to an increase in the extracellular glutamate levels. Hameyer et al. have reported that the CreERT2 deleter mouse has no detectable CreERT2 activity in the brain (Hameyer et al., 2007). Yet, our own preliminary data showed increased xCT levels in whole brain lysates of xCT transgenic mice after 5 weeks of Tamoxifen feeding. To ensure extensive broad xCT expression in the brain, *R26mxCT^{flSTOP}* mice will be crossed to Nestin-Cre mice, which express Cre in neuronal (and also some non-neuronal) cells. These mice will prove most suitable to dissect putative protective or detrimental effects of increased cystine uptake: either neuroprotection due to increased GSH synthesis or neurotoxicity due to increased glutamate levels. Of note, ongoing studies in our laboratory in collaboration with Dr. H. Beck (LMU München) and Dr. N. Plesnila (RCSI Dublin, Ireland) provided initial evidence that xCT knock-out mice have reduced infarct size upon transient ischemia/reperfusion (Beck et al, submitted) due to reduced levels of extracellular glutamate and hence reduced glutamate-mediated neurotoxicity. In addition to studying the role of xCT loss of function in xCT knock-out animals, the xCT transgenic mice will provide complementary data in a xCT gain of function model.

5. Summary

The thioredoxin system, along with the glutathione (GSH)-dependent system, is critically involved in the maintenance of the intracellular redox balance. The thioredoxin dependent system consists of thioredoxin reductases, thioredoxins and thioredoxin-dependent peroxidases. The mitochondrial thioredoxin reductase (Txnrd2) is an important component of the mitochondrial antioxidant system. Using Txnrd2 null cells we show that *Txnrd2*^{-/-} cells produced more ROS, and were highly susceptible to different prooxidants and GSH depletion. Administration of various antioxidants, such as NAC, GSH and α -Toc, reverted the phenotype of the *Txnrd2*^{-/-} cells. The up-regulation of the mitochondrial peroxiredoxins Prx III and Prx V and sulfiredoxin transcripts in *Txnrd2*^{-/-} cells could be a compensatory mechanism for loss of Txnrd2. However, under oxidative stress, *Txnrd2*^{-/-} cells showed higher amount of overoxidation of Prx I and PrxII/PrxIII indicating that in absence of Txnrd2 ROS scavenging efficiency of Trx2-Prx system is greatly compromised.

Oxidative stress has been implicated in cardiovascular diseases, including infarction and heart failure. Disruption of Txnrd2 leads to perturbed heart development and embryonic lethality in mice. Heart-specific Txnrd2 disruption causes post-natal death due to biventricular dilatation of the heart and mitochondrial aberrations of cardiomyocytes. Additional evidence for a possible involvement of Txnrd2 in the pathogenesis of cardiac diseases came from the study of the patients suffering from dilated cardiomyopathy (DCM). By DNA sequence analysis of these samples, we found two novel mutations (Ala59Thr and Gly375Arg) in TXNRD2. Stable expression of murine Txnrd2 harboring these two mutations in *Txnrd2*^{-/-} cells showed a dominant negative effect and were unable to rescue the cells from GSH depletion. Our data strongly suggest that the mutations found in a small percentage of DCM cases might be due to loss of Txnrd2 functions.

The cellular redox balance is maintained by thioredoxin- and GSH-dependent system along with Cys/(Cys)₂-cycle which is a distinct redox node of major importance. Previous study in the lab showed that the essential requirement of GSH can be bypassed by the Cys/(Cys)₂-cycle. To gain further insights into the role of the thioredoxin system being a driving force for the Cys/(Cys)₂-cycle, xCT was overexpressed in *Txnrd2*^{-/-} fibroblasts. xCT overexpression rescued the *Txnrd2*^{-/-} cells from GSH depletion. This suggests that the (Cys)₂/Cys redox cycle is functional and intact even in the absence of GSH and/or mitochondrial thioredoxin reductase. In a parallel study, we found that cytosolic thioredoxin reductase (Txnrd1) is the driving force behind the Cys/(Cys)₂ redox cycle.

xCT expression provided growth advantages in culture conditions. In order to recapitulate our findings *in vivo*, we generated xCT knock-in mice, in which xCT expression can be induced in a spatio-temporal manner by tamoxifen. To our great surprise, overexpression of xCT in mice resulted in adverse effects like atrophy of spleen, thymus and testis, defective erythropoiesis and ultimately death after 5 weeks of induction. Detailed analysis of the bone marrow revealed that although there is an increase in the hematopoietic stem cell population, xCT overexpression leads to impaired erythropoiesis. The observed paradox with xCT overexpression could be due to glutamate-mediated toxicity or impaired redox balance.

6. References

- Allamand, V., Richard, P., Lescure, A., Ledeuil, C., Desjardin, D., Petit, N., Gartioux, C., Ferreira, A., Krol, A., Pellegrini, N., *et al.* (2006). A single homozygous point mutation in a 3'untranslated region motif of selenoprotein N mRNA causes SEP1-related myopathy. *EMBO Rep* 7, 450-454.
- Anderson, C. L., Iyer, S. S., Ziegler, T. R., and Jones, D. P. (2007). Control of extracellular cysteine/cystine redox state by HT-29 cells is independent of cellular glutathione. *Am J Physiol Regul Integr Comp Physiol* 293, R1069-1075.
- Andersson, M., Holmgren, A., and Spyrou, G. (1996). NK-lysin, a disulfide-containing effector peptide of T-lymphocytes, is reduced and inactivated by human thioredoxin reductase. Implication for a protective mechanism against NK-lysin cytotoxicity. *J Biol Chem* 271, 10116-10120.
- Anestis, K., Prast-Nielsen, S., Cenas, N., and Arner, E. S. (2008). Cell Death by SecTRAPs: Thioredoxin Reductase as a Prooxidant Killer of Cells. *PLoS ONE* 3, e1846.
- Anversa, P., Cheng, W., Liu, Y., Leri, A., Redaelli, G., and Kajstura, J. (1998). Apoptosis and myocardial infarction. *Basic Res Cardiol* 93 Suppl 3, 8-12.
- Araki, M., Nanri, H., Ejima, K., Murasato, Y., Fujiwara, T., Nakashima, Y., and Ikeda, M. (1999). Antioxidant function of the mitochondrial protein SP-22 in the cardiovascular system. *J Biol Chem* 274, 2271-2278.
- Arner, E. S., and Holmgren, A. (2000). Physiological functions of thioredoxin and thioredoxin reductase. *Eur J Biochem* 267, 6102-6109.
- Arner, E. S., and Holmgren, A. (2006). The thioredoxin system in cancer. *Semin Cancer Biol* 16, 420-426.
- Arner, E. S., Nordberg, J., and Holmgren, A. (1996). Efficient reduction of lipoamide and lipoic acid by mammalian thioredoxin reductase. *Biochem Biophys Res Commun* 225, 268-274.
- Atkins, J. F., and Gesteland, R. F. (2000). The twenty-first amino acid. *Nature* 407, 463, 465.
- Bachur, N. R., Gordon, S. L., and Gee, M. V. (1977). Anthracycline antibiotic augmentation of microsomal electron transport and free radical formation. *Mol Pharmacol* 13, 901-910.
- Baker, A., Payne, C. M., Briehl, M. M., and Powis, G. (1997). Thioredoxin, a gene found overexpressed in human cancer, inhibits apoptosis in vitro and in vivo. *Cancer Res* 57, 5162-5167.
- Banjac, A. (2005) Cystine-Import and regulation of apoptosis in B-Lymphocytes. Dissertation, LMU, Munich.
- Banjac, A., Perisic, T., Sato, H., Seiler, A., Bannai, S., Weiss, N., Kolle, P., Tschoep, K., Issels, R. D., Daniel, P. T., *et al.* (2008). The cystine/cysteine cycle: a redox cycle regulating susceptibility versus resistance to cell death. *Oncogene* 27, 1618-1628.
- Banmeyer, I., Marchand, C., Clippe, A., and Knoops, B. (2005). Human mitochondrial peroxiredoxin 5 protects from mitochondrial DNA damages induced by hydrogen peroxide. *FEBS Lett* 579, 2327-2333.
- Bannai, S. (1984). Induction of cystine and glutamate transport activity in human fibroblasts by diethyl maleate and other electrophilic agents. *J Biol Chem* 259, 2435-2440.
- Bannai, S. (1986). Exchange of cystine and glutamate across plasma membrane of human fibroblasts. *J Biol Chem* 261, 2256-2263.

- Bannai, S., and Ishii, T. (1982). Transport of cystine and cysteine and cell growth in cultured human diploid fibroblasts: effect of glutamate and homocysteate. *J Cell Physiol* 112, 265-272.
- Bannai, S., and Kasuga, H. (1985). Anti-inflammatory drug inhibition of transport of cystine and glutamate in cultured human fibroblasts. *Biochem Pharmacol* 34, 1852-1854.
- Bannai, S., Sato, H., Ishii, T., and Sugita, Y. (1989). Induction of cystine transport activity in human fibroblasts by oxygen. *J Biol Chem* 264, 18480-18484.
- Bannai, S., Sato, H., Ishii, T., and Taketani, S. (1991). Enhancement of glutathione levels in mouse peritoneal macrophages by sodium arsenite, cadmium chloride and glucose/glucose oxidase. *Biochim Biophys Acta* 1092, 175-179.
- Bauer, H., Massey, V., Arscott, L. D., Schirmer, R. H., Ballou, D. P., and Williams, C. H., Jr. (2003). The mechanism of high Mr thioredoxin reductase from *Drosophila melanogaster*. *J Biol Chem* 278, 33020-33028.
- Beck, M. A., and Levander, O. A. (1998). Dietary oxidative stress and the potentiation of viral infection. *Annu Rev Nutr* 18, 93-116.
- Beck, M. A., Levander, O. A., and Handy, J. (2003a). Selenium deficiency and viral infection. *J Nutr* 133, 1463S-1467S.
- Beck, M. A., Williams-Toone, D., and Levander, O. A. (2003b). Coxsackievirus B3-resistant mice become susceptible in Se/vitamin E deficiency. *Free Radic Biol Med* 34, 1263-1270.
- Biaglow, J. E., and Miller, R. A. (2005). The thioredoxin reductase/thioredoxin system: novel redox targets for cancer therapy. *Cancer Biol Ther* 4, 6-13.
- Bilski, P., Belanger, A. G., and Chignell, C. F. (2002). Photosensitized oxidation of 2',7'-dichlorofluorescein: singlet oxygen does not contribute to the formation of fluorescent oxidation product 2',7'-dichlorofluorescein. *Free Radic Biol Med* 33, 938-946.
- Birringer, M., Pilawa, S., and Flohe, L. (2002). Trends in selenium biochemistry. *Nat Prod Rep* 19, 693-718.
- Biteau, B., Labarre, J., and Toledano, M. B. (2003). ATP-dependent reduction of cysteine-sulphinic acid by *S. cerevisiae* sulphiredoxin. *Nature* 425, 980-984.
- Biterova, E. I., Turanov, A. A., Gladyshev, V. N., and Barycki, J. J. (2005). Crystal structures of oxidized and reduced mitochondrial thioredoxin reductase provide molecular details of the reaction mechanism. *Proc Natl Acad Sci U S A* 102, 15018-15023.
- Bjornstedt, M., Hamberg, M., Kumar, S., Xue, J., and Holmgren, A. (1995). Human thioredoxin reductase directly reduces lipid hydroperoxides by NADPH and selenocystine strongly stimulates the reaction via catalytically generated selenols. *J Biol Chem* 270, 11761-11764.
- Bodenstein, N. P., McIntosh, W. A., Vlantis, A. C., and Urquhart, A. C. (1993). Clinical signs of orbital ischemia in rhino-orbitocerebral mucormycosis. *Laryngoscope* 103, 1357-1361.
- Bondareva, A. A., Capecchi, M. R., Iverson, S. V., Li, Y., Lopez, N. I., Lucas, O., Merrill, G. F., Prigge, J. R., Siders, A. M., Wakamiya, M., *et al.* (2007). Effects of thioredoxin reductase-1 deletion on embryogenesis and transcriptome. *Free Radic Biol Med* 43, 911-923.
- Bosl, M. R., Takaku, K., Oshima, M., Nishimura, S., and Taketo, M. M. (1997). Early embryonic lethality caused by targeted disruption of the mouse selenocysteine tRNA gene (*Trsp*). *Proc Natl Acad Sci U S A* 94, 5531-5534.
- Boveris, A. (1984). Determination of the production of superoxide radicals and hydrogen peroxide in mitochondria. *Methods Enzymol* 105, 429-435.

- Brandt, W., and Wessjohann, L. A. (2005). The functional role of selenocysteine (Sec) in the catalysis mechanism of large thioredoxin reductases: proposition of a swapping catalytic triad including a Sec-His-Glu state. *Chembiochem* 6, 386-394.
- Bridges, C. C., Hu, H., Miyauchi, S., Siddaramappa, U. N., Ganapathy, M. E., Ignatowicz, L., Maddox, D. M., Smith, S. B., and Ganapathy, V. (2004). Induction of cystine-glutamate transporter xc- by human immunodeficiency virus type 1 transactivator protein tat in retinal pigment epithelium. *Invest Ophthalmol Vis Sci* 45, 2906-2914.
- Brigelius-Flohe, R. (2008). Selenium compounds and selenoproteins in cancer. *Chem Biodivers* 5, 389-395.
- Brigelius-Flohe, R., and Banning, A. (2006). Part of the series: from dietary antioxidants to regulators in cellular signaling and gene regulation. Sulforaphane and selenium, partners in adaptive response and prevention of cancer. *Free Radic Res* 40, 775-787.
- Brown, K. K., Eriksson, S. E., Arner, E. S., and Hampton, M. B. (2008). Mitochondrial peroxiredoxin 3 is rapidly oxidized in cells treated with isothiocyanates. *Free Radic Biol Med* 45, 494-502.
- Burdo, J., Dargusch, R., and Schubert, D. (2006). Distribution of the cystine/glutamate antiporter system xc- in the brain, kidney, and duodenum. *J Histochem Cytochem* 54, 549-557.
- Carmel-Harel, O., Stearman, R., Gasch, A. P., Botstein, D., Brown, P. O., and Storz, G. (2001). Role of thioredoxin reductase in the Yap1p-dependent response to oxidative stress in *Saccharomyces cerevisiae*. *Mol Microbiol* 39, 595-605.
- Chae, H. Z., Chung, S. J., and Rhee, S. G. (1994). Thioredoxin-dependent peroxide reductase from yeast. *J Biol Chem* 269, 27670-27678.
- Chang, E. Y., Son, S. K., Ko, H. S., Baek, S. H., Kim, J. H., and Kim, J. R. (2005). Induction of apoptosis by the overexpression of an alternative splicing variant of mitochondrial thioredoxin reductase. *Free Radic Biol Med* 39, 1666-1675.
- Chang, M. C., Pralle, A., Isacoff, E. Y., and Chang, C. J. (2004a). A selective, cell-permeable optical probe for hydrogen peroxide in living cells. *J Am Chem Soc* 126, 15392-15393.
- Chang, T. S., Cho, C. S., Park, S., Yu, S., Kang, S. W., and Rhee, S. G. (2004b). Peroxiredoxin III, a mitochondrion-specific peroxidase, regulates apoptotic signaling by mitochondria. *J Biol Chem* 279, 41975-41984.
- Chang, T. S., Jeong, W., Woo, H. A., Lee, S. M., Park, S., and Rhee, S. G. (2004c). Characterization of mammalian sulfiredoxin and its reactivation of hyperoxidized peroxiredoxin through reduction of cysteine sulfinic acid in the active site to cysteine. *J Biol Chem* 279, 50994-51001.
- Chavatte, L., Brown, B. A., and Driscoll, D. M. (2005). Ribosomal protein L30 is a component of the UGA-selenocysteine recoding machinery in eukaryotes. *Nat Struct Mol Biol* 12, 408-416.
- Chen, Y. W., Bycroft, M., and Wong, K. B. (2003). Crystal structure of ribosomal protein L30e from the extreme thermophile *Thermococcus celer*: thermal stability and RNA binding. *Biochemistry* 42, 2857-2865.
- Choi, H. J., Kang, S. W., Yang, C. H., Rhee, S. G., and Ryu, S. E. (1998). Crystal structure of a novel human peroxidase enzyme at 2.0 Å resolution. *Nat Struct Biol* 5, 400-406.
- Choi, M. H., Sajed, D., Poole, L., Hirata, K., Herdman, S., Torian, B. E., and Reed, S. L. (2005). An unusual surface peroxiredoxin protects invasive *Entamoeba histolytica* from oxidant attack. *Mol Biochem Parasitol* 143, 80-89.

- Chung, W. J., Lyons, S. A., Nelson, G. M., Hamza, H., Gladson, C. L., Gillespie, G. Y., and Sontheimer, H. (2005). Inhibition of cystine uptake disrupts the growth of primary brain tumors. *J Neurosci* 25, 7101-7110.
- Conrad, M. (2009). Transgenic mouse models for the vital selenoenzymes cytosolic thioredoxin reductase, mitochondrial thioredoxin reductase and glutathione peroxidase 4. *Biochim Biophys Acta*.
- Conrad, M., Brielmeier, M., and Bornkamm, G. W. (2006). Mitochondrial and Cytosolic Thioredoxin Reductase Knockout Mice. *Selenium : Its Molecular Biology and Role in Human Health*: Springer, New York.).
- Conrad, M., Jakupoglu, C., Moreno, S. G., Lippl, S., Banjac, A., Schneider, M., Beck, H., Hatzopoulos, A. K., Just, U., Sinowatz, F., *et al.* (2004). Essential role for mitochondrial thioredoxin reductase in hematopoiesis, heart development, and heart function. *Mol Cell Biol* 24, 9414-9423.
- Copeland, P. R., and Driscoll, D. M. (1999). Purification, redox sensitivity, and RNA binding properties of SECIS-binding protein 2, a protein involved in selenoprotein biosynthesis. *J Biol Chem* 274, 25447-25454.
- Copeland, P. R., Fletcher, J. E., Carlson, B. A., Hatfield, D. L., and Driscoll, D. M. (2000). A novel RNA binding protein, SBP2, is required for the translation of mammalian selenoprotein mRNAs. *Embo J* 19, 306-314.
- Copeland, P. R., Stepanik, V. A., and Driscoll, D. M. (2001). Insight into mammalian selenocysteine insertion: domain structure and ribosome binding properties of Sec insertion sequence binding protein 2. *Mol Cell Biol* 21, 1491-1498.
- Crack, P. J., Taylor, J. M., Flentjar, N. J., de Haan, J., Hertzog, P., Iannello, R. C., and Kola, I. (2001). Increased infarct size and exacerbated apoptosis in the glutathione peroxidase-1 (Gpx-1) knockout mouse brain in response to ischemia/reperfusion injury. *J Neurochem* 78, 1389-1399.
- Cregan, S. P., Dawson, V. L., and Slack, R. S. (2004). Role of AIF in caspase-dependent and caspase-independent cell death. *Oncogene* 23, 2785-2796.
- D'Autreaux, B., and Toledano, M. B. (2007). ROS as signalling molecules: mechanisms that generate specificity in ROS homeostasis. *Nat Rev Mol Cell Biol* 8, 813-824.
- Da Silva-Azevedo, L., Jahne, S., Hoffmann, C., Stalder, D., Heller, M., Pries, A. R., Zakrzewicz, A., and Baum, O. (2009). Up-regulation of the peroxiredoxin-6 related metabolism of reactive oxygen species in skeletal muscle of mice lacking neuronal nitric oxide synthase. *J Physiol* 587, 655-668.
- Damdimopoulos, A. E., Miranda-Vizuete, A., Treuter, E., Gustafsson, J. A., and Spyrou, G. (2004). An alternative splicing variant of the selenoprotein thioredoxin reductase is a modulator of estrogen signaling. *J Biol Chem* 279, 38721-38729.
- Davies, K. J., Doroshov, J. H., and Hochstein, P. (1983). Mitochondrial NADH dehydrogenase-catalyzed oxygen radical production by adriamycin, and the relative inactivity of 5-iminodaunorubicin. *FEBS Lett* 153, 227-230.
- de Jesus, L. A., Hoffmann, P. R., Michaud, T., Forry, E. P., Small-Howard, A., Stillwell, R. J., Morozova, N., Harney, J. W., and Berry, M. J. (2006). Nuclear assembly of UGA decoding complexes on selenoprotein mRNAs: a mechanism for eluding nonsense-mediated decay? *Mol Cell Biol* 26, 1795-1805.
- DeYulia, G. J., Jr., Carcamo, J. M., Borquez-Ojeda, O., Shelton, C. C., and Golde, D. W. (2005). Hydrogen peroxide generated extracellularly by receptor-ligand interaction facilitates cell signaling. *Proc Natl Acad Sci U S A* 102, 5044-5049.
- Dickinson, B. C., and Chang, C. J. (2008). A targetable fluorescent probe for imaging hydrogen peroxide in the mitochondria of living cells. *J Am Chem Soc* 130, 9638-9639.

- Diehn, M., Cho, R. W., and Clarke, M. F. (2009a). Therapeutic implications of the cancer stem cell hypothesis. *Semin Radiat Oncol* 19, 78-86.
- Diehn, M., Cho, R. W., Lobo, N. A., Kalisky, T., Dorie, M. J., Kulp, A. N., Qian, D., Lam, J. S., Ailles, L. E., Wong, M., *et al.* (2009b). Association of reactive oxygen species levels and radioresistance in cancer stem cells. *Nature* 458, 780-783.
- Ding, F., and Grabowski, P. J. (1999). Identification of a protein component of a mammalian tRNA(Sec) complex implicated in the decoding of UGA as selenocysteine. *Rna* 5, 1561-1569.
- Driscoll, D. M., and Copeland, P. R. (2003). Mechanism and regulation of selenoprotein synthesis. *Annu Rev Nutr* 23, 17-40.
- Drummen, G. P., van Liebergen, L. C., Op den Kamp, J. A., and Post, J. A. (2002). C11-BODIPY(581/591), an oxidation-sensitive fluorescent lipid peroxidation probe: (micro)spectroscopic characterization and validation of methodology. *Free Radic Biol Med* 33, 473-490.
- Egler, R. A., Fernandes, E., Rothermund, K., Sereika, S., de Souza-Pinto, N., Jaruga, P., Dizdaroglu, M., and Prochownik, E. V. (2005). Regulation of reactive oxygen species, DNA damage, and c-Myc function by peroxiredoxin 1. *Oncogene* 24, 8038-8050.
- Eilken, H. M., Nishikawa, S., and Schroeder, T. (2009). Continuous single-cell imaging of blood generation from haemogenic endothelium. *Nature* 457, 896-900.
- Fagegaltier, D., Hubert, N., Yamada, K., Mizutani, T., Carbon, P., and Krol, A. (2000). Characterization of mSelB, a novel mammalian elongation factor for selenoprotein translation. *Embo J* 19, 4796-4805.
- Farley, F. W., Soriano, P., Steffen, L. S., and Dymecki, S. M. (2000). Widespread recombinase expression using FLP_{ER} (flipper) mice. *Genesis* 28, 106-110.
- Ferrari, R., Guardigli, G., Mele, D., Percoco, G. F., Ceconi, C., and Curello, S. (2004). Oxidative stress during myocardial ischaemia and heart failure. *Curr Pharm Des* 10, 1699-1711.
- Feussner, A., Rolinski, B., Weiss, N., Deufel, T., Wolfram, G., and Roscher, A. A. (1997). Determination of total homocysteine in human plasma by isocratic high-performance liquid chromatography. *Eur J Clin Chem Clin Biochem* 35, 687-691.
- Finkel, T. (1998). Oxygen radicals and signaling. *Curr Opin Cell Biol* 10, 248-253.
- Fisher, A. B., Dodia, C., Manevich, Y., Chen, J. W., and Feinstein, S. I. (1999). Phospholipid hydroperoxides are substrates for non-selenium glutathione peroxidase. *J Biol Chem* 274, 21326-21334.
- Fletcher, J. E., Copeland, P. R., Driscoll, D. M., and Krol, A. (2001). The selenocysteine incorporation machinery: interactions between the SECIS RNA and the SECIS-binding protein SBP2. *Rna* 7, 1442-1453.
- Fomenko, D. E., and Gladyshev, V. N. (2003). Identity and functions of CxxC-derived motifs. *Biochemistry* 42, 11214-11225.
- Forman, H. J., Williams, J. J., Nelson, J., Daniele, R. P., and Fisher, A. B. (1982). Hyperoxia inhibits stimulated superoxide release by rat alveolar macrophages. *J Appl Physiol* 53, 685-689.
- Francis, G. S. (2001). Pathophysiology of chronic heart failure. *Am J Med* 110 Suppl 7A, 37S-46S.
- Freemerman, A. J., Gallegos, A., and Powis, G. (1999). Nuclear factor kappaB transactivation is increased but is not involved in the proliferative effects of thioredoxin overexpression in MCF-7 breast cancer cells. *Cancer Res* 59, 4090-4094.

- Fujino, G., Noguchi, T., Takeda, K., and Ichijo, H. (2006). Thioredoxin and protein kinases in redox signaling. *Semin Cancer Biol* 16, 427-435.
- Gasdaska, J. R., Berggren, M., and Powis, G. (1995a). Cell growth stimulation by the redox protein thioredoxin occurs by a novel helper mechanism. *Cell Growth Differ* 6, 1643-1650.
- Gasdaska, J. R., Harney, J. W., Gasdaska, P. Y., Powis, G., and Berry, M. J. (1999a). Regulation of human thioredoxin reductase expression and activity by 3'-untranslated region selenocysteine insertion sequence and mRNA instability elements. *J Biol Chem* 274, 25379-25385.
- Gasdaska, P. Y., Berggren, M. M., Berry, M. J., and Powis, G. (1999b). Cloning, sequencing and functional expression of a novel human thioredoxin reductase. *FEBS Lett* 442, 105-111.
- Gasdaska, P. Y., Gasdaska, J. R., Cochran, S., and Powis, G. (1995b). Cloning and sequencing of a human thioredoxin reductase. *FEBS Lett* 373, 5-9.
- Gasdaska, P. Y., Oblong, J. E., Cotgreave, I. A., and Powis, G. (1994). The predicted amino acid sequence of human thioredoxin is identical to that of the autocrine growth factor human adult T-cell derived factor (ADF): thioredoxin mRNA is elevated in some human tumors. *Biochim Biophys Acta* 1218, 292-296.
- Gasol, E., Jimenez-Vidal, M., Chillaron, J., Zorzano, A., and Palacin, M. (2004). Membrane topology of system xc- light subunit reveals a re-entrant loop with substrate-restricted accessibility. *J Biol Chem* 279, 31228-31236.
- Geisberger, R., Kiermayer, C., Homig, C., Conrad, M., Schmidt, J., Zimmer-Strobl, U., and Brielmeier, M. (2007). B- and T-cell-specific inactivation of thioredoxin reductase 2 does not impair lymphocyte development and maintenance. *Biol Chem* 388, 1083-1090.
- Geiszt, M., and Leto, T. L. (2004). The Nox family of NAD(P)H oxidases: host defense and beyond. *J Biol Chem* 279, 51715-51718.
- Gelpi, C., Sontheimer, E. J., and Rodriguez-Sanchez, J. L. (1992). Autoantibodies against a serine tRNA-protein complex implicated in cotranslational selenocysteine insertion. *Proc Natl Acad Sci U S A* 89, 9739-9743.
- Gilberger, T. W., Walter, R. D., and Muller, S. (1997). Identification and characterization of the functional amino acids at the active site of the large thioredoxin reductase from *Plasmodium falciparum*. *J Biol Chem* 272, 29584-29589.
- Gladyshev, V. N., Jeang, K. T., and Stadtman, T. C. (1996). Selenocysteine, identified as the penultimate C-terminal residue in human T-cell thioredoxin reductase, corresponds to TGA in the human placental gene. *Proc Natl Acad Sci U S A* 93, 6146-6151.
- Griendling, K. K., and FitzGerald, G. A. (2003a). Oxidative stress and cardiovascular injury: Part I: basic mechanisms and in vivo monitoring of ROS. *Circulation* 108, 1912-1916.
- Griendling, K. K., and FitzGerald, G. A. (2003b). Oxidative stress and cardiovascular injury: Part II: animal and human studies. *Circulation* 108, 2034-2040.
- Gromer, S., and Gross, J. H. (2002). Methylseleninate is a substrate rather than an inhibitor of mammalian thioredoxin reductase. Implications for the antitumor effects of selenium. *J Biol Chem* 277, 9701-9706.
- Gromer, S., Urig, S., and Becker, K. (2004). The thioredoxin system--from science to clinic. *Med Res Rev* 24, 40-89.
- Gromer, S., Wissing, J., Behne, D., Ashman, K., Schirmer, R. H., Flohe, L., and Becker, K. (1998). A hypothesis on the catalytic mechanism of the selenoenzyme thioredoxin reductase. *Biochem J* 332 (Pt 2), 591-592.

- Gustafsson, A. B., and Gottlieb, R. A. (2008). Recycle or die: the role of autophagy in cardioprotection. *J Mol Cell Cardiol* 44, 654-661.
- Gutierrez, P. L., Gee, M. V., and Bachur, N. R. (1983). Kinetics of anthracycline antibiotic free radical formation and reductive glycosidase activity. *Arch Biochem Biophys* 223, 68-75.
- Gutscher, M., Pauleau, A. L., Marty, L., Brach, T., Wabnitz, G. H., Samstag, Y., Meyer, A. J., and Dick, T. P. (2008). Real-time imaging of the intracellular glutathione redox potential. *Nat Methods* 5, 553-559.
- Hameyer, D., Loonstra, A., Eshkind, L., Schmitt, S., Antunes, C., Groen, A., Bindels, E., Jonkers, J., Krimpenfort, P., Meuwissen, R., *et al.* (2007). Toxicity of ligand-dependent Cre recombinases and generation of a conditional Cre deleter mouse allowing mosaic recombination in peripheral tissues. *Physiol Genomics* 31, 32-41.
- Haridas, V., Ni, J., Meager, A., Su, J., Yu, G. L., Zhai, Y., Kyaw, H., Akama, K. T., Hu, J., Van Eldik, L. J., and Aggarwal, B. B. (1998). TRANK, a novel cytokine that activates NF-kappa B and c-Jun N-terminal kinase. *J Immunol* 161, 1-6.
- Hattori, H., Imai, H., Furuhashi, K., Sato, O., and Nakagawa, Y. (2005a). Induction of phospholipid hydroperoxide glutathione peroxidase in human polymorphonuclear neutrophils and HL60 cells stimulated with TNF-alpha. *Biochem Biophys Res Commun* 337, 464-473.
- Hattori, N., Machida, Y., and Noda, K. (2005b). [Pathogenesis of Parkinson's disease: a common pathway between alpha-synuclein and parkin and the mechanism of Lewy bodies formation]. *Rinsho Shinkeigaku* 45, 905-907.
- Hill, K. E., Zhou, J., Austin, L. M., Motley, A. K., Ham, A. J., Olson, G. E., Atkins, J. F., Gesteland, R. F., and Burk, R. F. (2007). The selenium-rich C-terminal domain of mouse selenoprotein P is necessary for the supply of selenium to brain and testis but not for the maintenance of whole body selenium. *J Biol Chem* 282, 10972-10980.
- Hirosawa-Takamori, M., Chung, H. R., and Jackle, H. (2004). Conserved selenoprotein synthesis is not critical for oxidative stress defence and the lifespan of *Drosophila*. *EMBO Rep* 5, 317-322.
- Hirosawa-Takamori, M., Jackle, H., and Vorbruggen, G. (2000). The class 2 selenophosphate synthetase gene of *Drosophila* contains a functional mammalian-type SECIS. *EMBO Rep* 1, 441-446.
- Hirotsu, S., Abe, Y., Okada, K., Nagahara, N., Hori, H., Nishino, T., and Hakoshima, T. (1999). Crystal structure of a multifunctional 2-Cys peroxiredoxin heme-binding protein 23 kDa/proliferation-associated gene product. *Proc Natl Acad Sci U S A* 96, 12333-12338.
- Holmgren, A. (1977). Bovine thioredoxin system. Purification of thioredoxin reductase from calf liver and thymus and studies of its function in disulfide reduction. *J Biol Chem* 252, 4600-4606.
- Holmgren, A. (1985). Thioredoxin. *Annu Rev Biochem* 54, 237-271.
- Holmgren, A. (1989). Thioredoxin and glutaredoxin systems. *J Biol Chem* 264, 13963-13966.
- Homig-Holzel, C., Hojer, C., Rastelli, J., Casola, S., Strobl, L. J., Muller, W., Quintanilla-Martinez, L., Gewies, A., Ruland, J., Rajewsky, K., and Zimmer-Strobl, U. (2008). Constitutive CD40 signaling in B cells selectively activates the noncanonical NF-kappaB pathway and promotes lymphomagenesis. *J Exp Med* 205, 1317-1329.
- Hömig, C. (2005) Einfluss der Epstein-Barr-Virus Proteine LMP1 und EBNA2 auf die B-Zellentwicklung in vivo, LMU, Munich.
- Hoshi, T., and Heinemann, S. (2001). Regulation of cell function by methionine oxidation and reduction. *J Physiol* 531, 1-11.

- Ide, T., Tsutsui, H., Kinugawa, S., Suematsu, N., Hayashidani, S., Ichikawa, K., Utsumi, H., Machida, Y., Egashira, K., and Takeshita, A. (2000). Direct evidence for increased hydroxyl radicals originating from superoxide in the failing myocardium. *Circ Res* 86, 152-157.
- Ikeda, K., Kumagai, Y., Nagano, Y., Matsuzawa, N., and Kojo, S. (2003). Change in the concentration of vitamins C and E in rat tissues by paraquat administration. *Biosci Biotechnol Biochem* 67, 1130-1131.
- Ito, K., Hirao, A., Arai, F., Matsuoka, S., Takubo, K., Hamaguchi, I., Nomiyama, K., Hosokawa, K., Sakurada, K., Nakagata, N., *et al.* (2004). Regulation of oxidative stress by ATM is required for self-renewal of haematopoietic stem cells. *Nature* 431, 997-1002.
- Ito, K., Hirao, A., Arai, F., Takubo, K., Matsuoka, S., Miyamoto, K., Ohmura, M., Naka, K., Hosokawa, K., Ikeda, Y., and Suda, T. (2006). Reactive oxygen species act through p38 MAPK to limit the lifespan of hematopoietic stem cells. *Nat Med* 12, 446-451.
- Itoh, N., Cao, J., Chen, Z. H., Yoshida, Y., and Niki, E. (2007). Advantages and limitation of BODIPY as a probe for the evaluation of lipid peroxidation and its inhibition by antioxidants in plasma. *Bioorg Med Chem Lett* 17, 2059-2063.
- Ivanova, A., Signore, M., Caro, N., Greene, N. D., Copp, A. J., and Martinez-Barbera, J. P. (2005). In vivo genetic ablation by Cre-mediated expression of diphtheria toxin fragment A. *Genesis* 43, 129-135.
- Jager, R., Maurer, J., Jacob, A., and Schorle, H. (2004). Cell type-specific conditional regulation of the c-myc proto-oncogene by combining Cre/loxP recombination and tamoxifen-mediated activation. *Genesis* 38, 145-150.
- Jakupoglu, C., Przemeck, G. K., Schneider, M., Moreno, S. G., Mayr, N., Hatzopoulos, A. K., de Angelis, M. H., Wurst, W., Bornkamm, G. W., Brielmeier, M., and Conrad, M. (2005). Cytoplasmic thioredoxin reductase is essential for embryogenesis but dispensable for cardiac development. *Mol Cell Biol* 25, 1980-1988.
- Jeong, W., Park, S. J., Chang, T. S., Lee, D. Y., and Rhee, S. G. (2006). Molecular mechanism of the reduction of cysteine sulfinic acid of peroxiredoxin to cysteine by mammalian sulfiredoxin. *J Biol Chem* 281, 14400-14407.
- Jin, D. Y., Chae, H. Z., Rhee, S. G., and Jeang, K. T. (1997). Regulatory role for a novel human thioredoxin peroxidase in NF-kappaB activation. *J Biol Chem* 272, 30952-30961.
- Jing, Y., Dai, J., Chalmers-Redman, R. M., Tatton, W. G., and Waxman, S. (1999). Arsenic trioxide selectively induces acute promyelocytic leukemia cell apoptosis via a hydrogen peroxide-dependent pathway. *Blood* 94, 2102-2111.
- Jones, D. P., Go, Y. M., Anderson, C. L., Ziegler, T. R., Kinkade, J. M., Jr., and Kirlin, W. G. (2004). Cysteine/cystine couple is a newly recognized node in the circuitry for biologic redox signaling and control. *Faseb J* 18, 1246-1248.
- Jonsson, T. J., Tsang, A. W., Lowther, W. T., and Furdai, C. M. (2008). Identification of intact protein thiosulfinate intermediate in the reduction of cysteine sulfinic acid in peroxiredoxin by human sulfiredoxin. *J Biol Chem* 283, 22890-22894.
- Kang, S. W., Baines, I. C., and Rhee, S. G. (1998a). Characterization of a mammalian peroxiredoxin that contains one conserved cysteine. *J Biol Chem* 273, 6303-6311.
- Kang, S. W., Chae, H. Z., Seo, M. S., Kim, K., Baines, I. C., and Rhee, S. G. (1998b). Mammalian peroxiredoxin isoforms can reduce hydrogen peroxide generated in response to growth factors and tumor necrosis factor-alpha. *J Biol Chem* 273, 6297-6302.
- Kang, S. W., Chang, T. S., Lee, T. H., Kim, E. S., Yu, D. Y., and Rhee, S. G. (2004). Cytosolic peroxiredoxin attenuates the activation of Jnk and p38 but potentiates that of Erk in Hela cells stimulated with tumor necrosis factor-alpha. *J Biol Chem* 279, 2535-2543.

- Karunagaran, D., Joseph, J., and Kumar, T. R. (2007). Cell growth regulation. *Adv Exp Med Biol* 595, 245-268.
- Keightley, J. A., Anitori, R., Burton, M. D., Quan, F., Buist, N. R., and Kennaway, N. G. (2000). Mitochondrial encephalomyopathy and complex III deficiency associated with a stop-codon mutation in the cytochrome b gene. *Am J Hum Genet* 67, 1400-1410.
- Kiermayer, C., Michalke, B., Schmidt, J., and Brielmeier, M. (2007). Effect of selenium on thioredoxin reductase activity in Txnrd1 or Txnrd2 hemizygous mice. *Biol Chem* 388, 1091-1097.
- Kim, H. J., Chae, H. Z., Kim, Y. J., Kim, Y. H., Hwangs, T. S., Park, E. M., and Park, Y. M. (2003a). Preferential elevation of Prx I and Trx expression in lung cancer cells following hypoxia and in human lung cancer tissues. *Cell Biol Toxicol* 19, 285-298.
- Kim, M. R., Chang, H. S., Kim, B. H., Kim, S., Baek, S. H., Kim, J. H., Lee, S. R., and Kim, J. R. (2003b). Involvements of mitochondrial thioredoxin reductase (TrxR2) in cell proliferation. *Biochem Biophys Res Commun* 304, 119-124.
- Kim, S. Y., Kim, T. J., and Lee, K. Y. (2008). A novel function of peroxiredoxin 1 (Prx-1) in apoptosis signal-regulating kinase 1 (ASK1)-mediated signaling pathway. *FEBS Lett* 582, 1913-1918.
- Kinnula, V. L., Lehtonen, S., Kaarteenaho-Wiik, R., Lakari, E., Paakko, P., Kang, S. W., Rhee, S. G., and Soini, Y. (2002). Cell specific expression of peroxiredoxins in human lung and pulmonary sarcoidosis. *Thorax* 57, 157-164.
- Kinzy, S. A., Caban, K., and Copeland, P. R. (2005). Characterization of the SECIS binding protein 2 complex required for the co-translational insertion of selenocysteine in mammals. *Nucleic Acids Res* 33, 5172-5180.
- Krol, A. (2002). Evolutionarily different RNA motifs and RNA-protein complexes to achieve selenoprotein synthesis. *Biochimie* 84, 765-774.
- Kumar, S., Bjornstedt, M., and Holmgren, A. (1992). Selenite is a substrate for calf thymus thioredoxin reductase and thioredoxin and elicits a large non-stoichiometric oxidation of NADPH in the presence of oxygen. *Eur J Biochem* 207, 435-439.
- Kwon, J., Lee, S. R., Yang, K. S., Ahn, Y., Kim, Y. J., Stadtman, E. R., and Rhee, S. G. (2004). Reversible oxidation and inactivation of the tumor suppressor PTEN in cells stimulated with peptide growth factors. *Proc Natl Acad Sci U S A* 101, 16419-16424.
- Lammers, M., and Follmann, H. (1984). Deoxyribonucleotide biosynthesis in yeast (*Saccharomyces cerevisiae*). A ribonucleotide reductase system of sufficient activity for DNA synthesis. *Eur J Biochem* 140, 281-287.
- Laurent, A., Nicco, C., Chereau, C., Goulvestre, C., Alexandre, J., Alves, A., Levy, E., Goldwasser, F., Panis, Y., Soubrane, O., *et al.* (2005). Controlling tumor growth by modulating endogenous production of reactive oxygen species. *Cancer Res* 65, 948-956.
- Laurent, T. C., Moore, E. C., and Reichard, P. (1964). Enzymatic Synthesis of Deoxyribonucleotides. Iv. Isolation and Characterization of Thioredoxin, the Hydrogen Donor from *Escherichia Coli* B. *J Biol Chem* 239, 3436-3444.
- Lebovitz, R. M., Zhang, H., Vogel, H., Cartwright, J., Jr., Dionne, L., Lu, N., Huang, S., and Matzuk, M. M. (1996). Neurodegeneration, myocardial injury, and perinatal death in mitochondrial superoxide dismutase-deficient mice. *Proc Natl Acad Sci U S A* 93, 9782-9787.
- Lee, S. R., Kim, J. R., Kwon, K. S., Yoon, H. W., Levine, R. L., Ginsburg, A., and Rhee, S. G. (1999). Molecular cloning and characterization of a mitochondrial selenocysteine-containing thioredoxin reductase from rat liver. *J Biol Chem* 274, 4722-4734.

- Lerman-Sagie, T., Rustin, P., Lev, D., Yanoov, M., Leshinsky-Silver, E., Sagie, A., Ben-Gal, T., and Munnich, A. (2001). Dramatic improvement in mitochondrial cardiomyopathy following treatment with idebenone. *J Inherit Metab Dis* 24, 28-34.
- Lescure, A., Gautheret, D., Carbon, P., and Krol, A. (1999). Novel selenoproteins identified in silico and in vivo by using a conserved RNA structural motif. *J Biol Chem* 274, 38147-38154.
- Li, L., Shoji, W., Takano, H., Nishimura, N., Aoki, Y., Takahashi, R., Goto, S., Kaifu, T., Takai, T., and Obinata, M. (2007). Increased susceptibility of MER5 (peroxiredoxin III) knockout mice to LPS-induced oxidative stress. *Biochem Biophys Res Commun* 355, 715-721.
- Lim, J. C., Choi, H. I., Park, Y. S., Nam, H. W., Woo, H. A., Kwon, K. S., Kim, Y. S., Rhee, S. G., Kim, K., and Chae, H. Z. (2008). Irreversible oxidation of the active-site cysteine of peroxiredoxin to cysteine sulfonic acid for enhanced molecular chaperone activity. *J Biol Chem* 283, 28873-28880.
- Lothrop, A. P., Ruggles, E. L., and Hondal, R. J. (2009). No selenium required: reactions catalyzed by mammalian thioredoxin reductase that are independent of a selenocysteine residue. *Biochemistry* 48, 6213-6223.
- Low, S. C., and Berry, M. J. (1996). Knowing when not to stop: selenocysteine incorporation in eukaryotes. *Trends Biochem Sci* 21, 203-208.
- Lu, J., Chew, E. H., and Holmgren, A. (2007). Targeting thioredoxin reductase is a basis for cancer therapy by arsenic trioxide. *Proc Natl Acad Sci U S A* 104, 12288-12293.
- Maiti, B., Arbogast, S., Allamand, V., Moyle, M. W., Anderson, C. B., Richard, P., Guicheney, P., Ferreira, A., Flanigan, K. M., and Howard, M. T. (2009). A mutation in the SEPNI selenocysteine redefinition element (SRE) reduces selenocysteine incorporation and leads to SEPNI-related myopathy. *Hum Mutat* 30, 411-416.
- Martins, N. M., Santos, N. A., Curti, C., Bianchi, M. L., and Santos, A. C. (2008). Cisplatin induces mitochondrial oxidative stress with resultant energetic metabolism impairment, membrane rigidification and apoptosis in rat liver. *J Appl Toxicol* 28, 337-344.
- Massie, A., Schallier, A., Mertens, B., Vermoesen, K., Bannai, S., Sato, H., Smolders, I., and Michotte, Y. (2008). Time-dependent changes in striatal xCT protein expression in hemi-Parkinson rats. *Neuroreport* 19, 1589-1592.
- Matsui, M., Oshima, M., Oshima, H., Takaku, K., Maruyama, T., Yodoi, J., and Taketo, M. M. (1996). Early embryonic lethality caused by targeted disruption of the mouse thioredoxin gene. *Dev Biol* 178, 179-185.
- Matsushima, S., Ide, T., Yamato, M., Matsusaka, H., Hattori, F., Ikeuchi, M., Kubota, T., Sunagawa, K., Hasegawa, Y., Kurihara, T., *et al.* (2006). Overexpression of mitochondrial peroxiredoxin-3 prevents left ventricular remodeling and failure after myocardial infarction in mice. *Circulation* 113, 1779-1786.
- Maulik, N., Yoshida, T., Engelman, R. M., Deaton, D., Flack, J. E., 3rd, Rousou, J. A., and Das, D. K. (1998). Ischemic preconditioning attenuates apoptotic cell death associated with ischemia/reperfusion. *Mol Cell Biochem* 186, 139-145.
- May, J. M., Cobb, C. E., Mendiratta, S., Hill, K. E., and Burk, R. F. (1998). Reduction of the ascorbyl free radical to ascorbate by thioredoxin reductase. *J Biol Chem* 273, 23039-23045.
- Mazumder, S., Plesca, D., and Almasan, A. (2007). A jekyll and hyde role of cyclin E in the genotoxic stress response: switching from cell cycle control to apoptosis regulation. *Cell Cycle* 6, 1437-1442.

- Miller, E. W., Albers, A. E., Pralle, A., Isacoff, E. Y., and Chang, C. J. (2005). Boronate-based fluorescent probes for imaging cellular hydrogen peroxide. *J Am Chem Soc* 127, 16652-16659.
- Miranda-Vizuete, A., Damdimopoulos, A. E., Pedrajas, J. R., Gustafsson, J. A., and Spyrou, G. (1999). Human mitochondrial thioredoxin reductase cDNA cloning, expression and genomic organization. *Eur J Biochem* 261, 405-412.
- Miranda-Vizuete, A., and Spyrou, G. (2002). Genomic organization and identification of a novel alternative splicing variant of mouse mitochondrial thioredoxin reductase (TrxR2) gene. *Mol Cells* 13, 488-492.
- Mizusawa, H., Ishii, T., and Bannai, S. (2000). Peroxiredoxin I (macrophage 23 kDa stress protein) is highly and widely expressed in the rat nervous system. *Neurosci Lett* 283, 57-60.
- Moghadaszadeh, B., Petit, N., Jaillard, C., Brockington, M., Roy, S. Q., Merlini, L., Romero, N., Estournet, B., Desguerre, I., Chaigne, D., *et al.* (2001). Mutations in SEPN1 cause congenital muscular dystrophy with spinal rigidity and restrictive respiratory syndrome. *Nat Genet* 29, 17-18.
- Moos, P. J., Edes, K., Cassidy, P., Massuda, E., and Fitzpatrick, F. A. (2003). Electrophilic prostaglandins and lipid aldehydes repress redox-sensitive transcription factors p53 and hypoxia-inducible factor by impairing the selenoprotein thioredoxin reductase. *J Biol Chem* 278, 745-750.
- Nalvarte, I., Damdimopoulos, A. E., Nystom, C., Nordman, T., Miranda-Vizuete, A., Olsson, J. M., Eriksson, L., Bjornstedt, M., Arner, E. S., and Spyrou, G. (2004a). Overexpression of enzymatically active human cytosolic and mitochondrial thioredoxin reductase in HEK-293 cells. Effect on cell growth and differentiation. *J Biol Chem* 279, 54510-54517.
- Nalvarte, I., Damdimopoulos, A. E., and Spyrou, G. (2004b). Human mitochondrial thioredoxin reductase reduces cytochrome c and confers resistance to complex III inhibition. *Free Radic Biol Med* 36, 1270-1278.
- Nguyen, P., Awwad, R. T., Smart, D. D., Spitz, D. R., and Gius, D. (2006). Thioredoxin reductase as a novel molecular target for cancer therapy. *Cancer Lett* 236, 164-174.
- Noh, D. Y., Ahn, S. J., Lee, R. A., Kim, S. W., Park, I. A., and Chae, H. Z. (2001). Overexpression of peroxiredoxin in human breast cancer. *Anticancer Res* 21, 2085-2090.
- Noh, Y. H., Baek, J. Y., Jeong, W., Rhee, S. G., and Chang, T. S. (2009). Sulfiredoxin Translocation into Mitochondria Plays a Crucial Role in Reducing Hyperoxidized Peroxiredoxin III. *J Biol Chem* 284, 8470-8477.
- Nonn, L., Berggren, M., and Powis, G. (2003a). Increased expression of mitochondrial peroxiredoxin-3 (thioredoxin peroxidase-2) protects cancer cells against hypoxia and drug-induced hydrogen peroxide-dependent apoptosis. *Mol Cancer Res* 1, 682-689.
- Nonn, L., Williams, R. R., Erickson, R. P., and Powis, G. (2003b). The absence of mitochondrial thioredoxin 2 causes massive apoptosis, exencephaly, and early embryonic lethality in homozygous mice. *Mol Cell Biol* 23, 916-922.
- Nordberg, J., and Arner, E. S. (2001). Reactive oxygen species, antioxidants, and the mammalian thioredoxin system. *Free Radic Biol Med* 31, 1287-1312.
- Oberley, T. D., Verwiebe, E., Zhong, W., Kang, S. W., and Rhee, S. G. (2001). Localization of the thioredoxin system in normal rat kidney. *Free Radic Biol Med* 30, 412-424.
- Ogasawara, M. A., and Zhang, H. (2008). Redox Regulation and its Emerging Roles in Stem Cells and Stem-Like Cancer Cells. *Antioxid Redox Signal*.

- Ohashi, T., Mizutani, A., Murakami, A., Kojo, S., Ishii, T., and Taketani, S. (2002). Rapid oxidation of dichlorodihydrofluorescein with heme and hemoproteins: formation of the fluorescein is independent of the generation of reactive oxygen species. *FEBS Lett* 511, 21-27.
- Okado-Matsumoto, A., Matsumoto, A., Fujii, J., and Taniguchi, N. (2000). Peroxiredoxin IV is a secretable protein with heparin-binding properties under reduced conditions. *J Biochem* 127, 493-501.
- Okuno, S., Sato, H., Kuriyama-Matsumura, K., Tamba, M., Wang, H., Sohda, S., Hamada, H., Yoshikawa, H., Kondo, T., and Bannai, S. (2003). Role of cystine transport in intracellular glutathione level and cisplatin resistance in human ovarian cancer cell lines. *Br J Cancer* 88, 951-956.
- Osawa, M., Hanada, K., Hamada, H., and Nakauchi, H. (1996). Long-term lymphohematopoietic reconstitution by a single CD34-low/negative hematopoietic stem cell. *Science* 273, 242-245.
- Pacheco, R., Gallart, T., Lluís, C., and Franco, R. (2007). Role of glutamate on T-cell mediated immunity. *J Neuroimmunol* 185, 9-19.
- Papp, L. V., Lu, J., Striebel, F., Kennedy, D., Holmgren, A., and Khanna, K. K. (2006). The redox state of SECIS binding protein 2 controls its localization and selenocysteine incorporation function. *Mol Cell Biol* 26, 4895-4910.
- Park, H. S., Lee, S. H., Park, D., Lee, J. S., Ryu, S. H., Lee, W. J., Rhee, S. G., and Bae, Y. S. (2004a). Sequential activation of phosphatidylinositol 3-kinase, beta Pix, Rac1, and Nox1 in growth factor-induced production of H₂O₂. *Mol Cell Biol* 24, 4384-4394.
- Park, J. Y., Seong, J. K., and Paik, Y. K. (2004b). Proteomic analysis of diet-induced hypercholesterolemic mice. *Proteomics* 4, 514-523.
- Patenaude, A., Ven Murthy, M. R., and Mirault, M. E. (2004). Mitochondrial thioredoxin system: effects of TrxR2 overexpression on redox balance, cell growth, and apoptosis. *J Biol Chem* 279, 27302-27314.
- Pedrajas, J. R., Miranda-Vizueté, A., Javanmardy, N., Gustafsson, J. A., and Spyrou, G. (2000). Mitochondria of *Saccharomyces cerevisiae* contain one-conserved cysteine type peroxiredoxin with thioredoxin peroxidase activity. *J Biol Chem* 275, 16296-16301.
- Pennington, J. D., Jacobs, K. M., Sun, L., Bar-Sela, G., Mishra, M., and Gius, D. (2007). Thioredoxin and thioredoxin reductase as redox-sensitive molecular targets for cancer therapy. *Curr Pharm Des* 13, 3368-3377.
- Persson-Moschos, M. E., Stavenow, L., Akesson, B., and Lindgarde, F. (2000). Selenoprotein P in plasma in relation to cancer morbidity in middle-aged Swedish men. *Nutr Cancer* 36, 19-26.
- Powis, G., Gasdaska, J. R., and Baker, A. (1997a). Redox signaling and the control of cell growth and death. *Adv Pharmacol* 38, 329-359.
- Powis, G., Gasdaska, J. R., Gasdaska, P. Y., Berggren, M., Kirkpatrick, D. L., Engman, L., Cotgreave, I. A., Angulo, M., and Baker, A. (1997b). Selenium and the thioredoxin redox system: effects on cell growth and death. *Oncol Res* 9, 303-312.
- Qiao, H. X., Hao, C. J., Li, Y., He, X., Chen, R. S., Cui, J., Xu, Z. H., and Li, W. (2008). JNK activation mediates the apoptosis of xCT-deficient cells. *Biochem Biophys Res Commun* 370, 584-588.
- Rabilloud, T., Heller, M., Gasnier, F., Luche, S., Rey, C., Aebersold, R., Benahmed, M., Louisot, P., and Lunardi, J. (2002). Proteomics analysis of cellular response to oxidative stress. Evidence for in vivo overoxidation of peroxiredoxins at their active site. *J Biol Chem* 277, 19396-19401.

- Reichard, P. (1988). Interactions between deoxyribonucleotide and DNA synthesis. *Annu Rev Biochem* 57, 349-374.
- Rhee, S. G. (1999). Redox signaling: hydrogen peroxide as intracellular messenger. *Exp Mol Med* 31, 53-59.
- Rhee, S. G., Bae, Y. S., Lee, S.-R. a., and Kwon, J. (2000). Hydrogen peroxide: a key messenger that modulates protein phosphorylation through cysteine oxidation. *Science'sstke* 2000, p. pe1-6.
- Rhee, S. G., Chae, H. Z., and Kim, K. (2005). Peroxiredoxins: a historical overview and speculative preview of novel mechanisms and emerging concepts in cell signaling. *Free Radic Biol Med* 38, 1543-1552.
- Rhee, S. G., Jeong, W., Chang, T. S., and Woo, H. A. (2007). Sulfiredoxin, the cysteine sulfinic acid reductase specific to 2-Cys peroxiredoxin: its discovery, mechanism of action, and biological significance. *Kidney Int Suppl*, S3-8.
- Rhee, S. G., Kang, S. W., Chang, T. S., Jeong, W., and Kim, K. (2001). Peroxiredoxin, a novel family of peroxidases. *IUBMB Life* 52, 35-41.
- Rieger, M. A., Hoppe, P. S., Smejkal, B. M., Eitelhuber, A. C., and Schroeder, T. (2009). Hematopoietic cytokines can instruct lineage choice. *Science* 325, 217-218.
- Rohrbach, S., Gruenler, S., Teschner, M., and Holtz, J. (2006). The thioredoxin system in aging muscle: key role of mitochondrial thioredoxin reductase in the protective effects of caloric restriction? *Am J Physiol Regul Integr Comp Physiol* 291, R927-935.
- Roussel, X., Bechade, G., Kriznik, A., Van Dorsselaer, A., Sanglier-Cianferani, S., Branlant, G., and Rahuel-Clermont, S. (2008). Evidence for the formation of a covalent thiosulfinate intermediate with peroxiredoxin in the catalytic mechanism of sulfiredoxin. *J Biol Chem* 283, 22371-22382.
- Rozen, S., and Skaletsky, H. (2000). Primer3 on the WWW for general users and for biologist programmers. *Methods Mol Biol* 132, 365-386.
- Rundlof, A. K., and Arner, E. S. (2004). Regulation of the mammalian selenoprotein thioredoxin reductase 1 in relation to cellular phenotype, growth, and signaling events. *Antioxid Redox Signal* 6, 41-52.
- Rundlof, A. K., Carlsten, M., Giacobini, M. M., and Arner, E. S. (2000). Prominent expression of the selenoprotein thioredoxin reductase in the medullary rays of the rat kidney and thioredoxin reductase mRNA variants differing at the 5' untranslated region. *Biochem J* 347 Pt 3, 661-668.
- Rundlof, A. K., Fernandes, A. P., Selenius, M., Babic, M., Shariatgorji, M., Nilsson, G., Ilag, L. L., Dobra, K., and Bjornstedt, M. (2007). Quantification of alternative mRNA species and identification of thioredoxin reductase 1 isoforms in human tumor cells. *Differentiation* 75, 123-132.
- Saelens, X., Festjens, N., Vande Walle, L., van Gurp, M., van Loo, G., and Vandenabeele, P. (2004). Toxic proteins released from mitochondria in cell death. *Oncogene* 23, 2861-2874.
- Sandalova, T., Zhong, L., Lindqvist, Y., Holmgren, A., and Schneider, G. (2001). Three-dimensional structure of a mammalian thioredoxin reductase: implications for mechanism and evolution of a selenocysteine-dependent enzyme. *Proc Natl Acad Sci U S A* 98, 9533-9538.
- Sasaki, H., Sato, H., Kuriyama-Matsumura, K., Sato, K., Maebara, K., Wang, H., Tamba, M., Itoh, K., Yamamoto, M., and Bannai, S. (2002). Electrophile response element-mediated induction of the cystine/glutamate exchange transporter gene expression. *J Biol Chem* 277, 44765-44771.

- Sato, H., Ishii, T., Sugita, Y., and Bannai, S. (1991). Induction of cationic amino acid transport activity in mouse peritoneal macrophages by lipopolysaccharide. *Biochim Biophys Acta* 1069, 46-52.
- Sato, H., Shiiya, A., Kimata, M., Maebara, K., Tamba, M., Sakakura, Y., Makino, N., Sugiyama, F., Yagami, K., Moriguchi, T., *et al.* (2005). Redox imbalance in cystine/glutamate transporter-deficient mice. *J Biol Chem* 280, 37423-37429.
- Sato, H., Tamba, M., Kuriyama-Matsumura, K., Okuno, S., and Bannai, S. (2000). Molecular cloning and expression of human xCT, the light chain of amino acid transport system xc. *Antioxid Redox Signal* 2, 665-671.
- Sato, H., Tamba, M., Okuno, S., Sato, K., Keino-Masu, K., Masu, M., and Bannai, S. (2002). Distribution of cystine/glutamate exchange transporter, system x(c)-, in the mouse brain. *J Neurosci* 22, 8028-8033.
- Sato, H., Watanabe, H., Ishii, T., and Bannai, S. (1987). Neutral amino acid transport in mouse peritoneal macrophages. *J Biol Chem* 262, 13015-13019.
- Savaskan, N. E., Heckel, A., Hahnen, E., Engelhorn, T., Doerfler, A., Ganslandt, O., Nimsky, C., Buchfelder, M., and Eyupoglu, I. Y. (2008). Small interfering RNA-mediated xCT silencing in gliomas inhibits neurodegeneration and alleviates brain edema. *Nat Med* 14, 629-632.
- Sawicki, J. A., Morris, R. J., Monks, B., Sakai, K., and Miyazaki, J. (1998). A composite CMV-IE enhancer/beta-actin promoter is ubiquitously expressed in mouse cutaneous epithelium. *Exp Cell Res* 244, 367-369.
- Schneider, M., Forster, H., Boersma, A., Seiler, A., Wehnes, H., Sinowatz, F., Neumuller, C., Deutsch, M. J., Walch, A., Hrabe de Angelis, M., *et al.* (2009). Mitochondrial glutathione peroxidase 4 disruption causes male infertility. *Faseb J*.
- Schroder, E., Littlechild, J. A., Lebedev, A. A., Errington, N., Vagin, A. A., and Isupov, M. N. (2000). Crystal structure of decameric 2-Cys peroxiredoxin from human erythrocytes at 1.7 Å resolution. *Structure* 8, 605-615.
- Schweizer, U., Brauer, A. U., Kohrle, J., Nitsch, R., and Savaskan, N. E. (2004). Selenium and brain function: a poorly recognized liaison. *Brain Res Brain Res Rev* 45, 164-178.
- Seemann, S., and Hainaut, P. (2005). Roles of thioredoxin reductase 1 and APE/Ref-1 in the control of basal p53 stability and activity. *Oncogene* 24, 3853-3863.
- Seiler, A. (2008). Dissecting the molecular mechanism of glutathione-dependent regulation of cell proliferation and cell death.
- Seiler, A., Schneider, M., Forster, H., Roth, S., Wirth, E. K., Culmsee, C., Plesnila, N., Kremmer, E., Radmark, O., Wurst, W., *et al.* (2008). Glutathione peroxidase 4 senses and translates oxidative stress into 12/15-lipoxygenase dependent- and AIF-mediated cell death. *Cell Metab* 8, 237-248.
- Selenius, M., Fernandes, A. P., Brodin, O., Bjornstedt, M., and Rundlof, A. K. (2008). Treatment of lung cancer cells with cytotoxic levels of sodium selenite: effects on the thioredoxin system. *Biochem Pharmacol* 75, 2092-2099.
- Seo, M. S., Kang, S. W., Kim, K., Baines, I. C., Lee, T. H., and Rhee, S. G. (2000). Identification of a new type of mammalian peroxiredoxin that forms an intramolecular disulfide as a reaction intermediate. *J Biol Chem* 275, 20346-20354.
- Shigenaga, M. K., Hagen, T. M., and Ames, B. N. (1994). Oxidative damage and mitochondrial decay in aging. *Proc Natl Acad Sci U S A* 91, 10771-10778.
- Shih, A. Y., and Murphy, T. H. (2001). xCt cystine transporter expression in HEK293 cells: pharmacology and localization. *Biochem Biophys Res Commun* 282, 1132-1137.

- Small-Howard, A., Morozova, N., Stoytcheva, Z., Forry, E. P., Mansell, J. B., Harney, J. W., Carlson, B. A., Xu, X. M., Hatfield, D. L., and Berry, M. J. (2006). Supramolecular complexes mediate selenocysteine incorporation in vivo. *Mol Cell Biol* 26, 2337-2346.
- Soerensen, J., Jakupoglu, C., Beck, H., Forster, H., Schmidt, J., Schmahl, W., Schweizer, U., Conrad, M., and Brielmeier, M. (2008). The role of thioredoxin reductases in brain development. *PLoS ONE* 3, e1813.
- Soriano, P. (1999). Generalized lacZ expression with the ROSA26 Cre reporter strain. *Nat Genet* 21, 70-71.
- Spyrou, G., Enmark, E., Miranda-Vizuet, A., and Gustafsson, J. (1997). Cloning and expression of a novel mammalian thioredoxin. *J Biol Chem* 272, 2936-2941.
- Srinivas, S., Watanabe, T., Lin, C. S., William, C. M., Tanabe, Y., Jessell, T. M., and Costantini, F. (2001). Cre reporter strains produced by targeted insertion of EYFP and ECFP into the ROSA26 locus. *BMC Dev Biol* 1, 4.
- Stadtman, T. C. (1991). Biosynthesis and function of selenocysteine-containing enzymes. *J Biol Chem* 266, 16257-16260.
- Su, D., and Gladyshev, V. N. (2004). Alternative splicing involving the thioredoxin reductase module in mammals: a glutaredoxin-containing thioredoxin reductase 1. *Biochemistry* 43, 12177-12188.
- Su, D., Novoselov, S. V., Sun, Q. A., Moustafa, M. E., Zhou, Y., Oko, R., Hatfield, D. L., and Gladyshev, V. N. (2005). Mammalian selenoprotein thioredoxin-glutathione reductase. Roles in disulfide bond formation and sperm maturation. *J Biol Chem* 280, 26491-26498.
- Sun, Q. A., Kirnarsky, L., Sherman, S., and Gladyshev, V. N. (2001a). Selenoprotein oxidoreductase with specificity for thioredoxin and glutathione systems. *Proc Natl Acad Sci U S A* 98, 3673-3678.
- Sun, Q. A., Su, D., Novoselov, S. V., Carlson, B. A., Hatfield, D. L., and Gladyshev, V. N. (2005). Reaction mechanism and regulation of mammalian thioredoxin/glutathione reductase. *Biochemistry* 44, 14528-14537.
- Sun, Q. A., Wu, Y., Zappacosta, F., Jeang, K. T., Lee, B. J., Hatfield, D. L., and Gladyshev, V. N. (1999). Redox regulation of cell signaling by selenocysteine in mammalian thioredoxin reductases. *J Biol Chem* 274, 24522-24530.
- Sun, Q. A., Zappacosta, F., Factor, V. M., Wirth, P. J., Hatfield, D. L., and Gladyshev, V. N. (2001b). Heterogeneity within animal thioredoxin reductases. Evidence for alternative first exon splicing. *J Biol Chem* 276, 3106-3114.
- Tagami, M., Yamagata, K., Ikeda, K., Nara, Y., Fujino, H., Kubota, A., Numano, F., and Yamori, Y. (1998). Vitamin E prevents apoptosis in cortical neurons during hypoxia and oxygen reperfusion. *Lab Invest* 78, 1415-1429.
- Tajsharghi, H., Darin, N., Tulinius, M., and Oldfors, A. (2005). Early onset myopathy with a novel mutation in the Selenoprotein N gene (SEPN1). *Neuromuscul Disord* 15, 299-302.
- Talbot, S., Nelson, R., and Self, W. T. (2008). Arsenic trioxide and auranofin inhibit selenoprotein synthesis: implications for chemotherapy for acute promyelocytic leukaemia. *Br J Pharmacol* 154, 940-948.
- Tamura, T., and Stadtman, T. C. (1996). A new selenoprotein from human lung adenocarcinoma cells: purification, properties, and thioredoxin reductase activity. *Proc Natl Acad Sci U S A* 93, 1006-1011.
- Tanaka, T., Hosoi, F., Yamaguchi-Iwai, Y., Nakamura, H., Masutani, H., Ueda, S., Nishiyama, A., Takeda, S., Wada, H., Spyrou, G., and Yodoi, J. (2002). Thioredoxin-2 (TRX-2) is an essential gene regulating mitochondria-dependent apoptosis. *Embo J* 21, 1695-1703.

- Tanaka, T., Nakamura, H., Nishiyama, A., Hosoi, F., Masutani, H., Wada, H., and Yodoi, J. (2000). Redox regulation by thioredoxin superfamily; protection against oxidative stress and aging. *Free Radical Research* 33, 851-855.
- Thelander, L., and Reichard, P. (1979). Reduction of ribonucleotides. *Annu Rev Biochem* 48, 133-158.
- Toohey, J. I. (1975). Sulfhydryl dependence in primary explant hematopoietic cells. Inhibition of growth in vitro with vitamin B12 compounds. *Proc Natl Acad Sci U S A* 72, 73-77.
- Trachootham, D., Zhou, Y., Zhang, H., Demizu, Y., Chen, Z., Pelicano, H., Chiao, P. J., Achanta, G., Arlinghaus, R. B., Liu, J., and Huang, P. (2006). Selective killing of oncogenically transformed cells through a ROS-mediated mechanism by beta-phenylethyl isothiocyanate. *Cancer Cell* 10, 241-252.
- Tsutsui, H., Kinugawa, S., and Matsushima, S. (2009). Mitochondrial oxidative stress and dysfunction in myocardial remodelling. *Cardiovasc Res* 81, 449-456.
- Tujebajeva, R. M., Copeland, P. R., Xu, X. M., Carlson, B. A., Harney, J. W., Driscoll, D. M., Hatfield, D. L., and Berry, M. J. (2000). Decoding apparatus for eukaryotic selenocysteine insertion. *EMBO Rep* 1, 158-163.
- Turanov, A. A., Su, D., and Gladyshev, V. N. (2006). Characterization of alternative cytosolic forms and cellular targets of mouse mitochondrial thioredoxin reductase. *J Biol Chem* 281, 22953-22963.
- van Zandwijk, N. (1995). N-acetylcysteine for lung cancer prevention. *Chest* 107, 1437-1441.
- Veal, E. A., Day, A. M., and Morgan, B. A. (2007). Hydrogen peroxide sensing and signaling. *Mol Cell* 26, 1-14.
- Veal, E. A., Findlay, V. J., Day, A. M., Bozonet, S. M., Evans, J. M., Quinn, J., and Morgan, B. A. (2004). A 2-Cys peroxiredoxin regulates peroxide-induced oxidation and activation of a stress-activated MAP kinase. *Mol Cell* 15, 129-139.
- Walczak, R., Carbon, P., and Krol, A. (1998). An essential non-Watson-Crick base pair motif in 3'UTR to mediate selenoprotein translation. *Rna* 4, 74-84.
- Watabe, S., Hasegawa, H., Takimoto, K., Yamamoto, Y., and Takahashi, S. Y. (1995). Possible function of SP-22, a substrate of mitochondrial ATP-dependent protease, as a radical scavenger. *Biochem Biophys Res Commun* 213, 1010-1016.
- Watabe, S., Hiroi, T., Yamamoto, Y., Fujioka, Y., Hasegawa, H., Yago, N., and Takahashi, S. Y. (1997). SP-22 is a thioredoxin-dependent peroxide reductase in mitochondria. *Eur J Biochem* 249, 52-60.
- Watabe, S., Makino, Y., Ogawa, K., Hiroi, T., Yamamoto, Y., and Takahashi, S. Y. (1999). Mitochondrial thioredoxin reductase in bovine adrenal cortex its purification, properties, nucleotide/amino acid sequences, and identification of selenocysteine. *Eur J Biochem* 264, 74-84.
- Watanabe, H., and Bannai, S. (1987). Induction of cystine transport activity in mouse peritoneal macrophages. *J Exp Med* 165, 628-640.
- Williams, C. H., Arscott, L. D., Muller, S., Lennon, B. W., Ludwig, M. L., Wang, P. F., Veine, D. M., Becker, K., and Schirmer, R. H. (2000). Thioredoxin reductase two modes of catalysis have evolved. *Eur J Biochem* 267, 6110-6117.
- Woo, H. A., Chae, H. Z., Hwang, S. C., Yang, K. S., Kang, S. W., Kim, K., and Rhee, S. G. (2003a). Reversing the inactivation of peroxiredoxins caused by cysteine sulfinic acid formation. *Science* 300, 653-656.
- Woo, H. A., Jeong, W., Chang, T. S., Park, K. J., Park, S. J., Yang, J. S., and Rhee, S. G. (2005). Reduction of cysteine sulfinic acid by sulfiredoxin is specific to 2-cys peroxiredoxins. *J Biol Chem* 280, 3125-3128.

- Woo, H. A., Kang, S. W., Kim, H. K., Yang, K. S., Chae, H. Z., and Rhee, S. G. (2003b). Reversible oxidation of the active site cysteine of peroxiredoxins to cysteine sulfinic acid. Immunoblot detection with antibodies specific for the hyperoxidized cysteine-containing sequence. *J Biol Chem* 278, 47361-47364.
- Wood, Z. A., Schroder, E., Robin Harris, J., and Poole, L. B. (2003). Structure, mechanism and regulation of peroxiredoxins. *Trends Biochem Sci* 28, 32-40.
- Wu, S. J., Ng, L. T., and Lin, C. C. (2005). Effects of antioxidants and caspase-3 inhibitor on the phenylethyl isothiocyanate-induced apoptotic signaling pathways in human PLC/PRF/5 cells. *Eur J Pharmacol* 518, 96-106.
- Xu, G. L., Wang, S. C., Gu, B. Q., Yang, Y. X., Song, H. B., Xue, W. L., Liang, W. S., and Zhang, P. Y. (1997). Further investigation on the role of selenium deficiency in the aetiology and pathogenesis of Keshan disease. *Biomed Environ Sci* 10, 316-326.
- Xu, X. M., Carlson, B. A., Mix, H., Zhang, Y., Saira, K., Glass, R. S., Berry, M. J., Gladyshev, V. N., and Hatfield, D. L. (2007). Biosynthesis of selenocysteine on its tRNA in eukaryotes. *PLoS Biol* 5, e4.
- Xu, X. M., Mix, H., Carlson, B. A., Grabowski, P. J., Gladyshev, V. N., Berry, M. J., and Hatfield, D. L. (2005). Evidence for direct roles of two additional factors, SECp43 and soluble liver antigen, in the selenoprotein synthesis machinery. *J Biol Chem* 280, 41568-41575.
- Yamamoto, Y., Nagata, Y., Niki, E., Watanabe, K., and Yoshimura, S. (1993). Plasma glutathione peroxidase reduces phosphatidylcholine hydroperoxide. *Biochem Biophys Res Commun* 193, 133-138.
- Yanagawa, T., Iwasa, S., Ishii, T., Tabuchi, K., Yusa, H., Onizawa, K., Omura, K., Harada, H., Suzuki, H., and Yoshida, H. (2000). Peroxiredoxin I expression in oral cancer: a potential new tumor marker. *Cancer Lett* 156, 27-35.
- Yang, K. S., Kang, S. W., Woo, H. A., Hwang, S. C., Chae, H. Z., Kim, K., and Rhee, S. G. (2002). Inactivation of human peroxiredoxin I during catalysis as the result of the oxidation of the catalytic site cysteine to cysteine-sulfinic acid. *J Biol Chem* 277, 38029-38036.
- Yang, M., Nazhat, N. B., Jiang, X., Kelsey, S. M., Blake, D. R., Newland, A. C., and Morris, C. J. (1996). Adriamycin stimulates proliferation of human lymphoblastic leukaemic cells via a mechanism of hydrogen peroxide (H₂O₂) production. *Br J Haematol* 95, 339-344.
- Yoo, M. H., Xu, X. M., Carlson, B. A., Patterson, A. D., Gladyshev, V. N., and Hatfield, D. L. (2007). Targeting thioredoxin reductase 1 reduction in cancer cells inhibits self-sufficient growth and DNA replication. *PLoS ONE* 2, e1112.
- Yoshida, T., Maulik, N., Engelman, R. M., Ho, Y. S., Magnenat, J. L., Rousou, J. A., Flack, J. E., 3rd, Deaton, D., and Das, D. K. (1997). Glutathione peroxidase knockout mice are susceptible to myocardial ischemia reperfusion injury. *Circulation* 96, II-216-220.
- Yu, R., Mandelkar, S., Harvey, K. J., Ucker, D. S., and Kong, A. N. (1998). Chemopreventive isothiocyanates induce apoptosis and caspase-3-like protease activity. *Cancer Res* 58, 402-408.
- Zavacki, A. M., Mansell, J. B., Chung, M., Klimovitsky, B., Harney, J. W., and Berry, M. J. (2003). Coupled tRNA(Sec)-dependent assembly of the selenocysteine decoding apparatus. *Mol Cell* 11, 773-781.
- Zhang, H., Go, Y. M., and Jones, D. P. (2007). Mitochondrial thioredoxin-2/peroxiredoxin-3 system functions in parallel with mitochondrial GSH system in protection against oxidative stress. *Arch Biochem Biophys* 465, 119-126.

- Zhang, P., Liu, B., Kang, S. W., Seo, M. S., Rhee, S. G., and Obeid, L. M. (1997). Thioredoxin peroxidase is a novel inhibitor of apoptosis with a mechanism distinct from that of Bcl-2. *J Biol Chem* 272, 30615-30618.
- Zhang, Y., Tang, L., and Gonzalez, V. (2003). Selected isothiocyanates rapidly induce growth inhibition of cancer cells. *Mol Cancer Ther* 2, 1045-1052.
- Zhao, W., Fan, G. C., Zhang, Z. G., Bandyopadhyay, A., Zhou, X., and Kranias, E. G. (2009). Protection of peroxiredoxin II on oxidative stress-induced cardiomyocyte death and apoptosis. *Basic Res Cardiol* 104, 377-389.
- Zhong, L., Arner, E. S., and Holmgren, A. (2000). Structure and mechanism of mammalian thioredoxin reductase: the active site is a redox-active selenolthiol/selenenylsulfide formed from the conserved cysteine-selenocysteine sequence. *Proc Natl Acad Sci U S A* 97, 5854-5859.
- Zhong, L., Arner, E. S., Ljung, J., Aslund, F., and Holmgren, A. (1998). Rat and calf thioredoxin reductase are homologous to glutathione reductase with a carboxyl-terminal elongation containing a conserved catalytically active penultimate selenocysteine residue. *J Biol Chem* 273, 8581-8591.
- Zhong, L., and Holmgren, A. (2000). Essential role of selenium in the catalytic activities of mammalian thioredoxin reductase revealed by characterization of recombinant enzymes with selenocysteine mutations. *J Biol Chem* 275, 18121-18128.
- Zhou, J., Eleni, C., Spyrou, G., and Brune, B. (2008). The mitochondrial thioredoxin system regulates nitric oxide-induced HIF-1alpha protein. *Free Radic Biol Med* 44, 91-98.
- Zhou, Y., Kok, K. H., Chun, A. C., Wong, C. M., Wu, H. W., Lin, M. C., Fung, P. C., Kung, H., and Jin, D. Y. (2000). Mouse peroxiredoxin V is a thioredoxin peroxidase that inhibits p53-induced apoptosis. *Biochem Biophys Res Commun* 268, 921-927.

7. Appendix

7.1. Acknowledgements

Standing at a crucial juncture of my academic journey and before I step across the finish line, its time to take a pause and to express my gratitude in retrospect to all those people who supported me throughout this learning process.

I would start and would like to thank to my supervisor Dr. Marcus Conrad for his support and guidance. I appreciate the freedom given to me while doing my PhD thesis. He was always accommodative to the suggestions or criticisms, which stimulated the independent thinking.

I am indebted to Prof. Georg W. Bornkamm for giving me the opportunity to do my PhD in Germany. It was a great experience working under him. His ideas and suggestions were very valuable which finally concluded in the form of the present manuscript.

I express my best regards to my Dr. father Prof. Dr. Dirk Eick, for his supportive attitude towards me. Without his help it would have not been possible to submit the thesis in such a smooth manner.

I thank my present and former lab members Ana Banjac, Madhu Sukumar, Pankaj Kumar Mandal, Alexander Seiler, Heidi Förster, Alexander Mannes and Katja Möllmann for supporting me during day-to-day work, sharing their valuable experiences and making the stay in the lab memorable. I wish all of them a great success in life.

I would like to put emphasis on the help and support provided by Dr. Heike Beck, and of course, the members of her group: Juliane Hrdina, Matthias Semisch and Markus Worthmann. The unselfish help provided by Manuela Schneider at the bigining of my days in Munich deserve a special note of appreciation. They were the integral part of numerous sessions of discussion on ongoing projects.

Also I would like to thank Pirkko Kölle from Medizinische Poliklinik Innenstadt des Klinikum der LMU for doing HPLC measurements which added substantial information to the thesis.

I want to thank Dr. Elisabeth Kremmer for raising monoclonal antibody against mouse thioredoxin reductase 2 and human xCT for us.

I express my sincere thank to the people of Prof. Dr. Dick Eicks lab, specially Thomas Harasim, Martin Heidemann, Anastassia Malamoussi, Anita Gruber-Eber for sparing reagents and providing support at the hour of need.

I am very obliged to Dr. Ralf Kühn for coming up with the precise solution at the needed moment; without his help some of the data included would have never seen the light of the day.

I am expressing my thankfulness to Dr. Josef Mautner, whom I tried to avoid at the end of my thesis. Time and time again I have tried to sneak through the 1st floor where he was working. Every time when being caught, I was compelled by unpleasant question: Why I am still working and not writing my thesis?

I would like to thank people of KMOLB for help and encouragement.

The effort done by people in the animal facility is really appreciated and I thank all of them.

Additionally, I would like to thank my friend Adriana Gil-Monux, for her support and sharing nice time in Munich.

At last I want to dedicate this paragraph to acknowledge my family. Mom and Dad, thank you for all your mental support which was giving me great strength. And I would highlight the help provided by my sister, for always believing in me, standing behind me, and having the time and patience when nobody would. I would like to thank Dominik Flüge, for being the flambeau in moments when I was stuck in dark labirinth.

Tamara Perisic

7.2. Curriculum vitae

Name: Tamara PERISIC

Date and place of Birth: 29th May 1978, Travnik, Bosnia and Herzegovina

Nationality: Montenegrinian

Permanent address: Lofererstr 17, 81671 München, Germany

E-Mail: tamara.perisic@helmholtz-muenchen.de

Educational profile

PhD student at the Institute Of Clinical Molecular Biology And Tumor Genetics, Helmholtz Zentrum München (Feb 2005 – May 2009)

University education in molecular biology and physiology, Faculty of biology, Belgrade University, Belgrade, Serbia (Oct 1997- July 2004)

List of Publications

Mitochondrial Thioredoxin reductase but not cytosolic Thioredoxin reductase protects against myocardial ischemia-reperfusion injury: role of intrinsic apoptosis induction.

Perisic T*, Horstkotte J*, Schneider M, Lange P, Schroeder M, Hinkel R, Foerster H, Neumüller C, Sinowatz F, Molkenti JD, Boekstegers P, Brielmeier M, Conrad M, Kupatt C (In preparation).

** These author contributed equally to the manuscript*

Mutations in the Gene encoding mitochondrial thioredoxin reductase are associated with dilated cardiomyopathy.

Perisic T*, Sibbing D*, Pfeufer A*, Akyol M, Unwin S, Sinner MF, Jalilzadeh S, Conrad M, Bornkamm GW, Gieger C, Glöckner J, Wichmann HE, Hinterseer M, Näbauer M, MD, Kääb S, Meitinger T, Schömig A, Kastrati A, von Beckerath N. (submitted)

** These author contributed equally to the manuscript*

System x_c^- and Thioredoxin Reductase 1 Cooperatively Rescue Glutathione Deficiency

Perisic T*, Mandal P K* Seiler A*, Banjac-Canak A, Förster H, Kölle P, Weiss N, Lieberman M, Bannai S, Sato H, Kuhlencordt P, Bornkamm G.W, and Conrad M (submitted)

** These author contributed equally to the manuscript*

The cystine/cysteine cycle: a redox cycle regulating susceptibility versus resistance to cell death.

Banjac A, **Perisic T**, Sato H, Seiler A, Bannai S, Weiss N, Kölle P, Tschöep K, Issels RD, Daniel PT, Conrad M, Bornkamm GW. (2007). *Oncogene* 27: 1618-1628